SYNTHESIS AND CHARACTERIZATION OF SOME NEW SERIES OF BIPHENYL BRIDGED POLYNUCLEATING LIGANDS AND THEIR BIVALENT METAL COMPLEXES AS POSSIBLE SUPRAMOLECULAR HOSTS

A THESIS
SUBMITTED TO THE
NATONAL INSTITUTE OF TECHNOLOGY WARANGAL
FOR THE AWARD OF THE DEGREE OF
DOCTOR OF PHILOSOPHY

BY

V. KRISHNA

DEPARTMENT OF CHEMISTRY
NATIONAL INSTITUTE OF TECHNOLOGY WARANGAL
WARANGAL: 506004, ANDHRA PRADESH, INDIA
JANUARY, 2013

Dedicated to
…..My Parents

CONTENTS

Chapter	Title	Page No
	Statement	i
	Certificate	ii
	Acknowledgement	iii-iv
I	Introduction	1-39
II	Synthesis of Materials and Experimental Methods **Part A:** Materials **Part B:** Methods and Measurements	40-64
III	Spectral and Electrochemical Characterization, X-Ray Crystallographic Molecular Structure Determination and Molecular Modeling Studies of Some Biphenyl Bridged Napthylidinimine Schiff Bases **Part A:** Physical, Analytical and Spectral Studies **Part B:** Electrochemical Studies **Part C:** Molecular Structure Determination by Single Crystal X-Ray Crystallography and Molecular Modeling of NDADPE	65-120
IV	Binuclear Co(II), Ni(II), Cu(II) and Zn(II) Complexes of Biphenyl Bridged Napthylidinimine Schiff Base Ligands **Part A:** Physical, Analytical and Spectral Studies **Part B:** Cryomagnetic and ESR Spectral Studies **Part C:** Thermal Studies **Part D:** Electrochemical Studies	121-166
V	Bis-Biphenyl Bridged 2,6-diformylidinimine Tetraazomethine Cyclic Hosts and Their Binuclear and Tetranuclear Metal Complexes as Possible Hosts **Part A:** Spectral and Electrochemical Characterization of the Tetraazomethine Schiff Base Ligands **Part B:** Bi-nuclear and Tetra-nuclear Complexes of the Tetraazomethine Schiff Base Ligands	167-204
VI	Kinetics of Hydrolysis and Biological Activity of the Binucleating and Tetranucleating Ligands and Their Complexes	205-221
	List of Publications / Conferences	222-223

STATEMENT

I hereby declare that the matter embodied in this thesis entitled ***"Synthesis and Characterization of Some New Series of Biphenyl Bridged Polynucleating Ligands and Their Bivalent Metal Complexes as Possible Supramolecular Hosts"*** is the result of the investigations carried out by me in the Department of Chemistry, National Institute of Technology Warangal, Warangal, A.P., India, under the guidance of **Prof. A. Ramachandraiah**, Professor of Chemistry, National Institute of Technology Warangal and the same has not been reported earlier in part or in full, elsewhere, for any degree or diploma.

Warangal **V. Krishna**
January, 2013

CERTIFICATE

This is to certify that the work presented in this thesis entitled *"**Synthesis and Characterization of Some New Series of Biphenyl Bridged Polynucleating Ligands and Their Bivalent Metal Complexes as Possible Supramolecular Hosts**"*, has been carried out in the Department of Chemistry, National Institute of Technology Warangal, Warangal, A.P., India, by **Mr. V. Krishna**, under my supervision and the same has not been submitted elsewhere for any degree or diploma.

Dr. A. RAMACHANDRAIAH
Professor of Chemistry
National Institute of Technology, Warangal
(Research Supervisor)

Warangal
January, 2013

ACKNOWLEDGEMENTS

It gives me immense pleasure to express my deep sense of gratitude and indebtedness to my research guide, ***Dr. A. Ramachandraiah***, Professor of Chemistry, National Institute of Technology, Warangal for his expert and inspiring guidance.

I had the privilege of associating with him who has given me direction to my career. His dedication to science, integrity and patience towards his students has inspired me.

I express my sincere thanks to the ***Director***, National Institute of Technology, Warangal (NITW) for having given me the opportunity by providing both an Institute Fellowship and ample infrastructure to carry out my research work.

I express my sincere thanks to ***Prof. Ms. B. Rajitha,*** Head, Department of Chemistry, NITW, for her valuable help and support.

I am very thankful to my DSC member and former Head, Department of Chemistry, ***Prof. K. Laxma Reddy,*** for his valuable suggestions and encouragement during my research work.

I wish to thank ***Prof. B. V. Appa Rao,*** Department of Chemistry, NITW, for his cooperation throughout my research work.

I express sincere thanks to my other DSC member ***Prof. M. Krishna Mohan,*** Department of Metallurgical and Material Engineering, NITW, for his valuable suggestions.

I would like to express my special thanks to ***Prof. G. V. P. Chandramouli, Prof. I. Ajit Kumar Reddy, Prof. P. Nageswar Rao, Prof. V. Rajeswar Rao, Dr. K. V. Gobi, Dr. P. V. Srilakshmi, Dr. N. Venkatathri Narayanan, Dr. Vishnu Shanker, Dr. Kashinath and Dr Vijay Kumar*** for their encouragement.

I express my special thanks to ***Dr. P. Raghavaih,*** University of Hyderabad, for his help of X-ray crystallographic studies.

I wish to express my special thanks to ***Dr. B. Srinivas,*** for his academic help in assigning the crystal data.

I am grateful to ***Prof. K. V. Ramanujachary,*** Department of Chemistry and Biochemistry, Rowan University, Newjerrsey, USA, for his help of in running special investigations such as tensorial ESR spectral studies, cryomagnetic susceptibility measurements, voltammetric solutions, thermometric studies, etc., among others.

I express my special thanks to ***Dr. M. Venkata Ramana,*** DFRL, Mysore***,*** for his help of antimicrobial activity.

I thank all my seniors ***Dr. T. Sarojini, Dr. D. Prabhakarchary, Dr N. Raju, Dr. P. Vijay Bhaskar,*** and colleagues ***G. Srinivas Rao, K. Rajamouli*** and ***E. Rajesh*** for their encouragement throughout my research work.

I am thankful to all my fellow research scholars, ***K. V. V. Satya Narayana, K. Chaitanya Kumar, M. Murili, B. Suresh Kuram, S. Vijaya Lakhsmi, Ch. VSR, P. Kavitha, K. Bhavani, V. Amarnath, T. Ramesh, S. Kanakaraju, K. Koti, M. N. Reddy, Janardhan, Satynarayana, Santhosh, Surender, Mallikharjun, Venkanna, Nagaraju, Ramesh, Ravi Babu, Lakshmi Narayana, Nookaraju, Rajini and Kannamba*** for their help and encouragement.

I am also grateful to many of the nonteaching staff of the institute who helped me in various ways.

I remember with affection, my sisters, brother, nephew and my brother-in-law for their patience in love.

V. KRISHNA

CHAPTER I

INTRODUCTION

It is the opinion of many popular scientists that more revolutionary breakthroughs have taken place in the area of chemistry than in any other branches of science and technology during the past 5 decades. This is mainly due to the chemistry's unique nature of overlapping with other areas of science. In the present day scenario, man faces several challenges: to combat deceases; to search for alternative sources of energy; to fight the menace of environmental pollution; to generate materials suitable for specific advanced engineering applications etc. Supramolecular Chemistry, a major area of advanced chemical research intertwined with nano materials and technology, is fast evolving that would help face these challenges.

1.1 Supramolecular Chemistry

The term "Supramolecular Chemistry" has been defined by Nobel Prize winner Jean-Marie Lehn, as "*chemistry beyond the molecule*", the association of molecular or ionic entities held together reversibly by intermolecular forces to yield organised arrays of higher complexity[1,2]. Supramolecular chemistry is a multidisciplinary field, encompassing the traditionally distinct disciplines of organic, inorganic and physical chemistry. The reversibility of supramolecular self-assembly is key to form the thermodynamically most favorable structure. Molecular recognition is one of the features of supramolecular chemistry. It is made possible by usually, guest-host complementarity[3,4]. Supramolecular, non-covalent interactions are understood to involve ion-ion interactions (100-350 kJ mol^{-1}), ion-dipole interactions (50-200 kJ mol^{-1}), dipole-dipole interactions (5-50 kJ mol^{-1}), hydrogen bonding (4-120 kJ mol^{-1}), π-π stacking (0-50 kJ mol^{-1}) and Van der Waals forces (<5 kJ mol^{-1}). Supramolecular assembly is extended to convey involve space-driven and steric factors driven paradigms.

1.2 Classification of Supramolecular Chemistry Areas

Although supramolecular chemistry is still a young field, it has developed rapidly. Nowadays, people study supramolecular chemistry mainly in three directions: (a) molecular recognition chemistry, (b) building specific shapes/architectures and (c) molecular assembly organized from numerous molecules that may even eventually pile up to nanomaterial scale.

1.3 Supramolecular Recognition, Transport and Delivery

One of the greatest aspects of supramolecular chemistry is the selective binding (recognition) of compatible molecules, ions or species by a macrocyclic host, followed by the transport of the guest driven by physic-chemical gradients and chemodynomics before the same is released at the desired or chemically specified target destination. The concept of molecular recognition has been developed following the observation of enzymatic reactions. By following these principles, effective supra molecular receptors can be designed.

In its simplest sense, molecular recognition can be regarded as selective binding or complexing. The process can be, generally, considered as one molecule (host) binding another molecule (guest) to produce a host-guest complex. The host is often a larger molecule such as a macrocycle or molecular capsule and the guest can be a monoatomic cation, an organic cation, an inorganic anion, or even a neutral molecule. Either the host or the guest, or both, have binding sites that are capable of taking part in non-covalent interactions with the other.

Host-guest chemistry was recognized as a fundamental aspect of molecular recognition and self-assembly. Using host-guest chemistry, some molecules can be self-assembled to give medium-sized supramolecular structures that can have very impressive shapes and interesting properties. For example, one can assemble a "rotaxane", a molecule composed of a macrocycle and an end-capped thread molecule that is threaded through the cavity of macrocycle. Molecular cages are composed of one or more molecules that are assembled by covalent or non-covalent bonds to form a 3D cage-like structure. Small guest molecules can be bound inside the cage via intermolecular weak forces. Examples of these supramolecular structures are illustrated in **Figure 1.1**.

Non-covalent interactions play a leading role in controlling the secondary and tertiary structures of natural macromolecules such as polypeptides and polynucleotides. In recent years, intermolecular interactions, such as hydrogen bonding, π-π stacking and metal coordination, have been exploited in the molecular self-assembly of synthetic highly directional polymeric architectures[5].

1.4 Host-Guest Chemistry

In 1967, Pedersen reported that an alkali metal ion binds with crown ethers to form highly structured complexes[6]. This discovery gave fundamentally new concepts to chemistry in general and prompted the generation of a new field of supramolecular chemistry. From the event decades, many kinds of novel macrocyclic hosts have been synthesized or discovered, many macro crown ethers besides a variety of cryptands, calixaranes, cyclodextrins and cyclophanes[7] a few examples of novel **1.1** rotaxane [8], **1.2** catenane[9], **1.3** foldamer[10] and **1.4** molecular cage[11]. crown ethers, calixaranes, cyclodextrins, rotaxanes, helicates, (single, double and multistranded), inter-locked knotted molecule are found to serve as hosts by covalent, coordinates, non-covalent, topological, hydrogen bond and other modes of supra molecular interaction. In host-guest chemistry, a host molecule may selectively recognize its guest through many kinds of non-covalent interactions, such as electrostatic attraction, hydrogen bonding, metal coordination, Van der Waals forces and π-π stacking. Many smart artificial systems have been designed by using principles of host-guest chemistry[12].

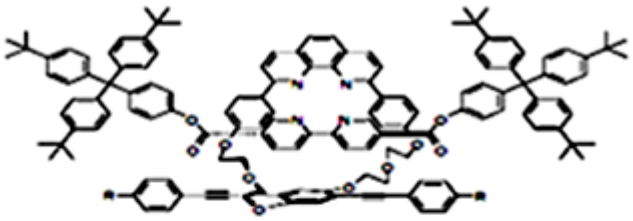

1.1

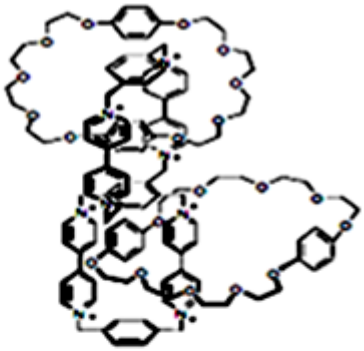

1.2

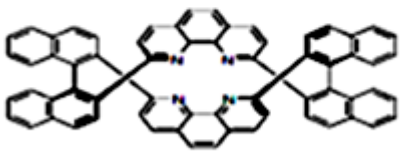

1.3

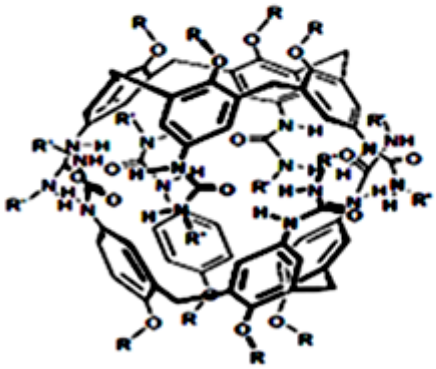

1.4

1.5 Helicates

The term 'helicate' was first introduced by Lehn and co-workers in 1987 as a description of a polymetallic helical double-stranded complex[13]. The concept of helicates extends the idea of classical coordination complexes towards more complex supermolecules in which two or more metal ions lie on a helical axis[14, 15]. Thus, a helicate is a discrete supramolecular complex formed by one or more covalent organic strands entwined and coordinated to a series of metal ions defining the helical axis.

The use of metal–ligand interactions to assemble sophisticated supramolecular architectures is a topic of considerable interest in recent years[16]. Achievements have included the deliberate design of catenanes and rotaxanes [17], knots [18], helicates [19], grids [20], and cylinders [21]. In particular, helical metallo-supramolecular arrays have attracted much attention because of the fundamental role of helicity in biology and the potential applications in the fields of asymmetric catalysis and non-linear optical materials[22-24]. Since Lehn and co-workers introduced the term helicates in 1987 for the description of a metal-containing double stranded helix[25], a variety of helical structures such as polymetallic double-stranded helicates, multiple-stranded homo and hetero metallic helicates and circular helicates have been described[26]. The suitably designed organic ligand (helicand) is necessary in the synthesis of metallo helicates. In order to allow for helical complex, the ligand should contain multiple metals binding sites whose donor sets are matched to the coordination geometric requirements of specific metal centers so as to give rise to multistranded arrays. In addition, the ligand must offer sufficient flexibility for multiple strands to wrap around the two (or more) metal centers, while also being sufficiently rigid to impose the same stereochemistry at both (or more) metal centers. Among the families of organic helicands, multidentate imines, such as pyridylimines [27-34], imidazolimines [35,36] and salicyladimines[37-42], are renowned for the generality of their easy syntheses by simple one-pot condensation reaction between aldehyde (or ketone) and amines, as well as their inherent advantage of coordinating with metal ions to form polynuclear aggregates with considerable structural diversity [43-47]. For a better understanding of the effects involved in the self-assembly process based on the imine ligand.

1.6 Self-Assembly in Nature

Naturally occurring DNA, perhaps the best known self-assembling structure in biological systems, exists in a double helical form[48]. The two single strands are held together

by a number of hydrogen bonds, involving acidic hydrogen atoms (hydrogen bonding donor), oxygen (hydrogen bonding acceptor) and nitrogen atoms (hydrogen bonding acceptor) of the purine and pyrimidine bases in order to maintain the double helical structure **Figure 1.1**. In this double helix guanine (G) forms triple hydrogen bonds with cytosine (C) and adenine (A) forms double hydrogen bonds with thymine (T) Guanine selectively interacts with cytosine because the G-C complex is much more stable than G-T complex which would form only one hydrogen bond. Similarly, adenine exclusively complexes with thymine because adenine would form no hydrogen bonds with cytosine. The X-ray diffraction studies revealed that the hydrogen bonds holding G-C and A-T complexes are about the same length (2.9 ± 0.1 Å).

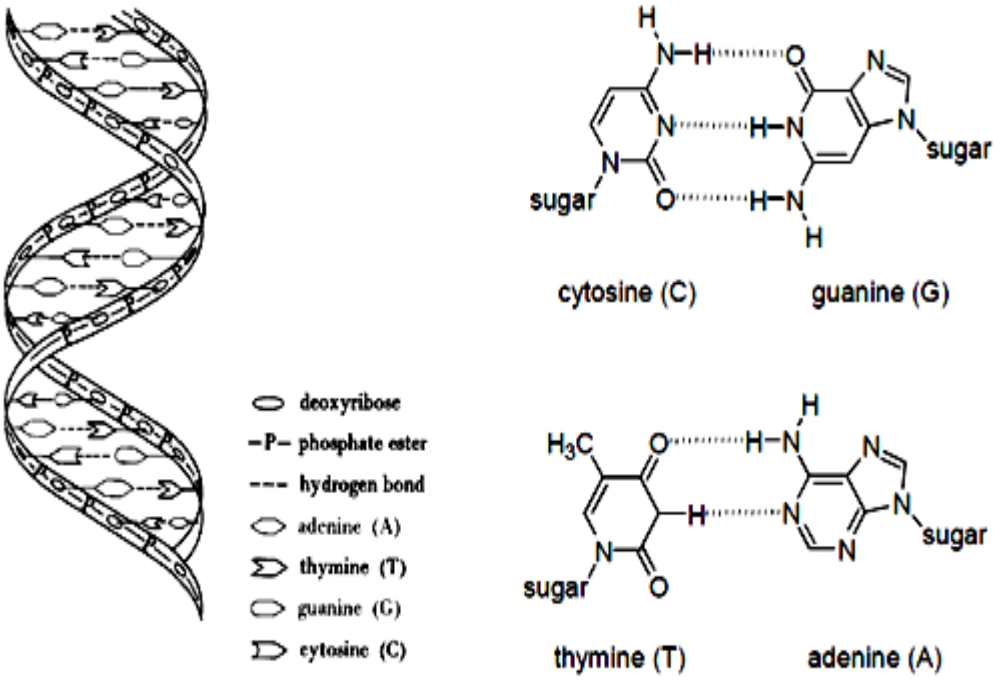

Figure 1.1: DNA helical structure of complementary base pairing.

1.7 Schiff Base Chemistry

As my thesis took examples of azomethine by systems with possible supramolecular cyclephenes is a general desripting Schiff bases is presented here briefly. By and large, all Schiff bases have been found to be a promising set of potential monodentate (**1.5**)[50], bidentate (**1.6**)[51], tridentate (**1.7**)[52], tetrdentate (**1.8**)[53] and polydentate (**1.9**)[54] ligands to a variety of metal ions. Thus, Schiff bases became the favourite systems for studies by many investigations of coordination chemistry. The possibility of all routine optical transitions, namely, n→π*, and σ→σ*, the coplaniarity of the lone-electron-pair-containing-orbital of

nitrogen to the -C=N- bond and I=1 of nitrogen give a great scope of electroning, ESR and magnetic studies of the complexes is now voluminous. However, their entry into the supramolecular arena is of recent phenomenon.

Condensation of carbonyl compounds with primary amines to form imines was discovered in 1864 by Hugo Schiff[55] and the product is now called a Schiff base compound.

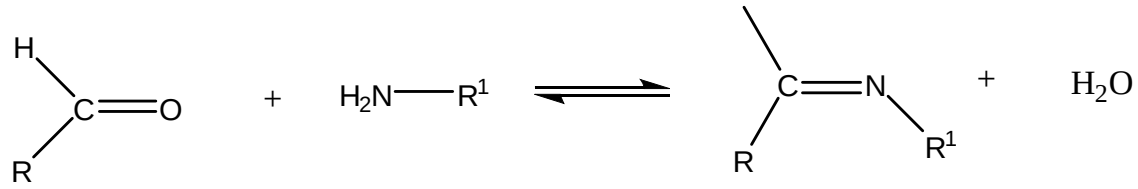

1.5

(R^1 = -CH_3, -Ph, etc)

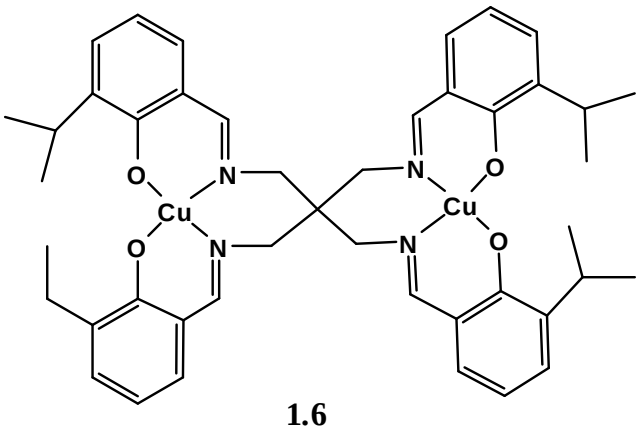

1.6

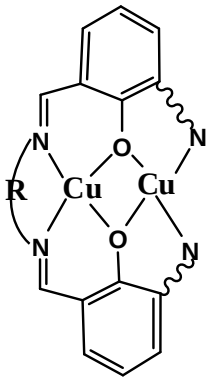

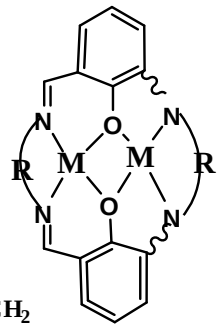

R= $(CH_2)_2$, $(CH_2)_3$ CH_2NHCH_2 etc

1.7

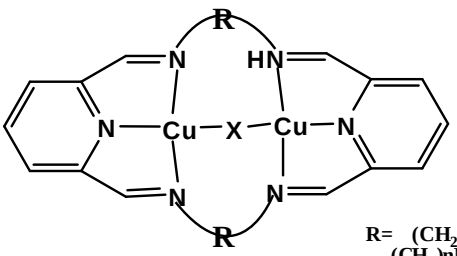

R= $(CH_2)n$, $(CH_2)nNH(CH_2)n$, $(CH_2)_2O(CH_2)_2$ etc.

1.8

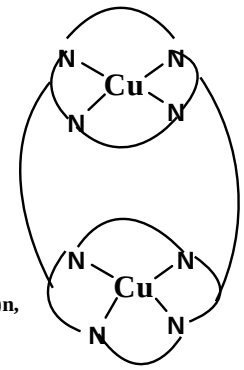

1.9

1.8 Schiff Base Macrocycles

During the last two decades, many kinds of methods of fabricating Schiff base macrocycles starting from various dicarbonyl compounds and diamines were developed towards the synthesis of symmetrical and unsymmetrical macrocycles[56].

Since the report of Robson's inaugural [2+2] macrocycle, Schiff base macrocycles have proved useful in the study of metal-ligand interactions[57]. These macrocycles, which are easily synthesized by reacting a diamine monomer with a diformyl monomer of an appropriate geometry to yield a single macrocycle, have been the subject of much recent investigation. A series of [2+2], [3+3], [4+4] and [6+6] Schiff base macrocycles were reported [58, 59]. The shape of the macrocycles depends on the geometry and stoichiometric ratio of the starting materials, as well as other conditions such as solubility of starting material, polarity of solvent, and presence of template.

The first Robson-type macrocycle was prepared by reaction of 2,6-diformyl-4-methylphenol **1** with 1,3-diaminopropane **2** in the presence of a metal salt. Synthesis of these macrocycles without a metal template only gave oligomers. However, it was found that by adding acid into the system, metal-free Robson-type macrocycles (e.g.,**3**) were formed[60], as shown in **Scheme 1.1**.

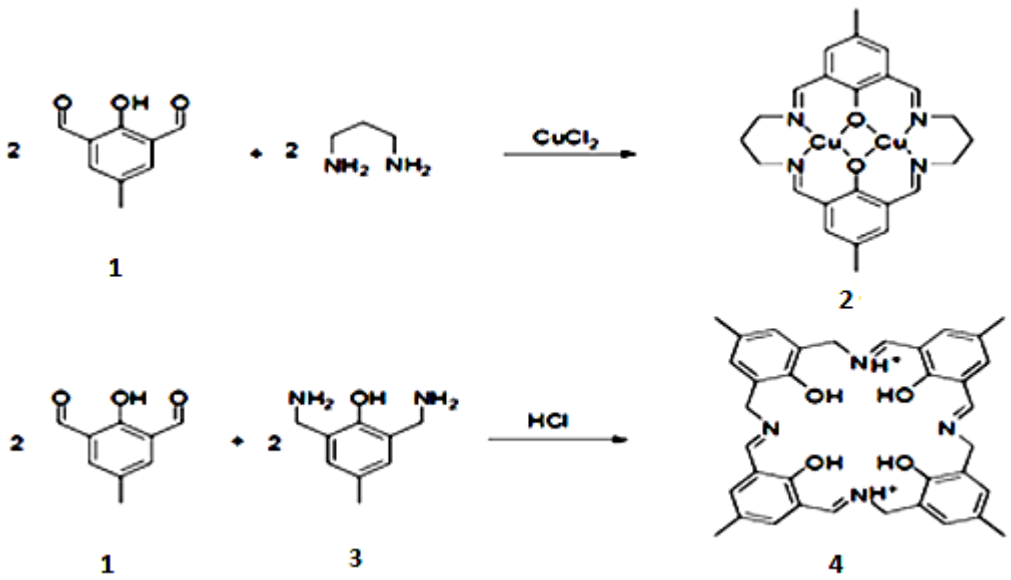

Scheme 1.1

1.9 Bi- and Poly-nuclear Schiff bases and Their Metal Complexes

Binuclear copper(II) complexes have received considerable attention in recent years partially due to the possible presence of coupled two copper centres in certain copper proteins and to their interesting magnetic and structural properties. Further evidence to the binuclear formulation comes from ESR studies, some data are presented in chloroform at room temperature which show seven line spectra very often observed for the binuclear system[61].

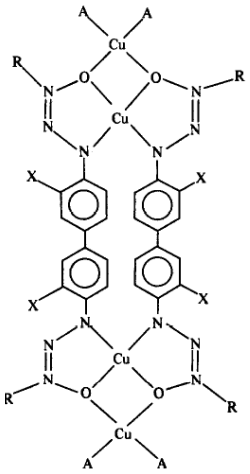

1.10

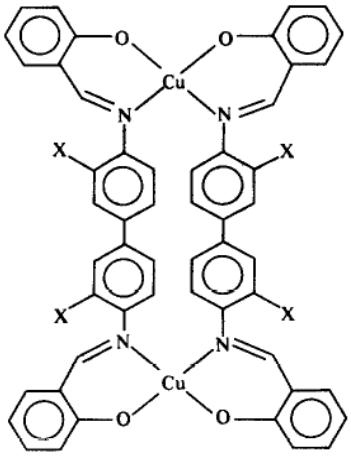

1.11

A Ramachandraiah et al have reported a new class of binuclear copper(II) complexes, Cu_2L_2, which yielded a series of tetranuclear copper(II) complexes, $Cu_4L_2A_4$ when mixed with CuA_2 in a 1:2 molar ratio in **1.10** and **1.11** (where LH_2 = 3,3'-dimethoxy-4,4'-bis(l-alkyl(R)triazene-l-oxide)biphenyl and A = Cl, Br) [62]**.**

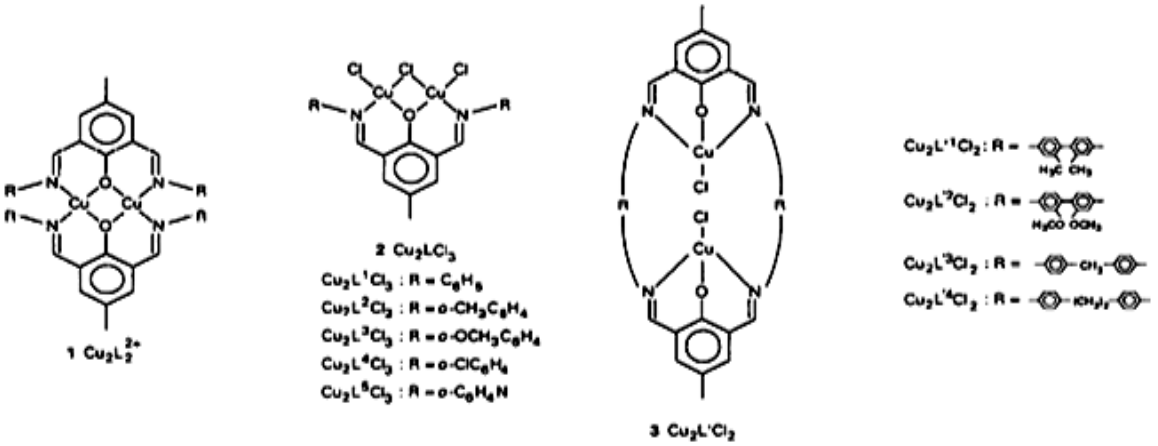

1.12

P S Zacharias et al have reported a series of binuclear copper(II) complexes of ligands derived from condensation of 2,6-diformyl-4-methylphenol with various aromatic mono and

diamines have been synthesized in **1.12**. Complexes derived from monoamines have the Cu_2LCl_3 composition and those from diamines have the $Cu_2L'Cl_2$, composition, where L and L' represent the ligands[63]. Homo and hetero-dinuclear copper(II), nickel(II) and zinc(II) complexes of a dinucleating ligand derived from the condensation of 2 mol of 2,6-diformyl-4-methylphenol and 1 mol of 1,3-diaminopropane (L) have been prepared as their perchlorate salts, and characterized and studied for their magnetic and redox properties[64].

Dinuclear copper(II), nickel(II), cobalt(II) and iron(III) complexes derived from the Schiff base ligands obtained from the condensation of 3,3'-dimethyl-4,4'-diaminobiphenyl and pyridine-2-aldehyde and mononuclear iron(III) complexes of some Schiff bases generated from substituted anilines and pyridine-2-aldehyde [65].

Dinuclear Cu(II), Ni(II) and Co(II) complexes of macrocyclic Schiff base ligands of 2,6-diformyl-4-methylphenol with α,ω-diamines have been synthesized and characterized. The effect of chelate ring size and saturation of azomethine groups of these ligands on stability, structure and electrochemical properties of the metal complexes has been investigated [66].

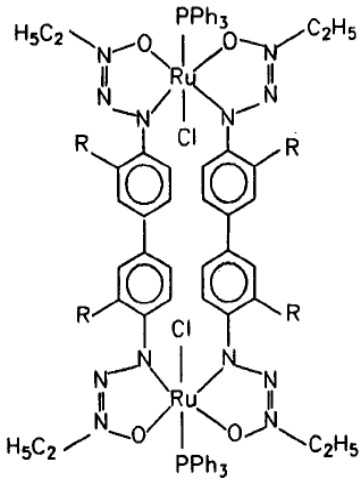

1.13

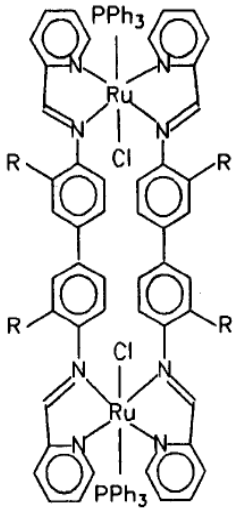

1.14

H Aneetha et al reported a number of dinuclear iron(III) and ruthenium(III) complexes and from dinucleating ligands in **1.13** and **1.14** have been synthesized and characterized[67].

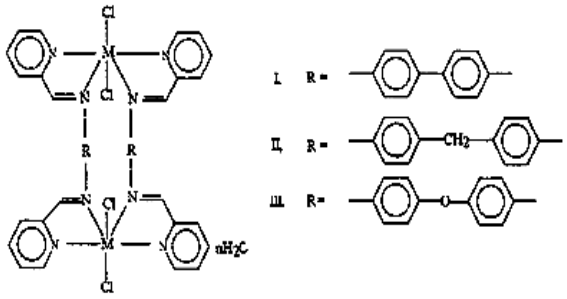

1.15

P K Bhattacharya et al reported Mn(II) binuclear complexes of Schiff base ligands have been synthesized **1.15** by the reaction of $Mncl_2$.$2H_2O$ in ethanolic solution with the Schiff base obtained by the condensation of pyridine carboxaldehyde and longer aromatic diamines like 4,4'- diamino diphenyl, 4,4'-diamino diphenyl methane and 4,4'-diamino diphenyl ether respectively[68].

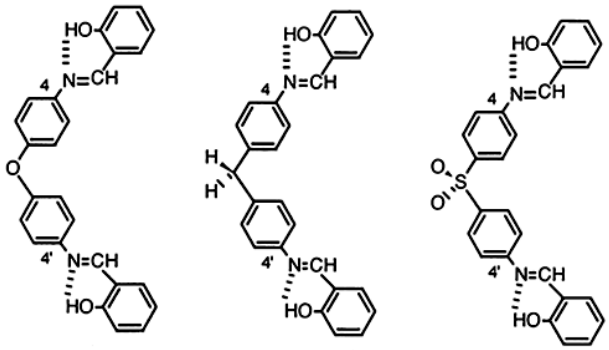

1.16

Noboru Yoshida et al reported copper(II) assisted self-assembly a series of new bis-*N*,*O*-bidentate Schiff base ligands, bis(*N*-salicylidene-3,3-diaminodiphenyl)sulfone, bis(*N*-salicylidene-4,4'-diaminodiphenyl)ether, bis(*N*-salicylidene-4,4'-diaminodiphenyl)methane has been prepared **1.16**. An analogous Schiff base, bis(*N*-salicylidene-4,4'-diaminodiphenyl)ether with a phenyl ether spacer (-$C_6H_4OC_6H_4$-) was also designed to self-assemble in the presence of metal ions, leading to a double-helical dinuclear supramolecular motif. Electrospray mass spectrometry proved a very useful characterization tool to detect a variety of supramolecular species in solution. These unprecedented double-helical motifs in solid and solution seem to be induced by the geometrical preference for tetrahedral and/or square-planar coordination of copper(II) ion and the inter ligand aromatic interactions between the bridging groups[69].

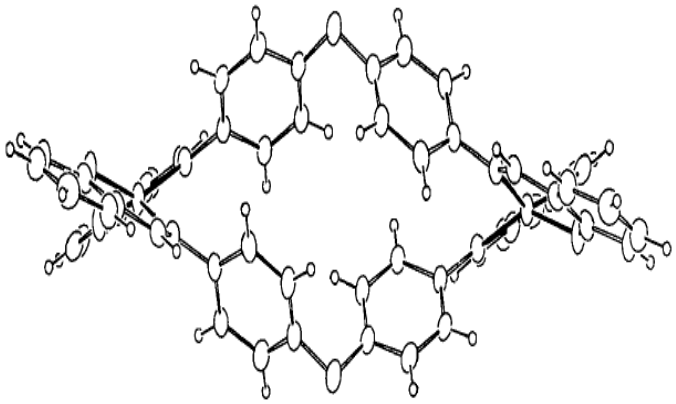

1.17

Structural characterization of two copper(II) complexes of bis-*N*,*O*-bidentate Schiff base ligands. The utilization and combination of Cu(II) and the bis-*N*,*O*-bidentate Schiff base having the flexible spacer group allow the facile formation of the tetranuclear and dinuclear Cu(II) complexes containing the double-helical motif. The weak π–π and CH–π aromatic interactions between the spacer groups and the flexible geometry of the Cu(II) ion would play an important role in determining the supramolecular in **1.17** structure[70].

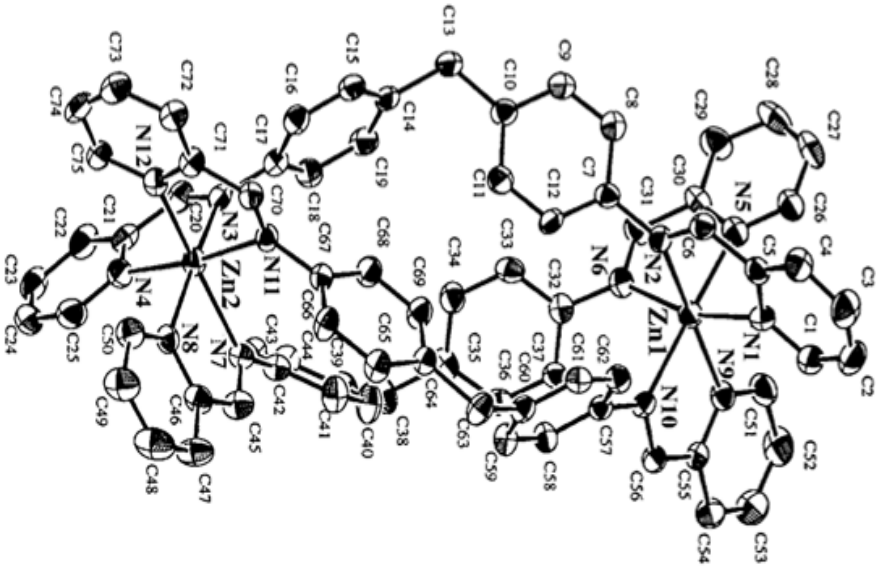

1.18

Noboru Yoshida, et al have reported the series of Zn(II) complexes with bis bidentate Schiff base ligand have been found to show interesting variations of structure in the solid state and solution. Three Zn(II)-assisted supramolecular motifs were presented using the bis-bidentate Schiff bases ligand, having flexible aromatic spacer groups. X-Ray crystal

diffraction characterization revealed that the Zn(II) complexes display dinuclear double-helical, dinuclear triple-helical and 1-D polynuclear architectures in **1.18** the solid-state, depending on subtle differences of coordination site and spacer group in the ligand[71].

Paul E Kruger et al have reported Self-assembly of the tetradentate ligand bis(*N*-salicylidene-4,4'-diaminodiphenyl)methane, **1.19** around Co(II) and Cu(II) gives rise to the dinuclear double helicates $[Co_2L_2]$ and $[Cu_2L_2]$, which have been characterised by a single crystal X-ray diffraction study[72].

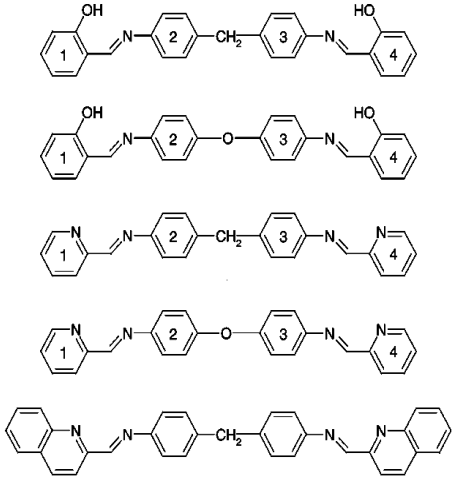

1.19

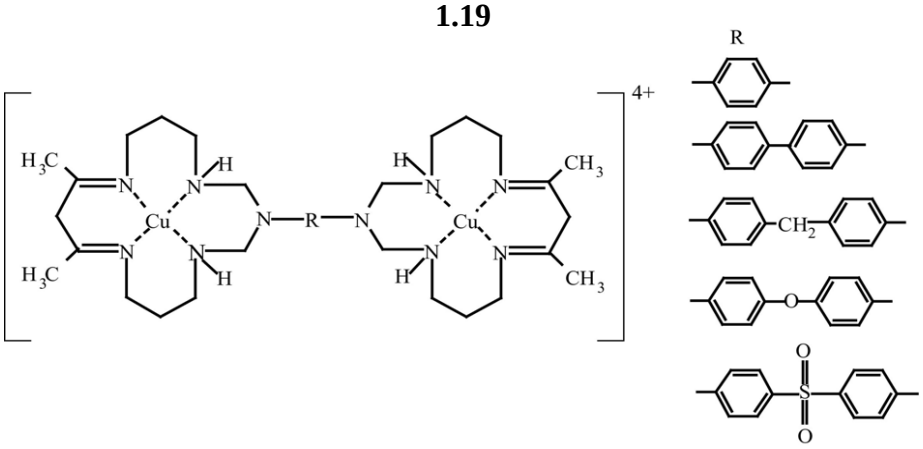

1.20

Masoud Salavati-Niasari et al have reported new bis(macrocyclic)dicopper(II) complexes containing phenylene bridges between 16 membered pentaaza macrocyclic subunits have been synthesized via one-pot template condensation of nitrogen–nitrogen linker (1,4-phenylenediamine; benzidine; 4,4'-diaminodiphenylmethane; 4,4'-diaminodiphenylether; 4,4'-diaminodiphenylsulfon), formaldehyde, 1,3-diaminopropane, copper(II) and 2,4-pentanedione in a 1:4:4:2:2 molar ratio results in the formation of new series of binuclear

copper(II) complexes in **1.20**; bis(8,10-dimethyl-1,3,7,11,15-pentaazacyclohexadeca-7,11-diene)copper(II) {[Cu(Me_2[16]aneN_5)]2RCl_4}". {[Cu(Me_2[16]aneN_5)]2R}(ClO_4)$_4$ was prepared by a method similar to that for {[Cu(Me_2[16]aneN_5)]2RCl_4} except that copper(II) perchlorate was used instead of copper(II) chloride[73].

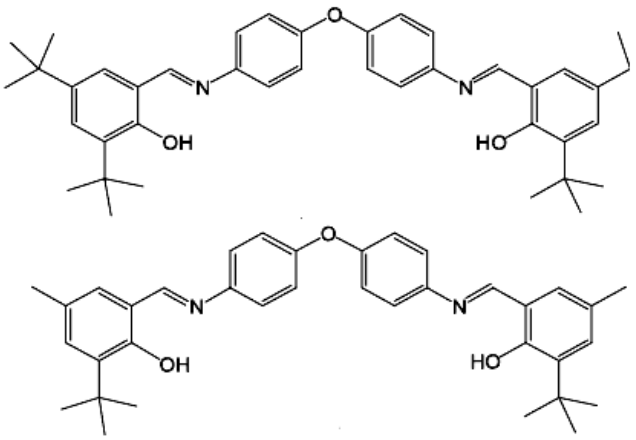

1.21

Wei Huang, et, al have reported two flexible Schiff base ligands bis-[(N,N'-3,5-di-tert-butylsalicylidene)-4,4'-diaminodiphenyl]ether and bis-[(N,N'-3-tert-butyl-5-methylsalicylidene)-4,4'-diaminodiphenyl]ether were prepared in high yields and their structures in **1.21** were determined by X-ray single-crystal diffraction. Different packing modes were observed. Due to the different spacial hindrance of substituted groups bonded to the phenol rings. Reaction of ligands with Cu(ClO_4)$_2$.6H_2O in hot methanol yielded neutral double helical dinuclear complexes where each Cu(II) center has a pseudo-tetrahedral coordination sphere with two-wrapped ligands[74].

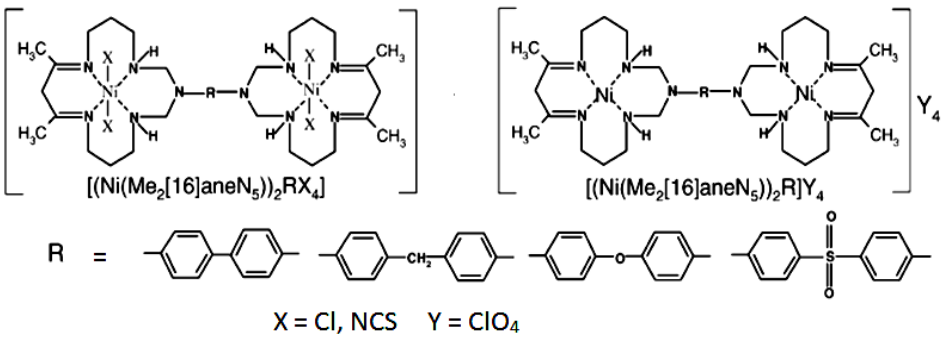

1.22

Masoud Salavati-Niasari et al have reported bis(macrocyclic)dinickel(II) complexes containing phenylene bridges between 16-membered pentaaza macrocyclic subunits have been synthesized via one-pot template condensation of nitrogen–nitrogen linker (1,4-

phenylenediamine; benzidine; 4,4'-diaminodiphenylmethane; 4,4'-diaminodiphenylether; 4,4'-diaminodiphenylsulfone), formaldehyde, 1,3-diaminopropane, nickel(II) and 2,4-pentanedione in **1.22** a 1:4:4:2:2 molar ratio[75].

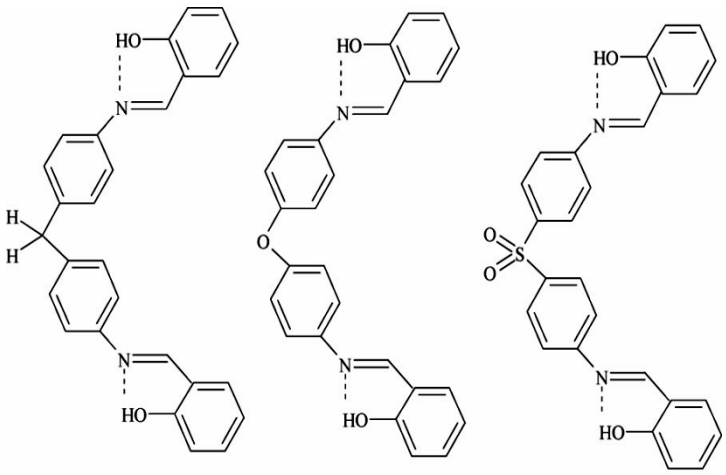

1.23

Masoud Salavati-Niasari et al have reported synthesis and characterisation of three dimeric *cis*-dioxomolybdenum(VI) complexes involving Schiff base ligands is described. Ligands were obtained by condensation of salicylaldehyde with aromatic nitrogen–nitrogen linkers(4,4'-diaminodiphenylmethane;4,4'-diaminodiphenylether;4,4'diaminodiphenylsulfone). $[MoO_2(acac)_2]$ reacted with the prepared ligands **1.23**; bis[(*N*,*O*-salicylidene)-4,4'-diaminodiphenyl]methane,bis[(*N*,*O*-salicylidene)-4,4'-diaminodiphenyl]ether, bis[(*N*,*O*-)-4,4'-diaminodiphenyl]sulfone, forming six-coordinated *cis*-dioxo Mo(VI) complexes; $[MoO_2L]_2$.

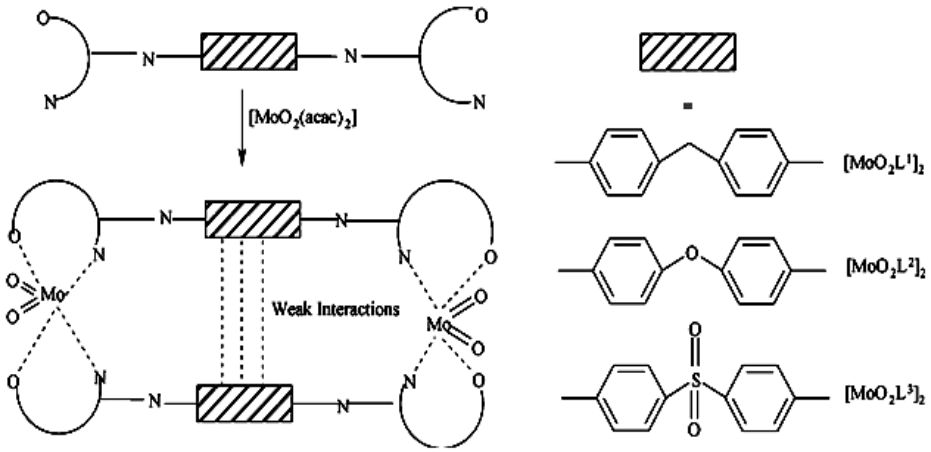

1.24

This set of dioxomolybdenum(VI) complexes **1.24** with bis-bidentate Schiff-base ligands derived from aromatic nitrogen–nitrogen linkers (4,4'-diaminodiphenylmethane; 4,4'-diaminodiphenylether; 4,4'-diaminodiphenylsulfone) exhibit good catalytic activities and selectivity in the epoxidation of cyclohexene with *t*-butylhydroperoxide. The electron withdrawing group on the aromatic nitrogen–nitrogen linkers of complex is advantageous over electron-donating one on the effectiveness of a catalyst but disadvantageous on the redox stability of a complex. SWNTs can also take up the Mo catalysts by adsorption and there by facilitate the reusability at a quite high conversion level[76].

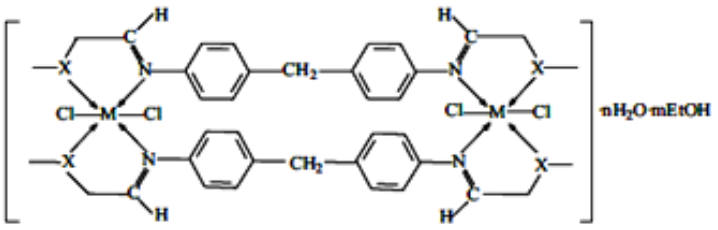

M = Co(II), Ni(II) and Cu(II)

1.25

S A AbouEl-Enein et al have reported cobalt(II), nickel(II) and copper(II) complexes of Schiff's bases derived from 4,4'-methylenedianiline and pyridine-2-carboxaldehyde(L^1), furan-2-carboxaldehyde(L^2) or thiophene-2-carboxaldehyde(L^3), were prepared and characterized by different analytical and spectral methods. The Schiff bases behave as neutral tetradentate ligands. The chloro-complexes of (L^2) with (2:3) mole ratio have a polymeric nature. However, that of L^1 and L^3 with (1:1) mole ratio showed **1.25** a sandwich structure [77].

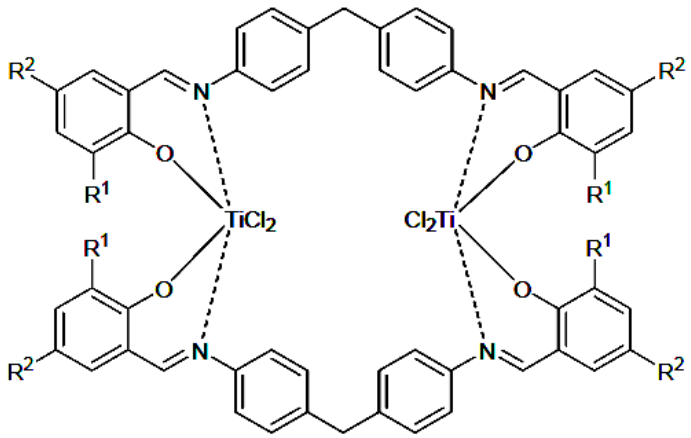

1.26

G A Tolstikov et al have reported reactions of salicylaldehyde, 3-*tert*-butylsalicylaldehyde, and 3,5-di-*tert*-butylsalicylaldehyde with1,4-diaminobutane, 1,6-diaminohexa,4,4′-diaminodiphenylmethane,4,4′diamino3,3′,5,5′tetramethyldiphenylmethane, 4,4′-diamino-5,5′-dicyclopentyl-3,3′-dimethyldiphenylmethane,4,4′-diamino-5,5′dicyclohexyl-3,3′-dimethyldiphenylmethane, bis(4-aminophenyl) sulfone, *o*,*o*′- and *p*,*p*′-diaminodiphenyl ethers, 1,4-bis(4-aminophenoxy)benzene, 2,2-bis[4-(4-aminophenoxy)phenyl]propane, and 4,4'-diamino-*p*-terphenyl gave a series of the corresponding Schiff bases which can be used as tetradentate ligands for the synthesis of titanium in **1.26** and zirconium complexes[78].

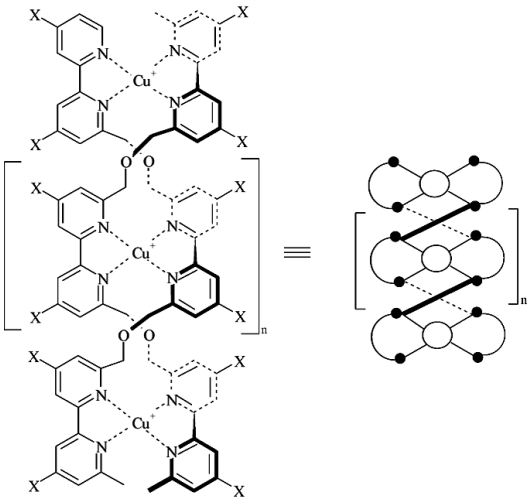

1.27

B I Kharisov et al have reported describe the contribution of coordination chemistry to the creation and development of supramolecular chemistry in **1.27**. Both discrete and infinite buildups are examined. The first group comprises metal-containing host molecules and organic acceptors for metal cations; the second includes coordination polymers, ionic and liquid crystals. Their potential- and practical applications are briefly explained[79].

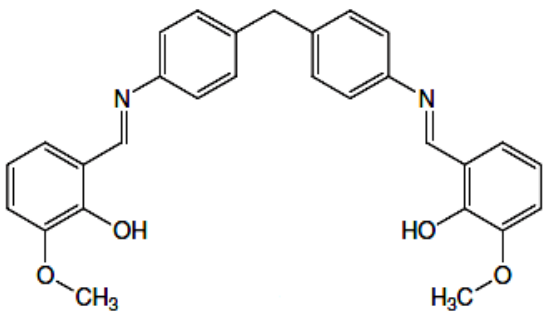

1.28

Cai-feng Bi et al have reported a Schiff base compound (L) was synthesized using o-vanillin and 4,4'-diaminodiphenylmethane and characterized by elemental analysis, ^{1}H NMR, ^{13}C NMR, IR, electronic absorption spectra and X-ray diffraction single crystal analysis in **1.28**. The title compound(L) has no fluorescence intensity in a range of 450–650 nm, but its fluorescence spectrum shows enhancement in the intensity of the signal at 372 nm on binding with the Zn(II) cation from pH=6 to 14. No such significant change was observed for other metal ions. Fluorescence intensity was linear with concentration of Zn(II) cation in a range from 1×10^{-7} mol·L^{-1} to 1.2×10^{-5} mol·L^{-1}. This Schiff base compound is a promising system for the development of new fluorescent probes for the detection of Zn(II) cation [80].

Synthesized a novel Schiff base fluorescent probe for Zn(II) derived from o-vanillin and 4,4'-diaminodi-phenylmethane. This fluorescent probe is based on a significant enhancement in fluorescence intensity after adding Zn(II) in DMF, DMSO, THF, toluene and chloroform. This fluorescent probe has high selectivity for binding Zn(II). This is reflected in competitive binding experiments with a range of metal cations. This L–Zn(II) system is stable at pH 6 to 14. A very good linear relationship of fluorescence intensity is observed.

R. Rajavel et al have reported new series of macrocyclic binuclear metal complexes Cu(II), Ni(II) and VO(IV) having the general composition $[ML]X_2$. The binucleating Schiff base ligand has been synthesized from freshly prepared o-aminobenzaldehyde and benzidine. This synthesized ligand reacts with 2,3-pentanedione and metal salts to form macrocyclic binuclear Schiff base complexes. Both ligand and complexes were characterized by elemental analysis, IR, UV-Vis spectral data, conductivity, magnetic moment, ^{1}H NMR and ESR spectra. The parent Schiff base and its complexes are assayed against gram negative bacteria like Klebsiella pneumoniae, Escherichia coli and gram positive bacteria like staphylococcus aureus at 37°C by disc diffusion technique. The inhibition of bacterial growth high at copper(II) complex.

Novel macrocyclic binuclear Schiff base complexes have been synthesized by template method. The Schiff base ligand can be prepared by fresh o-aminobenzaldehyde with benzidine. The ligand react with 2,3-pentanedione and respective metal salts. The metal-ligand ratio of 1:1 has been arrived at by estimating the nitrogen and metal contents. The complexes are electrolytic as indicated by the high molar conductivity values. The involvement of the azomethine nitrogen atoms of the ligand in binding with the metal has been inferred from the IR spectra. The lower value of magnetic moment of binuclear

complexes are attributed to the weak anti-ferromagnetic interaction between two central metal ions, this indication was the formation of binuclear complexes in **1.29**.

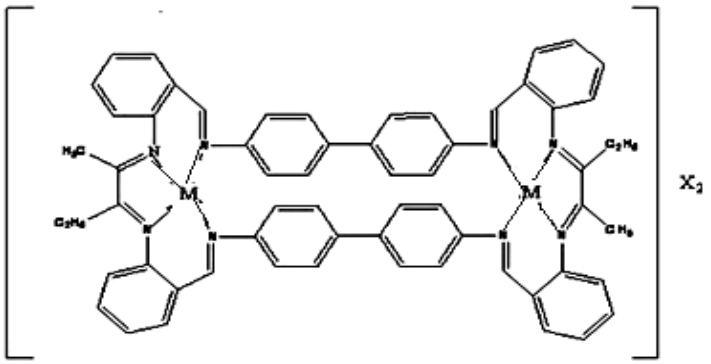

Where M=Cu & Ni $X=ClO_4^-$; M=VO $X=SO_4^{2-}$

1.29

The presence of counter ion has been confirmed from the IR and high conductivity values. The antibacterial activity more pronounced in Cu(II) complex because of the Chelation theory[81].

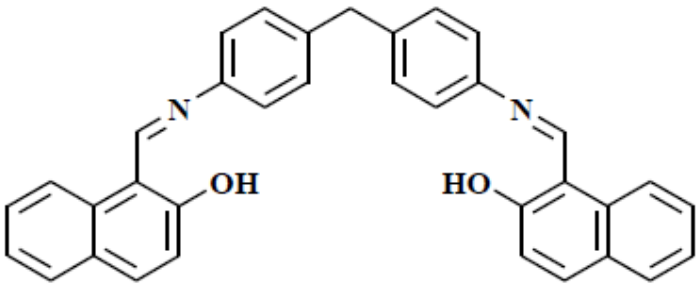

1.30

Narinder Singh et al have reported azomethanine linked chemosensor has been synthesized and examined for cation recognition properties in **1.30**. The sensor shows strong affinity for Al^{3+} over other cations [82].

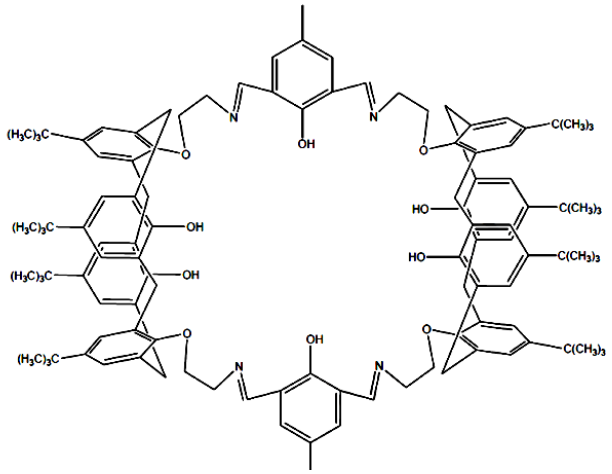

1.31

PA Vigato et al have reported the structural and physico-chemical aspects of planar or tridimensional cyclic and acyclic compartmental Schiff bases, their polyamine homologues and related polynuclear complexes in **1.31**. The selective generation of helically folden strands, which can modify their structure into a linear one upon complexation and return to the helical form by demetalation cycling between contracted and extended structures. Also the ability of acyclic and macrocyclic ligands without endogenous bridging groups to in capsulate two or more metal ions and to act as building blocks in the construction of oligomeric or polymeric systems is also analyzed. The magneto-structural correlation of the homo and hetero dinuclear or polynuclear complexes, together with the photochemical and photo physical properties resulting from these specific recognition processes, were also considered[83].

In our laboratory we have recently reported the acyclic synthesis of N_2O_2 donor biphenyl bridged Schiff bases viz. 2,2'-(4,4'-oxybis(4,1-phenylene)bis(azan-1-yl-1-ylidene))bis(methan-1-yl-1-ylidene)dinaphthalen-1-ol(NDADPE),2,2'-(4,4'-methylenebis(4,1-phenylene)bis(azan-1-yl-1-ylidene))bis(methan-1-yl-1-ylidene)dinaphthalen-1-ol(NDADPM), 2,2'-(3,3'-dimethoxybiphenyl-4,4'-diyl)bis(azan-1-yl-1-ylidene)bis(methylidene)dinaphthalen-1-ol(NDADPO), 2,2'-(3,3'-dimethylbiphenyl-4,4'-diyl)bis(azan-1-yl-1-ylidene)bis(methan-1-yl-1-ylidene)dinaphthalen-1-ol(NDADPT),2,2'-(biphenyl-4,4'-diylbis(azalidene))bis(methan-1-yl-1-ylidene)dinaphthalen-1-ol(NDADPB) and their Co(II), Ni(II), Cu(II) and Zn(II) compounds. The ligands were characterised by elemental, IR, ^{1}H, ^{13}C NMR, mass spectral analysis, electrochemical, thermal, single X-ray Crystallography and molecular modeling studies. The Co(II), Ni(II), Cu(II) and Zn(II) complexes of biphenyl bridged Schiff base ligands were characterised by molar conductance, electronic spectral studies, cryomagnetic

susceptibility, ESR, electrochemical and thermal were presented. Magnetic behaviour of all metal complexes was paramagnetic. Thermal behavior of metal complexes was studied by the thermogravimetric analysis. An octahedral and tetrahedral geometry was proposed for all of these complexes. All the biphenyl bridged Schiff base metal compounds were found to be active against Gram +ve and Gram -ve bacteria [84-87].

Macrocyclic synthesis of N_4O_2 donor biphenyl bridged Schiff bases viz. DFMDE, DFMDPM, DFMDPD, DFMDPT and DFMDPB also reported from this laboratory. The ligands are characterised by spectral (electronic, IR, ^{1}H NMR, ^{13}C NMR, mass), thermal, electrochemical and molecular modeling studies.

The Co(II), Ni(II), Cu(II) and Zn(II) complexes of macrocyclic biphenyl bridged Schiff base ligands were characterised by elemental analysis, thermal analysis, cryomagnetic susceptibility measurements, ESR, electrochemical and antimicrobial activities of these complexes are also studied and ligand found to be more active than the Gentamycin and Fluconazole [88, 89].

I have presented the foregoing gist on the research activity reported in the literature and various kinds of Schiff bases to establish their versatility in both coordination chemistry and supramolecular chemistry. The presence of potentially well known coordinating atoms, N and O, with nuclear spin quantum values I = 1 and I = 0, respectively, enable a typical Schiff base one of the most sought after ligand systems.

Condensation of either an aliphatic or an aromatic primary amine with a carbonyl compound takes place at ambient to moderate laboratory conditions. Incorporation of auxiliary or functional moieties either on the primary amine or on the carbonyl compound would provide scope for generating a wide variety of Schiff bases. Many a time the carbonyl compound is selected such a way that the azomethine nitrogen finds a partner ligating atom a few atom away to enable the total Schiff base a bidentate or polydentate ligand. Further, the collective manipulations of substituents on the primary amine or/and the carbonyl compound would provide variable degree of structural, electronic, magnetic, stereochemical, thermodynamic, electrochemical and quantum mechanical properties for both the ligands as well as the ensuing complexes. Some of these properties may be conveniently preplaned to result, finally as the supramolecular properties.

As already mentioned above, the most prominent tasks of supramolecular systems is their ability to serve as hosts of ions, atoms, molecules and particles to first bind, transport and release when needed.

Depending on the way the hosts bind to the guests, the supramolecular host for have been classified in several types. A definitively brief description of each of these classes is presented hereunder.

1.9.1 *Catenanes and Rotaxanes*

In 1960 Wasserman reported the preparation of interlocked organic rings and named the complex a 'catenane' from the Latin for chain, *catena*[90]. In his paper he noted that other workers, notably Lüttringhaus[91], had attempted similar molecular entanglements but had been unsuccessful. Such entanglements are only possible because many of the key compounds used in supramolecular chemistry, such as polyethers, polyamines and crown ethers, are flexible. Furthermore they may also incorporate potential donor atoms, hydrogen bonding motifs, aromatic or hydrophobic groups that have affinities for complementary species. The resulting combination of flexibility and functionality can generate inter- and intermolecular attractions leading to entangled molecules such as the catenanes and related rotaxanes, which are illustrated in **1.32** catenane and **1.33** rotaxane.

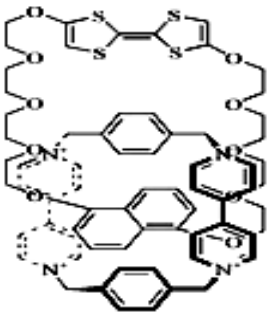

1.32

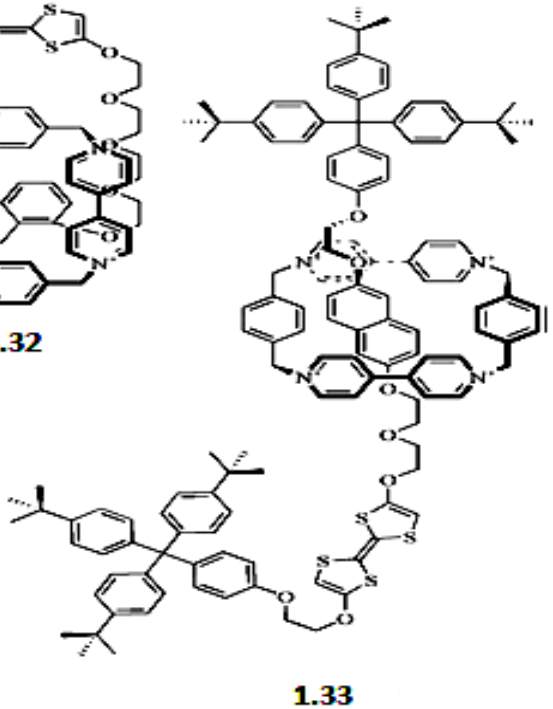

1.33

1.9.2 *Molecular Clefts and Tweezers*

Molecular clips and tweezers are two closely related types of compound. Molecular tweezers represent a simple kind of receptor in which two guest-binding domains usually comprising flat, aromatic groups, are positioned by a relatively rigid tether (in a more or less preorganised fashion) on either side of the proposed binding site. The guest is then held between the two 'pincers' of the host. In general, aromatic rings or alkynes are used as rigid spaces in order to hold the host pincers at the required distance apart, typically about 7Å in the case of aromatic guests that π-stack with aromatic binding sites. The spacer and nature of the binding sites should also prevent selfassociation. The types of tweezers have been expanded greatly since the original definition and terms such as tweezers or clips are used almost interchangeably in a descriptive way.

We have already seen a molecular clip based on Tröger's base in action where we noted the interesting effects of solvation on its binding ability. The molecular tweezers concept originated in 1978 with Howard Whitlock[91] of the University of Wisconsin, USA, exemplified in molecular tweezers **1.34**, which rely upon a combination of *π–π* stacking and ion–dipole interactions for guest binding. Whitlock's work was inspired by the observation, in 1970, that the hydrolysis of aspirin in water is inhibited by caffeine, suggesting some kind of binding of the drug by the caffeine. Whitlock anticipated that this binding might be studied using better defined systems such as host **1.34** with guests such as the potassium salt of 1,3-dihydroxy-2-naphthoate (KDN). The distance between the two theophylline pincers in **1.34** is held fairly rigidly by a six-carbon diyne spacer, which allows some pivoting at the sp3 methylene linkers (**Scheme 1.2**). The complex studied between **1.34** and KDN is highly insoluble and so could not be studied by NMR spectroscopy. Instead, the binding constant was measured by the assessment of partition coefficients by UV–Visible spectroscopy between phosphate-buffered aqueous solution and dichloroethane. This gave respectable binding constants in the region of 10^4.

The molecular tweezers concept has been extended by Zimmerman[92, 93] to the double recognition of guests *via π–π* stacking pincers with a hydrogen bonding core. The compounds incorporate a rigid backbone that enforces a *syn* conformation hence increasing preorganisation and 'turning off' the kind of conformational mobility.

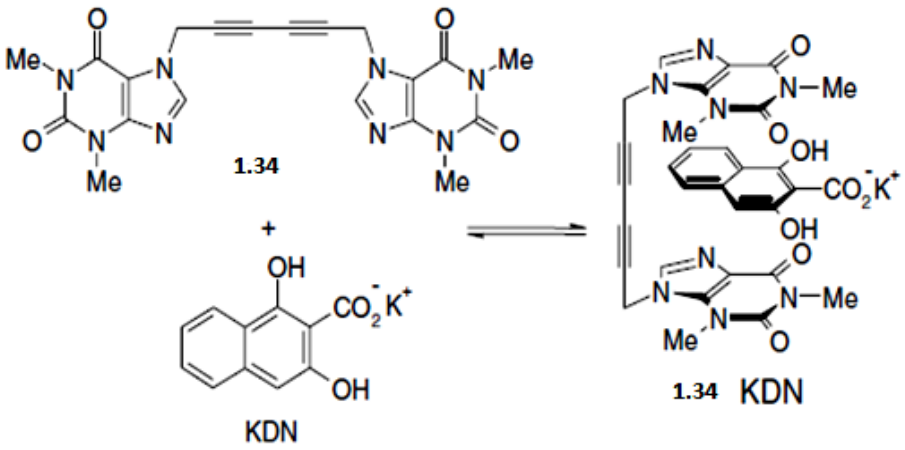

Scheme 1.2

1.9.3 *Spherands*

In addition to Pedersen and Lehn, the 1987 Nobel Prize for Chemistry was shared by a third supramolecular chemist, Donald Cram, for his development of a further type of macrocyclic cation host: the spherands[94]. While the crown ethers and even the cryptands are relatively flexible in solution, Cram realised that if a rigid host could be designed, which had donor sites that were forced to converge on a central binding pocket even before the addition of a metal cation, then strong binding and excellent selectivities between cations should be observed. Using space-filling molecular models (termed Corey–Pauling–Koltun or CPK models, in **Figure 1.2**, Cram and co-workers designed the rigid, three-dimensional spherands **1.35** and **1.36**, whose cation-binding oxygen atoms are preorganised in an octahedral array, ready to receive a metal ion.

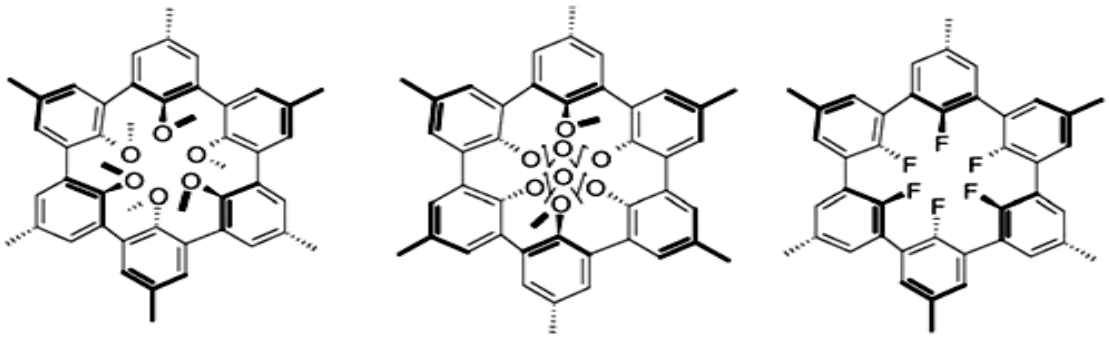

1.35 **1.36** **1.37**

In the case of compound **1.37**, three of the aryl rings are pointing upwards (out of the page) and three downwards. This results in the anisyl oxygen atoms being fixed in a nearly perfect octahedral array, while the *p*-methyl and anisyl methyl groups present a lipophilic surface to the solvent. This host selectively binds small cations such as Li^+ and, to a lesser extent, Na^+, in its cavity. Indeed, **1.35** is one of the strongest complexants known for Li^+. All other cations are excluded because they are simply too big to fit within the binding pocket. Spherand **1.36** has a binding pocket of similar size, formed from the tethering of the rings in pairs with diethylene glycol linkages, resulting in four rings being down and two up. The analogous fluoro compound **1.37**, along with an octameric analogue,

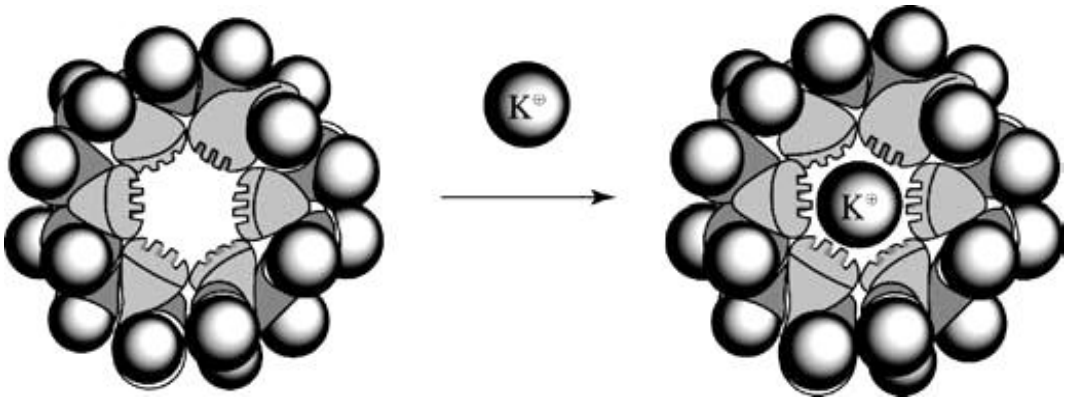

Figure 1.2: CPK models of crown ether and spherand complexes

1.9.4. *Podands*

At the same time that crown ethers were first being investigated in the 1960s some simple reactions were used to functionalize polyethers. The terminal hydroxyl groups were found to be amenable to tosylation and subsequent reaction with nucleophiles could introduce variations in ligand donor groups. Vögtle [95] and co-workers, notably Weber [96], used this route to incorporate a number of benzoic acid and quinoline groups. The new polyether derivatives were classed as podands in recognition of their two ligating 'feet'. Numerous variations, as illustrated in **1.38-1.41,** have since been prepared with the aim of broadening the range of metals that could be bound.

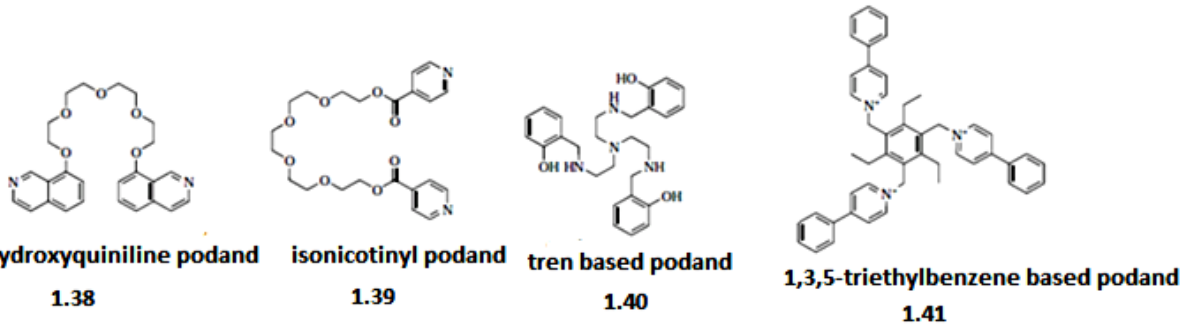

6-hydroxyquiniline podand 1.38 | isonicotinyl podand 1.39 | tren based podand 1.40 | 1,3,5-triethylbenzene based podand 1.41

The earliest compounds could coordinate to oxophilic metals, those classed as hard acids to use Pearson's terminology, while further development opened up the possibility of ligation to metals with borderline and soft characteristics through donors such as pyridine and sulfur. One interesting multifunctional podand was reported by the Hosseini group in 2001 which demonstrated that even compounds with simple structures can generate surprising supramolecular architectures[97-100]. Hexaethylene glycol was terminated in isonicotinic groups and reacted with silver salts to form a linear polymer in which each silver cation was held in a polyether loop around its equatorial plane and coordinated axially to the nitrogen atoms from the isonicotinyl termini of two adjacent ligands. An elegant interpenetrating linear structure resulted in which one linear network interpenetrated another running in the opposite direction, the same motif that runs through self-complementary double strand DNA and RNA. Despite some interesting results podands with two feet remain limited in their utility, particularly those created from polyethers, as most examples merely wrap up metals by coordinating to all available binding sites. Multifunctional podands can also be prepared from nonlinear parent compounds.

1.9.5 *Calixaranes*

Calixarenes are macrocycles or cyclic oligomers based on a hydroxyalkylation product of a phenol and an aldehyde[101]. The term generally describes cyclic arrays of *n* phenol moieties linked by methylene groups even though the larger systems do not form calyx (vase) shaped structures. Calixarene nomenclature is straightforward and involves counting the number

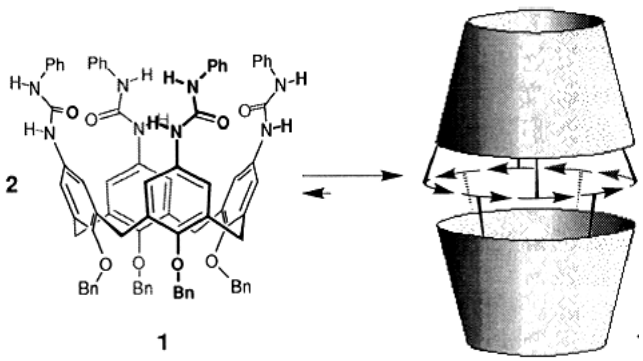

Figure 1.3: Dimerization of urea-substituted calix[4]arene

of repeating units in the ring and includes it in the name (e.g., calix[4]arene). Calixarenes are usually depicted with their phenolic groups down (lower rim) and their para-substituents pointing upward (upper rim). Calixarenes with free hydroxyl groups are conformationally flexible and the molecule can adopt different extreme conformations. For example, from the low-temperature ^{1}H NMR spectrum of calix[4]arene in solution, it consists of a mixture four conformations cone, partial cone, 1,3-alternate and 1,2-alternate. Both the upper and lower rims of calixarenes can be functionalized and the properties of these vase-like hosts can be altered[102-104]. In addition to the modification on the lower rim of calixarene to bind cations, calixarenes with four urea substituents on their upper rims can dimerize into a molecular capsule via hydrogen bonding in **Figure 1.3**.

The cavity inside the capsule can reversibly encapsulate smaller molecules such as chloroform, benzene, and toluene, as shown in **Figure 1.4**[105-110].

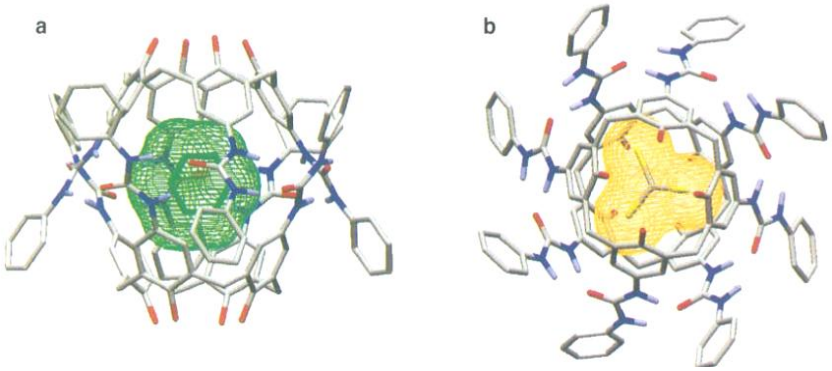

Figure 1.4: Calixaranes of (a) side view of dimer containing an encapsulated benzene guest and (b) top view of dimer containing chloroform

We must have seen that some of the above mentioned hosts are chemically Schiff bases. At the sites of metal binding and carriage, the azomethanine group plays important role.

Keeping in view the importance, relevance, variance and convenience biphenyl bridged Schiff bases offer, I have considered it appropriate to synthesise new classes of Schiff bases in order to exhibit them as potential supramolecular entities.

With the scope, available as suggested above, I have set the following objectives for my investigations.

1.10 Objectives of the Present Work

i. To thoroughly exploit the abilities of selected biphenyl bridged salicylidinimines as binucleating and polynucleating ligand systems.

ii. To synthesise and characterize a variety of biphenyl bridged naphthalidimines as binucleating and polynucleating ligand systems.

iii. To synthesise biphenyl bridged 2,6-diformylidininophenols as binucleating and polynucleating ligand systems.

iv. To characterise the ligands, mentioned through in (i) through (iii) and their bi- and poly-nuclear divalent metal complexes by various advanced physicochemical, spectral, thermochemical, etc., methods.

v. To explore the possibilities of extending the chemistry of the selected Schiff bases, mentioned at objectives (i) through (iii) and their binuclear and polynuclear complexes as supramolecular hosts.

vi. To study the stability against and the kinetics of hydrolysis of the selected Schiff bases and their complexes.

vii. To correlate the properties of the compounds to those obtained by molecular modeling.

viii. To study the pharmacological activity of the selected Schiff bases and their complexes as fungicides and bactericides.

ix. To apply the selected Schiff bases as complexmetric analytical reagents for the analysis of some bivalent metal ions.

x. To strive to undertake the above cited investigations under 'Green Chemistry' regimes.

The biphenyl bridged Schiff bases and their complexes prepared, and investigated in my researches are shown in **1.42-1.46** hereunder.

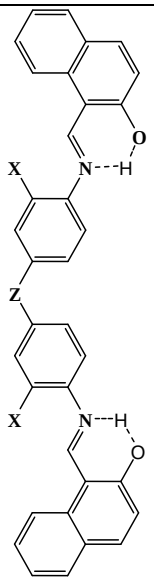

1.42 H_2L^i

Z	X	row combination labelled as H_2L^i
-O-	-	NDADPE or H_2L^1
$-CH_2-$	-	NDADPM or H_2L^2
	$-OCH_3$	NDADPD or H_2L^3
-	$-CH_3$	NDADPT or H_2L^4
-	-H	NDADPB or H_2L^5

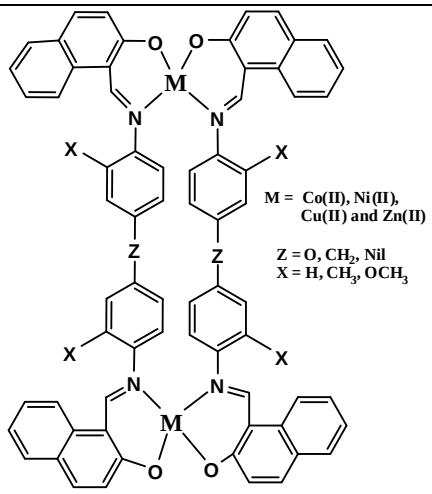

1.43 $M_2L_2^i$

Z	X	i	row combination $M_2L_2^i$
O	H	1	$M_2L_2^1$
CH_2	H	2	$M_2L_2^2$
-	OCH_3	3	$M_2L_2^3$
-	CH_3	4	$M_2L_2^4$
-	H	5	$M_2L_2^5$

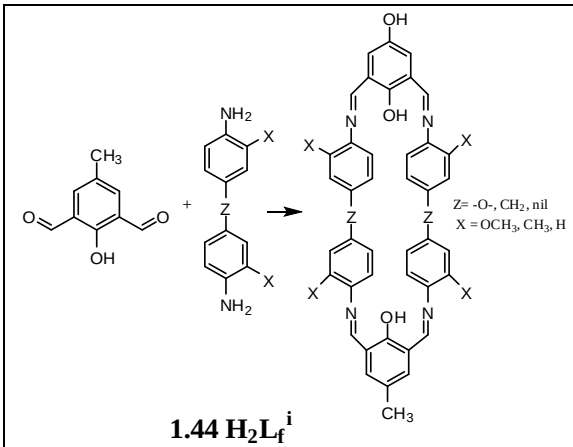

1.44 $H_2L_f^i$

Z	X	$H_2L_f^i$
-O-	H	DFMDPE or $H_2L_f^1$
$-CH_2-$	H	DFMDPM or $H_2L_f^2$
nil	OCH_3	DFMDPD or $H_2L_f^3$
nil	CH_3	DFMDPT or $H_2L_f^4$
nil	H	DFMDPB or $H_2L_f^5$

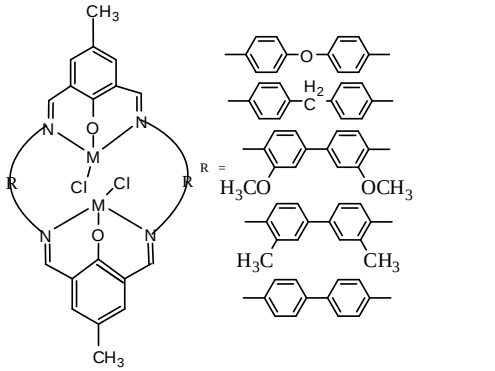

1.45 $M_2L_f^i$

L	i	$M_2L_f^i$
DFMDE	1	$M_2L_f^1$
DFMDM	2	$M_2L_f^2$
DFMDD	3	$M_2L_f^3$
DFMDT	4	$M_2L_f^4$
DFMDB	5	$M_2L_f^5$

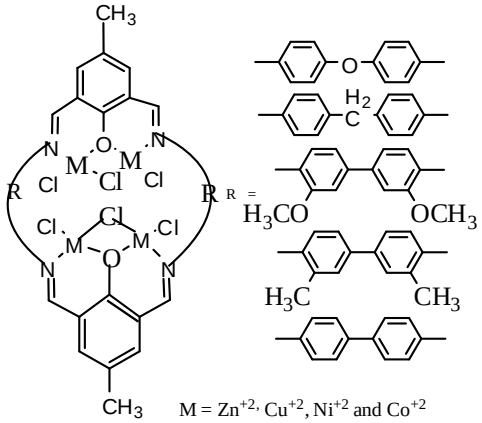

1.46 $M_4L_f^i$

$H_2L_f^i$	$M_4L_f^i$
DFMDPE or $H_2L_f^1$	$M_4L_f^1$
DFMDPM or $H_2L_f^2$	$M_4L_f^2$
DFMDPD or $H_2L_f^3$	$M_4L_f^3$
DFMDPT or $H_2L_f^4$	$M_4L_f^4$
DFMDPB or $H_2L_f^5$	$M_4L_f^5$

The manner in which these Schiff bases and their bivalent bi and polynuclear complexes can serve as supramolecular hosts is shown schematically in **Schemes 1.3-1.5** here:

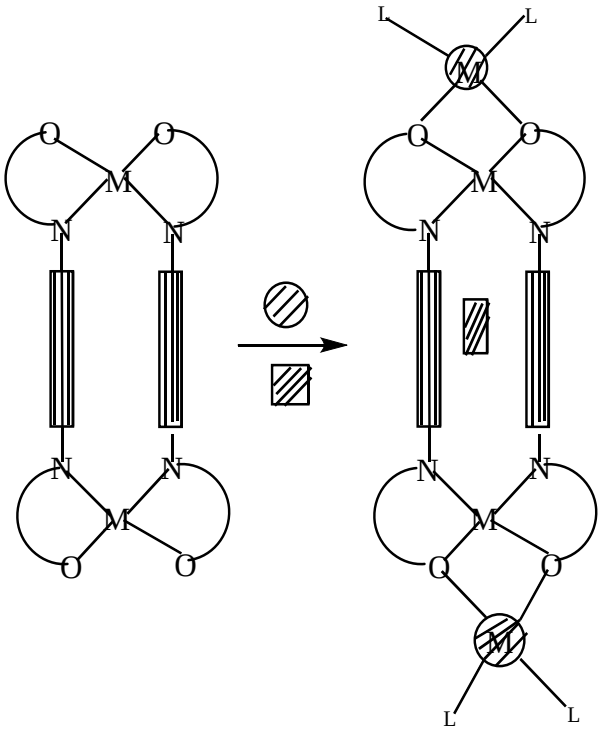

Scheme 1.3

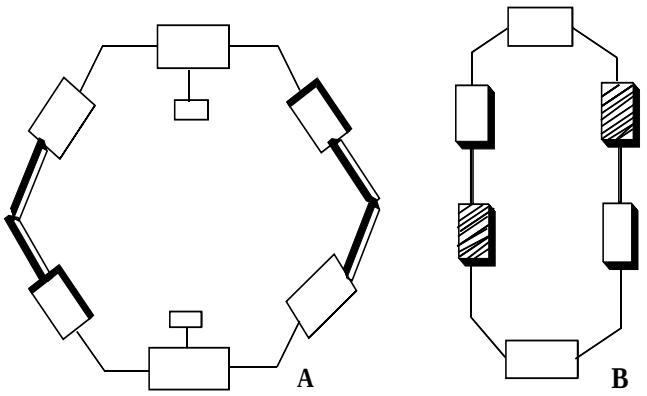

Scheme 1.4

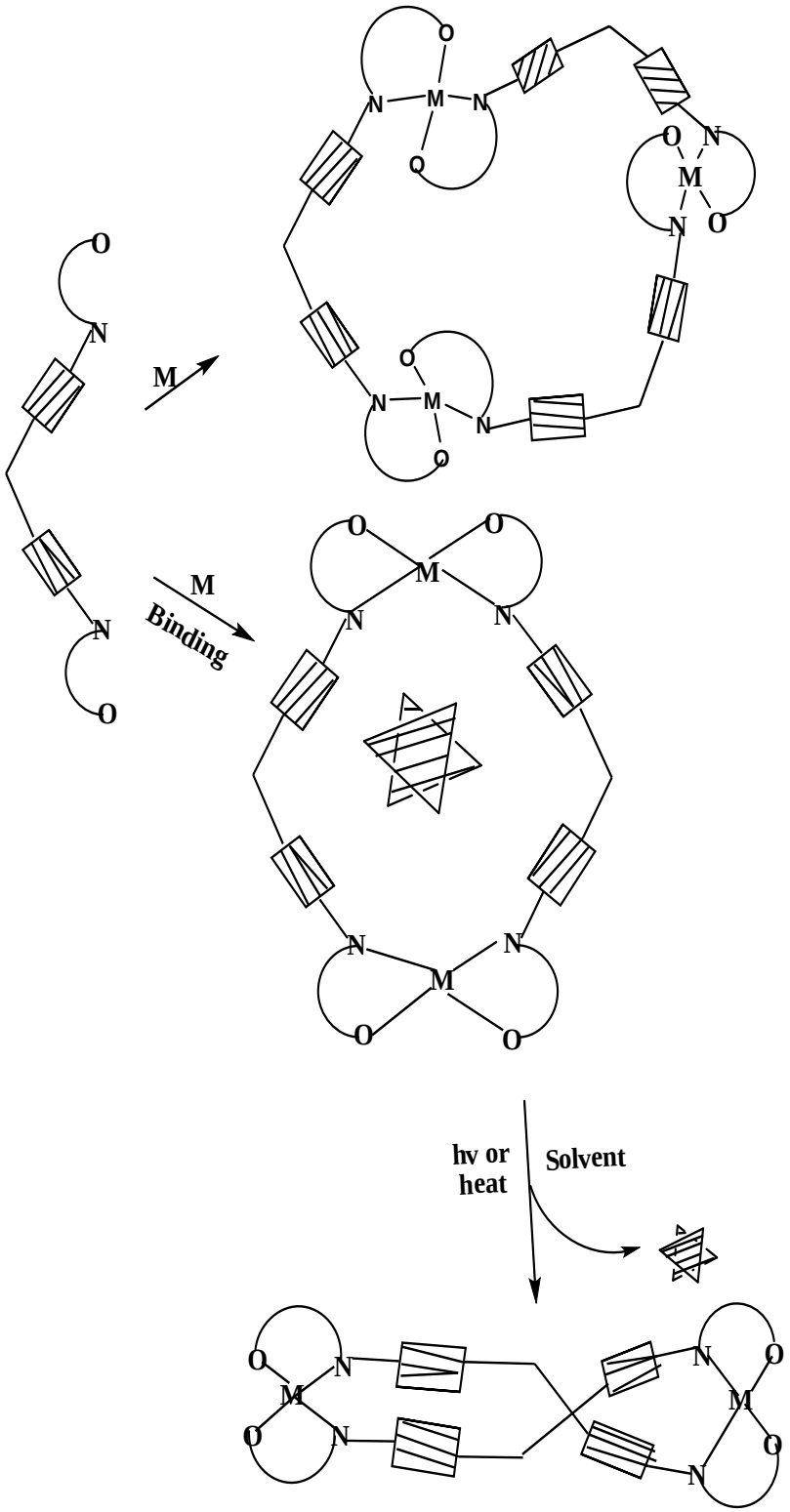

Scheme 1.5

The studies made on these systems are embodied in this thesis entitled, **"Synthesis and Characterization of Some New Series of Biphenyl Bridged Polynucleating Ligands and Their Bivalent Metal Complexes as Possible Supramolecular Hosts".** It presents the

physicochemical, analytical, electronic spectral, fluorescence, electrochemical, molecular modeling, single crystal X-ray diffraction, ESR spectral, *etc*., of the ligands besides similar and cryomagnetic, thermal and bioassying studies of the complexes.

The thesis is divided into 6 chapters including this 'Introduction' **Chapter I**.

In **Chapter II**, the details of synthesis of new compounds, preparation reported compounds, reagents, buffers, etc are given.

The experimental conditions set for investigations, advanced instrumental techniques employed, brief introductions to supramolecular mechanics, X-Ray diffractometry of helical molecular stacking, cryomagnetic methods (low temp ESR and susceptibility), fast scan voltammetry, molecular modeling, conformational analysis by Surfer and Grapher, antibacterial assaying, *etc.*, are provided for the benefit of general readership of this thesis. The names and brands of major instruments used during our investigations are mentioned.

In **Chapter III**, spectral and electrochemical characterization, X-Ray crystallographic structure determination and molecular modeling studies of some biphenyl bridged napthylidinimine Schiff bases are presented and discussed.

Chapter IV, contains the results and discussion of the investigations on binuclear Co(II), Ni(II), Cu(II), and Zn(II) complexes of biphenyl bridged napthylidinimine Schiff base ligands.

In **Chapter V**, spectral and electrochemical characterization of bis-biphenyl bridged 2,6-diformylidinimine tetraazomethine cyclic hosts and their binuclear and tetranuclear metal complexes are presented and discussed

In the last chapter, i.e., **Chapter VI,** the kinetics of hydrolysis and biological activity of a few binucleating and tetranucleating ligands and their complexes are briefly described.

Wherever and whenever woks of other scientists and investigations were taken for support of synthesis, interpretation and lead, due acknowledgements have been made by citing their works in the list of literature at the end of each chapter.

References

1. J M Lehn, *Acc Chem Rev*, 11, **1978**, 49
2. J M Lehn, *Angew Chem*, 100, **1988**, 91
3. P A Gale, *Phil. Trans. R Soc Lond*, 358, **2000,** 431
4. J W Steed, J L Atwood, *In Supramolecular Chemistry*, John Wiley & Sons, Ltd, **1999**
5. J K Klosterman, Y Yamauchi, M Fujita, *Chem Soc Rev*, 38, **2009**, 1714.
6. (a) C J Pedersen , *J Am Chem Soc*, 89, **1967**, 2495 (b) C J Pedersen, *J Am Chem Soc*, 89, **1967**, 7017
7. K Gloe, Macrocyclic Chemistry, *Current Trends and Future Perspectives Springer*, **2005**
8. M J MacLachlan, A Rose, T M Swager, *J Am Chem Soc*, 123, **2001**, 9180
9. P R Ashton, A S Reder, N Spencer, J F Stoddart, *J Am Chem Soc*, 115, **1993**, 5286
10. T W, Bell, H Jousselin, *Nature*, 367, **1994**, 441
11. K D Shimizu, J Rebek, *Proc Natl Acad Sci. USA*, 92, **1995**, 12403
12. K Ghosh, H B Yang, B H Northrop, M M Lyndon, Y R Zheng, D C Muddiman, P J Stang, *J Am Chem Soc*, 130, **2008**, 5320
13. J M Lehn, A Rigault, J Siegel, J Harrowfield, B Chevrier, D Moras, *Proc Natl Acad Sci, USA, 84*, **1987**, 2565
14. A D Cutland-Van Noord, J W Kampf, V L Pecoraro, *Angew Chem*, Int Ed, 41, **2002**, 4667
15. J A Johnson, J W Kampf, V L Pecoraro, *Angew Chem*, Int Ed, 42, **2003**, 546
16. J M Lehn, *Supramolecular Chemistry, Concepts and Perspectives*, VCH: Weinheim, **1995**
17. J P Collin, C Dietrich-Buchecker, P Gavina, M C Jimenez-Molero, J P Sauvage, *Acc Chem Res*, 34, **2001**, 477
18. C Dietrich-Buchecker, G Rapenne, J P Sauvage, *Coord Chem Rev*, 186, **1999**, 167.
19. M. Albrecht, *Chem Rev*, 101, **2001**, 3457
20. M T Youinou, N Rahmouni, J Fischer, J A Osbon, *Angew Chem*, 104, **1992**, 771
21. D W Johnson, J D Xu, R W Saalfrank, K N Raymond, *Angew Chem*, Int Ed Engl, 38, **1999**, 2882
22. S. James, *J Chem Soc Rev*, 32, **2003**, 276
23. C Piguet, G Bernardinelli, G Hopfgartner, *Chem Rev*, 97, **1997**, 2005
24. J Hamacek, M Borkovec, C Piguet, *Dalton Trans*, **2006**, 1473

25. J M Lehn, A Rigault, J Siegel, J Harrowfield, B Chevrier, D Moras, *Proc Natl Acad Sci*, USA, 84, **1987**, 2565
26. M Albrecht, *Chem Rev*, 101, **2001**, 3457
27. D Guo, K L Pang, C Y Duan, C He, Q J Meng, *Inorg Chem*, 41, **2002**, 5978
28. D Guo, C He, C Y Duan, C O Qian, Q J Meng, *New J Chem*, 26, **2002**, 796
29. L Xu, X T Chen, Y Xu, D R Zhu, X Z You, L H Weng, *J Mol Struct*, 559, 2001, 361
30. L J Childs, M Pascu, A J Clarke, N W Alcock, M J Hannon, *Chem Eur J*, 10, **2004**, 4291
31. M J Hannon, C L Painting, A Jackson, J Hamblin, W Errington, *Chem Commun*, **1997** 1807
32. N Yoshida, K Ichikawa, *Chem Commun*, **1997**, 1091
33. A T Vallina, H Stoeckli-Evans, *Acta Crystallogr C*, 57, **2001**, 489
34. Q Wang, X D Pi, C Y Su, *Acta Crystallogr C*, 61, **2005**, 73
35. F Tuna, M R Lees, G J Clarkson, M J Hannon, *Chem Eur J*, 10, **2004**, 5737
36. Z K Wu, Q Q Chen, S X Xiong, B Xin, Z W Zhao, L J Jiang, J S Ma, *Angew Chem*, Int Ed, 42, **2003,** 3271
37. J Keegan, P E Kruger, M Nieuwenhuyzen, N Martin, *Cryst Growth Des*, 2, **2002**, 329
38. N Yoshida, H Oshio, T Ito, *J Chem Soc*, Perkin Trans, 2, **1999**, 975.
39. P E Kruger, N Martin, M Nieuwenhuyzen, *J Chem Soc*, Dalton Trans, **2001** 1966
40. X C Su, Z F Zhou, S R Zhu, H K Lin, L H Weng, X B Leng, Y T Chen, *Chin J Chem*, 18, **2000**, 773
41. N Yoshida, K Ichikawa, M Shiro, *J Chem Soc*, Perkin Trans. 2, **2000**, 17
42. M Taneda, K Amimoto, H Koyama, T Kawato, *Org Biomol Chem*, 2, **2004**, 499
43. H Birkedal, P Pattison, *Acta Crystallogr C*, 62, **2006**, 139
44. A Lavalette, F Tuna, G Clarkson, N W Alcock, M J Hannon, *Chem Commun*, **2003** 2666
45. M J Hannon, C L Painting, N W Alcock, *Chem Commun*, **1999**, 2023
46. H Gudbjartson, K Biradha, K M Poirier, M J Zaworotko, *J Am Chem Soc*, 121, **1999** 2599
47. J Keegan, P E Kruger, M Nieuwenhuyzen, J O'Brien, N Martin, *Chem Commun*, **2001** 2192
48. L Stryer, *Biochemistry*, Fourth Edition Ed, W H Freeman and Company, New York, **1995**

49. R H Petrucci, *General Chemistry*, Principles and Modern Applications, Fifth Edition Ed, Macmillan Publishing Company: New York, **1989**
50. Y Journaux and O Kahn, J C S, *Dalton Trans*, **1979**, 1575
51. H Doine, F F Stephens and R D Cannon, *Inorg Chim Acta*, 75, **1983**, 155
52. a) J P Beale, J A Cunningham and D J Phillips, *Inorg Chim Acta*, 83, **1979**, 113
    b) W Kanda, M Nakamura, H Okawa and S Kida, *Bull Chem Soc*, Jpn, 55, **1982**, 471
    c) J Journaux, O Kahn, J Zarembowitch, J Galy and J Jaud, *J Am Chem Soc* 105, 1983, 7585
53. L Banci, A Bencini, D Gatteschi, A Dei, *Inorg Chim Acta*, 36, **1979**, 419
    S L Lambert, C L Spiro, R R Gangne, D N Hendrickson, *Inorg Chem*, 21, **1982**, 68
    S K Mandal, K Nag, *J C S*, Dalton Trans, **1983**, 2429
    D E Fenton, S E Gayda, *J C S*, Chem Commun, **1974**, 96
54. a) M G B Drew J Nelson, F Esho, V Mc Kee, S M Nelson, *J C S*, Dalton Trans, **1982**,1837
    b) J De O Cabral, M F Cabral, M Mc Cann, S M Nelson, *Inorg Chim Acta*, 15, **1984**, 86
55. H. Schiff, *Annalen,* 131, **1864**, 118, (55) 2nd time N E Borisova, M D Reshetova, Y A Ustynyuk, *Chem Rev*, 46, **2007**, 107
56. N H Pilkington, R Robson, *Aust J Chem*, 23, **1970**, 2225
57. M Bell, A J Edwards, B F Hoskins, E H Kachab, R Robson, *J Am Chem Soc,* 111, **1989**, 3603
58. A J Gallant, M J MacLachlan, *Angew Chem,* Int ed, 42, **2003**, 5307
59. A J Gallant, M Yun, M Sauer, C S Yeung, M J MacLachlan, *Org Lett*, 7, **2005**, 4827
60. M Bell, A J Edwards, B F Hoskins, E H Kachab, R Robson, *J Am Chem Soc,* 111, **1989**, 3603
61. A Ramachandraiah, P S Zacharias, *Inorg Nucl Chem Letters*, 16, **1980**, 433-435,
62. A Ramachandraiah, T Sarojini, K Laxma Reddy, P S Zacharias, *Polyhedron*, 9, **1990**, 2659-2664
63. B Srinivas, N Arulsamy, P S Zacharias, *Polyhedron*, 10, **1991**, 731-736
64. B Srinivas, N Arulsamy, P S Zacharias, *Polyhedron*, 11, **1992**, 211-215
65. A Ramachandraiah, Chepuri R K Rao, H Aneetha, B Srinivas, P S Zacharias, *Polyhedron*, 13, **1994**, 2659-2664
66. Chepuri R K Rao, P S Zacharias, *Polyhedron*, 16, **1997**, 1201-1209
67. H Aneetha, J Padmaja, P S Zacharias, *Polyhedron*, 15, **1996**, 2445-2451
68. C A Sureshan, P K Bhattacharya, *Journal of Molecular Catalysis A*, 30, **1998**, 73-78

69. Noboru Yoshida, Hiroki Oshio, Tasuku Ito, *J Chem Soc*, Perkin Trans. 2, **1999**, 975–983
70. N Yoshida, K Ichikawa, *Chem Commun*, **1997**, 1091
71. Noboru Yoshida, Kazuhiko Ichikawa, Motoo Shiro, *J Chem Soc*, Perkin Trans, 2, **2000**, 17–26
72. Paul E Kruger, Noreen Martin, Mark Nieuwenhuyzen, *J Chem Soc*, Dalton Trans., **2001**, 1966–1970
73. Masoud Salavati-Niasari, Ahmad Amiri, *J Mol Catal A, Chem*, 235, **2005,** 114–121
74. Z Chu, W Huang, *J Mol Struct*, 837, **2007**, 15–22
75. Masoud Salavati-Niasari, Ahmad Amiri, *Transition Met Chem*, 31, **2006**, 157–162
76. Masoud Salavati-Niasari, Mehdi Bazarganipour, *J Mol Catal A Chem*, 278, **2007**, 173–180
77. S A AbouEl-Enein, *J Therm Anal Cal*, 91, **2008**, 929–936
78. I I Oleini*a*, I V Oleinik, S S Ivanchev, G A Tolstikov, *Russ J Gen Chem*, 45, **2009**, 528-535
79. Yu E Alexeev, B I Kharisov, T C Hernandez Garciab, A D Garnovskiia, *Coord Chem Rev*, 254, **2010,** 794-831
80. Shan-bin Liu, Cai-feng Bi, Yu-hua Fan, Yu Zhao, Peng-fei Zhang, Qing-dan Luo, Dong-mei Zhang, *Inorg Chem Commun*, 14, **2011**, 1297–1301
81. K Anuradha, R Rajavel , *International Journal Of Pharmacy & Technology*, 3, **2011**, 2217-2227
82. Kamalpreet Kaur, K Vimal, Bhardwaj, Navneet Kaur, Narinder Singh , *Inorg Chem Commun*, 18, **2012**, 79-82
83. P A Vigato, V Peruzzo, S Tamburini, *Coord Chem Rev*, 256, **2012**, 953-1114
84. P Muralidhar Reddy, AVSS Prasad, Ch Kista Reddy, V Ravinder, *Transition Met Chem*, 33, **2008**, 251
85. P Muralidhar Reddy, K R Shanker Rohini M Sarangapani V Ravinder , *Spectrochim Acta A* , 70, **2008**, 1231
86. P Muralidhar Reddy., AVSS Prasad, K Shanker, V Ravinder, *Spectrochim Acta*, *A*, 68, **2007**, 1000
87. T Sarojini, *Studies of some new classes of polynuclear coordination compounds*, PhD thesis, Regional Engg College Warangal, **1993**
88. J G Collee, J P Duguid, A G Farser, B D Marmion (Eds*), Practical MedicalMicrobiology*, Churchill Livingstone, New York, **1989**
89. Z H Chohan, A Scozzafava, C T Supran, *J Enzyme Inhib Med Chem*, 17, **2003**, 261

90. HL Frisch, E Wasserman,. *J Am Chem Soc*, Chemical topology, 83, **1961**, 3789–3795
91. A Lüttringhaus, et al, Cyclisationen von Langkettigen Dithiolen, Versuche zur Darstellung sich umfassender Ringe mit Hilfe von Einschlußverbindungen, *Ann*, 613, **1958**, 185–198
92. M Descamps, J F Willart, E Dudognon, V Caron, Transformation of pharmaceutical compounds upon milling and comilling, The role of T-g, *Journal of Pharmaceutical Sciences*, 96, **2007**, 1398–1407
93. D Braga, S L Giaffreda, F Grepioni, et al, *Mechanochemical preparation of molecular and supramolecular organometallic materials and coordination networks*. Dalton Trans. **2006**, 1249–1263.
94. E Maverick D J Cram, 'Spherands, Hosts preorganised for binding cations', in *Comprehensive Supramolecular Chemistry*, J L Atwood, J E D Davies, D D MacNicol, F Vögtle (eds), Pergamon, Oxford, 1, **1996**, 213–243
95. B Tummler, et al, 'Open-chain polyethers – influence of aromatic donor end groups on thermodynamics and kinetics of alkali-metal ion complex-formation', *J Am Chem Soc* , 101, **1979,** 2588–2598
96. E Weber, F Vögtle, ,Crystal 1,1-alkali metal-complexes of non-cyclic neutral ligands', *Tetrahedron Lett*, 29, **1975**, 2415–2418,
97. Schmaltz et al, 'Double stranded interwound infinite silver coordination network', *Chem Commun*, **2001**, 1242–1243
98. LO Abouderbala, et al, 'Cooperative anion binding and electrochemical sensing by modular podands' *Proc Nat Acad Sci*, USA, 99, **2002**, 5001–5006
99. Liu S, et al, 'Synthesis and characterization of lanthanide $[Ln(L)]_2$ complexes of N_4O_3 amine phenol ligands with phenolate oxygen bridges evidence for very weak magnetic exchange between lanthanide ions' *J Am Chem Soc*, 114, **1992**, 6081–6087
100. M A Hossain, et al, 'Anion binding with a tripodal amine' *Inorg Chem*, 43, **2004**, 3751–3755
101. C D Gutsche, Calixarenes, Cambridge, *Royal Society of Chemistry*, **1989**
102. J Vicens, V Bohmer, Eds, Calixarenes, *Kluwer Academic Press*, Dordrecht, **1991**
103. A Arduini, A Pochini, S Reverbi, R Ungaro, *J Chem Soc Chem Commun*, **1984,** 981
104. A Arduini, A Pochini, S Reverbi, R Ungaro, G D Andreetti, F Ugozzoli, *Tetrahedron*, 7, **1986**, 2089
105. M A McKervey, E M Seward, G Ferguson, B Ruhl, S J Harris, *J Chem Soc, Chem. Commun*, **1985**, 388
106. S K Chang, I *J* Cho, *Chem Soc*, Perkin Trans, 1, **1986**, 211

107. Yamamoto, S Shinkai, *Chem Lett*, **1994**, 1115

108. E Ghidini, F Ugozzoli, R Ungaro, S Harkerma, A Abu EI-Fadl, D N Reinhoudt, *J Am Chem Soc*, 112, **1990**, 6979

109. T McKittrick, D Diamond, D J Marrs, P O'Hagan, M A McKervey, *Talanta*, 43, **1996**, 1145

110. J F Malone, D J Marrs, M A Mckervey, P O'Hagan, N Thompson, A Walker, F Arnaud-Neu, O Mauprivez, M J Schwing-Weill, J F Dozol, H Rouquette, N *J* Simon, *Chem Soc Chem Commun*, **1995**, 2151

CHAPTER II

SYNTHESIS OF MATERIALS AND EXPERIMENTAL METHODS

It is highlighted in **CHAPTER I** that our objectives were to generate new classes of biphenyl bridged polynucleating ligands and their ensuing coordination compounds as possible supramolecular hosts and for possible model applications. I can confidently state that as many as 90 distinct and individual compounds ligands, complexes and intermediates etc, have been synthesized for the first time by me. These compounds fall into different classes on the basis of their structural features. The compounds were characterized by various physiochemical techniques employing modern analytical instruments. Hence, it is considered appropriate to compile all the experimental aspects into one account. This chapter, meant for this purpose, is divided into two parts.

Part A discusses the laboratory procedural details for the synthesis of various ligands, intermediates and complexes whereas **PART B** covers the instrumental techniques and procedures employed to obtain qualitative and quantitative information.

Advanced versions of some useful software and packages such as MERCURY-2.3, WIN-GX and DIAMOND-10.0 were used for single crystal refinement data. CHEMOFFICE-11.0, ORIGIN-8.0, MSEXCEL-2007, SURFUR-10.0, etc, were used for calculations, statistical treatment and graphical projections of the analytical data and molecular structures word processors like MSWORD-2007, etc were used to typeset the documents and for graphics embedding.

2A.1 Biphenyl Bridged Naphthalidinimine Schiff Bases and Their Complexes

THE LIGANDS, H_2L^i

The general structure of these compounds is provided in structure **2A.1.** By independent and coupled variation through Z and X, nearly five biphenyl bridged polynucleating ligands were synthesized. The synthetic procedure is same for all compounds and is given below.

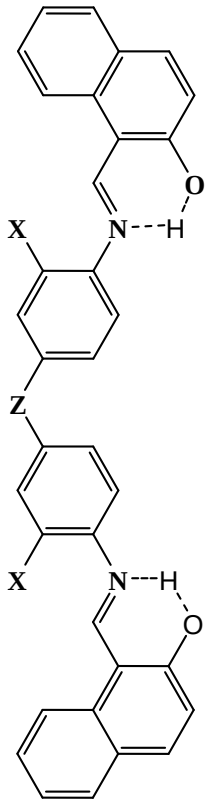

2A.1 (H_2L^i)

Z	X	row combination labelled as H_2L^i
-O-	-	NDADPE or H_2L^1
$-CH_2-$	-	NDADPM or H_2L^2
	$-OCH_3$	NDADPD or H_2L^3
-	$-CH_3$	NDADPT or H_2L^4
-	-H	NDADPB or H_2L^5

Biphenyl bridged bis-bidentate Schiff base ligands were prepared by mixing methanol solution of any biphenyl bridged primary diamine, like (4-aminophenoxy)benzenamine, (4-aminobenzyl)phenylamine, o-diansidine, o-tolidine and benzidine, with that of 2-hydroxy-1-naphthalidimine. The ligands precipitated were filtered through suction and washed repeatedly with hot methanol followed by acetone and dried in vacuo at 90^0C over night.

The procedure for the preparation of a Schiff base ligand, NDADPE (i.e. H_2L^1) is given here. 2.002 gm (10 m moles) of 4,4'-diaminodiphenylether and 3.443 gm (20 m moles) of 2-hydroxy-1-naphthyaldhyde were dissolved in methanol separately in 100 ml beakers. When the two solutions were mixed with vigorous stirring while heating at ~50 ^{0}C, a bright yellow colored substance was obtained, which on standing over night, gave an yellow crystalline solid. The mass was recrystallized from methanol and dried in vacuo. The other ligands, i.e., NDADPM, NDADPD, NDADPT and NDADPB were prepared by employing the same procedure.

The physical and chemical characteristics along with that of these ligands are mentioned in **PART A** of **CHAPTER III**.

THE COMPLEXES, $M_2L_2^i$

The H_2L biphenyl bridged napthylidinimine ligand systems are potential bis-binucleating ligands. If the ligands are generalized as H_2L^i, the anticipated binuclear structure is given in structure **2A.2** for the complexes, $M_2L_2^i$. The synthetic procedure of generating the metal complexes, $M_2L_2^i$, is nearly the same for any M and $H_2L_f^i$ combination. Representative synthetic method for the preparation of a few complexes, are provided here.

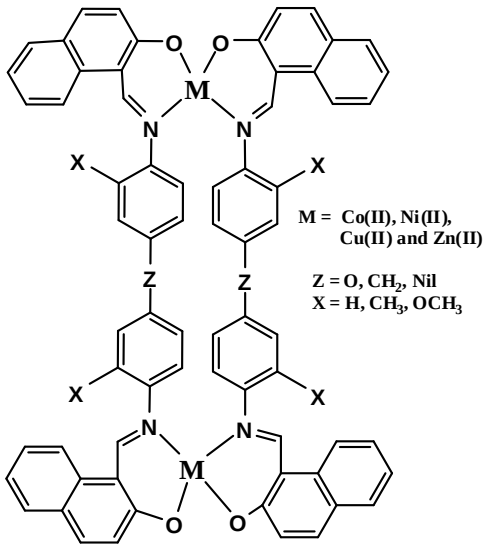

2A.2 ($M_2L_2^i$)

Z	**X**	**i**	**row combination $M_2L_2^i$**
O	H	1	$M_2L_2^1$
CH_2	H	2	$M_2L_2^2$
-	OCH_3	3	$M_2L_2^3$
-	CH_3	4	$M_2L_2^4$
-	H	5	$M_2L_2^5$

Cobalt(II) Complexes

A warm solution, containing 2 m moles (1.0138 gm) of cobalt acetate in methanol was added, while stirring, to a solution containing 1.017 gm (2 m moles) of 2,2'-(4,4'-oxybis(4,1-phenylene)bis(azan-1-yl-1-ylidene))bis(methan-1-yl-1-ylidene)dinaphthalen-1-ol (NDADPE) in chloroform. The mixture turned deep red and the contents were kept standing overnight to yield a bright crystalline red coloured binuclear cobalt(II) complex.

Nickel(II) Complexes

A like warm solution, containing 2 m moles (0.3996 gm) of nickel acetate in methanol was added, was added to a solution containing 1.013 gm (2 m moles) of 2,2'-(4,4'-methylenebis(4,1-phenylene)bis(azan-1-yl-1-ylidene))bis(methan-1-yl-1-lidene)dinaphthalen-1-ol (NDADPM) in chloroform while stirring. The mixture turned green and the contents were kept standing overnight to yield a bright crystalline green coloured binuclear nickel(II) complex.

Copper(II) Complexes

A warm solution, containing 2 m moles (0.439 gm) of copper acetate in methanol was added, while stirring, to a chloroform solution of 1.1057 gm (2 m moles) of 2,2'-(3,3'-dimethoxybiphenyl-4,4'-diyl)bis(azan-1-yl-1-ylidene)bis(methan-1-yl-1-ylidene)dinaphthalen-1-ol (NDADPD). The brownish black contents yielded a crystalline binuclear copper(II) complex, when kept standing overnight.

Zinc(II) Complexes

A moderately hot solution, of 2 m moles (0.439 gm) of zinc acetate in methanol was added, to a solution of 1.041 gm (2 m moles) of 2,2'-(3,3'-dimethylbiphenyl-4,4'-diyl)bis(azan-1-yl-1-ylidene)bis(methan-1-yl-1-ylidene)dinaphthalen-1-ol (NDADPT) in chloroform. The mixture turned brownish black and the contents gave a crystalline binuclear zinc(II) complex upon standing overnight.

2A.2 Biphenyl Bridged of Macrocyclic Schiff Base Ligands and Their Complexes

THE MACROCYCLIC LIGANDS, $H_2L_f^i$

Another series of polynucleating ligands with macrocyclic nature have been prepared. The general structure of these ligands is shown in **2A.3.** Condensation of a biphenyl bridged diamine with 2,6-diformyl-4-methyl phenol is expected to give such ligand series.

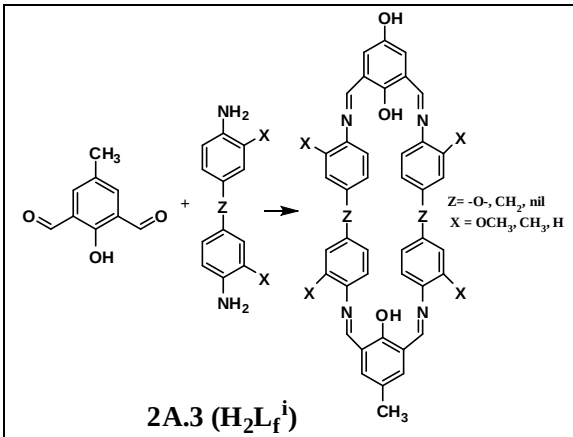

2A.3 ($H_2L_f^i$)

Z	**X**	**row combination $H_2L_f^i$**
-O-	H	DFMDPE or $H_2L_f^1$
$-CH_2-$	H	DFMDPM or $H_2L_f^2$
nil	OCH_3	DFMDPD or $H_2L_f^3$
nil	CH_3	DFMDPT or $H_2L_f^4$
nil	H	DFMDPB or $H_2L_f^5$

2,6-diformyl-4-methylphenol was prepared by the reported procedure[1]. An amount of 0.4004 gm (2 m moles) of 4,4'-diaminodiphenylether and 0.328 gm (2 m moles) of 2,6-diformyl-4-methylphenol were dissolved in methanol separately in 100 ml beakers. When the two solutions were mixed with vigorous stirring at ~50 ^{0}C, an orange red colored substance was obtained, which on standing over night gave an orange red crystalline solid. The mass was recrystallized from methanol and dried in vacuo. The other ligands, i.e., DFMDPM, DFMDPD, DFMDPT and DFMDPB were prepared by employing the same procedure.

The physical and chemical characteristics of these ligands, mentioned in structure **2A.3** are given in **PART A** of **CHAPTER V**.

THE COMPLEXES, $M_2L_f^i$ and $M_4L_f^i$

Coordination compounds of several metal ions were synthesised from the H_2L^i systems. The anticipated binuclear ***($M_2L_f^i$)*** and tetranuclear ***($M_4L_f^i$***) structures are given in structures **2A.3a** and **2A.3b,** respectively. The binuclear complexes were prepared by dissolving 1 m mole of the ligand in chloroform and 2 or 4 m moles of the metal salts in acetone with an aim

of obtaining complexes of $M_2L_f^i$. A representative synthetic method to obtain $Cu_2L_f^i$ is provided here.

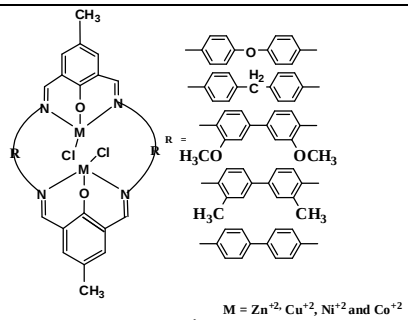

2A.3a ($M_2L_f^i$)

L	**i**	**$M_2L_f^i$**
DFMDE	1	$M_2L_f^1$
DFMDM	2	$M_2L_f^2$
DFMDD	3	$M_2L_f^3$
DFMDT	4	$M_2L_f^4$
DFMDB	5	$M_2L_f^5$

A mixture of DFMDE (0.01 m mol, 0.6567 gm) and copper chloride (0.02 m mol, 0.3409 gm) was refluxed for an hour in alcohol. Brown colour complex was obtained which was washed with methanol and air dried. (Yield: 82%).

The complexes of cobalt, nickel and zinc(II) ions have been generated, employing the same procedure used in the preparation of $Cu_2L_f^i$ complex described above.

The method to get $M_4L_f^i$ type complexes is given here for the case of come L_fi.

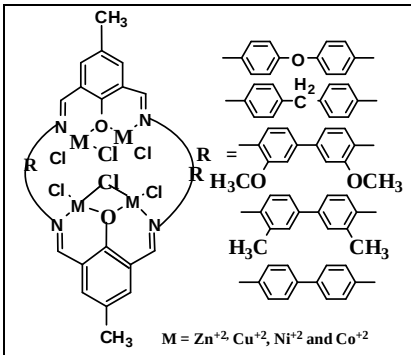

2A.3b ($M_4L_f^i$)

$H_2L_f^i$	**$M_4L_f^i$**
DFMDPE or $H_2L_f^1$	$M_4L_f^1$
DFMDPM or $H_2L_f^2$	$M_4L_f^2$
DFMDPD or $H_2L_f^3$	$M_4L_f^3$
DFMDPT or $H_2L_f^4$	$M_4L_f^4$
DFMDPB or $H_2L_f^5$	$M_4L_f^5$

A mixture of DFMDE (0.01 m mol, 0.6567 gm) and copper chloride (0.04 m mol, 0.6818 gm) was refluxed for an hour in alcohol. Brown colour complex was obtained which was washed with methanol and air dried. (Yield: 75%). The other complexes like those of cobalt, nickel and zinc have been generated by employing the same procedure used in the preparation of Cu_4L^i complex described above.

2A.3 The Buffers

Since the spectral and electrochemical studies of the all compounds have been carried out in aqueous buffers, a series of aqueous buffer solutions of constant ionic strength of 0.1M covering a wide pH range (0.5-12.0) was prepared. The stock solutions mentioned in **Table 2A.1** were first prepared and used in different combinations according to the reported procedure to get the solution of the desired pH[2-4].

Table 2A.1: *Stock solutions for preparing the buffers*

Index No.	Solute	Concentration
I	Hydrochloric Acid (HCl)	0.10 M
II	Potassium Chloride (KCl)	0.10 M
III	Sodium Chloride (NaCl)	0.10 M
IV	Sodium Citrate ($Na_3C_6H_5O_7$)	0.10 M
V	Sodium Acetate ($NaOOCCH_3$)	0.10 M
VI	Acetic Acid (CH_3COOH)	0.10 M
VII	Sodium Tetra Borate ($Na_2B_4O_7$)	0.05 M
VIII	Glycine (H_2NCH_2COOH)	0.10 M
IX	Sodium Hydroxide (NaOH)	0.10 M

The pH values expected Henderson's equation and measured by pH metry are collected in **Table 2A.2**.

Table 2A.2: *Preparation of buffer solutions with the stock solutions*

(a) ***pH Range 1.10 - 4.50***

S.No.	$Na_3C_6H_5O_7$	HCl	Capacity (ml)	pH Calculated	pH Measured
1	4.80	95.20	100	1.10	1.13
2	22.20	77.80	100	1.50	1.49
3	30.60	69.40	100	2.00	1.98
4	35.40	64.60	100	2.50	2.42
5	40.30	59.70	100	3.00	2.93
6	46.80	53.20	100	3.50	3.54
7	56.00	44.00	100	4.00	3.95
8	71.90	28.10	100	4.50	4.55

(b) ***pH Range 5.00 - 6.50***

S.No.	CH_3COONa	CH_3COOH	Capacity (ml)	pH Calculated	pH Measured
1	64.00	36.00	100	5.00	5.19
2	84.80	15.20	100	5.50	5.63
3	94.40	5.60	100	6.00	6.23
4	98.40	1.60	100	6.50	6.71

(c) ***Neutral pH Range***

The stock KCl solution was pH-metrically tuned by KOH / HCl

(d) ***pH Range 7.75 - 9.00***

S.No.	$Na_2B_4O_7$	HCl	Capacity (ml)	pH Calculated	pH Measured
1	52.90	47.10	100	7.75	7.84
2	55.85	44.15	100	8.00	8.14
3	65.25	34.75	100	8.50	8.61
4	85.60	14.40	100	9.00	9.21

(e) ***pH Range 9.50 - 11.00***

S.No.	$Na_2B_4O_7$	NaOH	Capacity (ml)	pH Calculated	pH Measured
1	79.00	21.00	100	9.50	9.61
2	59.00	41.00	100	10.00	10.13
3	52.80	7.20	100	10.50	10.64
4	50.10	49.90	100	11.00	11.03

(f) ***pH Range 11.50 - 12.90***

S.No.	Glycine	NaOH	Capacity (ml)	pH Calculated	pH Measured
1	49.00	51.00	100	11.50	11.62
2	45.55	54.45	100	12.00	12.19
3	34.60	65.40	100	12.50	12.64
4	10.00	90.00	100	12.90	13.19

PART-B: METHODS AND MEASUREMENTS

The methods of sampling for various instrumental investigations along with the types of instrumental techniques are boringly presented in this part. For the benefit of readers of the thesis who would take leads from our investigations and studies, a brief essaying is portrayed at the end of this chapter about the principles of some of the modern methods of investigation that we have utilized.

2B.1 Sampling Methods and Instrumental Operations

2B.1.1 *Melting point determination*

Conventional Zeldal method and Buchi model melting point apparatus were used to measure the melting points and were uncorrected. The melting points of all the Schiff base ligands and their metal complexes were also obtained on DSC Model: Q 10 TA Instruments.

2B.1.2 *Elemental analysis*

The C, H, N and S elemental analysis of the ligands and complexes were done on a Carlo terbo Model EA 1108 CHNS-O Elemental Analyser equipped with DP 200 Data Processor and a microgram sensitive Mettle Balance at Rowan University, USA. The metal analysis of copper, cobalt, nickel, and zinc present in the complexes were analysed adapting standard chemical and spectrophotometric procedures. The analyses of a few metal ions were found by ICP-OES at Rowan University, USA and the values were in good agreement with spectrophotometric analysis.

2B.1.3 *Mass spectra*

Electrospray ionisation Mass Spectra (ESI-MS) were determined on a Perkin Elmer Model (SCIEX API- 2000, ESI-MS) Spectrometer at 12.5 eV plate potential.

2B.1.4 *Infrared spectral studies*

The IR spectra were recorded in Nujoll/KBr pellets on a Shimadzu 8201 model FT-IR spectrophotometer at a 1 cm^{-1} resolution. Additionally, JASCO Model FTIR-5300 spectrophotometer and Perkin Elemer model spectrum 100 S were also used for a greater reproducibility.

2B.1.5 *NMR spectral studies*

The ligands and some of the soluble diamagnetic complexes were characterised by ^{1}H and ^{13}C NMR spectra, recorded on a Bruker DPX FT-NMR spectrometer, using TMS as an internal reference at room temperature operating at 400 MHz. Deuteriated solvents were used to prepare the solutions of ~10-12 mg/ml. During the ^{13}C NMR studies, Deuteriated solvent, itself, several as the locking isotope.

2B.1.6 *ESR spectral studies*

EPR spectra were measured using a Bruker EMX Micro Premium X Spectrometer at X-band (9.17, GHz) on the powder, solution and frozen glass in toluene/dichloromethane (90/10 v/v) at Rowan Univesity, USA.

2B.1.7 *Magnetic susceptibility studies*

The solid-state magnetic susceptibility of crystalline samples was measured between 4 and 300 K at a field of 1 kOe using a Super Conducting Quantum Design Model MPMS SQUID magnetometer at Rowan University, USA. Diamagnetic corrections were made using Pascal's constants.

2B.1.8 *Thermal studies*

Differential Scanning Calorimetric thermal analyses of the samples were performed on a Thermal Advantage DSC Q2000 V9.8 Build 296 (TA Instrument, USA) module which was calibrated for temperature and cell constants using indium and sapphire. Thermogravimetric (TGA) and Differential thermal analysis (DTA) were carried out using SDT Q600 V8.0 Build

95 TGA and DTA system on well ground samples in flowing nitrogen atmosphere with a heating rate of 5 °C/min. On the basis of the TGA/DTA studies. The instrument was equipped with refrigerator cooling system (RCS). The crystals (3-5 mg) were crimped in aluminum pans (non-hermetic, 30 μL) scanned at a heating rate of 10 °C/min in the range 30–300 ºC under a dry nitrogen atmosphere (flow rate 50 mL/min).

2B.2 UV-Visible Spectral Methods

The UV-Visible electronic spectra of all compounds were recorded on either a Shimadzu Model 160A ratio recording spectrometer or a Analyticzena specord 205 spectrophotometer in the wavelength range 1100-200 nm. The double-walled sample cuvette holder has a provision for circulating thermostatted water from a constant temperature bath. Thus pH-metric spectrophotometric titration for studying the protanation deprotonation equlibria and chemical kinetics were monitored by viewing the spectral variation. The overlay spectral feature was used for recording the spectra at different pH for a fixed concentration to see the effect of pH on the electronic spectra and hence, on the structure of the analyte chromophore.

2B.3 Electrochemical Methods

The work presented in this thesis is considerably electrochemical and spectroelctrochemical in nature. Hence, a number of electroanalytical methods were used during the studies of the compounds. Since electrochemical techniques usually need ultra pure materials and methods of reproducibility, the purification of the materials and setting up experiments were done with utmost care.

The pH of the buffers, stock solutions and reaction mixtures were measured by an Orion Model EA 940 Expandable Ion Meter equipped with 91-01 Ag|AgCl combined glass electrode. Preliminary electrochemical measurements were taken on a EG & G Prineiton Applied Research Corporation (PARC) Model 264 A3 Polarographic Analyzer/Stripping Voltammeter and on a Bio Analytical System Model CV-27 voltamograph equipped with an EG & G PARC Model 303 A SMDE. Metrohm 663 VA and CHI 619D Electrochemical Analyzers were used for final studies. We set the mercury electrode surface area as 0.26 mm^2 for our studies.

PRE-RUN PREPARATORY METHODS

Purification of Mercury

AR grade mercury was purchased from S.D Fine Chemicals Ltd. 1 Kg of mercury was filtered through chemoise leather. Then it was treated with saturated solution of mercuric chloride for separation of other metals from mercury. This operation was repeated thrice. The mercury, thus obtained, was again dried with pieces of Whitman filter paper several times. Finally, it was purified by double distillation under reduced pressure and was stored in dark polythene bottles.

Treatment of Platinum Wire and Auxiliary Electrode

Platinum wire which was used as auxiliary electrode in our studies was activated by heating in blue flame of Bunsen burner. Ignition was done after the electrode was dipped in ethyl alcohol and retrieved. During the electrochemical measurements the above procedure was carried out quite often.

Cleaning of Ag|AgCl Reference Electrode

The Ag|AgCl was used as reference electrode. It contains a saturated solution of AgCl and KCl filled in glass tube. The Ag|AgCl electrode was always kept in saturated KCl solution. Whenever it was needed, AgCl and KCl solution of reference electrode were changed.

Electrochemical Measurement

The electrochemical measurements were done in a thermostatted three-electrode system cell, comprising of the working (SMDE), electrode or solid Pt or graphite reference electrode [Ag|AgCl|Cl (sat) or SCE] and auxiliary electrode (Pt foil or wire). The three electrode assembly is shown in **Figure 2B.1**.

Stock solutions of 10^{-3} M concentration of the compounds were prepared in 50 ml standard flasks. 20 ml of the buffer was taken in the electrochemical cell and 2 ml of the pure solvent of the stock solution of compound was added to it. This mixture was the blank. The contents of the cell were purged with AR grade nitrogen gas for 8 minutes to remove the dissolved oxygen. Then under the bed of the same nitrogen gas the electrochemical measurements were carried out as per the set experimental conditions. Mixing of 2 ml the relevant solution instead of the solvent alone to 20 ml of the buffer gave the solution for which the baseline correction was done under similar experimental conditions.

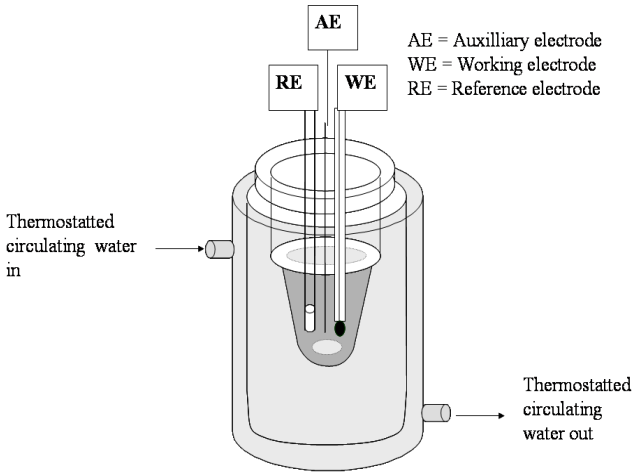

Figure 2B.1: Thermostatted three-electrode electrochemical cell

2B.4 X-Ray Crystallographic Studies

2B.4.1 *Growing crystals*

Whenever XRD measurement were undertaken, the respective recrystallised pure Schiff base compounds were first dissolved in dichloromethane (10 mg per 2 ml). To this solution were added a few drops of methanol and the test tubes were closed with aluminum foils with one or two perforations. The test tubes were then kept buried in a stout sheet of thermocoal to avoid sudden temperature fluctuations; the whole setup was secluded into a wooden chest for 10 days. The tubes were then removed after a couple of weeks to see single crystals of varied sizes. These crystals were sorted by looking through a compound microscope. The best crystal, suitable for the single crystal XRD studies, was carefully picked, washed with pure ether to remove solvent residues and then air dried before; it was taken for mounting on the single crystal XRD machine.

2B.4.2 *Crystallographic data collection*

After obtaining a suitable crystal for an X-ray experiment, the single crystal X-ray data was collected on Bruker-Nonius SMART APEX CCD diffractometer at 293(2) K using graphite-monochromated Cu Kα radiation (λ = 1.54184 Å). This instrument is designed to aim X-ray beams through a crystal and record where the beams diffract and to measure the intensity of the reflection. A schematic of the setup is shown in **Figure 2B.2**.

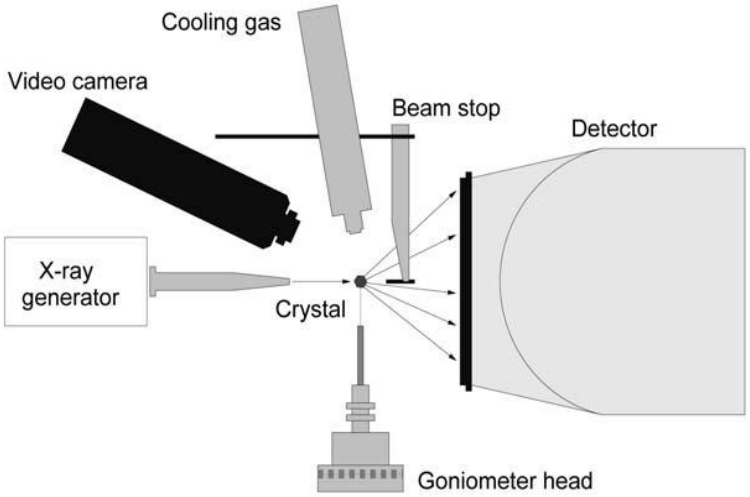

Figure 2B.2: Schematic of a single crystal X-ray diffractometer

2B.5 Magnetic Susceptibility Measurements

A Super Conducting Quantum Interference Device (SQUID) Magnetometer was used

Figure 2B.3: Photograph of the Superconducting Quantum Design Model, MPMS (SQUID) Magnetometer

for solid-state magnetic susceptibility at 300 K a field of 1 kOe using a Quantum Design Model, MPMS (SQUID) magnetometer as shown in **Figure 2B.3**. Each sample was placed in a gelatine capsule. The susceptibility of the capsule was measured separately and its contribution was subtracted from the overall susceptibility. A temperature-independent susceptibility parameter ($\chi 0$) was included in the fitting procedures. Material of known mass was mounted on to the sample probe and inserted into the Vibrating Sample Magnetometer (VSM) for Cryomagnetic measurements between 4-300 K at a 1 Tesla field strength.

2B.6 Molecular Modeling

ChemOffice 2010 was used for molecular modeling of the compounds. Thermodynamic parameters such as heat of formation, dipole movement, and HOMO-LUMO energies were obtained using this molecular modeling software. HOMO-LUMO energy values were used to verify the observed λ_{max} values for different species. The energy minimized structures were put to single axis and double dihedral conformational analysis.

2B.6 Antimicrobial Studies

The antimicrobial activity of the compounds was determined by paper disc method and the minimum inhibitory concentration by liquid dilution method at Defense Food Research Laboratory, Mysore. Details are given in **Chapter VI**.

2B.7 Functional Priniciples of Some Important Techniques

A brief sketch of some of the modern methods of characterisation of ligands and complexes that I have investigated is presented here. Though excellent books, review articles and resource material are available on these methods, a brief introduction may be a ready-reckoner. Only those methods, which gave deeper insight into the thermodynamic, electronic, structural, redox, magnetic and spectral character of the compounds are covered hereunder.

2B.7.1 ***Cyclic voltammetry***

Cyclicvoltammetry is a modern electrochemical technique[5-7], in this technique, a potential programme such as the one shown in **Figure 2B.4** applied between stationary working electrode and a reference electrode while the resulting current is measured as an outcome of the possible electron transfer process between the solution-working electrode interface and an auxiliary electrode (counter electrode).

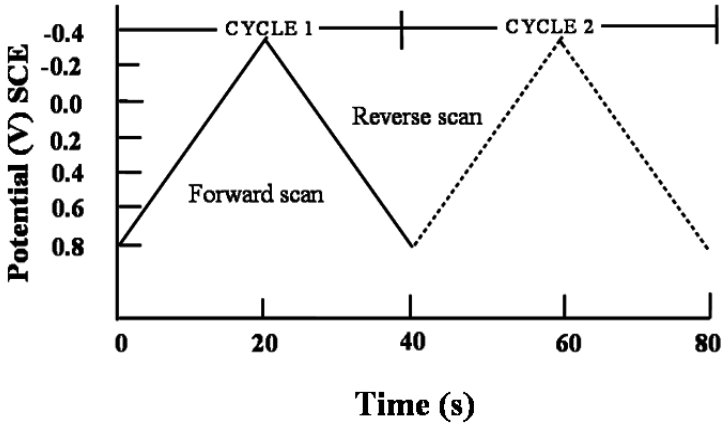

Figure 2B.4: Typical triangular potential ramps for cyclic voltammetry technique (e.g., between +0.8 and -0.4V vs SCE)

The cathodic or forward potential sweep gives a reduction wave, whereas or backward potential sweep gives an oxidation wave. This complete reduction-oxidation current potential curve is called a cyclic voltammogram.

A series of papers by Shain and coworkers present a detailed theory of cyclic voltammetry[8-10]. The utility of the techniques was worked out by Randels[11] for reversible processes and Delahey for irreversible processes[12].

The current potential wave provides four measurements, the net current at the peak of the cathodic response, the potential at peak of the cathodic response, the net current at the peak of anodic response and the potential at the peak of the anodic response. In **Figure 2B.5** is shown a typical cyclic voltammogram for reversible charge transfer.

For a general electrode process,

$$i_p = 2.99x10^5 n(\alpha n_a)^{1/2} AD^{1/2} v^{1/2} C \qquad 2.1$$

where

i_p = peak current in μA

n = number of electrons

A = area of the working electrode in cm^{-1}

D = diffusion coefficient in cm^2

C = concentration in mol lit^{-1}

ν = scan rate in volts

α = transfer coefficient (usually 0.5)

n_a = number of electrons involved in the rate determining step.

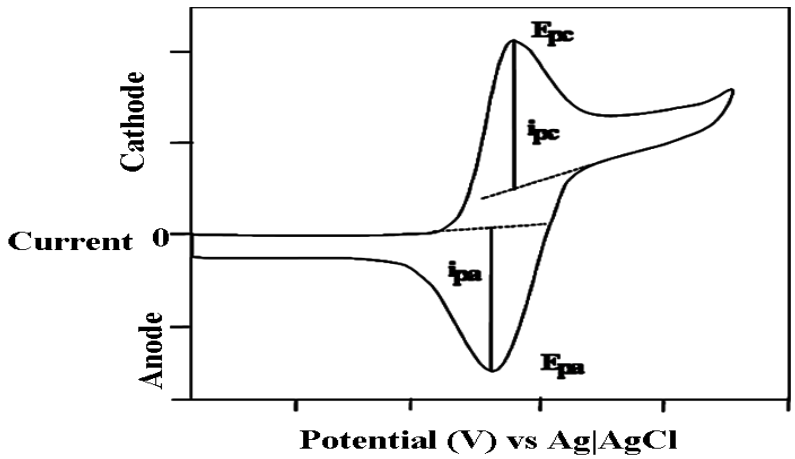

Figure 2B.5: Typical riverssible cyclic voltammogram

The value of α_{na} is given through

$$E_{p\,1/2} - E_p = \frac{0.048}{\alpha n_a} \qquad 2.2$$

where E_p and $E_{p1/2}$ are the peak and half peak potentials, respectively.

For a reversible system,

$$\left|E_{pa} - E_{pc}\right| = \frac{0.059}{n} \qquad 2.3$$

$$\frac{i_{pc}}{i_{pa}} = 1 \qquad 2.4$$

The peak current in reversible process is given by the Randel-Sevcik equation

$$i_p = kn^{3/2} AD^{1/2} C\upsilon^{1/2} \qquad 2.5$$

where

i_p = peak current in μA

n = number of electrons

A = area of the working electrode in cm^{-1}

D = diffusion coefficient in cm^2

C = concentration in mol lit^{-1}

ν = scan rate in volts

k = Randel-Sevcik constant

The peak current in irrireversible process is given by equation

$$i_p = 0.227nFAC^{o}{}_0 k_f \exp\left[\frac{-\alpha nF}{RT}\right]\{E_p - E^o\} \qquad 2.6$$

A plot of log i_p vs Ep-E^o of different scan rates yields, α from the slope and k from the intercept, provide E_o is known.

Shain and Nicholson calculated the peak potential for an irreversible response

$$E_p = E_o - \frac{RT}{\alpha_n F}\left[0.780 + \ln(D_o \alpha a)^{1/2} - \ln k_s\right] \qquad 2.7$$

There is 30/αn mV cathodic shift in peak potential for every 10-fold increase in scan rate, and this criterion can be used to characterize an irreversible response.

The heterogeneous forward rate constant (k^0 f, h) values can be calculated using the equation,

$$Ep = \frac{RT}{(\alpha naF)}\{(\ln(k_o f, h/D^{1/2}) - 1.14) - (0.5\ln(\alpha n_a V)\} \qquad 2.8$$

where R is the gas constant, F is the Faraday constant and T is the absolute temperature.

Eqn. 2.3 and 2.4 are usually employed for checking the reversibility of an electrochemical process. For a given analyte and other experimental set of conditions, Eqn 2.1 states that i_p proportion to $\nu^{1/2}$. Hence, a plot between the square root of scan rate and peak current, i_p of the corresponding cyclic voltammograms should be straight line. Deviations from this rule are quite frequent in organic voltammetry[13].

Usually, The shape of the peak of irreversible response is independent of scan rate and the separation of E_p and $E_{p1/2}$ is given by

$$E_p - E_{p1/2} = \frac{-1.857RT}{\alpha nF} \qquad 2.9$$

In **Figure 2B.6** are shown the three cases of reversible, quasi-reversible and irreversible voltammetric profiles presented in an arbitrary scale. If the electron transfer is diffusion controlled process and the scan rate is faster than chemical reaction, one can find the kinetics of chemical reaction by monitoring the variation of peak current and peak potential with time and concentrations.

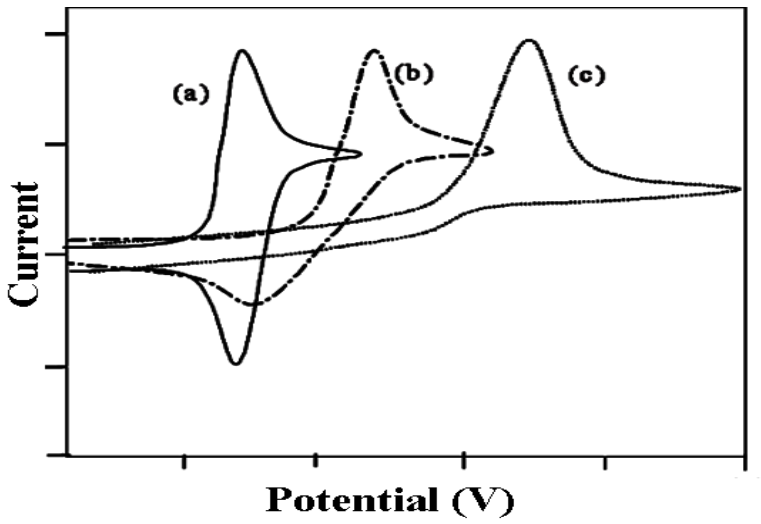

Figure 2B.6: Typical cyclic voltammograms for (a) the reversible, (b) quasi-reversible and (c) irreversible charge transfer (taken in arbitrary scale)

The current flowing through the cell due to the application of the pulse has been divided into three components:

2B.7.2 *Molecular modeling*

Computational chemistry/molecular modeling is the science of representing molecular structures numerically and simulating their behavior with the equations of quantum and classical physics. The 1998 Nobel Prize in Chemistry was awarded to Pople and Kohn for their work in Computational Chemistry and Molecular Modeling.

Computational methods are used to perform the following basic types of calculations:

a) Single Point Energy: The energy of atoms in a particular spatial arrangement in model
b) Geometrical Optimization: Systematic 3-dimensional arrangement of atoms to represent the local energy minima.
c) Property Calculations: To predict certain physical and chemical properties such as heat of formation, HOMO-LUMO, energies, dipole moment.

Molecular modeling/Computational chemistry encompasses a variety of mathematical methods which fall into two broad categories called Molecular Mechanics and Quantum Mechanics.

Molecular Mechanics

In the early years, the force field or molecular mechanics calculations were also known as the *Westheimer Method*[14]. Westheimer is considered as father of molecular mechanics. Molecular Mechanics based on the laws of classical physics to molecular nuclei without explicit consideration of electrons.

Most of the MM_2 calculations on the fundamental concept that a ball-and-spring to approximate a molecule[15,16].

Molecular mechanical methods are based on following principles[17]

- Nuclei and electrons are clubbed together and treated as unified atom-like particles.

- ❖ Bonds between particles are viewed as harmonic oscillators.
- ❖ Non bonding interactions between these particles are treated using potential functions derived using classical mechanics.
- ❖ Individual potential functions are used to describe the different interaction: bond stretching, angle bending, and torsional energies, through-space interactions.
- ❖ Molecular mechanical energies are not absolute energies; they are relative steric energies between two or more conformations of the same molecule.

The total energy of molecule is sum of the stretching ($E_{stretching}$), angle bending ($E_{bending}$), nonbonding interactions ($E_{nonbonding}$), torsional interactions ($E_{torsion}$) and coupled energy terms ($E_{cross\text{-}term}$). The cross-term is combination of two inter related motions (bend-stretch, stretch-stretch, torsion-stretch, etc).

$$E_{total} = \Sigma E_{stretching} + \Sigma E_{bending} + \Sigma (E_{nonbonding} + \Sigma E_{electrostatic}) + \Sigma E_{torsion} + \Sigma E_{cross\text{-}term} \quad 2.10$$

Quantum Mechanics

This method based on the Schrodinger equation to describe a molecule with explicit treatment of electron structure. Quantum mechanical methods can be subdivided into two classes: *ab initio* and semiempirical. Quantum mechanical methods described molecule in terms of explicit interactions between electrons and nuclei.

Both *ab initio* and semiempirical methods are based on the following principles[18]:

- ❖ Nuclei and electron are distinguished from each other
- ❖ Electron-electron and electron-nuclear interactions are explicit
- ❖ Interactions are governed by electron charges and motion of electron
- ❖ Interactions determine the spatial distribution of nuclei and electrons and their energies

All type of calculations are not possible for all methods and no one method is best for all purposes. Choice of method depends on a number of factors, including, nature of molecule, type of information sought, and computer resources.

Molecular mechanics, which attempts to reproduce molecular geometries, energies and other features by adjusting bond lengths, bond angles and torsion angles to equilibrium values that are dependent on the hybridization of an atom and its bonding scheme (this atom description is referred to as the atom type).

Geometry Optimization

Geometry optimization is a first step for the Molecular Mechanics and Quantum Mechanics calculations and Molecular Dynamics Stimulations. Hence, it is subjected to energy minimization, the goal of energy minimization or geometric optimization is to minimizing the potential energy functions with respect to coordinates reduce the steric and electrostatic interactions. Energy minimization required a series of iterations.

Typical molecular structures are entered in to molecular modeling software and perform geometry optimization. Geometric optimization is using first-order and second-order methods. The second-order method is also known as Newton-Raphson method. This method uses information obtained from first and second derivatives of the energy with respect to the coordinates.

The combination of both methods gives a power full tool to find the local minima.

- Calculate the single point energy of starting geometry **Figure 2B.7.**
- Change the coordinates of some subset of atoms and calculate the energy of the new conformer.
- First or second derivative of the energy with respective to the atomic coordinates determine how large and in what direction the next increment of geometry change should be A typical plot of potential energy vs variable is shown below.

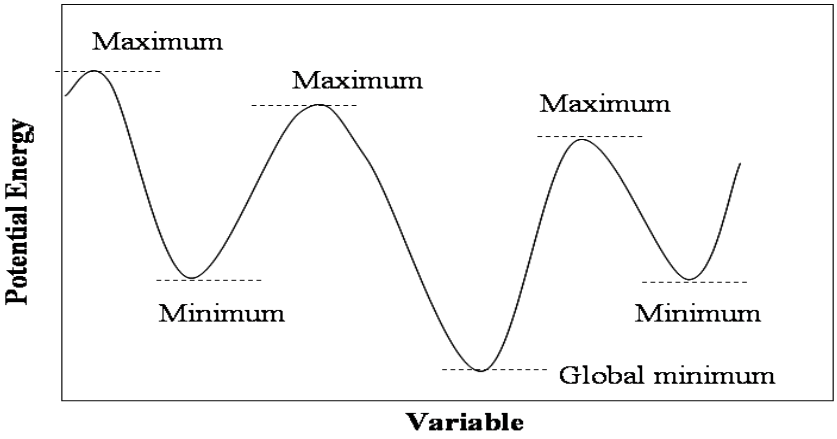

Figure 2B.7*:* A typical plot of potential energy vs variable

Conformational search

Conformations refer to both maxima and minima and all positions in between a conformer refers to the conformational at the bottom of potential energy, which is minimum. The aim of conformational search is to explore all the possible values of dihedral angles that could be assigned to each rotatable bond in a molecular structure.

Boltzmann statistics give the number of possible conformers (auxial and equatorial ration in cyclohexane). Boltzmann eqn. 2.11 is given below

$$P_j = \frac{n_j}{\sum n_i} = \frac{f_i e - E / RT}{\sum f_i e - E / RT} \qquad 2.11$$

P_j = Probability of finding one conformation

f = Frequency factor indicating the degeneracy of energy

E = Relative energy (kcal/mol)

R = Gas constant (0.0199 kcal/mol-K)

T = Temperature (K)

Conformational search is an exhaustive process, but the possibility of finding global minima is a function of number increments used to explore each rotatable dihedral angle.

References

1. R R Gange, C L Sipro, T J Smith, C A Hamann, W R Thies, A K Shienke, *J Am Chem Soc*, 103, **1981**, 4073
2. "*Preparation of Most Common Buffers Used in Polarographic determination*" in Education system Labs Guide-documentation supplied by EG&G Princeton Applied Research Corporation
3. D T Sawyer, A Sobkowiak, J L Roberts, "*Electrochemistry for Chemists*" 2nd Edn, John Wiley & Sons, **1995**
4. J Lawrence, H Henderson, *Am J Physiol*, 21, **1908**, 173-179
5. K B Oldham, J C Myland, "*Fundamentals of Electrochemical Science*" Academic Science, New York, **1994**
6. L A Matheson, N Nichols, *Trans Am Electrochem Soc*, 73, **1938**, 193
7. A Sevcick, *Collect Chem Commun*, 13, **1948**, 349
8. R S Nicholson, M L Olmstead, *Anal Chem*, 41, **1969**, 851
9. A J Bard, Larry Faulkner, "*Electrochemical Methods-Fundamentals and Applications*" John Wiley & Sons Inc, **1980**
10. H H Bauer, *J Electroanal Chem*, 16, **1968**, 2111
11. J E B Randles, *Trans Faraday Soc*, 44, **1948**, 327
12. P Delahay, "*New Instrumental Methods in Electrochemistry*" Inter Science, New York, **1954**, 132
13. F H Westheimer, J F J Mayer, *J Chem Phys*, 14, **1946**, 733
14. U Burkert, N L Allinger, "*Molecular mechanics"* American Chemical Society Monograph, Wasington, DC, 177, **1982**
15. A K Rappe, C Casewit, "*Molecular Mechanics Across Chemistry*" University Science Books, Sausalito, CA, **1992**
16. *Cambridge Soft ChemOffie-2006,* Textbook supplied by Cambridge Soft Corporation, Cambridge, MA, USA
17. Wilson, Gisvolds " *Text book of Organic Medicinal and Pharmaceutical Chemistry*" 11th edn, Lippincott Williams & Wilkins, **2003**
18. O Ermer, *Struct Bonding*, 27, **1976**, 161

CHAPTER III

SPECTRAL AND ELECTROCHEMICAL CHARACTERIZATION, X-RAY CRYSTALLOGRAPHIC MOLECULAR STRUCTURE DETERMINATION AND MOLECULAR MODELING STUDIES OF SOME BIPHENYL BRIDGED NAPTHYLIDINIMINE SCHIFF BASES

Portions of the results of this chapter are published as "*Crystal structure analysis and conformational isomerism of 2,2'-(4,4'-oxybis(4,1-phenylene)bis(azan-1-yl-1-ylidene))bis(methan-1-yl-1-ylidene)dinaphthalen-1-ol''* in Molecular Crystals and Liquid Crystals, (Taylor and Francis),Volume 562, Issue 1, Page 265-290, July 2012

In this Chapter, the characterization of biphenyl bridged Schiff base ligands is discussed. These ligands were characterized by spectral (IR, electronic, NMR and mass), elemental analysis, electrochemical, thermal, single crystal X-ray crystallographic and molecular modeling studies.

Diamines such as 4-(4-aminophenoxy)aniline, 4.4'-diamino biphenyls, when treated with 2-hydroxy-1-napthaladehyde to obtain binucleating and tetradentate Schiff base ligands. The details of the synthesis are presented in **Chapter II**. The general structure of these Schiff bases is given in **3.1**.

Based on the structural vividity, this Chapter is divided into three parts, **PARTS, A**, **B**, and **C**.

In **PART A**, the physical, analytical and spectral data of the biphenyl bridged Schiff base ligands, **2A.1** are present and discussed.

In **PART B**, the electrochemical studies of **3.1** are reported, whereas in **PART C**, the single crystal X-ray diffraction studies, molecular helical stacking and molecular modeling studies of the Schiff bases are described.

The structure of the class of biphenyl bridged Schiff base ligands is furnished in **3.1** and is referred to as H_2L^i, hereafter.

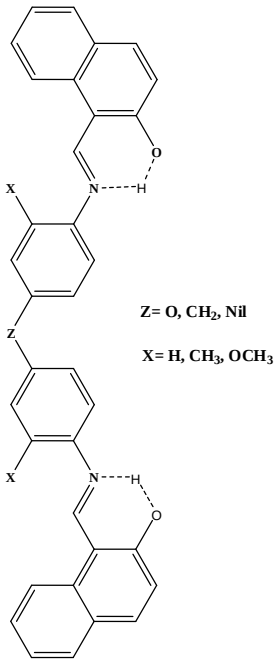

3.1 H_2L^i

Z	X	Row Combination Labelled as H_2L^i
-O-	-	NDADPE or H_2L^1
$-CH_2-$	-	NDADPM or H_2L^2
	$-OCH_3$	NDADPD or H_2L^3
-	$-CH_3$	NDADPT or H_2L^4
-	-H	NDADPB or H_2L^5

3A.1 General Characterization of the Biphenyl Bridged Schiff Base Ligands

The physical and analytical data of the H_2L^i are presented in **Table 3A.1.** The elemental data are in good agreement with the structure shown in **3.1.** The spectral studies are briefly presented here.

3A.2 Infrared Spectral Studies

The FT-IR spectra for **3.1** in KBr pellet were recorded in 400-4000 cm^{-1}. The FTIR spectra of NDADPE are shown in **Figure 3A.1.** Relevant frequencies are presented in **Table 3A.2**. The lowering of the presence of upon condensation is a strong indicator of the Schiff base formation as well as improved intramolecular hydrogen bonding (see **3.1**). The bands present at 1624-1618 cm^{-1} attributable to $\nu_{C=N}$ stretch the C=O of the naphthaldehyde owes in frequencies at 1740-1720 cm^{-1}. In the ligands NDADPE, NDADPM, NDADPD, NDADPT and NDADPB a medium intensity band is present around 3500 cm^{-1} corresponding to the ν_{OH}

stretch. Aromatic ring frequencies are observed for all the ligands in the range of 1498-1378 cm^{-1} and wagging frequencies are observed in the range of 3058-3021 cm^{-1}.

3A.3 ^{1}H NMR and ^{13}C NMR Spectral Studies

Representative ^{1}H NMR and ^{13}C NMR spectra of NDADPE, NDADPM, NDADPD, NDADPT and NDADPB are present in **Figures 3A.2-3A.4,** respectively. Important chemical shift values all the compounds. The spectral patterns and the relative intensities (integrals) are compatible with the respective spectra.

In all the Schiff bases δ values characteristic to the deshielded CH=N protons (2H). The ligands were observed. A signal appears around δ 15.5, due to the OH protons. Useful ^{1}H NMR and ^{13}C NMR data are collected in **Table 3A.4**. All the ligands contain signals in the range of δ 156-170 values characteristic of the azomethanine (C=N) carbon signals. Whereas at δ ~170 values due to the phenolic C-O carbon. The ligand core contains signal at δ 32.8-56.9 corresponding to the methylene carbons. The aryl carbons are resonate in the range of δ 109.2-154.7.

Table 3A.1: *Physical and analytical data of biphenyl bridged Schiff base ligands*

Compound	Appearance	M.Point (^{0}C)	Molecular Formula	Molecular Weight #	Elemental Analysis*		
					C %	H%	N%
NDADPE	Yellow	194.14	$C_{34}H_{24}N_2O_3$	509	80.17	4.83	5.50
				(509)	(80.30)	(4.76)	(5.51)
NDADPM	Yellow	207.02	$C_{35}H_{26}N_2O_2$	507	82.53	5.24	5.49
				(507)	(82.92)	(5.17)	(5.53)
NDADPD	Red	174.03	$C_{36}H_{28}N_2O_4$	553	78.05	4.97	4.67
				(553)	(78.24)	(5.11)	(5.07)
NDADPT	Pale Orange	182.54	$C_{36}H_{28}N_2O_2$	521	82.75	5.65	6.15
				(521)	(83.05)	(5.42)	(5.38)
NDADPB	Orange	185.03	$C_{34}H_{24}N_2O_2$	493	82.50	4.15	5.91
				(493)	(82.91)	(4.91)	(5.69)

* data in parenthesis are calculated ones # data in parenthesis are obtained from ESI^{+} Mass spectra, vide intra

Table 3A.2: *Infrared spectral data of biphenyl bridged Schiff base ligands*

S. No.	Compound	IR spectral data (cm^{-1})*			
		$\nu_{C=N}$	ν_{OH}	ν_{C-O}	Aromatic
1	NDADPE	1620	3415	1541	3045w, 1494, 1323
2	NDADPM	1624	3420	1543	3032w, 1510, 1319
3	NDADPD	1618	3605	1541	2939w, 1487, 1329
4	NDADPT	1618	3441	1543	3024w, 1405, 1321
5	NDADPB	1620	3515	1541	3038w, 1409, 1307

* in KBr pellet, w; weak

Table 3A.3: *UV-Visible and fluorescence spectra of biphenyl bridged Schiff base ligands*

S. No.	Compound	Electronic data in $CHCl_3$ λ_{max} ($\bar{\upsilon}$) (ε)[a]	Fluorescence data Exited (nm)	Fluorescence data Emission (nm)
1.	NDADPE	388(26,547)(25,772)	370	420,442,465,490
2.	NDADPM	380.5(16,795)(26,282) 321.5(18.885)(31.105)	360	404,465,489
3.	NDADPD	493(38,370)(20,284)	360	410,539
4.	NDADPT	404.5(34,195)(24,722)	380	409,430,524
5.	NDADPB	400(49,607)(25,000)	380	415,433, 525

a, λ_{max} (in nm), $\bar{\upsilon}$ (in cm^{-1}), ε (lit. $mol^{-1}.cm^{-1}$)

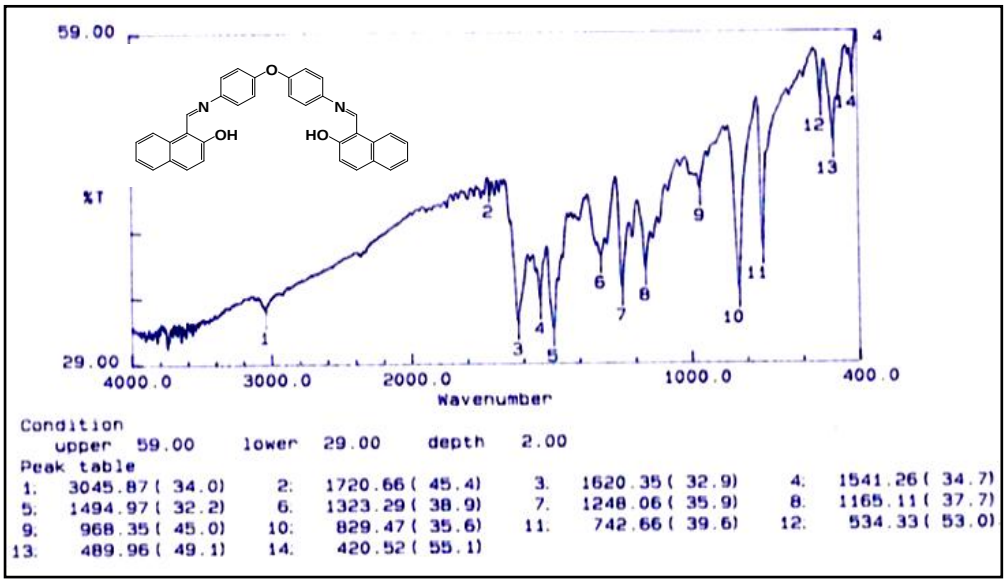

Figure 3A.1: FT-IR spectrum of NDADPE

Table 3A.4: *^{1}H NMR and ^{13}C NMR spectral data of biphenyl bridged Schiff base ligands*

Compound	δ ^{1}H NMR (ppm)	δ ^{13}C NMR (ppm)
NDADPE	15.54 (s) 2H, O...H...N, 9.38(s,) 2H,C=N), 8.16(4H, d,aminophenyl), 7.37(4H,d,aminophenyl), 7.41(4H, s, naphthyl), 7.55 (4H, s, naphthyl), 7.77-8.16 (4H, s, naphthyl)	161.54 (CH=N), 155.83 (Ar-C), 155.09, 141.64 (C-O) 136.29, 133.11, 129.42, 128.06, 127.44, 123.57, 121.98, 121.70, 119.94, 118.95, 108.98
NDADPM	15.38 (s) 2H, O...H...N, 9.33 (s) 2H, C=N, 8.09(d) 4H,aminophenyl, 7.32(d) 4H,aminophenyl, 7.33 (s) 4H, naphthyl, 7.52 (s) 4H, naphthyl, 7.69-8.09(m) 4H, naphthyl, 4.20 (s) 2H, CH_2	161.64 (CH=N), 159.83 (Ar-C), 155.09, 141.64 (C-O), 136.29, 133.11, 129.42, 128.06, 127.44, 123.57, 121.98, 121.70, 119.94, 118.95, 109.98, 45.07
NDADPD	9.40 (s) 2H, O...H, 8.16 (s) 2H, C=N, 3.59(s) aminophenylmethoxy, 7.38(d) 4H, 6H, aminophenyl, 7.36 (s) 4H, naphthyl, 7.53(s) 4H, naphthyl, 7.72-8.14 (m) 4H, naphthyl, 7.26 (s) 2H, aminophenyl	32.8, 56.9 (4C, CH_2-CH_2), 119, 121.8, 123.4, 127.8, 129.1, 133.4, 134.2, 135.9, 136.5, 137.6, 138.7 (22C, Ar-C), 161.3 (2C, CH=N)
NDADPT	9.42(s) 2H, O...H, 8.06(s) 2H, C=N, 2.35(s) 6H, aminophenyl, 7.38(d) 4H, aminophenyl, 7.36 (s) 4H, naphthyl, 7.53 (s) 4H, naphthyl, 7.72-8.14 (m) 4H, naphthyl 7.26 (s) 2H,aminophenyl	123.3, 128.6, 130.5, 132.8, 136.9, 140.0, 146.7, 151.2 (16C, Ar-C), 158.7 (2C, CH=N), 168.3 (2C, C=O)
NDADPB	9.40 (s) 2H, O...H, 8.15 (s) 2H, C=N, 7.10 (d) 4H, aminophenyl, 7.38 (d) 4H, aminophenyl, 7.36 (s) 4H, naphthyl, 7.53 (s) 4H, naphthyl, 7.73-8.15 (m) 4H, naphthyl	110.3, 117.5, 123.2, 125.5, 126.7, 129.0, 129.7, 132.3, 133.3, 135.4, 138.7 (26C, Ar-C), 147.3(C-O), 161.2 (2C, CH=N)

s = singlet, d = doublet, m = multiplet

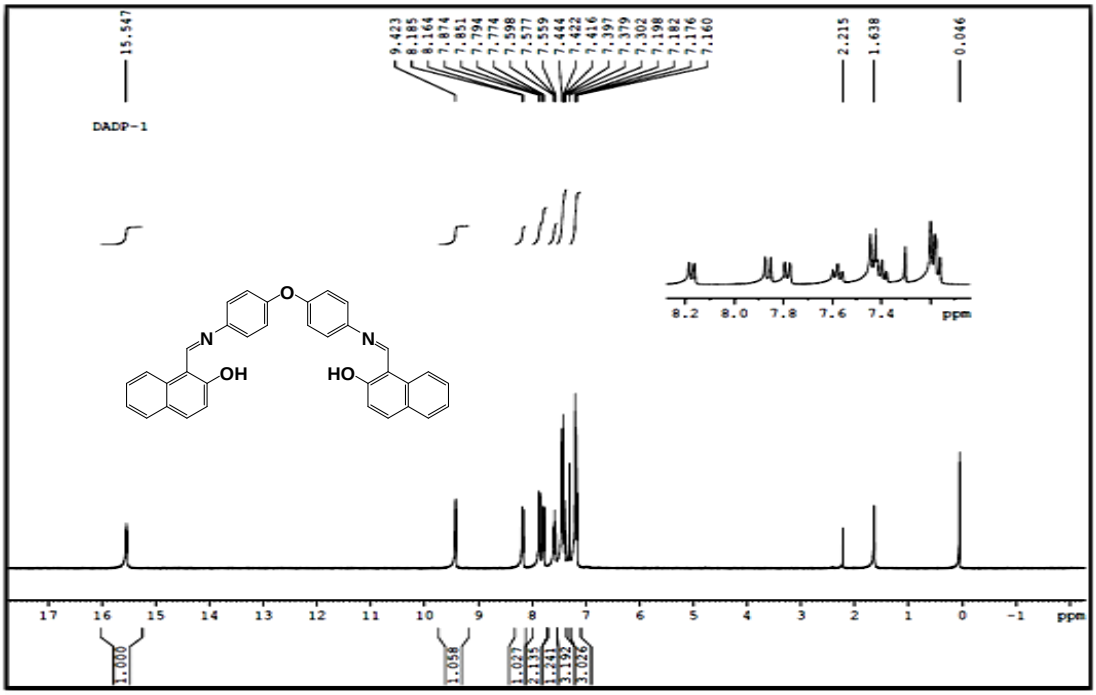

Figure 3A.2: ^{1}H NMR spectrum of NDADPE

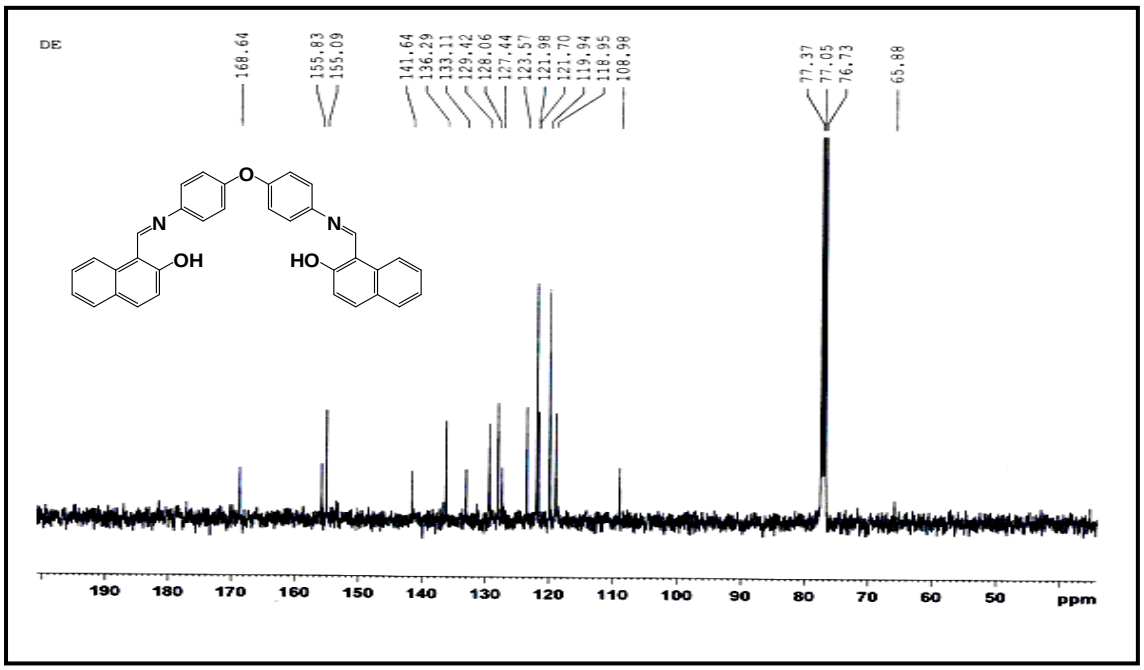

Figure 3A.3: ^{13}C NMR spectrum of NDADPE

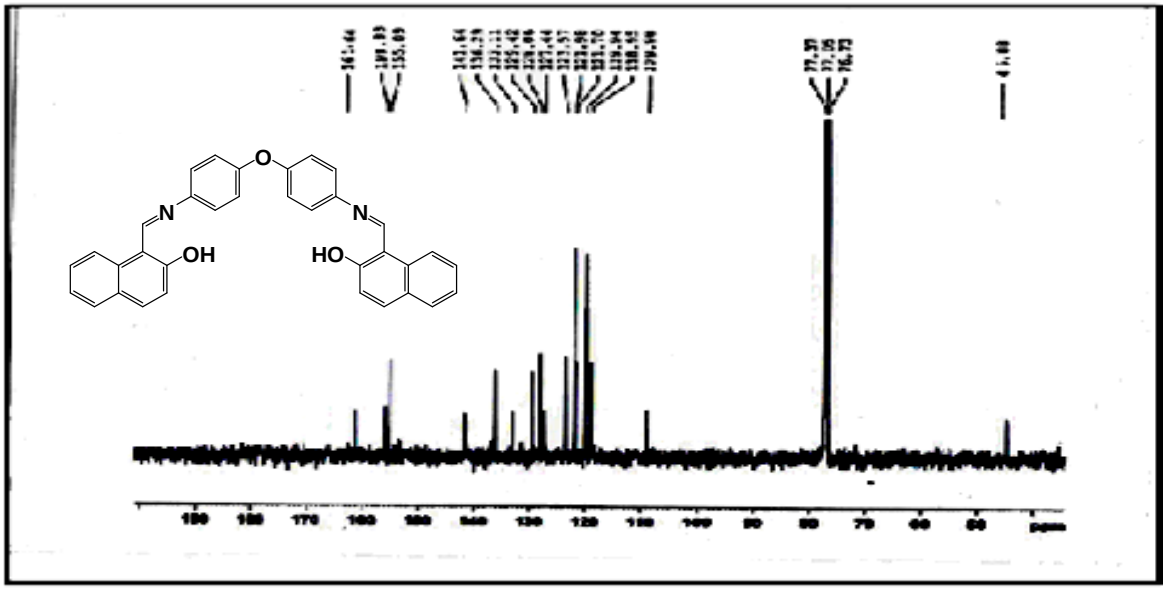

Figure 3A.4: ^{13}C NMR spectrum of NDADPM

3A.4 Mass Spectral Studies

The Electrospray ionization mass spectra (MS-ESI$^+$) of H_2L^i have been investigated. Typical such spectra are presented in **Figures 3A.5** for NDADPE and NDADPM respectively. The molecular ion peaks were obtained for NDADPE, NDADPM, NDADPD, NDADPT, and NDADPB are at 509 (100%), 507 (100%), 553 (100%), 521 (100%), 493 (100%), values respectively.

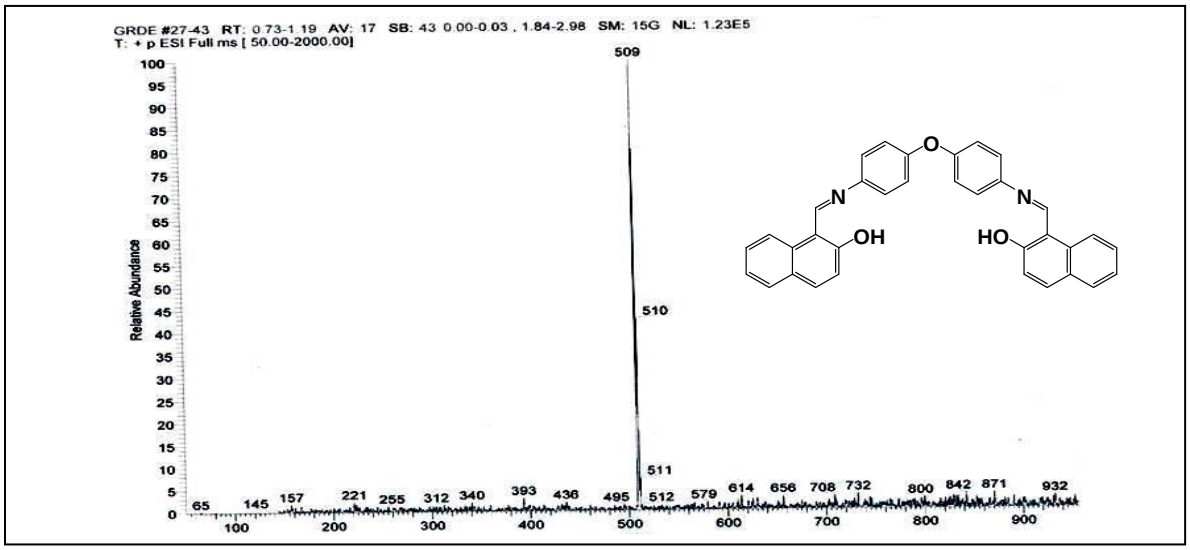

Figure 3A.5: Mass spectrum of NDADPE

3A.5 Electronic Spectral Studies

3A.5.1 *UV-Vis absorption spectra of biphenyl bridged Schiff base ligands*

The UV-Vis electronic spectra and the respective of NDADPE, NDADPM, NDADPD, NDADPT and NDADPB are shown in **Figure 3A.6.** The ligands showed absorption bands of (-C=N-) $\pi \rightarrow \pi^*$ and $n \rightarrow \pi^*$ at 380 and 500 nm, some of the relevant data are collected in **Table 3A.3.**

3A.5.2 *Fluorescence emission spectra of biphenyl bridged Schiff base ligands*

Naphthalidimines connected to conjugated rings are famous for fluorescence emission, some of the H_2L^i Schiff bases have been investigated by spectrofluorimetry. The fluorescence emission and electronic spectra of a few selected NDADPE are present in **Figure 3A.6,** the emission spectra of compounds NDADPE in diluted dichloromethane solutions. Some of the relevant data are collected in **Table 3A.3**. These Compounds exhibit color emissions with peaks at 420, 465, 449 and 489 nm, respectively. The maximum emission wavelength of compounds bathochromically shifted by about 30 and 20 nm, respectively, compared with that of NDADPD because of the electron repelling methoxyl group in their molecular structure.

3A.6 Thermal Studies

The thermal studies of biphenyl bridged Schiff base ligands were carried on by differential scanning calorigram (DSC)**.** A few representative thermograms are shown in **Figures 3A.7** and **3A.8,** along with their onset slope curves. All the ligands are endothermic peaks. There is only one endothermic phase transition at 200 ^{0}C throughout temperature range studied at 25-600 ^{0}C. This endothermic peak is attributed to the melting process of **3.1**. The sharp ramp of the endothermic peak reveals that the compound closer a distinct isothermal phase transition. The ΔH_{PT} or ΔH_{MP} to be ~2.19 kJ mol^{-1}. Their heat of fusion thermal data of all **3.1** are placed in **Table 3A.5.** The compounds, NDADPE, NDADPM exhibit slightly higher melting points than compounds, NDADPD, NDADPT and NDADPB. This difference is attributed to the bent diphenyl skeleton due to the presence of bridging atom between the two benzene rings.

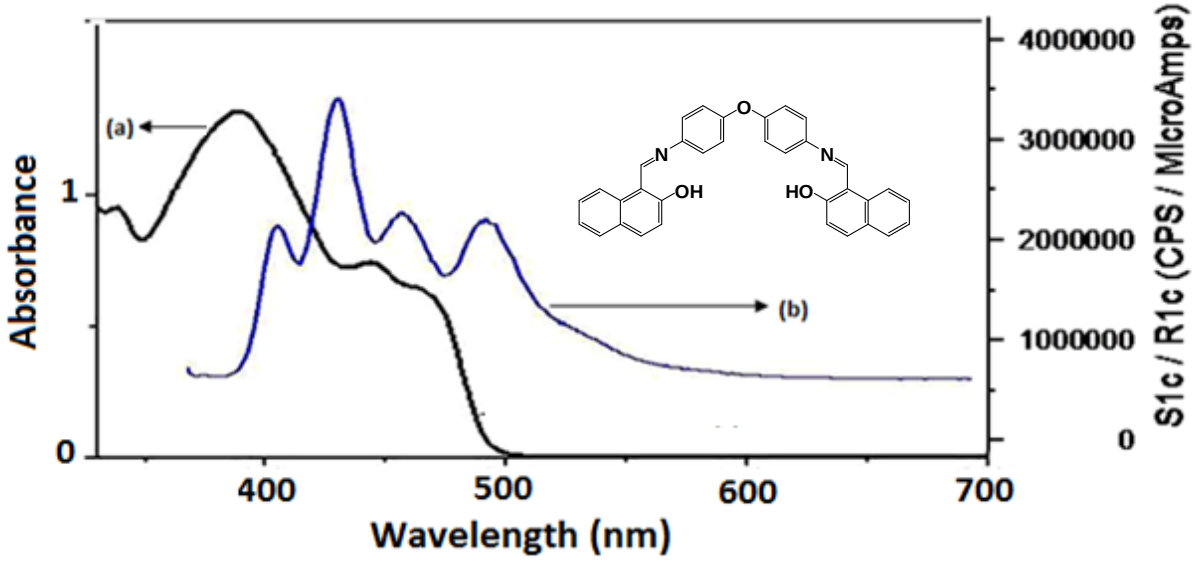

Figure 3A.6: Electronic spectra of a) UV–vis absorption b) Fluorescence spectra of NDADPE (4 x 10^{-5} M) in chloroform at room temperature

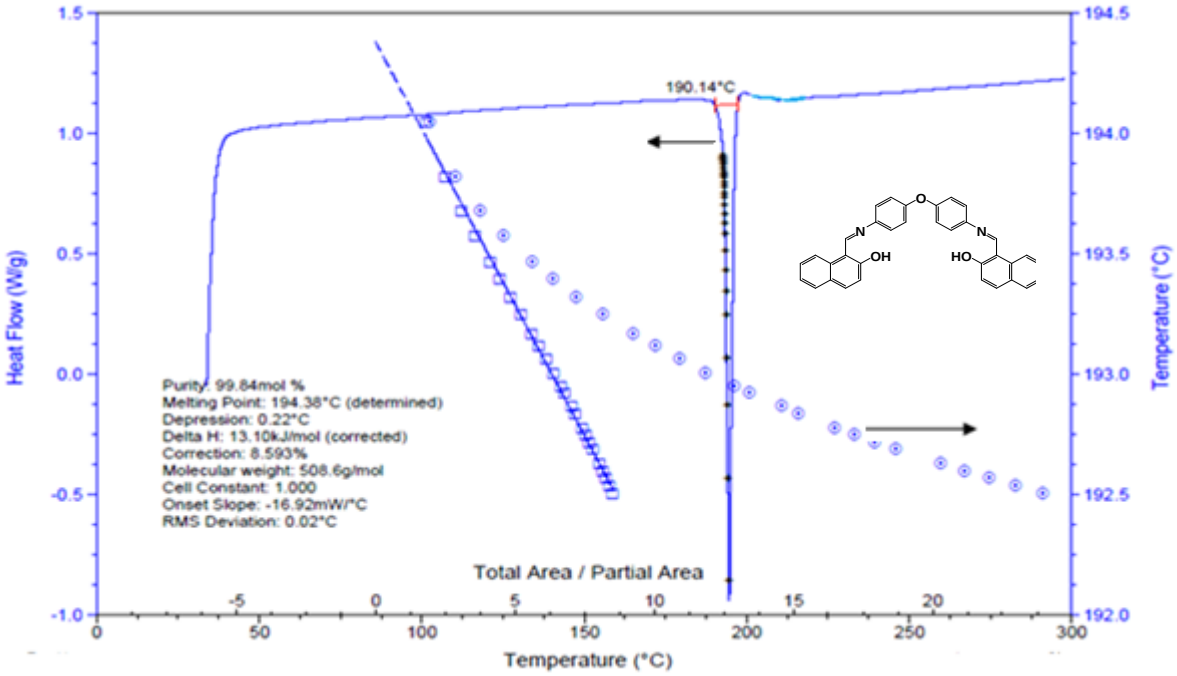

Figure 3A.7: Differential scanning calorigram of NDADPE (3 mg) under N_2 atmosphere

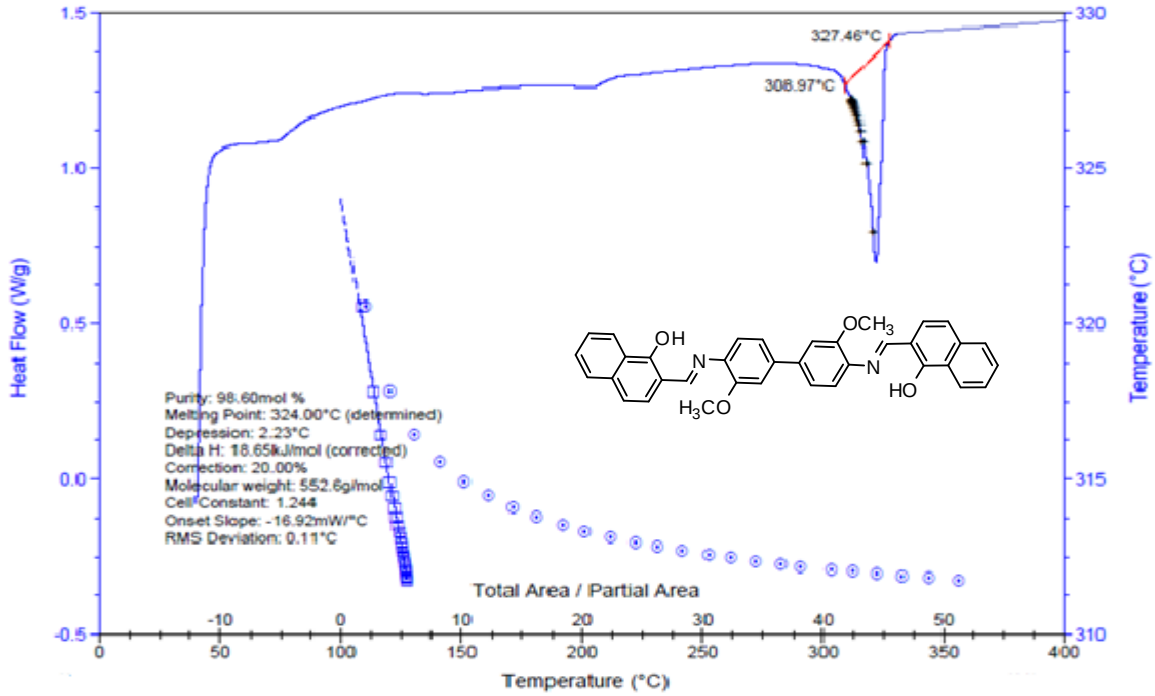

Figure 3A.8: Differential scanning calorigram of NDADPD (3 mg) under N_2 atmosphere

Table 3A.5: *Differential scanning calorimetry data of biphenyl bridged Schiff base ligands*

S.No	Compound	Melting point (^{0}C)	ΔH (kJ/mol)
1	NDADPE	194.14	13.00
2	NDADPM	207.12	3.713
3	NDADPD	174.02	18.16
4	NDADPT	182.54	4.913
5	NDADPB	185.03	2.043

PART B: ELECTROCHEMICAL STUDIES

The results presented in **Part A** reveal that H_2L^i Schiff bases, exist in several conjugate acid-base forms and that the naphtholate ion appears to undergo resonance isomerisation between bezenoid and quinonoid forms. A brief scan through literature reveals that protonation of Lewis base affects its voltammetric behavior of any compound. Hence, H_2L^i are expected to exhibit pH-dependent electrochemical features.

3B.1 Electrochemical Studies in Aqueous Buffers

The electrochemical behavior of H_2L^i have been examined in aqueous buffers at static mercury drop electrode (SMDE) and glass carbon electrode(GCE) over the pH range 2-12 using cyclic voltammetry and other voltammetric techniques. Cyclic voltammetry has been done on H_2L in non aqueous media. Typical cyclic voltammograms of H_2L^i are presented in **Figures 3B.1-3B.3**.

3B.2 Aqueous Electrochemistry of H_2L^i

The compounds were characterized by electrochemical investigation also to understand the effect of concentration of H_2L^i and structure of the molecular Skelton as a function of P^H, solvent nature of metal ion, etc,. Cyclic voltammetry was used as the routine one before extending to other studies. In **Figure 3B.1** are displayed the cyclic voltammograms of NDADPE at various pHs and in the cathodic potential range (from-0.400 V to -2.00V vs Ag/AgCl) measured on SMDE (drop size 0.26 mm^2). Similar features are observed for other H_2L. The following features are observed from these voltammograms.

(i) The compounds exhibit an irreversible reduction electron transfer reduction process.

(ii) Though each molecule has two azomethine sites both the electrophores are near simultaneously reduced.

(iii) The peak potential is found to be cathodically shifted with increasing analytical concentration, pH and scan rate suggesting the involvement of a following chemical reaction at low scan rates wherein the chemical event (C) competes with another the electrochemical event (E) that accompanies with a participation of H^+ ion in the electron transfer process

(iv) The current function ($i_p/ \nu^{1/2}$) is found to be near independent of scan rates at higher range of scan rates indicating the absence of any chemical even following the electrochemical event.

(v) The peak potentials are linear to pH suggesting a fixed number of H^+ ions participating in the electrochemical reduction.

(vi) The peak current is linear to $\nu^{1/2}$ indicating non-absorptive and simple diffusion controlled electron transfer.

(vii) At higher P^H buffers, however, the CV response i in two steps.

(viii) Compounds with Z= nil have different kind of CV profile from those with Z= CH_2 or –O-

The electron transfer is attributed to the reduction of the -C=N- moiety[1, 2] as

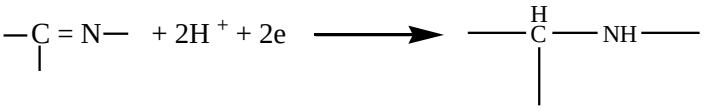

3.1

It is thermodynamically, electrostatically and quantum mechanically least favoured to have an electron transfer with a pair of electrons in one elementary reduction step. The 2-electron reduction of Schiff bases intrinsically happens in a consecutive pair of addition of $1e^-$, $1H^+$. In other words the net reaction is due to two steps of intrinsic reduction.

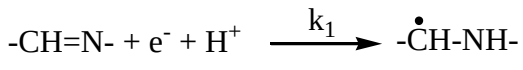

3.2

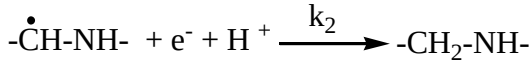

3.3

where k_1 and k_2 are the intrinsic heterogeneous rate constants.

when k1 >>>k_2, the first reaction triggers a parallel dimerisation process[3,4] as

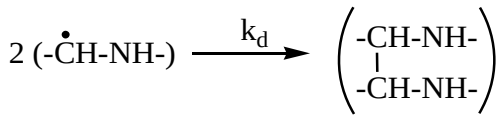

3.4

with a homogeneous dimerisation constant of k_d. Usually, the k_d value is far slower than k_2.

Electrochemical heterogeneous rate constants depend on the potential and hence on the scan rates.

If the commencement of the potential at which the second consecutive reduction (with k_2) is delayed, there is a finite probability for the dimerisation (with k_d) which would subsequently undergo reduction as

$$\begin{pmatrix}\text{-CH-NH-}\\ |\\ \text{-CH-NH-}\end{pmatrix} + 2e^- + 2H^+ \longrightarrow 2\ (\text{-}CH_2\text{-NH-}) \qquad 3.5$$

In such case the formation of dimer through equation (3.4) and its eventual reduction through the electrochemical reduction equation (5) is expected to be more prominent at lower scan rate than that at higher. Further, since the reduction of a sterically strained is more feasible than the 2-electron reduction of parent azomethine, one expects cyclic voltammetric reduction peak for the reduction of the dimer preceding that of the parent. That the reduction peaks appear a big broader than normal, may be an indicator of a closely preceding peak.

At very alkaline buffers, the cyclic voltammograms exhibit two irreversible reduction peaks at ~ 1.2 and -1.65 V vs Ag/AgCl. Such a wide separation cannot be attributed to a consecutive 2-step electron transfer at a single site, such as in equations [(3.2) + (3.3)] and (3.5). These two steps suggest a distinct pair of electrophoreses.

It has been already mentioned that LH_2 systems exist as LH_4^{2+}, LH_3^+, LH_2, LH^- and L^{2-} depending on the pH. It a pH $Pka_3<Ph<Pka_4$ LH_2 exists predominately as LH^-. The structure of LH^- may be shown in **Scheme 3.1**

Since naphthone, napthoxide differ electronically and the benzoide-quinoid isomersiationly LH^- is extendable up to the bridging 'Z', we have in LH^- two kinds of electrochemically reducible electrophores in equilibrium. The reason for obtaining two peaks at higher pHs is attributed to the presence of the two species. Even if LH_2 is present in L^{2-}, both the napthylidinimine sites

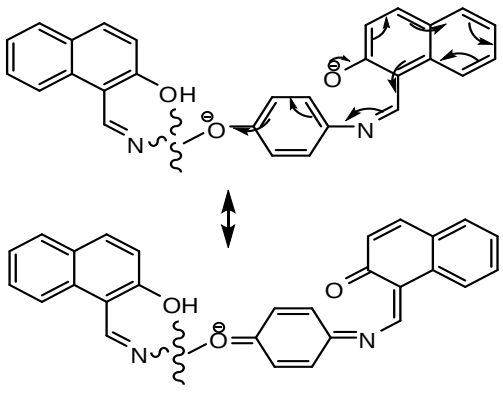

Scheme 3.1

cannot become quinonoid or bezenoid under simultaneously due to the presence of only one 'Z' atom. One of them is stabilized by quinonoid form whereas the other site remains as the bezenoid. Hence, one would get two CV responses. The experimental results are in line with this proposed scheme.

The electrochemical response of the LH_2 with Z= nil are observed to be slightly different. As the conjugate with Z=nil cannot extend over the bridging biphenyl benzenes and stop at azomethanine nitrogen, the LH_2 compounds with Z = nil do not show any split CV patterns even at elevated pHs. A series of CV profile for NDADPT as a representative case is presented in **Figure 3B.3.**

The electrochemical anodic behaviour of LH_2 was also examined in aqueous buffers on glass carbon electrode (GCE) in the potential range -1.2 to +1.2 Vs^{-1}. A representative set of CV of NDADPE is presented in **Figure 3B.5-3B.7** for 3 different pHs. Interestingly the reduction of LH_2 on SMDE because at pH ≈ 4.0 NDADPE undergoes reduction at ~-1.2 V on SMDE whereas on GCE its reduction is at ~-0.60 V. This much large anodic shift is attributed to the dissimilar substrate-electrode interface. Further, the reduction on GCE appears to be not complicated by the formation of free radical intermediates as it is evident from a single reduction peak at all pHs.

The LH_2 molecules undergo a two-step oxidation in the alkaline pHs as indicated in **Figure 3B.1**, whereas in the acidic and neutral media LH_2 are oxidatively stable on GCE till +1.1 Vs^{-1} Ag/AgCl. At neutral and acidic pHs the -N=CH- moiety's lone pair of electrons on the nitrogen is stabilized by intramolecular hydrogen bond[5-7]. Hence, oxidation of –N=CH- as

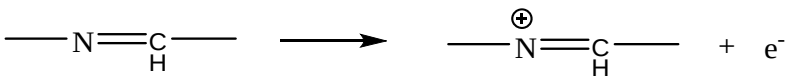

3.6

is not effective till +1.1 V. However, when the pH ≥10, one observers a distinct pair of anodic (irreversible) peaks. With the loss of phenolic hydrogen at higher pHs, the stability of the –N=CH- is reduced. Besides, as mentioned earlier, the two sites of the azomethanine are not similar in CH^- and L^{2-} . On one side, it is $^{\ominus}$=N-CH= whereas on the other, it is still-N=CH-. Hence oxidation of $^{\ominus}$=N-CH= moiety as

$$=\overset{\ominus}{N}\text{-CH}= \rightarrow =\text{N-CH}= + e^- \qquad 3.7$$

has to be more feasible than (less anodic) that fated to the –N=CH- as in eqn. In **Figures 3B.1** is shown the effect of pH on the electrochemical reduction potential, E_p. one can see from here that there is a great discontinuity of relationship between pH and E_p. This is possible only in case the two regions of pH are exhibiting the behaviour of two different chemical entities. From this we can ascertain that the species LH_3^{+2}, -LH is structurally intact where as L^- is structurally different from LH_3^{+2}, -LH. Hence, the electrochemical responses of H_2L in the pH range 6<pH<14 is essentially structurally reorganized form of LH. The absorptive character of azo group is well studies and it is reported that -C=N- is reduced at less negative potential than is -C=N-[8,9].

Coulometric measurements at potential more than 100 mV of the peak potential in all the pH range were made. It confirms that the reduction involves 2 electrons in acidic, basic and neutral pH range. The number of protons involved in the reduction process calculated as 2 from the plot of E_p vs pH. Relevant electrochemical data collected in **Table 3B.1.**

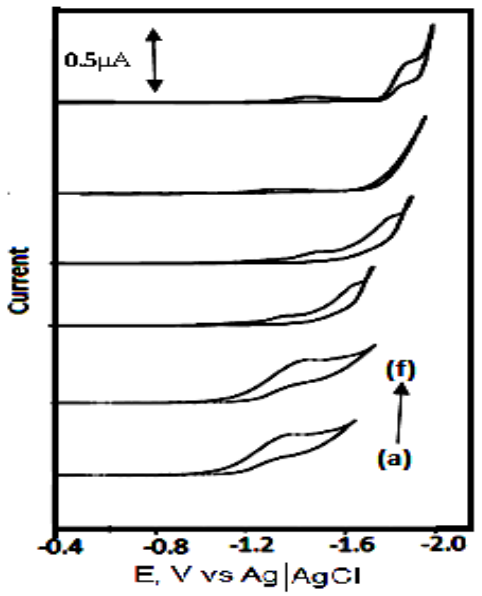

Figure 3B.1: Cyclic voltammograms of NDADPE (4 x 10^{-5} M) at a pH of (a) 2.07, (b) 4.02, (c) 6.01, (d) 8.20, (e) 10.12, (f) 12.01 (scan rate, 50 mV/s) on SMDE

For an n-electron, an m-proton electrochemical reduction, the cyclic voltammetric peak, E_p is shifted cathodically with pH as

$$E_p = E^o p - \frac{0.0591m}{n} pH \qquad 3.8$$

where E^0_p is Ep at $a_{H+} = 1$. Hence, the plot of E_p vs pH should be straight line with a slope of (0.05916 m)/n from which one can get the value of m with knowledge of n. The value of m evaluated from the linear segments of **Figure 3B.4** turn out to be 2 in both in acidic and basic range, relevant data collected in **Table 3B.1**.

The electrochemical data of H_2L such as peak potential, i_p, peak potential, E_p, diffusion coefficient, D_o, and heterogeneous electron transfer coefficient, k_h values of **H_2L** are collected in **Table 3B.1.** The plots of E_p vs log ν at different pH values were straight line, with slope **(S_1)** values of 15-85 mV (slope = $59/\alpha n_a$) is proportional to αn_a. Some of the plots of E_p vs log ν at selected pH are show in H_2L **.**The value of αn_a is obtained in the range 0.2-0.6 and vales of α are as 0.34-0.96 and relevant electrochemical data collected in **Table 3B.1.**

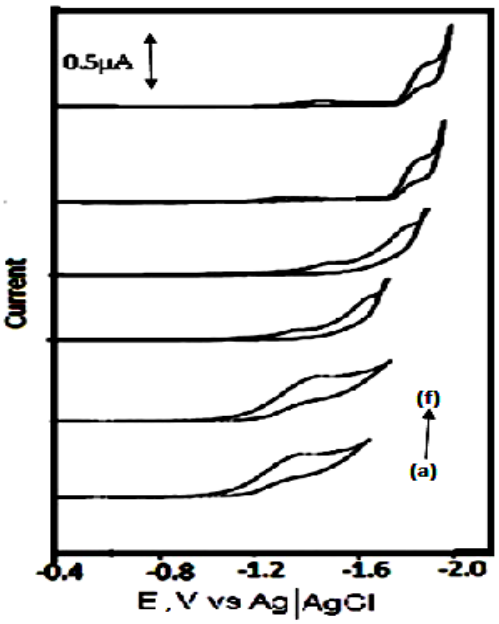

Figure3B.2: Cyclic voltammograms of NDADPM **(**4 x 10^{-5} M) at a pH of (a) 2.07, (b) 4.02, (c) 6.01, (d) 8.20, (e) 10.12, (f) 12.01 (scan rate, 50 mV/s) on SMDE

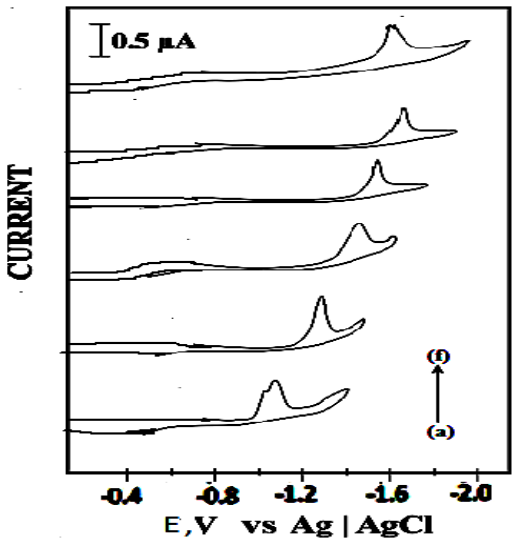

Figure 3B.3: Cyclic voltammograms of NDADPT **(**4 x 10^{-5} M) at a pH of (a) 2.07, (b) 4.02, (c) 6.01, (d) 8.20, (e) 10.12, (f) 12.01 (scan rate, 50 mV/s) on SMDE

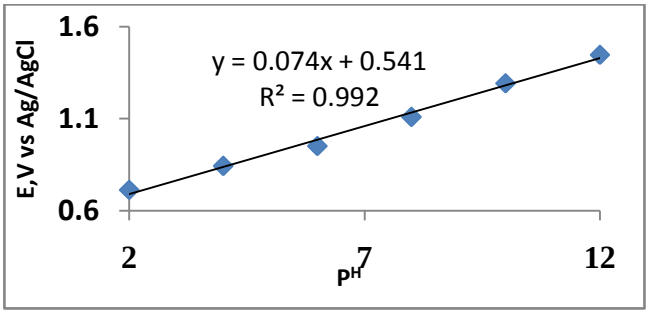

Figure 3B.4: Effect of pH vs. peak potential of NDADPE (2.06 x 10^{-4} M) (scan rate, 50 mV/s and drop size of 0.26 mm^2 on SMDE)

Table 3B.1: *Voltammetric data of biphenyl bridged Schiff base ligand*

Compound	pH	$-E_p$ (V)	α_{na}	k^o_h x10^9 (cm^2 /s)	D_o x 10^6 (cm^2 /s)
NDADPE	2.07	0.713	0.62	6.31	1.21
	4.02	0.843	0.55	1.73	3.01
	6.01	0.952	0.77	1.08	6.32
	8.20	1.109	0.29	2.68	1.70
	10.12	1.293	0.44	1.16	3.30
	12.01	1.447	0.55	5.95	2.39
NDADPM	2.07	0.691	0.59	6.23	1.22
	4.02	0.841	0.53	1.69	3.02
	6.01	0.951	0.76	1.07	6.25
	8.20	1.098	0.30	2.65	1.68
	10.12	1.292	0.56	1.17	3.34
	12.01	1.352	0.50	5.98	2.32
NDADPD	2.07	0.645	0.43	5.12	8.88
	4.02	0.774	0.44	4.31	8.23
	6.01	0.813	0.45	3.44	8.15
	8.20	0.936	0.47	2.20	8.82
	10.12	1.143	0.58	2.01	9.13
	12.01	1.231	0.62	1.89	9.16
NDADPT	2.07	0.734	0.39	5.47	5.46
	4.02	0.863	0.45	4.41	5.03
	6.01	0.904	0.47	4.07	5.71
	8.20	1.025	0.49	3.34	6.02
	10.12	1.257	0.53	2.74	5.53
	12.01	1.321	0.57	2.62	6.01
NDADPB	2.07	0.721	0.42	6.91	2.45
	4.02	0.833	0.44	6.09	2.16
	6.01	0.879	0.45	5.41	2.33
	8.20	1.038	0.48	4.97	1.38
	10.12	1.271	0.56	4.30	1.27
	12.01	1.301	0.51	4.18	1.28

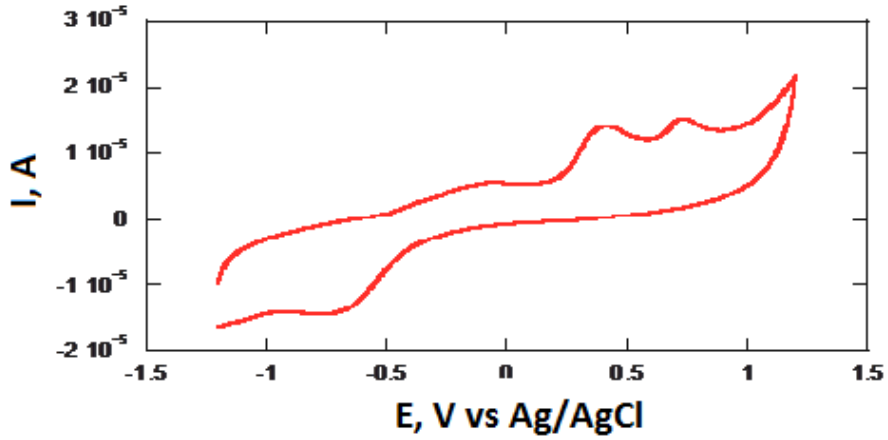

Figure 3B.5: Cyclic voltammogram of NDADPE **(**4 x 10^{-5} M) at a pH of 12.01 (scan rate, 100 mV/s) on GCE

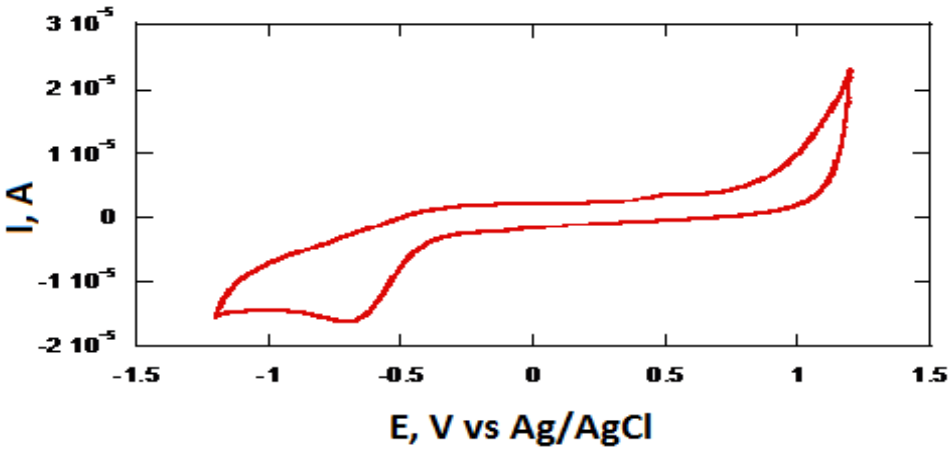

Figure 3B.6: Cyclic voltammogram of NDADPE **(**4 x 10^{-5} M) at a pH of 9. 01 (scan rate, 100 mV/s) on GCE

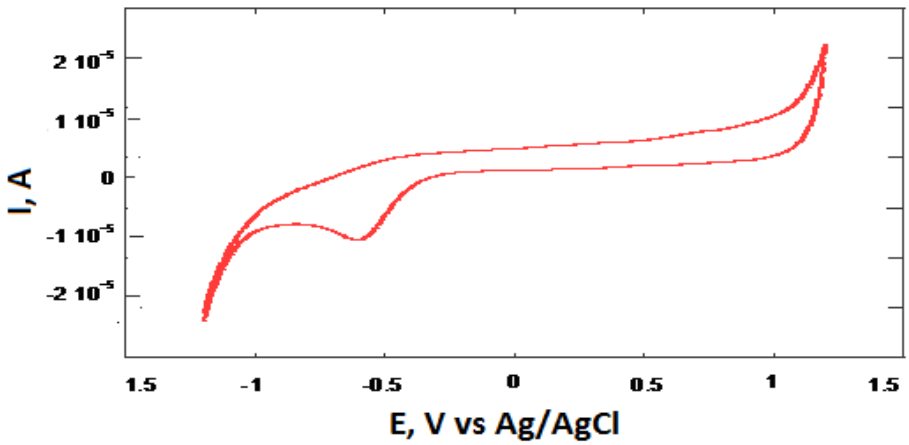

Figure 3B.7: Cyclic voltammogram of NDADPE **(**4 x 10^{-5} M) at a pH of 3. 01 (scan rate, 100 mV/s) on GCE

3B.3 Non-aqueous Electrochemistry

The electron transfer properties of the compounds were studied in DMF with tetra ethyl ammonium perchlorate (TEAP) as the supporting electrolyte. A typical cyclic voltammogram obtained in the anodic region on GCE for all compounds is presented in **Figures 3B.8-3B.12**. An irreversible reduction peak at ~ -0.850 V and another irreversible oxidation peak at ~ 1.250 V are observed in **Scheme 3.2**.

The cathodic Cyclicvoltammetry seams of NDADPE and NDADPM are shown in **Figures 3B.13** and **3B.14,** respectively in DMF solvent. Intense reduction peaks appears at ~0.8V (Ag/AgCl) with TEAP as the supporting electrolyte. The absence of H^+ in DMF restrictive the azomethine group to a free radical and irreversible electron transfer mechanism.

Anodic

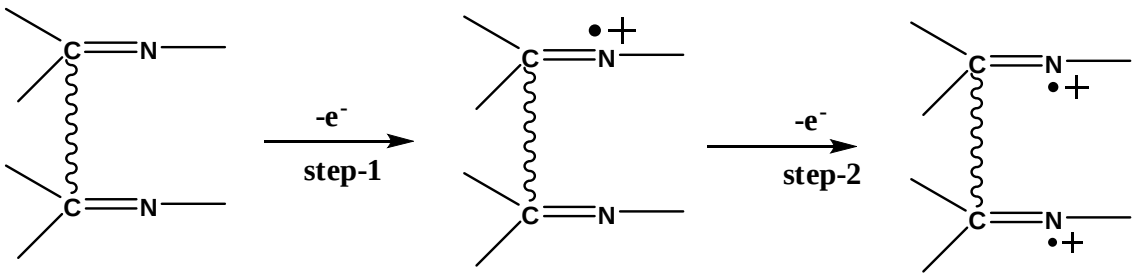

Cathodic

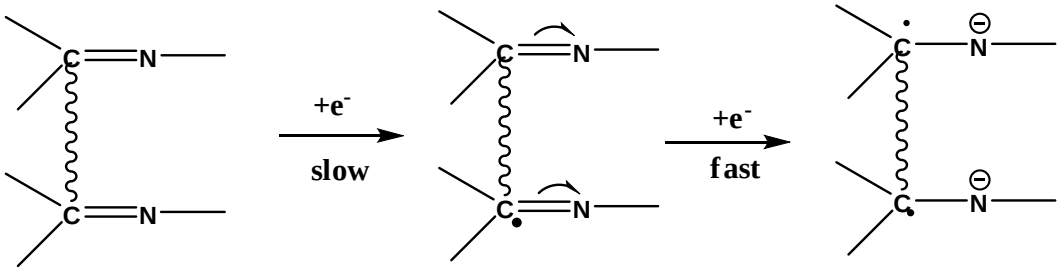

Scheme 3.2

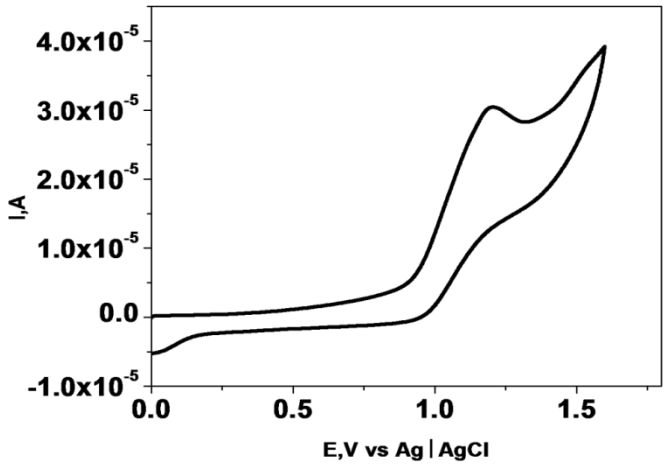

Figure 3B.8: Cyclic voltammogram of NDADPE **(**4 x 10^{-5} M) in DMF on GCE at scan rate, 0.1 Vs^{-1}, with TEAP (0.1 M)

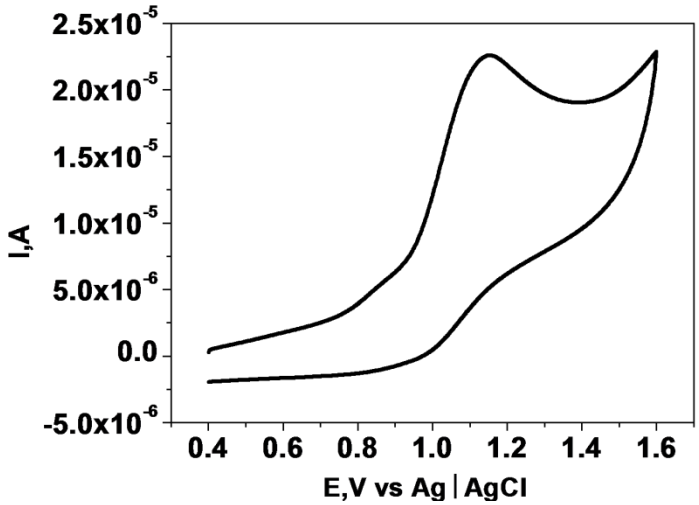

Figure 3B.9: Cyclic voltammogram of NDADPM **(**4 x 10^{-5} M) in DMF on GCE at scan rate, 0.1 Vs^{-1}, with TEAP (0.1 M)

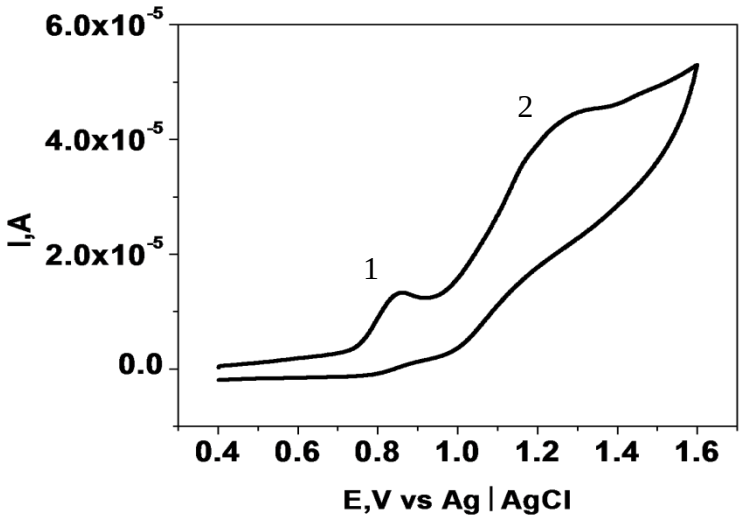

Figure 3B.10: Cyclic voltammogram of NDADPD **(**4 x 10^{-5} M) in DMF on GCE at scan rate, 0.1 Vs^{-1}, with TEAP (0.1 M)

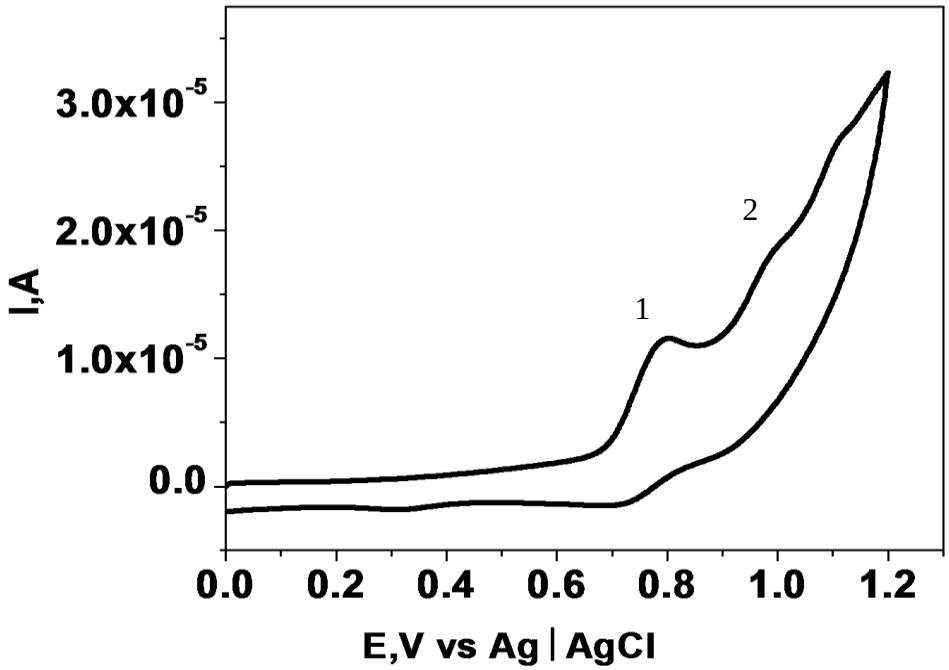

Figure 3B.11: Cyclic voltammogram of NDADPT **(**4 x 10^{-5} M) in DMF on GCE at scan rate, 0.1 Vs^{-1}, with TEAP (0.1 M)

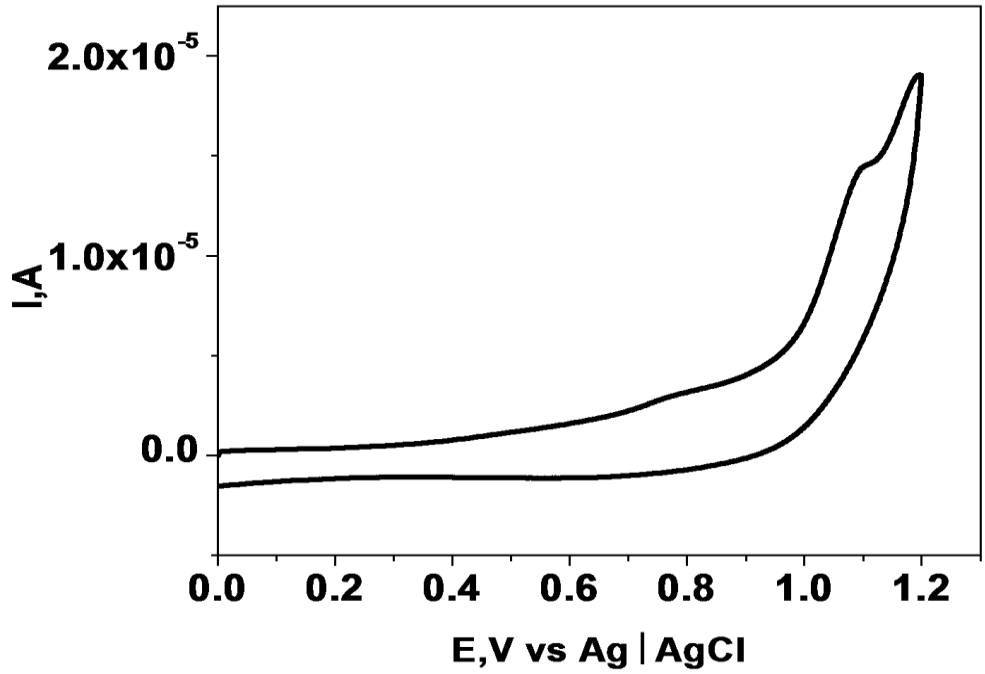

Figure 3B.12: Cyclic voltammograms of NDADPB **(**4 x 10^{-5} M) using the GCE at non aqueous solution with TEAP (0.1M) at scan rate, 100 mV/s

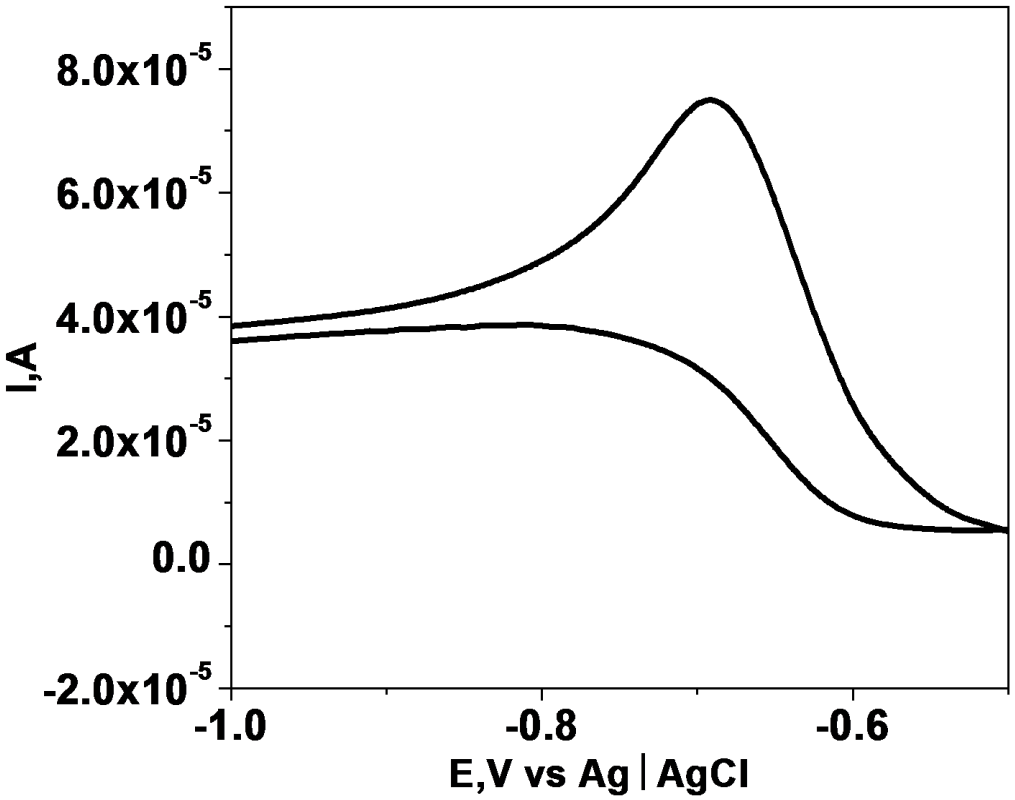

Figure 3B.13: Cyclic voltammogram of NDADPE **(**4 x 10^{-5} M) in DMF on SMDE at scan rate, 0.1 Vs^{-1}, with TEAP (0.1 M)

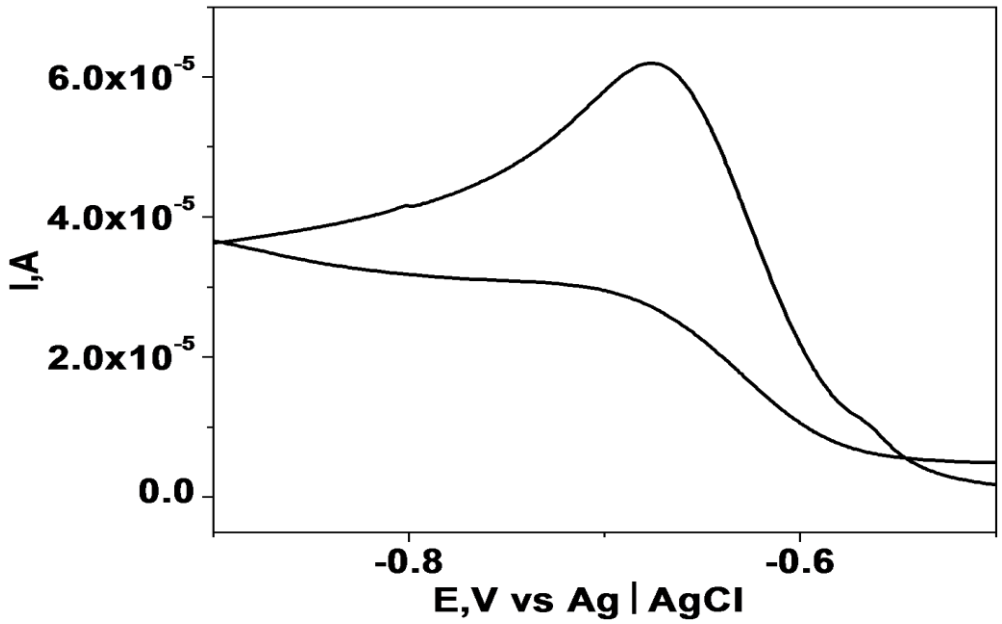

Figure 3B.14: Cyclic voltammogram of NDADPM **(**4 x 10^{-5} M) in DMF on SMDE at scan rate, 0.1 Vs^{-1}, with TEAP (0.1 M)

PART C: MOLECULAR STRUCTURE DETERMINATION BY SINGLE CRYSTAL X-RAY CRYSTALLOGRAPHY AND MOLECULAR MODELING OF NDADPE

Molecular structure determination of NDADPE was undertaken by single crystal XRD. The experimental details are already described in **Chapter II**. Diffraction quality crystals of NDADPE were chosen and the single crystal X-ray diffraction data were collected. No absorption correction was applied. The lattice parameters were determined from least-squares analysis, and reflection data were integrated using the program SHELXTL[10]. The structure was solved by direct methods using SHELXS-97 and refined by full-matrix least squares on F^2 with anisotropic displacement parameters for non-H atoms, using SHELXL-97. The positions of all aromatic and aliphatic C–H hydrogen atoms were calculated geometrically, and a riding model was used in the refinement, with C–H distances in the range of 0.93–0.98 Å and $U_{iso}(H) = 1.2U_{eq}(C)$. All the O–H and N–H hydrogens were refined from difference Fourier maps. The software used to prepare material for publication was Mercury 2.3 (Build RC4), ORTEP-3 and X-Seed[11]. The details of crystal data and refinements are given in **Table 3C.1**. The geometrical parameters of hydrogen bonds in NDADPE are listed in **Table 3C.2**. The selected bond lengths, bond angles and dihedral angles of all the non-hydrogen atoms are given in **Table 3C.3**. The list of atomic coordinate's equivalent, isotropic and anisotropic displacement parameters of the non-hydrogen atoms information file is available in .cif format.

3C.1 Crystal Structure Analysis

The compound NDADPE was crystallizes in triclinic *P*-1 space group with two symmetry. Independent molecular conformers, A&B in the asymmetric unit (Z' = 2). The ORTEP diagrams of the two conformers are shown in **Figure 3C.1**. The way the two conformers stack is exhibited in a stereographic disposition in **Figure 3C.2**. These two molecules are conformational isomers (**Figure 3C.10**). The torsion angles at diphenylether linkage in two molecules are different with each other (C6-C5-O1-C7; –134.25º; C42-C41-O4-C39; 153.5º). In the two conformers, the four naphthol O–H groups form intramolecular interactions with imine N-atoms with O–H···N hydrogen bonds. The two conformers (**A** and **B**) form different hydrogen bonding in the crystal structure. The inversion related molecules of conformer **A,** forms a supramolecular dimer with bifurcated C–H···O hydrogen bond synthon (**Figure 3C.3**). Conformer **B,** also forms a supramolecular dimer synthon with C–H···O hydrogen bonds (**Figure 3C.4**). The two dimers of **A** and **B** conformers interact with the

single and bifurcated C–H···O hydrogen bonds (**Figure 3C.5**). But the molecules of conformer **B,** form a supramolecular helix due to bifurcated C–H···O hydrogen bond synthons (**Figures 3C.6 a& b**). The dimers of conformer **A** and helices of conformer **B** connect via C–H···O hydrogen bonding. The overall molecular aggregation of conformers, **A** and **B** of NDADPE results in a corrugated tape like structure (**Figure 3C.7**), and in such corrugation conformers of **B** form a helical structure due to the bifurcated C–H···O interactions.

3C.2 Hirshfeld Surface Analysis

The challenging task is to successfully differentiate the conformational polymorphism by analyzing the crystal structures. The Hirshfeld surface analysis makes it easy to differentiate the polymorphic forms and conformational polymorphism[12]. Since the Hirshfeld surfaces are directly depend on the molecular environment, these are unique in the given crystal structure and they depend on the number of crystallographically independent molecules present in the asymmetric unit. Here we have applied the Hirshfeld surface and 2D fingerprint plots to analyze the conformers **A** and **B** of NDADPE**.**

The 2D fingerprint plots of Schiff base NDADPE were derived from the Hirshfeld surface by plotting the fraction of points on the surface as a function of the pair (d_i, d_e). Each point on the standard 2D graph represents a bin formed by discrete intervals of d_i and d_e (0.01 X 0.01 Å), and the points are colored as a function of the fraction of surface points in that bin, with a range from blue (relatively fewer points) through green (moderate fraction). The Hirshfeld surfaces and 2D fingerprint plots are given in **Figure 3C.8**. It is obvious from this analysis that the two conformers **A** and **B** of NDADPE are completely different and exhibit the conformational isomerism. Inspection of the fingerprint plots in **Figure 3C.9** highlights the major differences between the two conformers. Conformer **A** features the diffuse region of the blue points between the hydrogen bond spikes, while this feature is sharpened with extra spike in the fingerprint plot of conformer **B.**

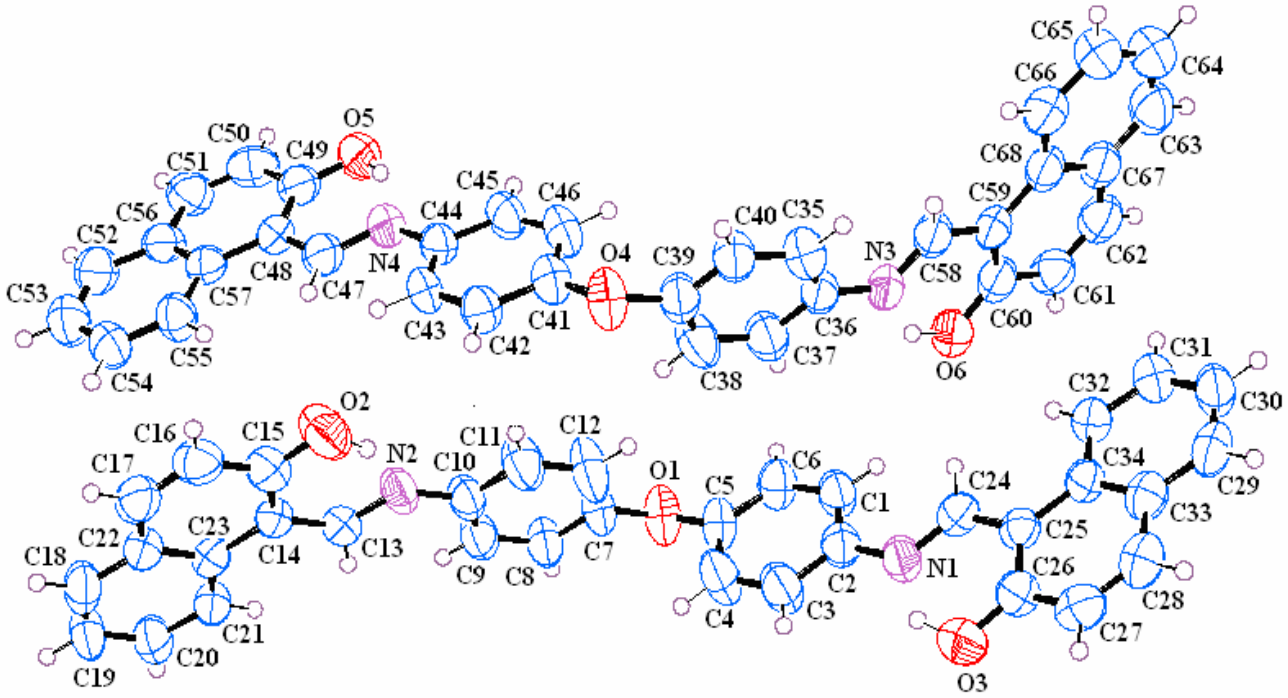

Figure 3C.1: ORTEP representation of conformers **A** and **B** of NDADPE ligand. Thermal ellipsoids are drawn at 50% probability level

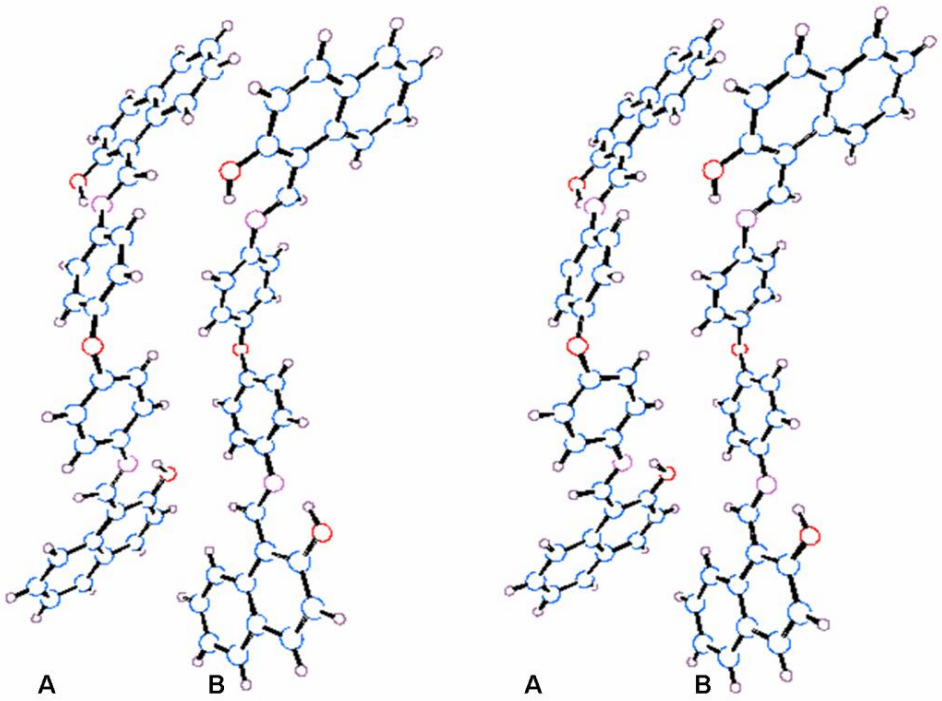

Figure 3C.2: Stereovision of the two conformers **A** and **B**, of NDADPE in the asymmetric unit

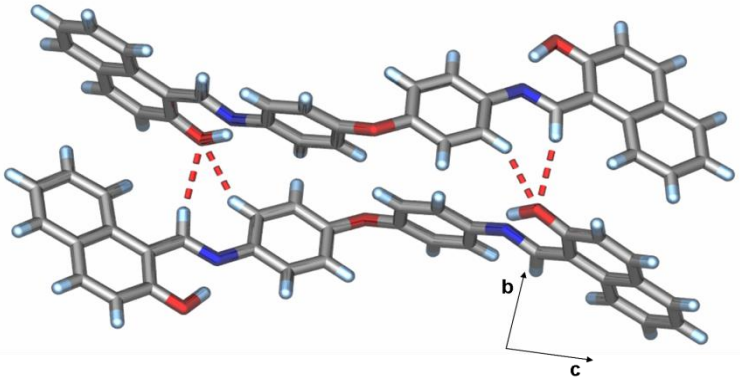

Figure 3C.3: Supramolecular dimer of conformer **A.** The two conformer **A** molecules interacting with bifurcated C–H···O hydrogen bonds

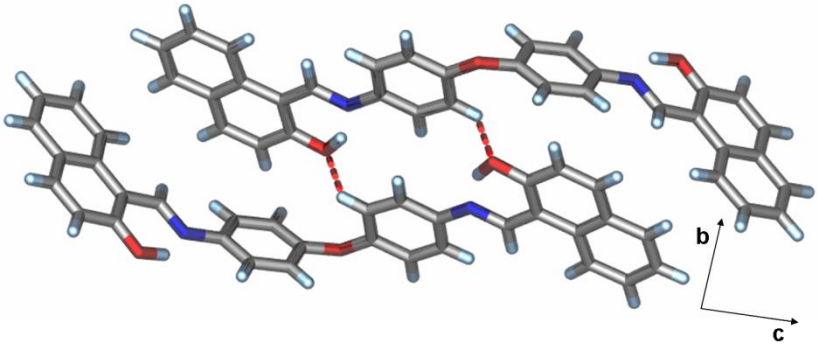

Figure 3C.4: Supramolecular dimer of conformer **B.** The two conformer **B** molecules interacting with the C–H···O hydrogen bonds

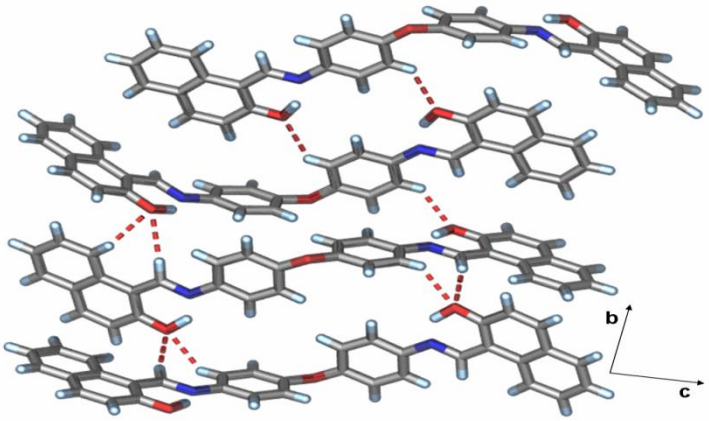

Figure 3C.5: Spatial disposition of the two conformers **A** and **B** as viewed along the bc-planes. The two supramolecular dimers of conformer **A** and **B** connect via C–H···O and bifurcated C–H···O hydrogen bonds

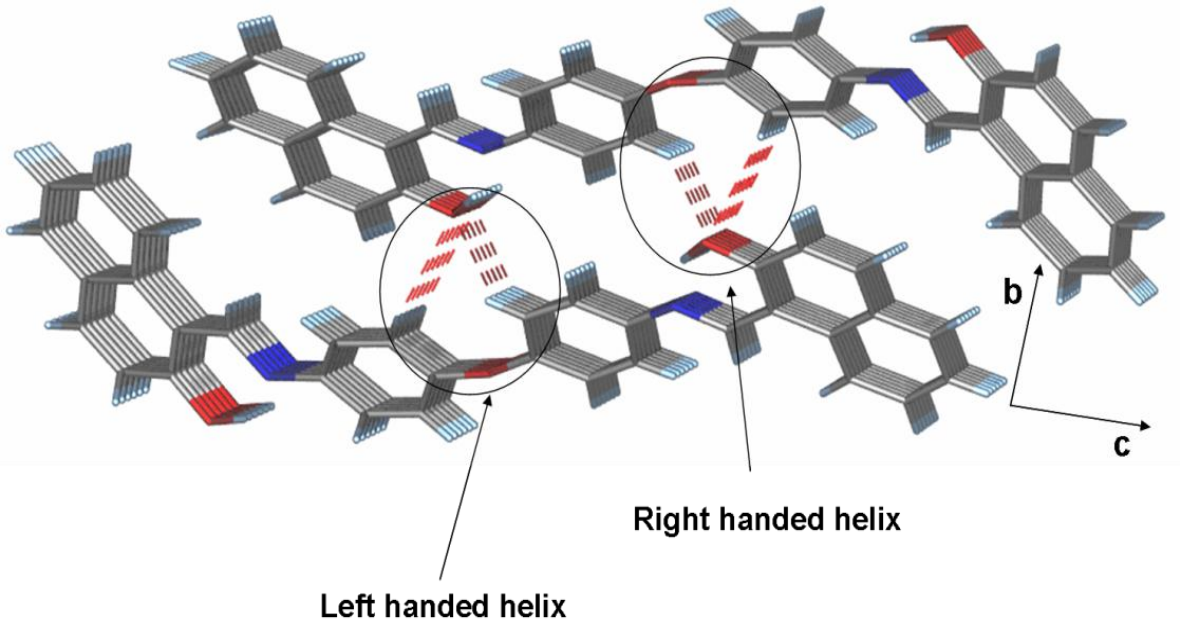

(**a**)

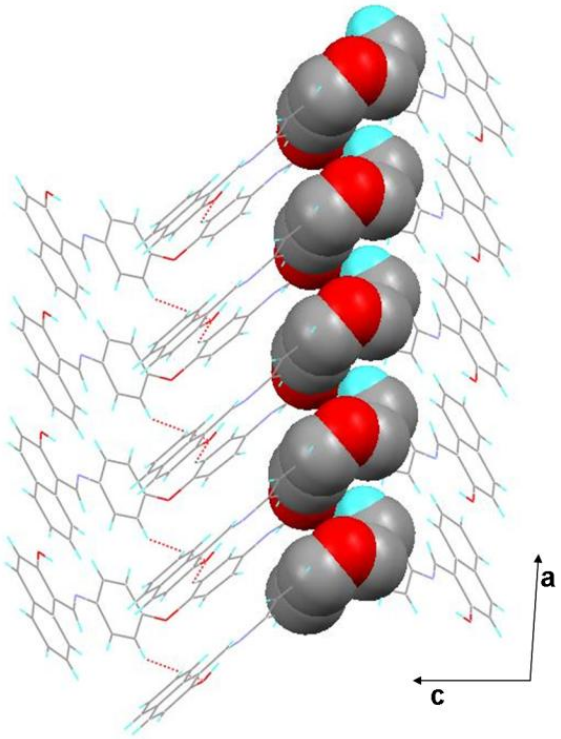

(**b**)

Figure 3C.6: Molecular packing array of conformer **B**, (a) viewed along bc plane; ((b) viewed along ac plane (atomic segments forming the helical structure shown in CPK spacefilling manner)

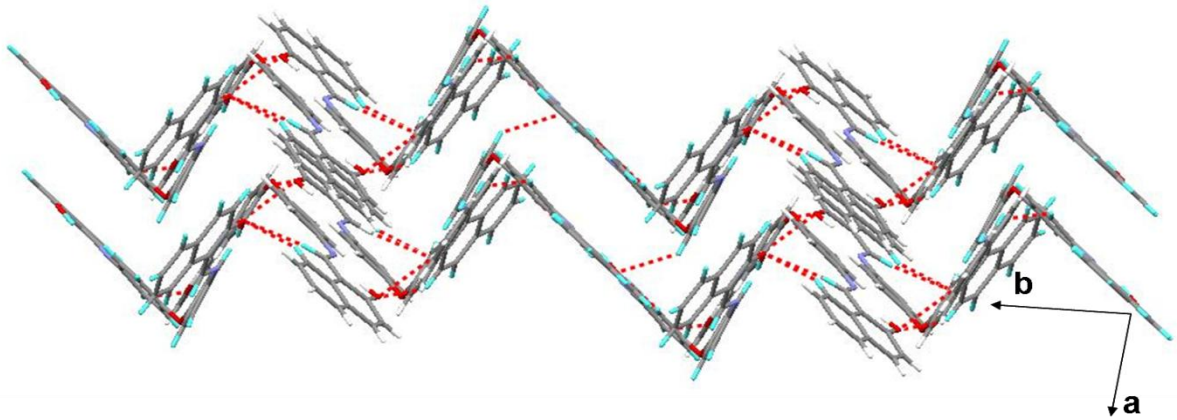

Figure 3C.7: Corrugated layered structure formed by conformers, **A** and **B** of NDADPE, viewed over ab plane

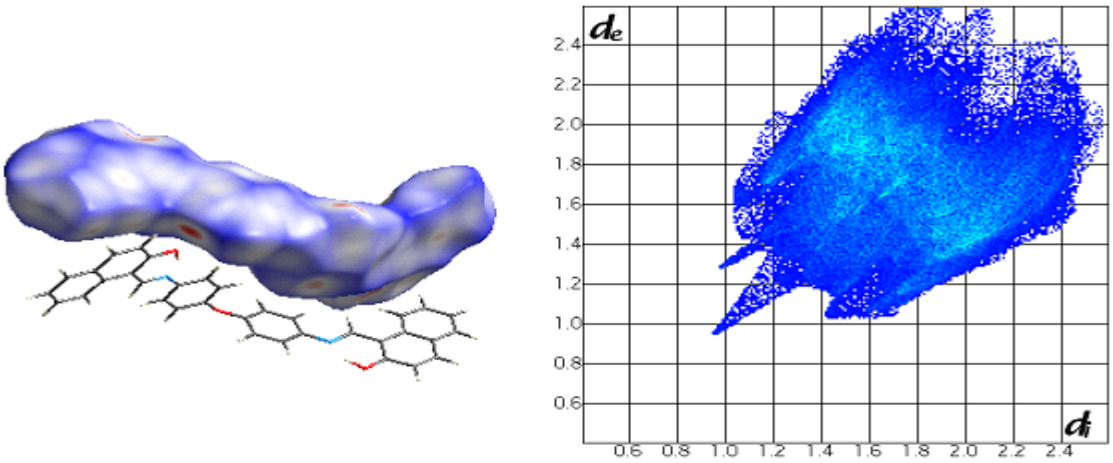

Figure 3C.8: Hirshfeld surface and 2D fingerplots of conformer **A**

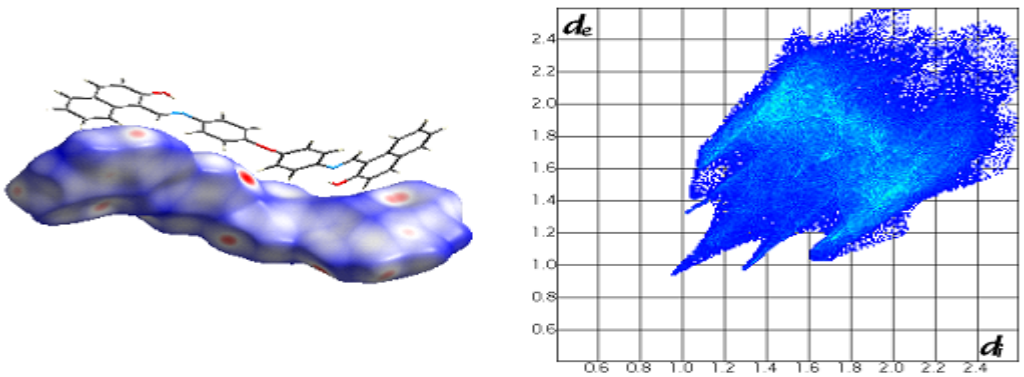

Figure 3C.9: Hirshfeld surface and 2D fingerplots of conformer **B**

Table 3C.1: *Crystallographic and experimental data of NDADPE*

Empirical formula	$C_{34}\ H_{24}\ N_2\ O_3$
Formula weight	508.55
Temperature	293(2) K
Wavelength	1.54184 Å
Crystal system	Triclinic
Space group	*P*-1
a/Å	a = 5.2902(6)
b/Å	b = 20.195(2)
c/Å	c = 23.832(3)
α/°	α= 87.860(9)
β/°.	β= 86.386(9)
γ/°	γ = 85.286(9)
Volume	2531.1(5) $Å^3$
Z	4
Density (calculated)	1.335 mg/m^3
Absorption coefficient	0.684 mm^{-1}
F(000)	1064
Crystal size	0.42 x 0.18 x 0.08 mm^3
Theta range for data collection	2.83 to 58.92°.
Index ranges	-5<=h<=4, -21<=k<=22, -26<=l<=25
Reflections collected	11529
Independent reflections	7043 [R(int) = 0.0580]
Completeness to theta = 58.92°	96.9 %
Absorption correction	multi-scan
Max. and min. transmission	0.947 and 0.8623
Refinement method	Full-matrix least-squares on F^2
Data / restraints / parameters	7043 / 0 / 736
Goodness-of-fit on F^2	0.973
Final R indices [I>2sigma(I)]	R1 = 0.0649, wR2 = 0.1796
R indices (all data)	R1 = 0.1492, wR2 = 0.1280
Extinction coefficient	0.00048(7)
Largest diff. peak and hole	0.162 and -0.199 $e.Å^{-3}$
CCDC	833469

Table 3C.2: *Geometrical parameters of hydrogen bonds in NDADPE*

Compound	D–H···A[a]	D–A (Å)	H···A (Å)	D–H···A (°)
NDADPE	Intra O(2)–H(2)···N(2)	2.519(6)	1.61(11)	153(11)
	Intra O(3)–H(3A)···N(1)	2.510(6)	1.69(10)	136(8)
	Intra O(5)–H(5)···N(4)	2.525(6)	1.60(8)	154(9)
	Intra O(6)–H(6A)···N(3)	2.504(6)	1.67(8)	139(6)
	C(9)–H(9)···O(3)	3.235(7)	2.4	141
	C(43)–H(43)···O(2)	3.087(6)	2.37	134

[a] All of the C–H, N–H and O–H bonds are neutron normalized to 1.083, 1.009 and 0.983Å respectively.

3C.3 Molecular Modeling Studies

Molecular modeling studies have been done on NDADPE, NDADPM, NDADPD, NDADPT and NDADPB to understand the stability, intramolecular hydrogen bonding and conformational analysis and to verify whether the mechanisms proposed for the thermodynamic, spectroscopic and electrochemical behavior of the compound are tenable.

Molecular modeling was performed on NDADPE using ChemOffice Ultra (version 11.0**)** to arrive at the molecular geometric properties and an intramolecular interaction such as H-bonding, etc. In **Table 3C.3** are shown some of the most relevant bond lengths and bond angles obtained from X-ray crystallography (excerpts of **Table 3C.3**) along with those from molecular modeling. There is an excellent agreement among the respective experimental and modelled data. In **Figures 3C.11-3C.13** are shown the torsional

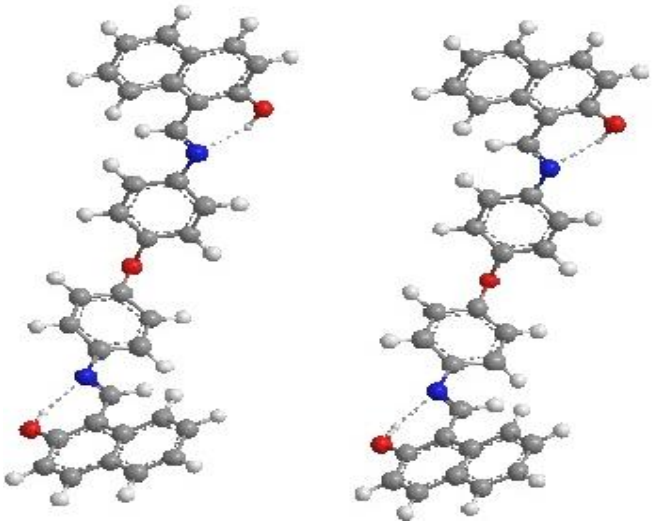

Figure 3C.10: Stereographic view of NDADPE after global minimization along with the scheme of the atoms

energy conformational 3-d plots. It is found that the free molecule has the stablest disposition with C(7)-O(1)-C(5)-C(6) dihedral angle of C(7)-O(1)-C(5) and with C(2)-N(1)-C(24)-C(25) of C(2)-N(1)-C(24) this is slightly different from the experimental X-ray data of **Table 3C.3**. This slight difference is attributed to the fact that modeling considers only one molecule. The structure of the energy minimised free molecule is shown in **Figure 3C.10** in its stereographic projection.

The quantum mechanical HOMO-LUMO orbital energy calculations have been used for computing the expected gas-phase electronic transitions. Some of the important molecular LUMO, HOMO orbitals are shown in **Figures 3C.14**. These values are collected in **Table 3C.4** along with the experimental spectral data. The theoretical and experimental absorption maxima are in great agreement. The solvent accessible zonal cloud is NDADPE in **Figure 3C.15**.

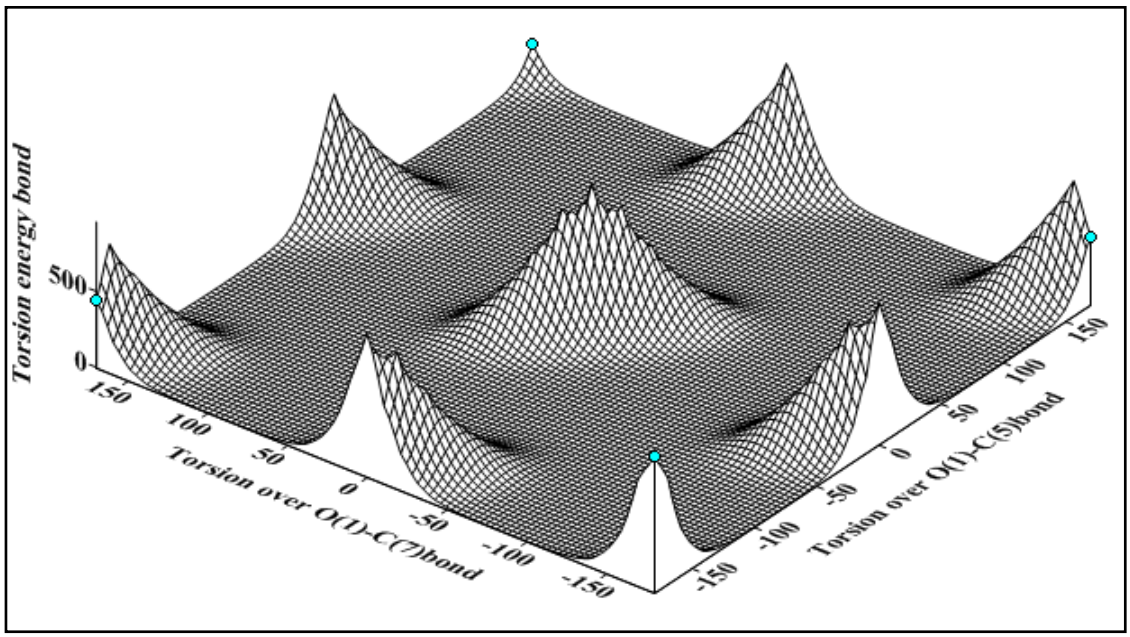

Figure 3C.11: Double dihedral torsional energy plot of NDADPE (left) over O(1)-C(7) and C(18-C(19) bonds from -180 to +180^{o} and (right) double dihedral plot over C(7)-O(1)-C(5) bonds (Refer **Figure 3C.10** for numbering scheme for the atoms)

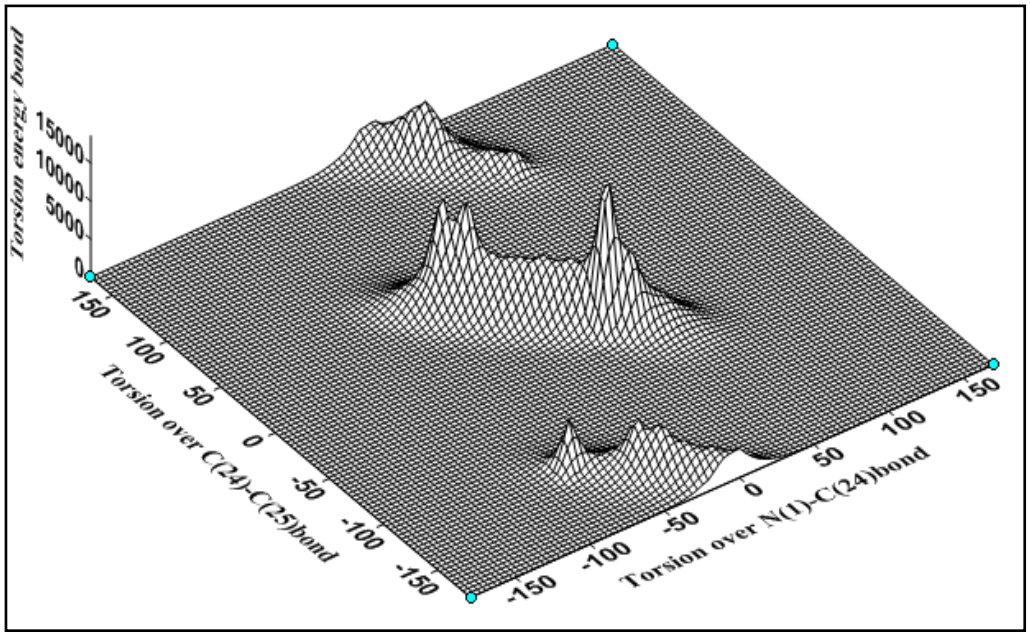

Figure 3C.12: Double dihedral torsional energy plot of NDADPE (left) over C(24)-C(25)and N(1)-C(24) bonds from -180 to +180^{o} and (right) double dihedral plot over N(1)-C(24)-C(25) bonds (Refer **Figure 3C.10** for numbering scheme for atoms)

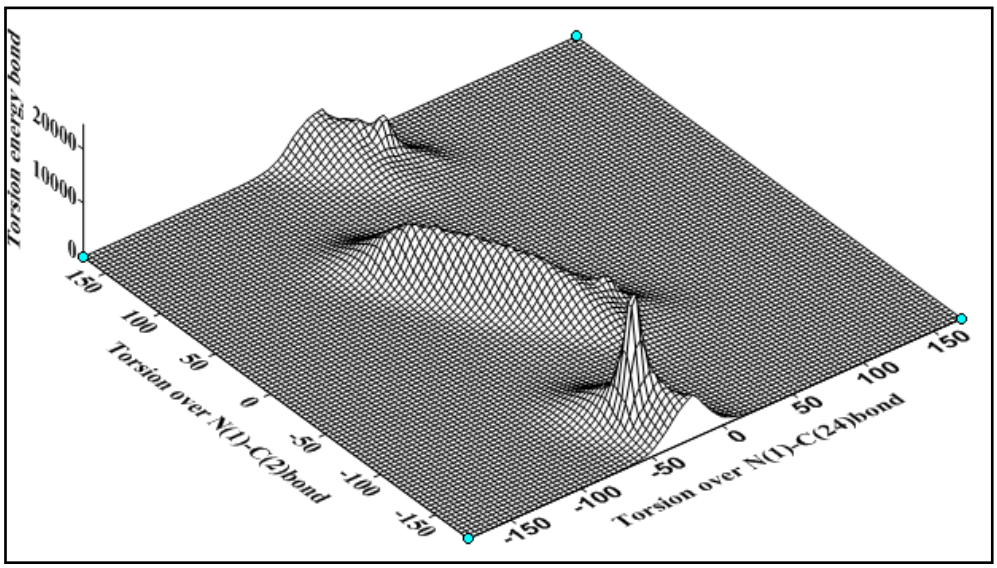

Figure 3C.13: Double dihedral torsional energy plot of NDADPE (left) over N(1)-C(2)and N(1)-C(24) bonds from -180 to +180^{o} and (right) double dihedral plot over C(2)-N(1)-C(24) bonds (Refer **Figure 3C.10** for numbering scheme for atoms)

Table 3C.3: *Bond lengths (Å), bond angles (deg) and dihedral angles (deg) for NDADPE*

Atoms	**XRD Data(q_1)**	**Molecular modeling data(q_2)**	**$\Delta q = q_1 - q_2$**
O(2)-C(15)	1.301(6)	1.361	0.06
C(14)-C(13)	1.425(7)	1.431	0.006
C(36)-C(37)	1.364(6)	1.376	0.0156
C(34)-C(33)	1.412(6)	1.419	0.0065
C(44)-C(45)	1.367(6)	1.373	0.0061
C(48)-C(49)	1.422(7)	1.429	0.0067
C(34)-C(25)	1.448(6)	1.439	-0.0093
C(23)-C(21)	1.404(6)	1.411	0.0066
C(33)-C(28)	1.420(7)	1.424	0.0038
C(10)-C(11)	1.371(7)	1.373	0.0022
C(57)-C(55)	1.410(7)	1.420	0.0095
C(41)-C(46)	1.389(7)	1.389	0.0003
C(34)-C(25)	1.448(6)	1.478	0.0297
N(3)-C(58)	1.284(6)	1.284	0.0003
N(4)-C(44)	1.429(6)	1.432	0.0032
C(34)-C(32)	1.401(6)	1.402	0.0006
C(57)-C(56)	1.396(7)	1.397	0.0012
C(34)-C(32)	1.401(6)	1.402	0.0007
C(23)-C(21)	1.404(6)	1.403	-0.0013
C(54)-C(53)	1.391(7)	1.394	0.003
C(34)-C(32)	1.401(6)	1.402	0.0007
O(1)-C(5)	1.382(6)	1.369	-0.0135
O(6)-C(60)	1.315(6)	1.368	0.0532
C(22)-C(18)	1.392(7)	1.402	0.0103
C(10)-C(9)	1.390(7)	1.397	0.0068
C(20)-C(19)	1.390(7)	1.401	0.0114
C(54)-C(53)	1.391(7)	1.401	0.0104
C(56)-C(52)	1.409(7)	1.394	-0.0148
C(34)-C(32)	1.401(6)	1.403	0.0023
C(58)-C(59)	1.428(7)	1.432	0.0043
O(3)-C(26)	1.303(6)	1.361	0.058
N(3)-C(58)	1.289(6)	1.285	-0.0037

C(34)-C(25)	1.448(6)	1.477	0.0285
C(24)-C(25)	1.428(6)	1.425	-0.0032
C(43)-C(42)	1.364(6)	1.372	0.0076
C(33)-C(28)	1.420(7)	1.422	0.002
C(44)-C(43)	1.389(6)	1.389	0
C(14)-C(23)	1.441(6)	1.442	0.0008
C(6)-C(1)	1.378(6)	1.374	-0.0044
C(67)-C(62)	1.426(7)	1.428	0.0015
C(57)-C(56)	1.396(7)	1.410	0.0136
C(58)-C(59)	1.428(7)	1.431	0.0028
C(6)-C(1)	1.375(6)	1.376	0.0011
C(34)-C(33)	1.412(6)	1.418	0.0056
C(41)-O(4)-C(39)	116.6(4)	116.7	0.1000
C(13)-N(2)-C(10)	125.9(5)	125.9	0.0000
C(58)-N(3)-C(36)	124.4(5)	124.5	0.1000
C(24)-N(1)-C(2)	124.1(5)	124.3	0.2000
C(49)-O(5)-H(5)	103(6)	103.0	0.0000
C(47)-N(4)-C(44)	124.8(5)	124.9	0.1000
C(26)-O(3)-H(3A)	113(6)	113.0	0.0000
C(60)-O(6)-H(6A)	113(5)	113.0	0.0000
C(45)-C(44)-C(43)	119.6(5)	119.7	0.1000
C(45)-C(44)-N(4)	116.8(5)	116.9	0.1000

Table 3C.4: *HOMO-LUMO energies of* H_2L^i

Species	$\Delta H^o_{f(kcal/mol)}$	**HOMO (eV)**	**LUMO (eV)**	**Calculated λ_{max} (nm)**	**Observed λ_{max} (nm)**
NDADPE	214.89	-9.746	-4.658	235	388
NDADPM	326.47	-9.570	-4.856	254	380
NDADPD	18.45	-9.21	-5.15	254.5	321.5
NDADPT	347.11	-9.96	-4.73	254.5	321.5
NDADPB	347.10	-9.676	-4.962	254	400

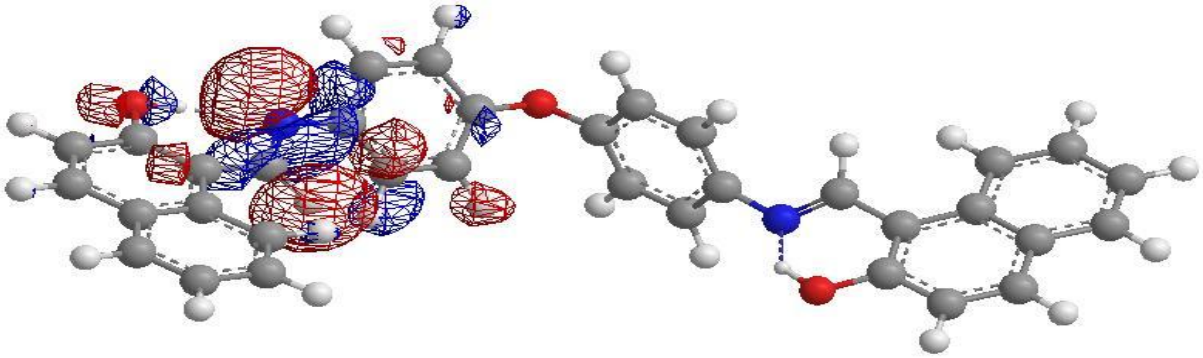

HOMO

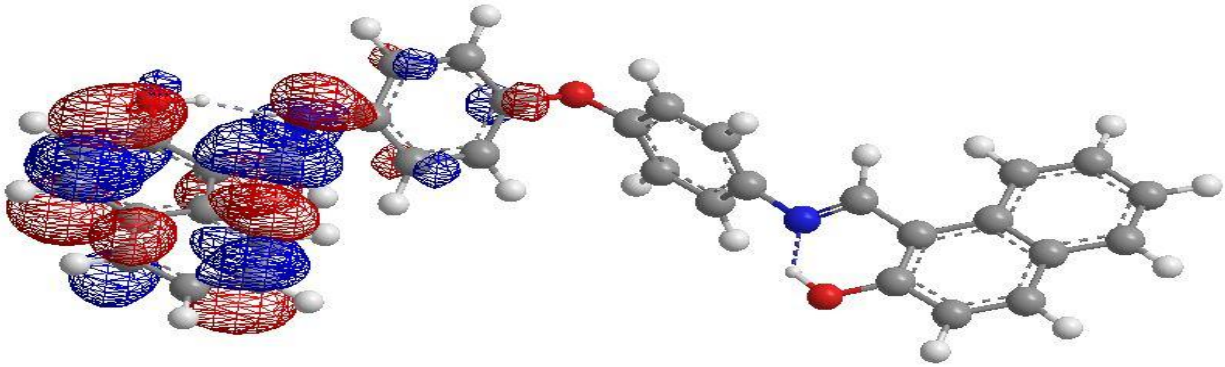

LUMO

Figure 3C.14: HOMO, LUMO molecular orbitals of NDADPE in wire mesh format

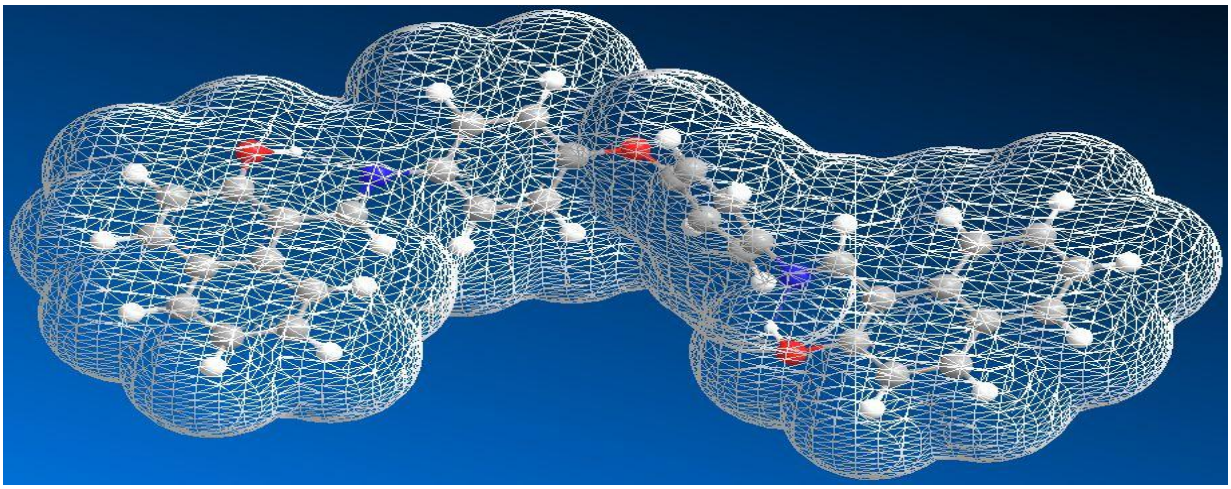

Figure 3C.15: Solvent accessible zonal cloud of NDADPE in wire mesh found

The possible energy minimized structure of NDADPM shown in **Figure 3C.16** along with stereographical projection and the numbering pattern is follows as shown in energy minimized structure in **Figure 3C.17**.

Single and double dihedral rotations were carried out over various bonds to acquire the global minima of the compound. Some of the 3d-plots torsional angle vs torsional energy are presented in **Figures 3C.18-3C.20.**

The conformational energy profiles of NDADPM for torsional angles over a few selected bonds are shown in **Figure 3C.22**. Some of the important Geometric Parameters of NDADPM is presented in **Table 3C.5**

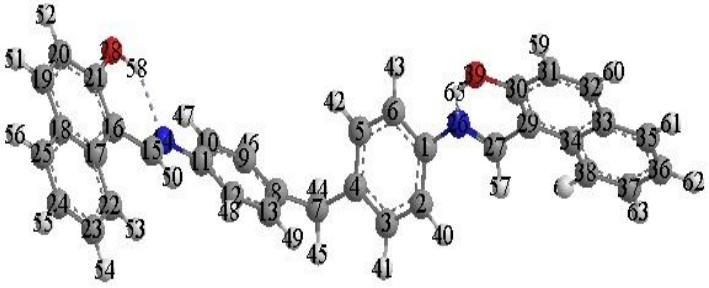

Figure 3C.16: Energy minimized monographic stereographic image of NDADPM generated from energy minimization through MM_2 calculations (lone pairs of electrons are removed for clarity)

To verify the observed wavelengths we have calculated the λ values from HOMO, LUMO energy values and they are presented in **Table 3C.4**. The molecular orbital surface of the HOMO and LUMO are shown in **Figure 3C.21**. The minor deviations are understood to be due to the fact that the molecular modeling does not take the crystal packing and multidirectional intermolecular interactions into reliable consideration of NDADPM

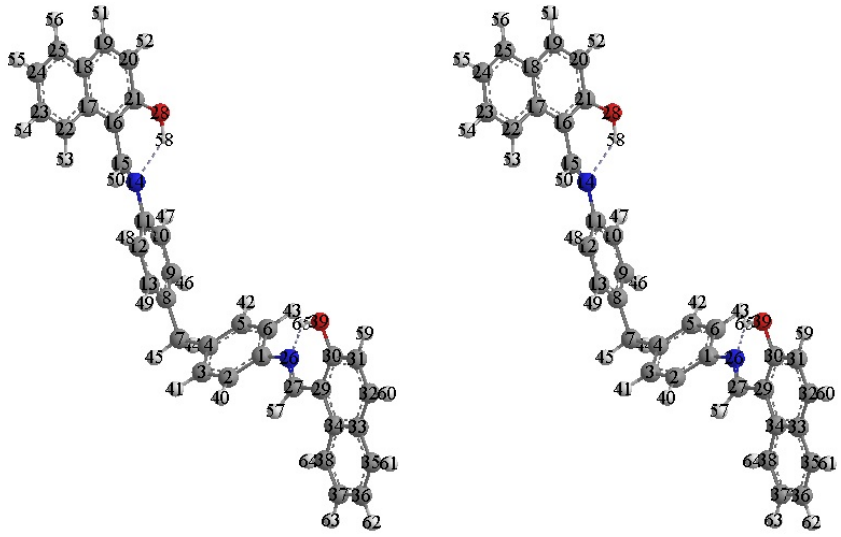

Figure 3C.17: Energy minimized structure and stereographic image of NDADPM generated from energy minimization through MM_2 calculations (lone pairs of electrons are removed for clarity)

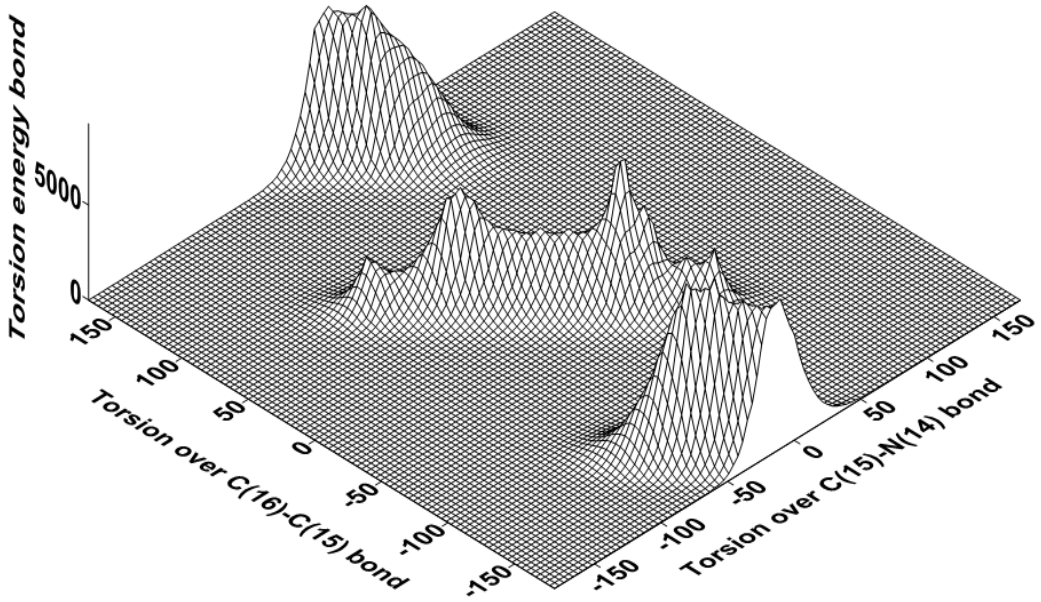

Figure 3C.18: Double dihedral torsional energy plot of NDADPM (left) over C(16)-C(15) and C(15)-N(14) bonds from -180 to +180^{o} and (right) double dihedral plot over C(16)-C(15)-N(14) bonds (Refer **Figure 3C.17** for numbering scheme for the atoms)

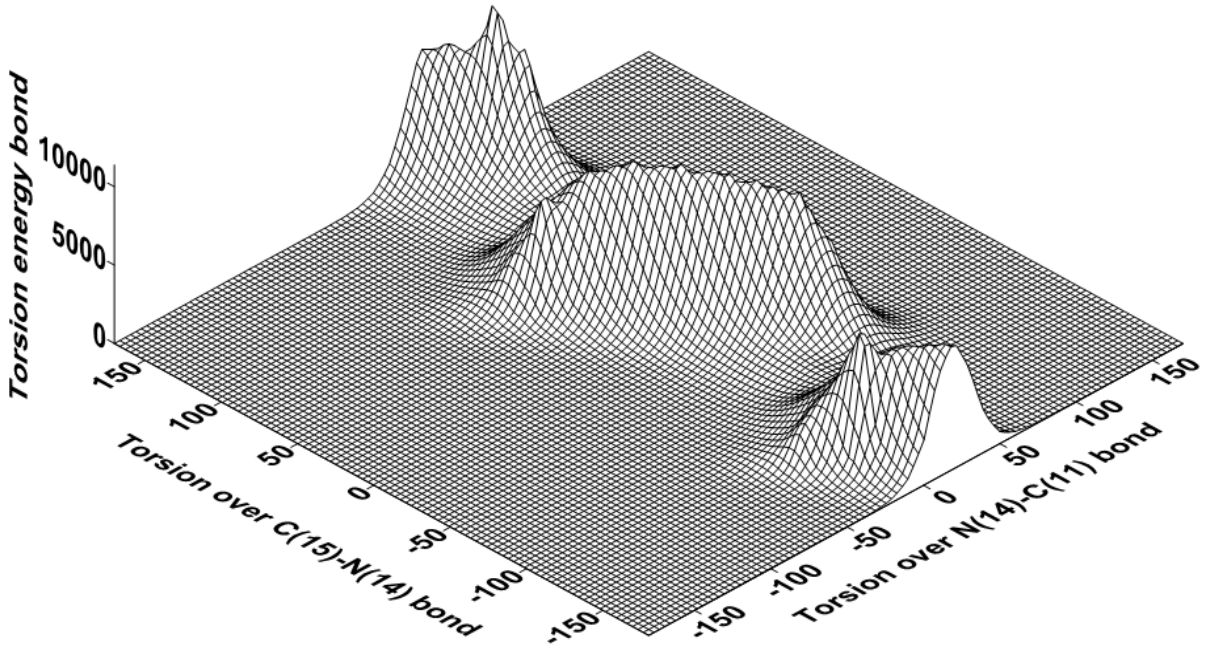

Figure 3C.19: Double dihedral torsional energy plot of NDADPM (left)over C(15)-N(14) and N(14)-C(11) bonds from -180 to +180^{o} and (right) double dihedral plot over C(15)-N(14)-C(11) bonds (Refer **Figure 3C.17** for numbering scheme for the atoms)

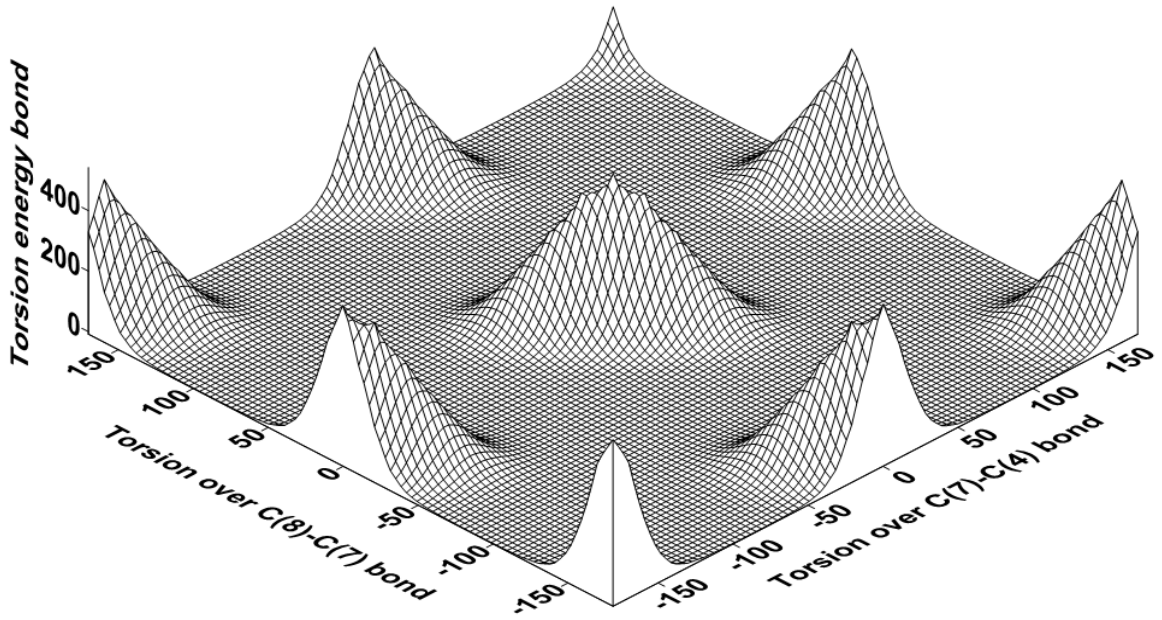

Figure 3C.20: Double dihedral torsional energy plot of NDADPM (left)over C(8)-C(7) and C(14)-C(4) bonds from -180 to +180^{o} and (right) double dihedral plot over C(8)-C(7)-C(4) bonds (Refer **Figure 3C.17** for numbering scheme for the atoms)

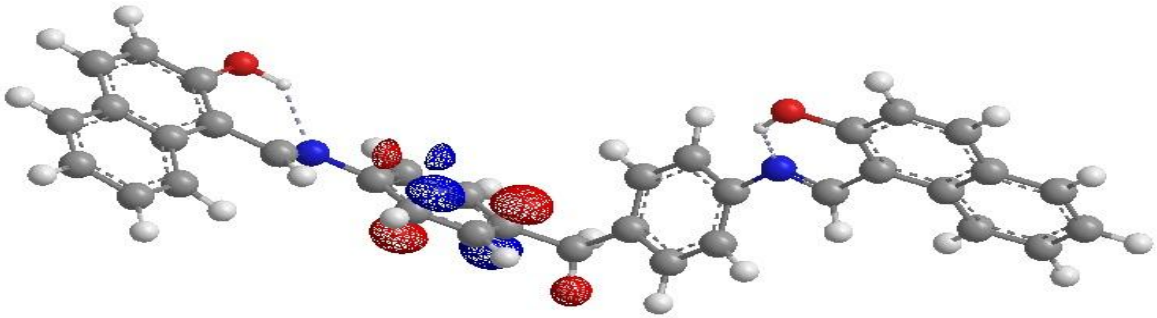

LUMO

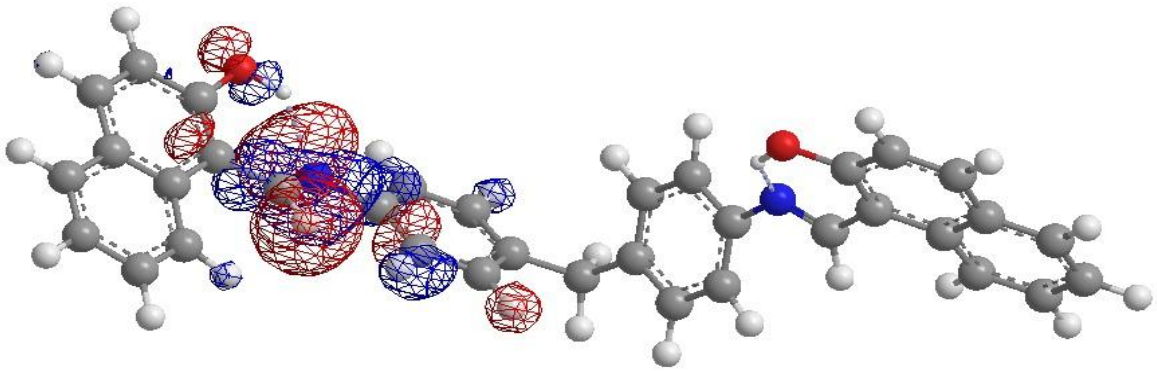

HOMO

3C.21: HOMO, LUMO molecular orbitals of NDADPM in wire mesh format

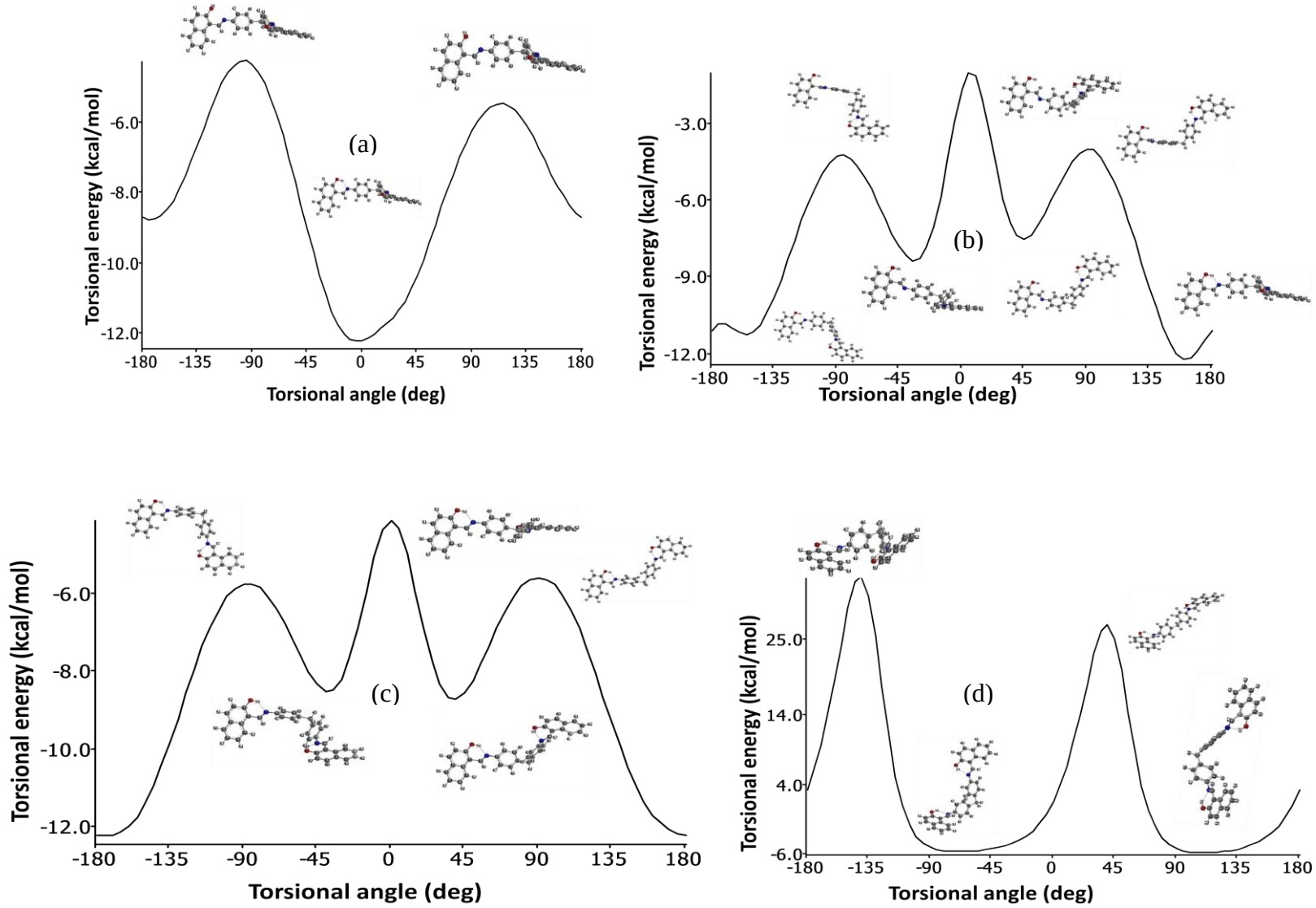

Figure 3C.22: Conformational analysis of NDADPM over (a) C_{21}-O_{28}, (b) C_{16}-C_{15}, (c) $N1_4$-C_{11} and (d) C_8-C_7

Table 3C.5: *Some of the important geometric parameters of NDADPM*

Bond	Bond length (A^o)	Bond	Bond angle (deg)	Bond	Dihedral angle (deg)
C_{16}-C_{15}	1.47	C_8-C_7-C_{14}	111.4	-C_8-C_7-C_4-C_3-	117.0
C_{15}-N_{14}	1.28	C_{15}-N_{14}-C_{11}	123.2	-C_{16}-C_{15}-N_{14}-C_{11}-	-180
N_{14}-C_{11}	1.43	C_{16}-C_{15}-N_{14}	125.8	-C_{15}-N_{14}-C_{11}-C_{11}-	160
O_{28}-C_{21}	1.36	O_{28}-C_{21}-C_{16}	122.9	-O_{28}-C_{21}-C_{16}-C15-	-0.9
C_8-C_7	1.51			-C_{21}-C_{16}-C_{15}-N_{14}-	-17.3

The possible energy minimized structure of NDADPD shown in **Figure 3C.23** along with stereographical projection and the numbering pattern is follows as shown in energy minimized structure in **Figure 3C.24**.

Single and double dihedral rotations were carried out over various bonds to acquire the global minima of the compound. Some of the 3d-plots torsional angle vs torsional energy are presented in **Figures 3C.25-3C.27.**

The conformational energy profiles of NDADPD for torsional angles over a few selected bonds are shown in **Figure 3C.29**. Some of the important Geometric Parameters of NDADPD is presented in **Table 3C.6.**

To verify the observed wavelengths we have calculated the λ values from HOMO, LUMO energy values and they are presented in **Table 3C.4**. The molecular orbital surface of the HOMO and LUMO are shown in **Figure 3C.28**. The minor deviations are understood to be due to the fact that the molecular modeling does not take the crystal packing and multidirectional intermolecular interactions into reliable consideration of NDADPD**.**

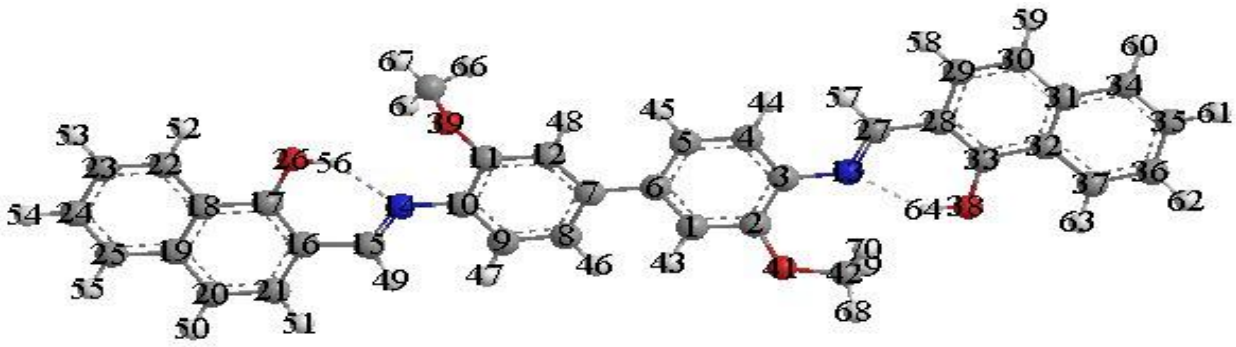

Figure 3C.23: Energy minimized monographic stereographic image of NDADPD generated from energy minimization through MM_2 calculations (lone pairs of electrons are removed for clarity)

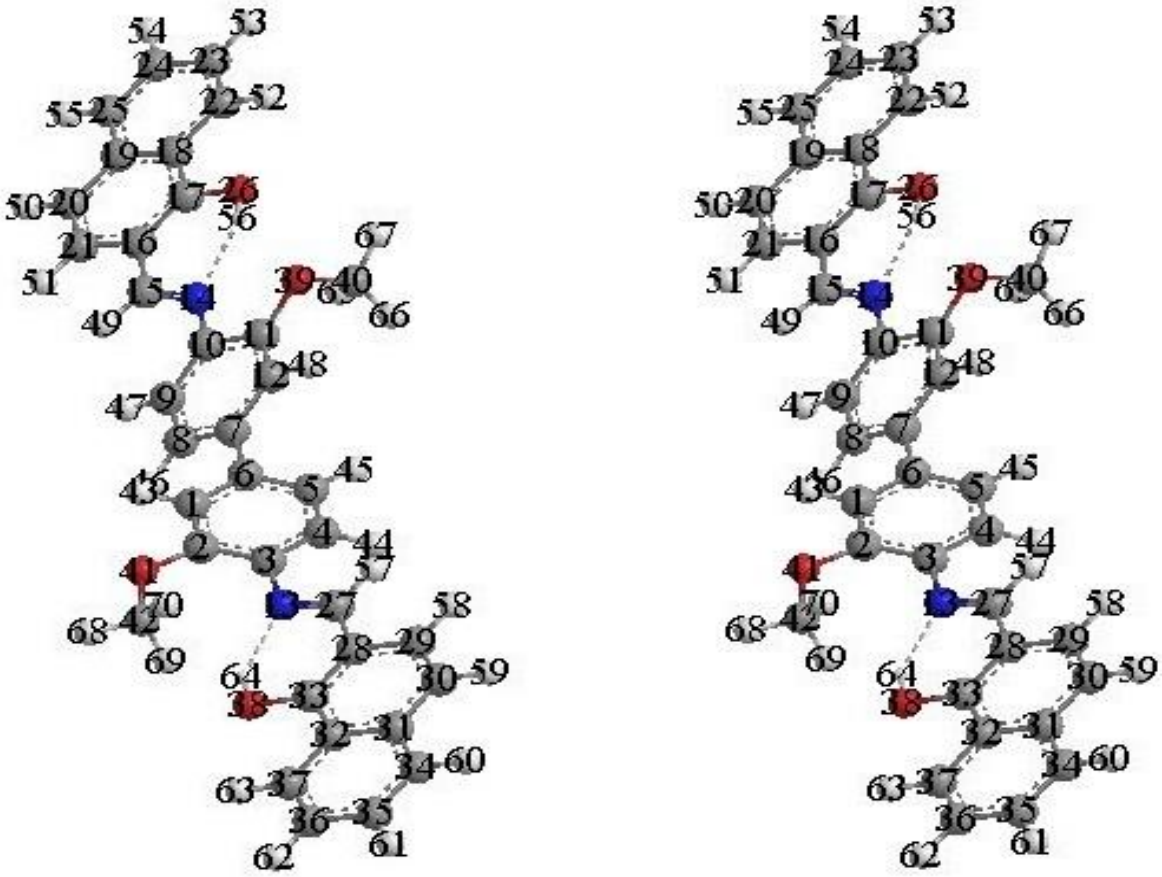

Figure 3C.24: Stereographic view of NDADPD after global minimization

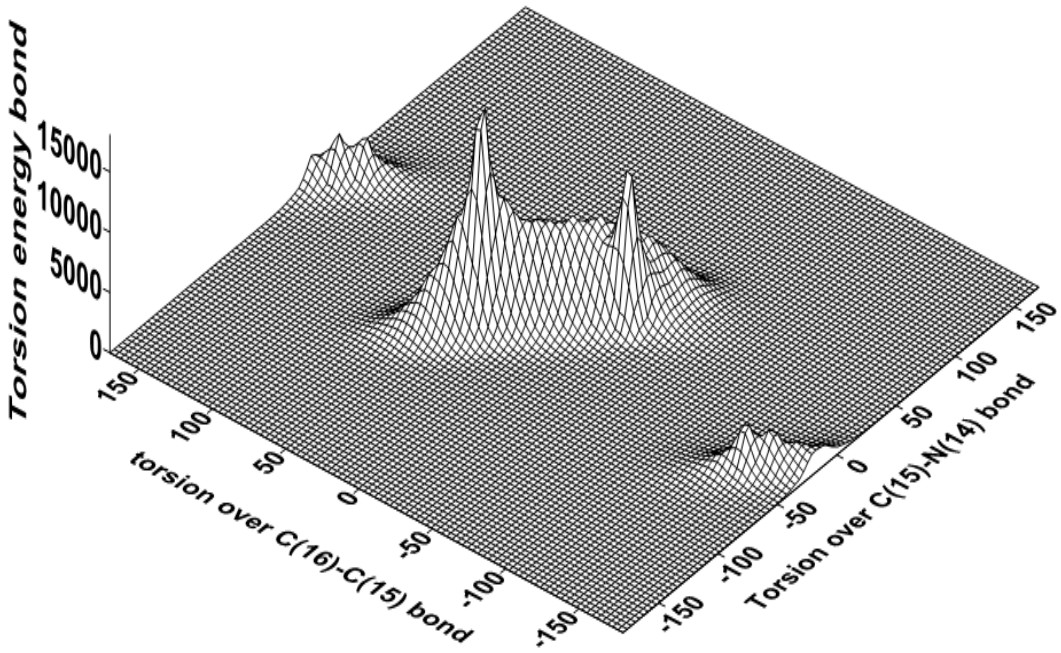

Figure 3C.25: Double dihedral torsional energy plot of NDADPD (left)over C(16)-C(15) and C(15)-N(14) bonds from -180 to +180^{o} and (right) double dihedral plot over C(16)-C(15)-N(14) bonds (Refer **Figure 3C.24** for numbering scheme for the atoms)

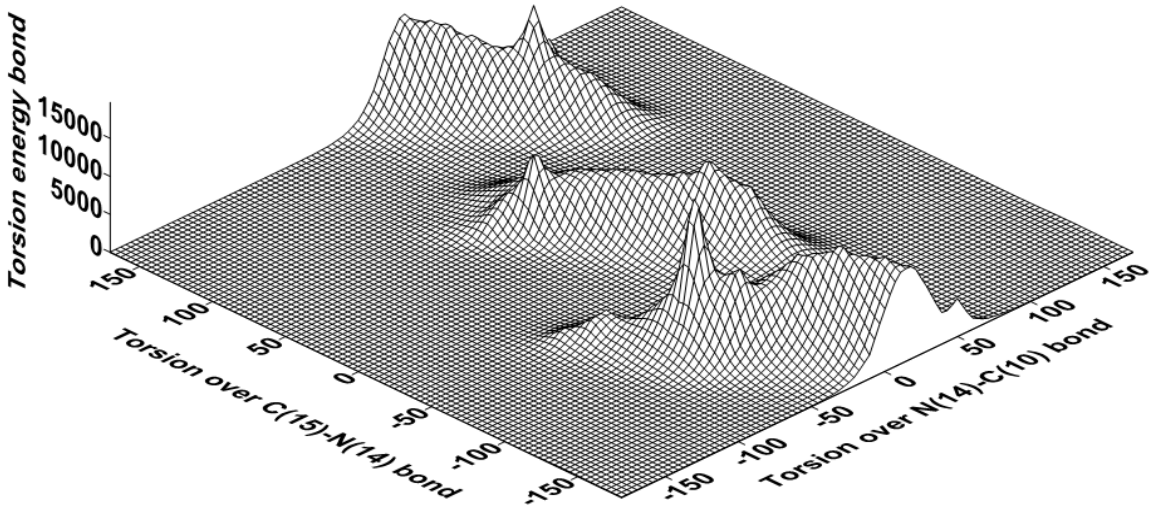

Figure 3C.26: Double dihedral torsional energy plot of NDADPD (left)over C(15)-N(14) and N(14)-C(11) bonds from -180 to +180^{o} and (right) double dihedral plot over C(15)-N(14)-C(11) bonds (Refer **Figure 3C.24** for numbering scheme for the atoms)

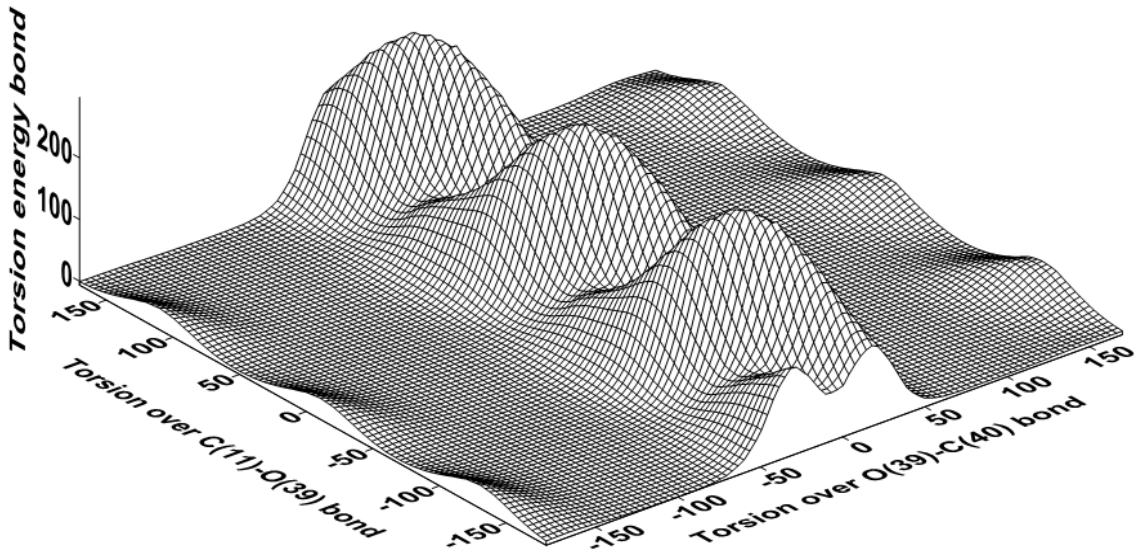

Figure 3C.27: Double dihedral torsional energy plot of NDADPD (left) over C(8)-C(7) and C(14)-C(4) bonds from -180 to +180^{o} and (right) double dihedral plot over C(8)-C(7)-C(4) bonds (Refer **Figure 3C.24** for numbering scheme for the atoms)

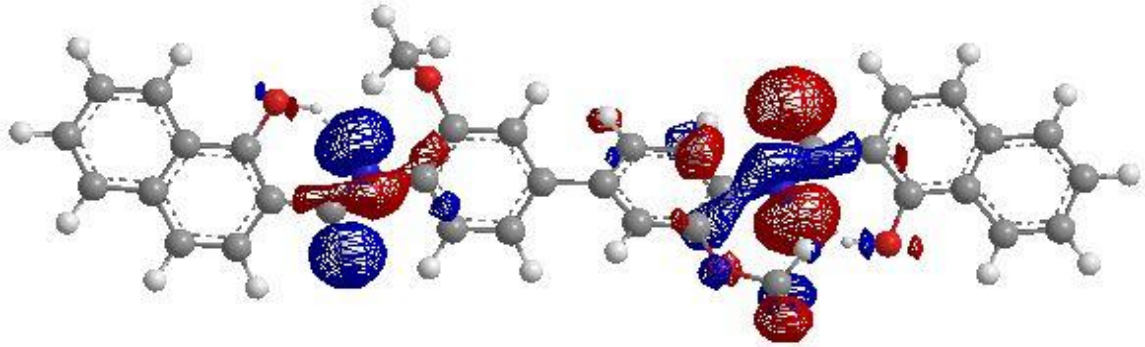

HOMO

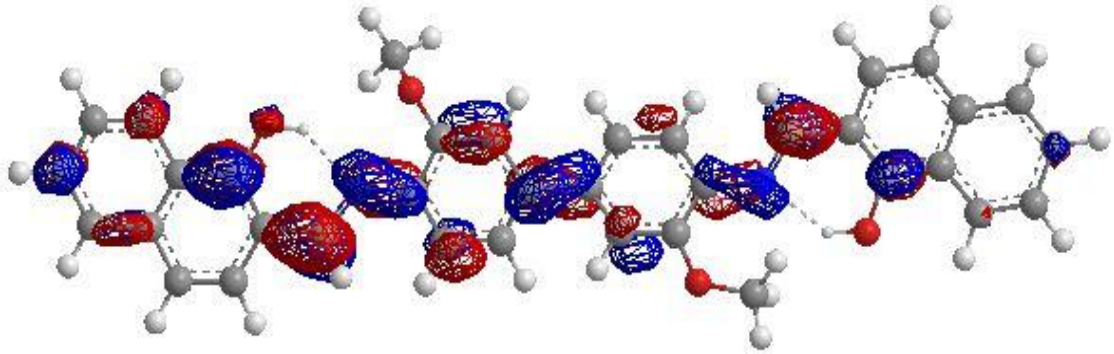

LUMO

Figure 3C.28: HOMO, LUMO molecular orbitals of NDADPD

Table 3C.6: *Some of the important geometric parameters of NDADPD*

Bond	Bond length (A^o)	Bond	Bond angle (deg)	Bond	Dihedral angle (deg)
C_{15}-C_{16}	1.47	C_{16}-N_4-C_{13}	125.8	-C_{10}-C_{11}-O_{39}-C_{40}-	-178.0
C_{17}-O_{26}	1.36	N_{14}-C_{10}-C_9	126	-O_{38}-C_{33}-C_{28}-C_{27}-	8.1
N_{14}-C_{15}	1.44	C_{27}-N_{13}-C_3	122.9	-C_{33}-C_{28}-C_{27}-N_{13}-	11.9
C_{10}-N_{14}	1.36	N_{13}-C_{28}-C_{27}	133.2	-C_{28}-C_{27}-N_{13}-C3-	-161.6
C_{11}-O_{39}	1.37			-C27-N13-C3-C2-	43.0

The possible energy minimized structure of NDADPT shown in **Figure 3C.30** along with stereographical projection and the numbering pattern is follows as shown in energy minimized structure in **Figure 3C.31**.

Single and double dihedral rotations were carried out over various bonds to acquire the global minima of the compound. Some of the 3d-plots torsional angle vs torsional energy are presented in **Figures 3C.32** and **3C.33.**

The conformational energy profiles of NDADPT for torsional angles over a few selected bonds are shown in **Figure 3C.35**. Some of the important Geometric Parameters of NDADPT is presented in **Table 3C.7.**

To verify the observed wavelengths we have calculated the λ values from HOMO, LUMO energy values and they are presented in **Table 3C.4**. The molecular orbital surface of the HOMO and LUMO are shown in **Figure 3C.34**. The minor deviations are understood to be due to the fact that the molecular modeling does not take the crystal packing and multidirectional intermolecular interactions into reliable consideration of NDADPT.

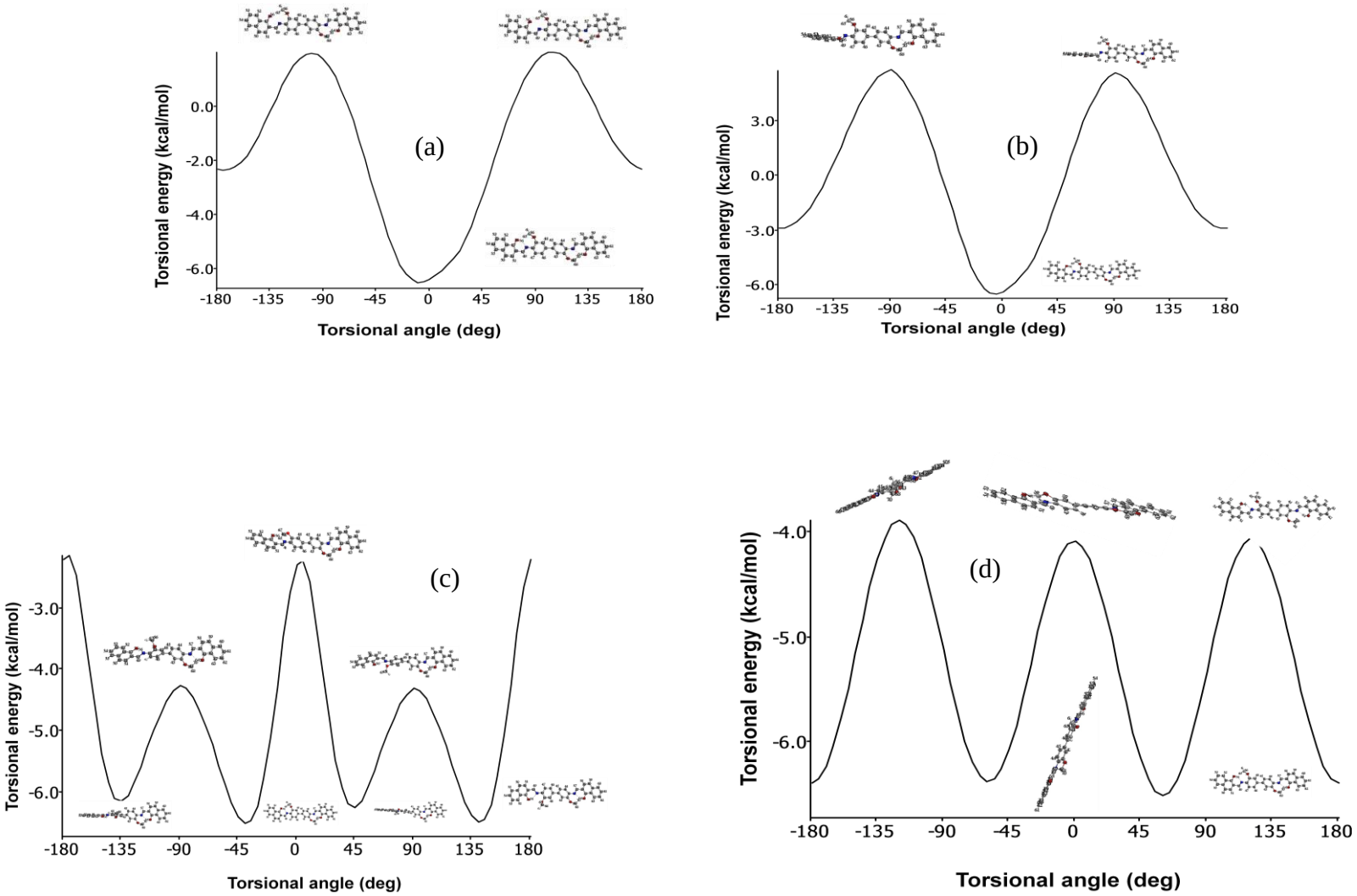

Figure 3C.29: Conformational analysis of NDADPD over (a) C_{17}-O_{26}, (b) C_{16}-C_{15}, (c) C_6-C_7, (d) C_{40}-O_{39}

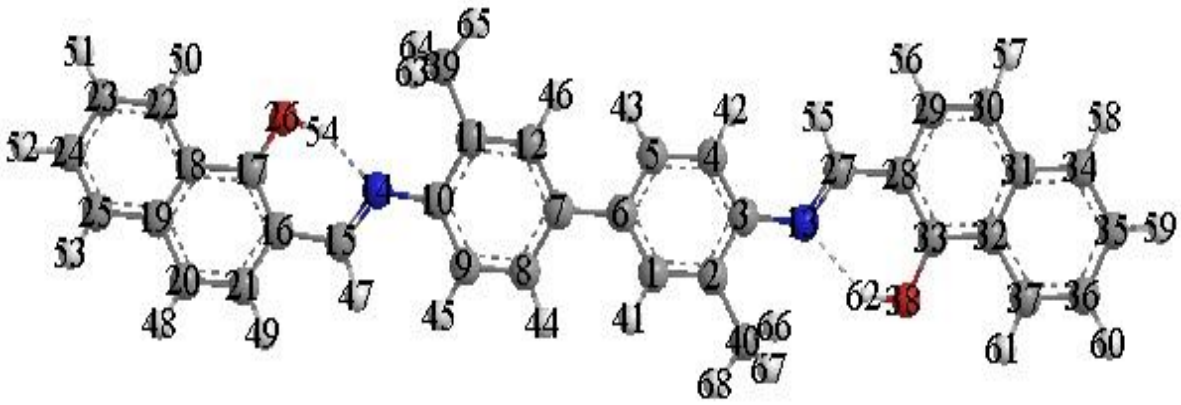

Figure 3C.30: Energy minimized monographic stereographic image of NDADPT generated from energy minimization through MM_2 calculations (lone pairs of electrons are removed for clarity)

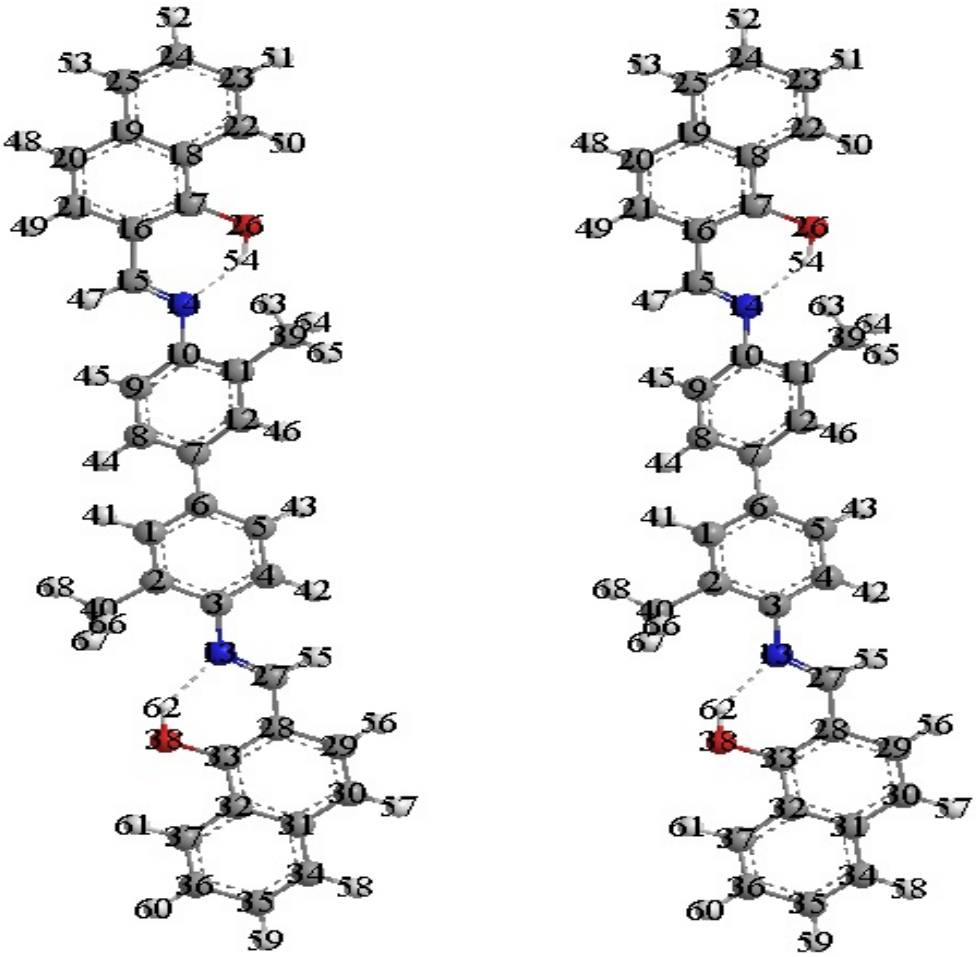

Figure 3C.31: Stereographic view of NDADPT after global minimization

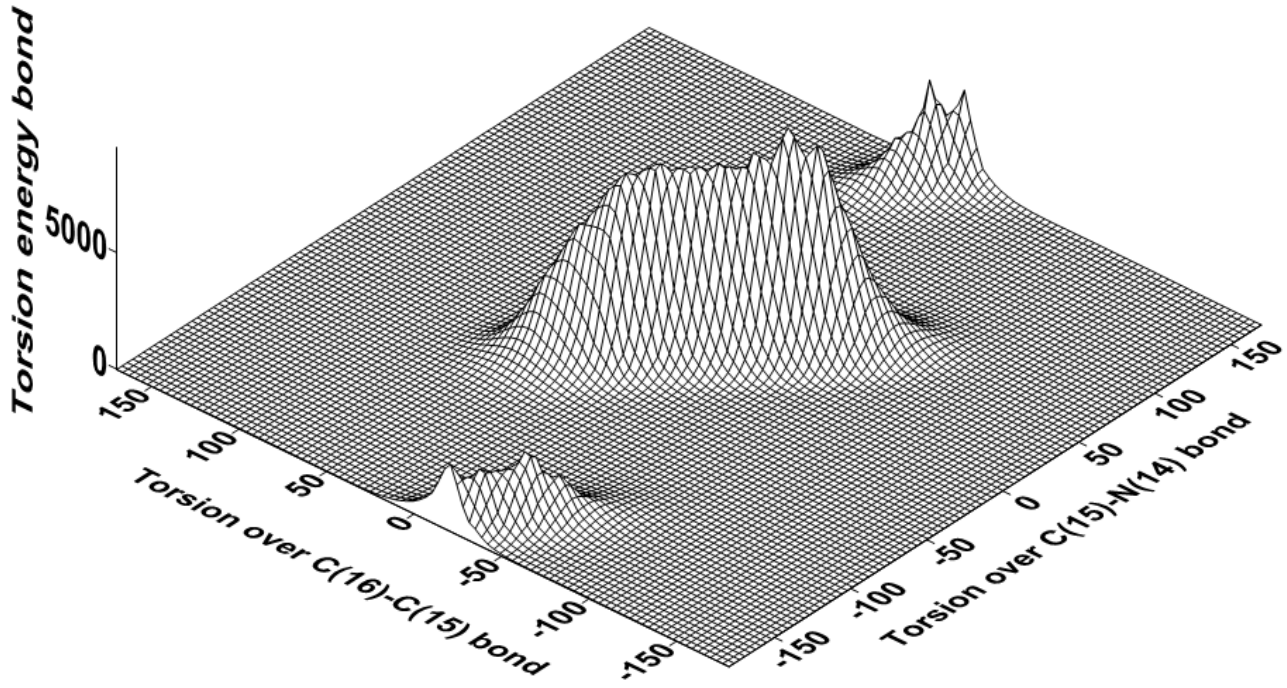

Figure 3C.32: Double dihedral torsional energy plot of NDADPT (left) over C(16)-C(15) and C(15)-N(14) bonds from -180 to +180^{o} and (right) double dihedral plot over C(16)-C(15)-N(14) bonds (Refer **Figure 3C.31** for numbering scheme for the atoms)

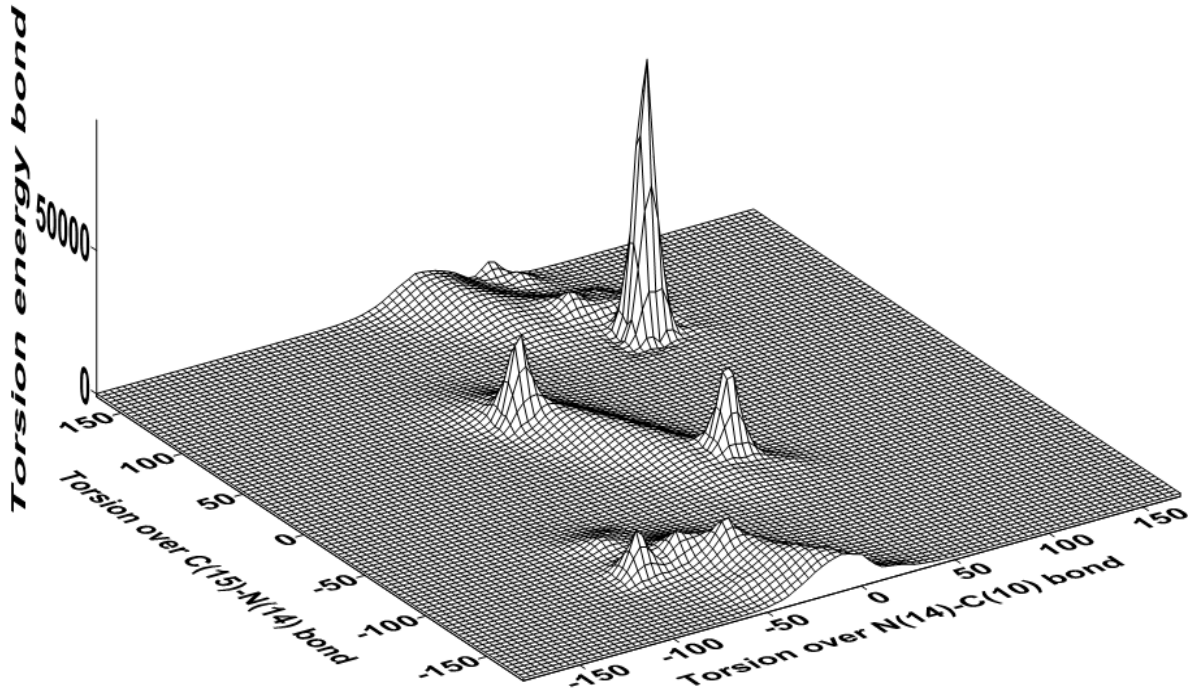

Figure 3C.33: Double dihedral torsional energy plot of NDADPT (left) over C(16)-C(15) and C(15)-N(14) bonds from -180 to +180^{o} and (right) double dihedral plot over C(16)-C(15)-N(14) bonds (Refer **Figure 3C.32** for numbering scheme for the atoms)

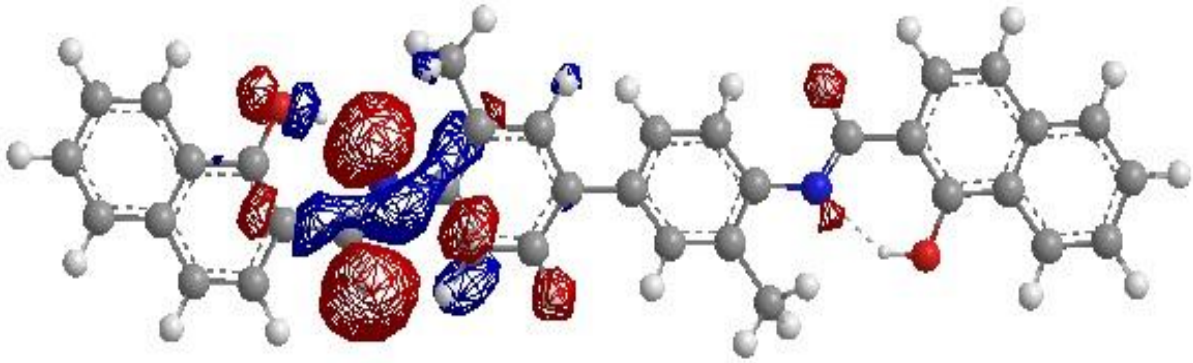

HOMO

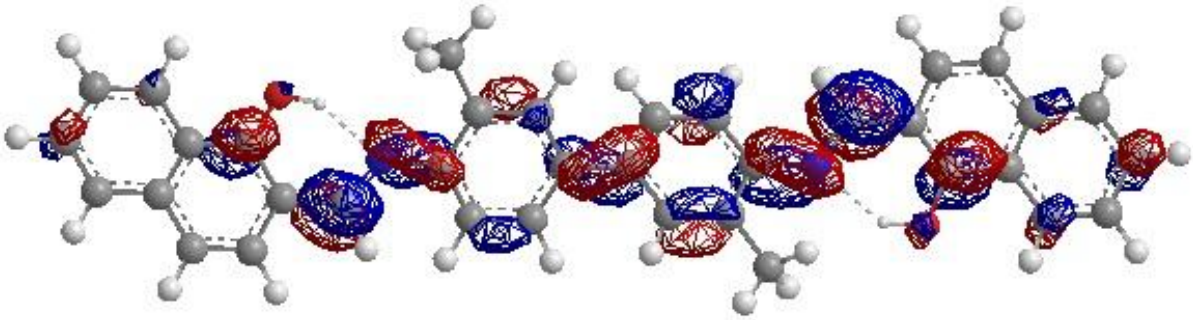

LUMO

Figure 3C.34: HOMO, LUMO molecular orbitals of NDADPT in wire mesh format

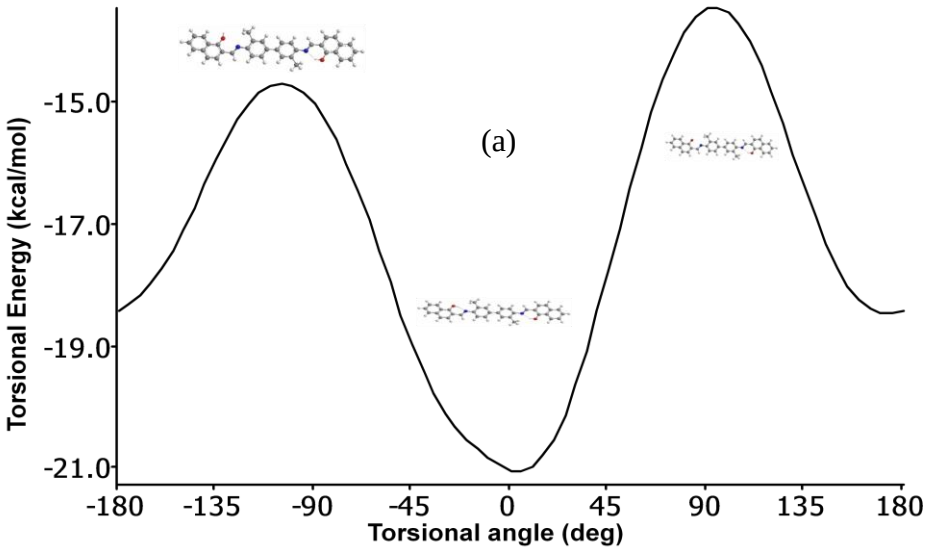

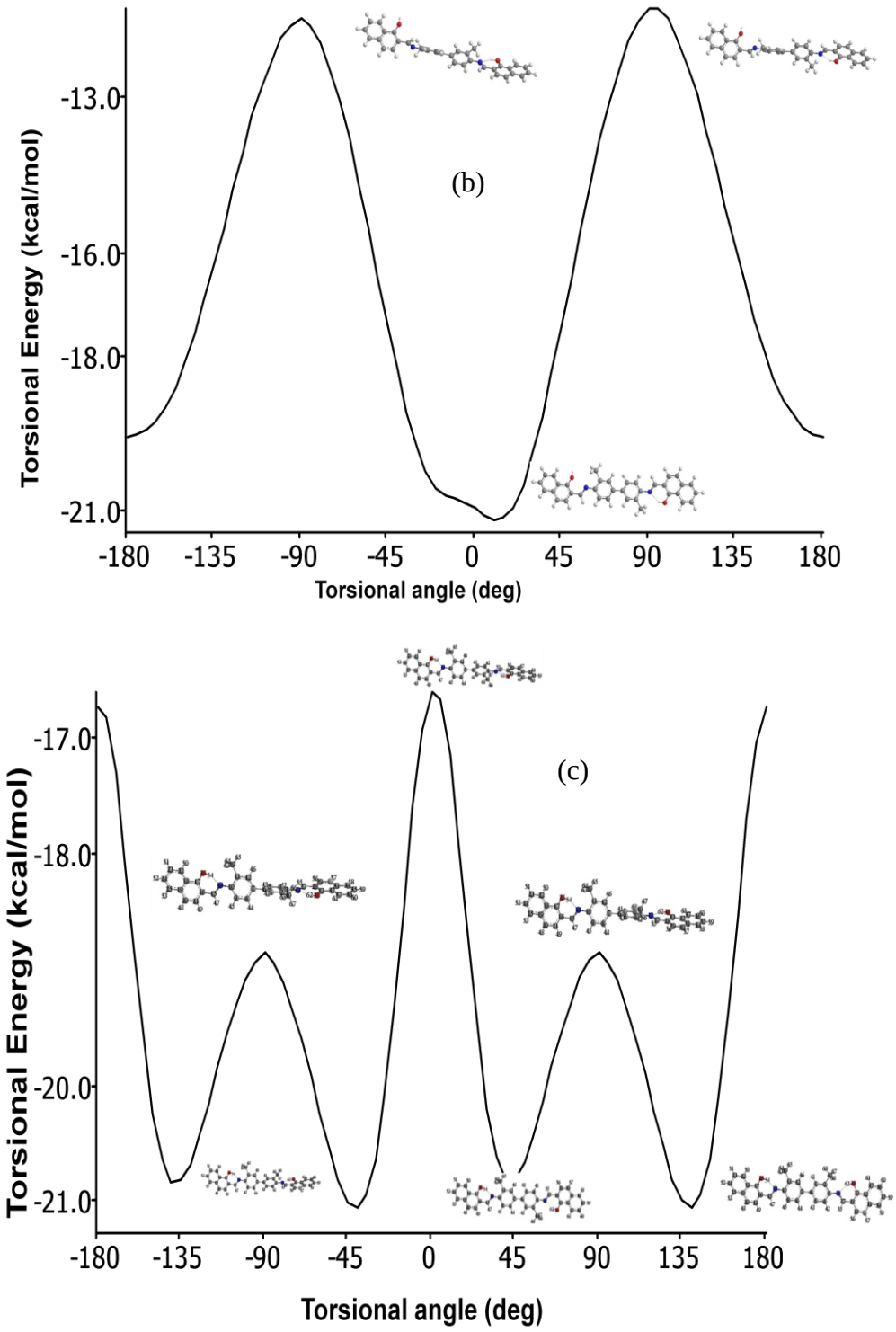

Figure 3C.35: Conformational analysis of NDADPT over (a) C_{17}-O_{26}, (b) C_{16}-C_{15}, (c) C_7-C_6

Table 3C.7: *Some of the important geometric parameters of NDADPT*

Bond	Bond length (A^o)	Bond	Bond angle (deg)	Bond	Dihedral angle (deg)
$-C_{33}-O_{38}$	1.51	$-C_{10}-N_{14}-C_{15}$	123.5	$-O_{38}-C_{33}-C_{28}-C_{29}-$	-179.0
$-C_{28}-C_{27}-$	1.47	$-N_{14}-C_{15}-C_{16}-$	133.6	$-O_{38}-C_{33}-C_{28}-C_{27}-$	8.1
$-N_{13}-C_{27}-$	1.28	$-C_{27}-N_{13}-C_3-$	122.9	$-C_{33}-C_{28}-C_{27}-N_{13}-$	11.9
$-C_3-N_{13}-$	1.36	$-N_{13}-C_{28}-C_{27}-$	133.2	$-C_{28}-C_{27}-N_{13}-C3-$	-161.6
$-C_6-C_7-$	1.48			$-C_{27}-N_{13}-C_3-C_2-$	43.0

The possible energy minimized structure of NDADPB shown in **Figure 3C.36** along with stereographical projection and the numbering pattern is follows as shown in energy minimized structure in **Figure 3C.37**.

Single and double dihedral rotations were carried out over various bonds to acquire the global minima of the compound. Some of the 3d-plots torsional angle vs torsional energy are presented in **Figures 3C.38** and **3C.39.**

The conformational energy profiles of NDADPB for torsional angles over a few selected bonds are shown in **Figure 3C.40**. Some of the important Geometric Parameters of NDADPB is presented in **Table 3C.8.**

To verify the observed wavelengths we have calculated the λ values from HOMO, LUMO energy values and they are presented in **Table 3C.4**. The molecular orbital surface of the HOMO and LUMO are shown in **Figure 3C.41**. The minor deviations are understood to be due to the fact that the molecular modeling does not take the crystal packing and multidirectional intermolecular interactions into reliable consideration of NDADPB.

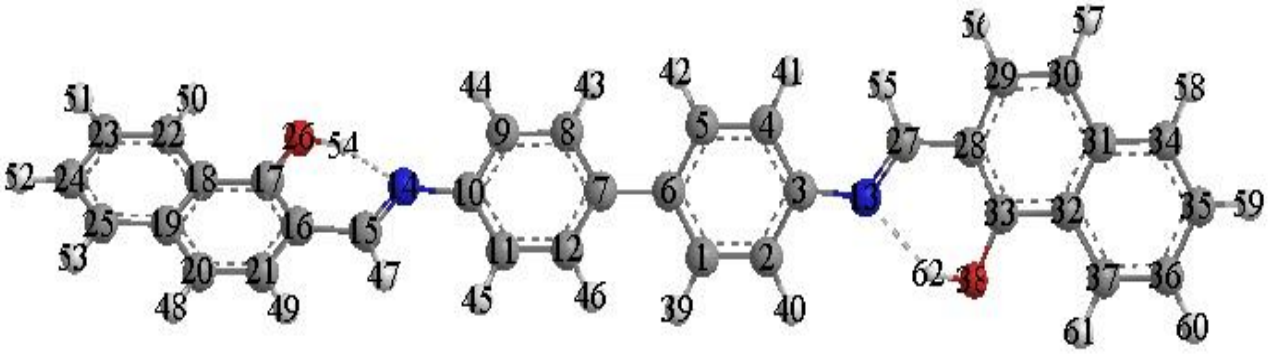

Figure 3C.36: Energy minimized monographic stereographic image of NDADPB generated from energy minimization through MM_2 calculations (lone pairs of electrons are removed for clarity)

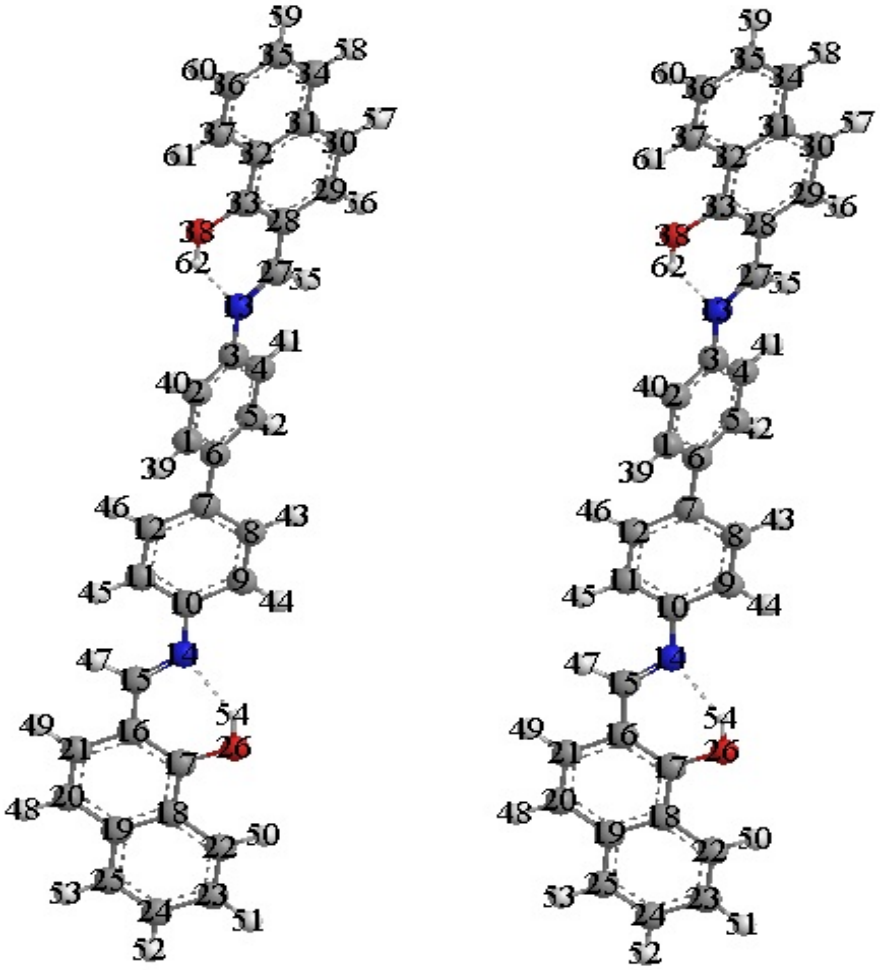

Figure 3C.37: Stereographic view of NDADPB after global minimization.

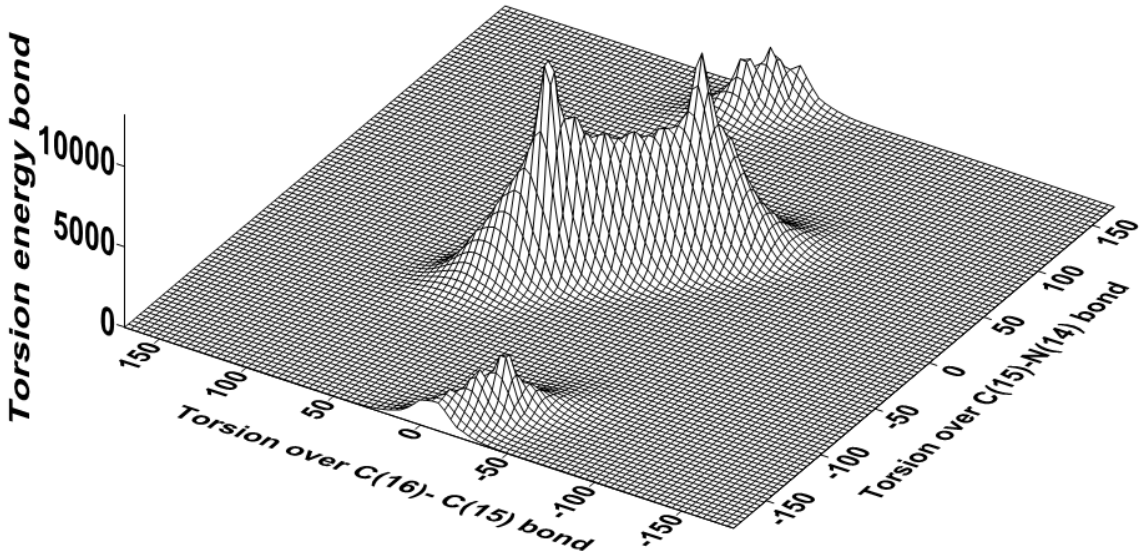

Figure 3C.38: Double dihedral torsional energy plot of NDADPB (left) over C(16)-C(15) and C(15)-N(14) bonds from -180 to +180^{o} and (right) double dihedral plot over C(16)-C(15)-N(14) bonds (Refer **Figure 3C.37** for numbering scheme for the atoms)

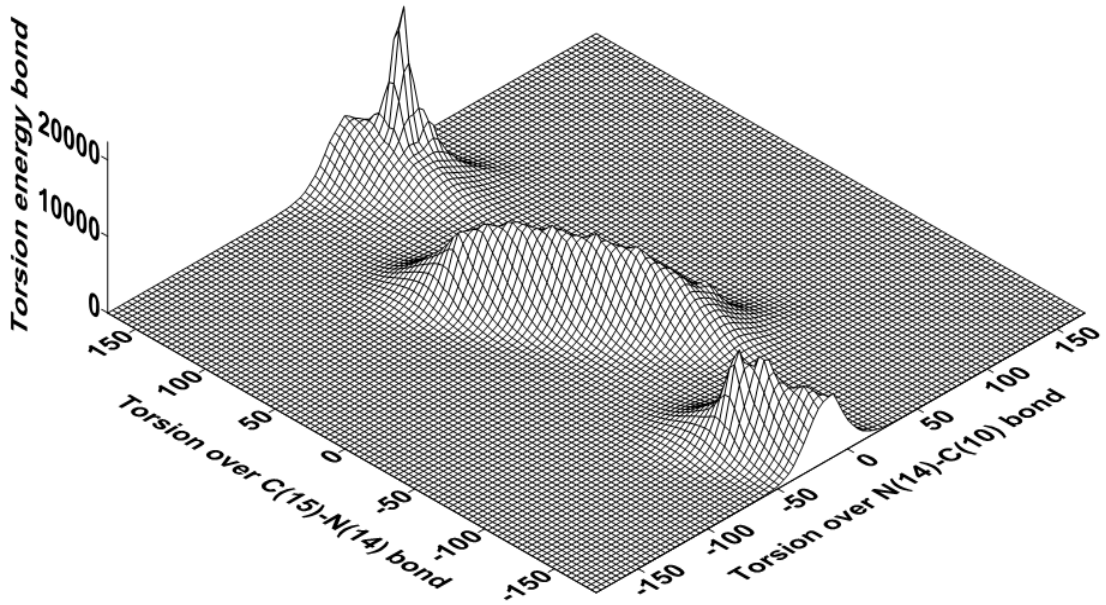

Figure 3C.39: Double dihedral torsional energy plot of NDADPB (left) over C(15)-N(14) and N(14)-C(10) bonds from -180 to +180^{o} and (right) double dihedral plot over C(15)-N(14)-C(10) bonds (Refer **Figure 3C.37** for numbering scheme for the atoms)

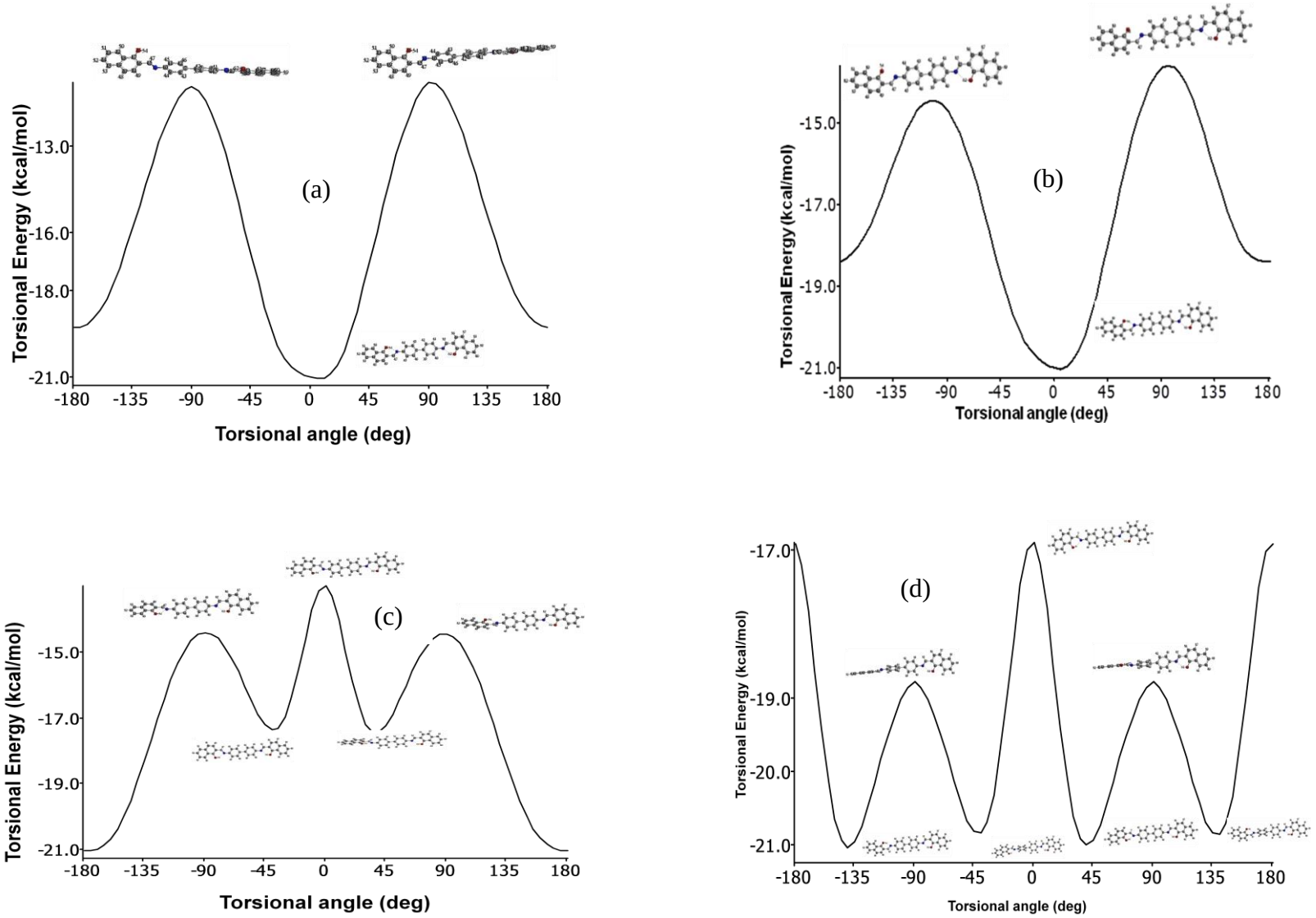

Figure 3C.40: Conformational analysis of NDADPB over (a) C_{16}-C_{15}, (b) C_{17}-O_{26}, (c) C_{10}-N_{14}, d) C_6-C_7

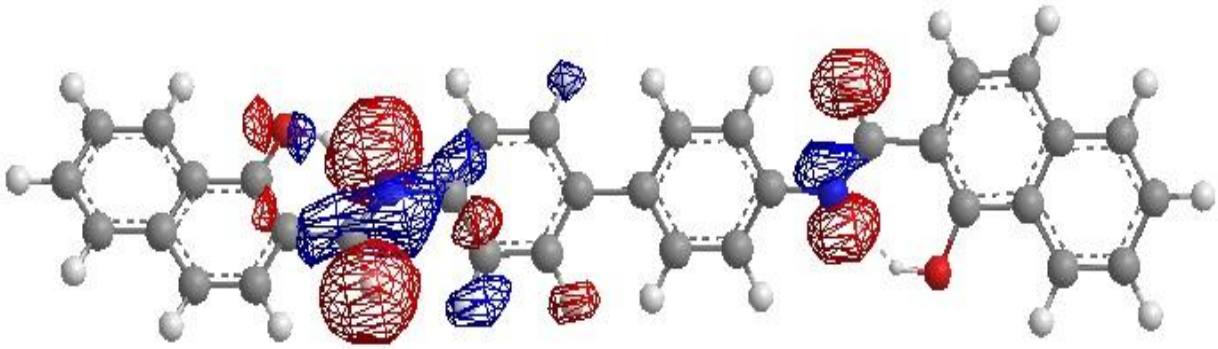

HOMO

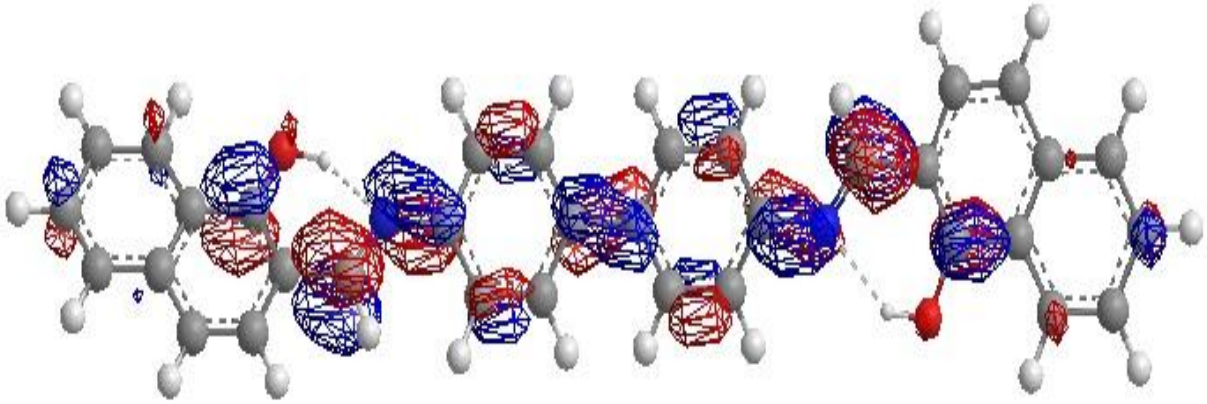

LUMO

Figure 3C.41: HOMO, LUMO molecular orbitals of NDADPB in wire mesh format

Table 3C.8: *Some of the important geometric parameters of NDADPB*

Bond	Bond length (A^o)	Bond	Bond angle (deg)	Bond	Dihedral angle (deg)
C_{17}-O_{26}	1.51	C_{16}-C_{15}-N_{14}	125.2	-O_{26}-C_{17}-C_{16}-C_{15}-	1.20
C_{16}-C_{15}	1.47	C_{15}-N_{14}-C_{10}	124.9	-C_{21}-C_{16}-C_{15}-N_{14}-	-169.8
N_{14}-C_{10}	1.42	C_3-N_{13}-C_{27}	124.3	-C_{10}-C_{15}-N_{14}-C_{10}-	-179.5
C_{15}-N_{14}	1.36	N_{13}-C_{27}-C_{28}	126.2	-C_{15}-N_{14}-C_{10}-C_9-	-172.6
C_7-C_6	1.48				

REFERENCES

1. E Paspalaev, A Pavlova, *C R Acad Bulg Sci*, 18, **1965,** 533
2. V N Dmitrieva, L V Kononenko, V D Benzuglyi, *Teor Eksp Khim*, 1, **1965,** 456
3. P Zuman, "*The Elucidation of Organic Electrode Processes*", Academic Press, New York, **1969**
4. E Hammam, A Tawfik, M M Ghoneim, *J Pharm Biomed Anal*, 36, **2004**, 149
5. V N Dmitrieva, V B Smelyakova, B M Krasovitskii, V D Bezulglyi, *Zh Obshch Khim*, 36, **1966**, 405
6. N F Levchenko, L Sh Afanasiadi, V D Benzuglyi, *Zh Obshch Khim*, 37, **1969**, 666
7. U Mustafa, P Kamran, M Levent, U Huseyin, *Anal Sci*, 20, **2004**, 1179
8. W U Malik, Goyal and R. Jain, *J Electroanal Chem*, 87, **1978**, 129
9. W U Malik and Goyal, *Talanta*, 23, **1976**, 705,
10. G M Sheldrick. SHELX-97: SHELXTL, Program for the Solution and Refinement of Crystal Structures, (version 6.14); Bruker AXS: Wisconsin, USA, 2000. Program for the Solution and refinement of Crystal Structures, University of Göttingen, Germany, **1997**
11. (a) C F Macrae, I J Bruno, J A Chisholm, P R Edgington, P McCabe, E Pidcock, L Rodriguez-Monge, R Taylor, J van de Streek, & P A Wood,. *J Appl Cryst***,** 41, **2008**, 466; (b) L J Farrugia, *J Appl Cryst, 30,* **1997**, 565; (c) L J Barbour, "X-Seed-A software tool for supramolecular crystallography" *J Supramol Chem, 1*, **2001**, 189
12. (a) M A Spackman, J J McKinnon, *Cryst Eng Comm,* 4, **2002** 378-392; (b) J J McKinnon, F P A Fabbiani, & M A Spackman, *Crystal Growth & Design*, 7, **2007**

CHAPTER IV

BINUCLEAR Co(II), Ni(II), Cu(II) AND Zn(II) COMPLEXES OF BIPHENYL BRIDGED NAPTHYLIDINIMINE SCHIFF BASE LIGANDS

Portions of the results of this chapter are presented in conference "*Synthesis and characterization of a novel series of homo aryl bridged binuclear and tetranuclear of Co(II), Ni(II), Cu(II) and Zn(II) complexes*" 3rd Asian Conference Coordination Chemistry, page-108, Oct. 2011, at IIT, Delhi

The biphenyl bridged Schiff base ligands reported in **Chapter III** have been complexed with various metal ions such as cobalt(II), nickel(II), copper(II), zinc(II), etc. The details of synthesis and purification of the complexes are presented in **Chapter II**. These complexes were characterized by physical, analytical, spectral, thermal, cryomagnetic, electron spin resonance and electrochemical studies are presented in this Chapter.

For further reference these complexes are labeled as $M_2L_2^i$ where M, L and i are defined in structure **4.1.** Based on the structural vividity, this Chapter is divided into four, **PARTS**, **A**, **B**, **C** and **D**.

In **PART A**, the physical, analytical and spectral data of binuclear bivalent metal complexes of biphenyl bridged napthylidinimine Schiff base ligands are presented and discussed. In **PART B**, the cryomagnetic and ESR spectral studies of these complexes are reported.

In **PART C** is dedicated for the discussion of their thermal studies. Whereas the same in **PART D**, the electrochemical studies of complexes are reported.

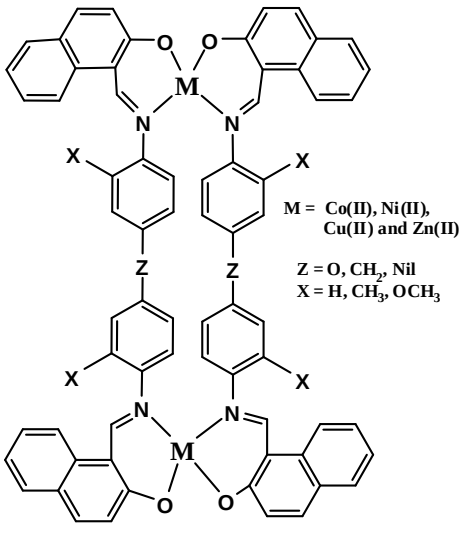

4.1 ($M_2L_2^i$)

Z	**X**	**i**	**Row Combination $M_2L_2^i$**
O	H	1	$M_2L_2^1$
CH_2	H	2	$M_2L_2^2$
-	OCH_3	3	$M_2L_2^3$
-	CH_3	4	$M_2L_2^4$
-	H	5	$M_2L_2^5$

4A.1 General Characterization of $M_2L_2^i$

The physical and analytical data of the metal (II) complexes are given in **Table 4A.1.** These analytical data are consistent with the proposed binuclear structure shown in **4.1**. The metal analysis were determined by ICP-MS are shown in **Figures 4A.1-4A.3.** Relevant data of analysis as given in **Table 4A.3**.

Table 4A.1: *Physical, analytical and magnetic data of the biphenyl bridged Schiff base Co(II) and Ni(II) complexes*

Complex	Mol. Wt	Color	M. P (^{0}C) #	Elemental analysis*				μ_{eff} (BM)
				% C	% H	% N	% M[a]	
$[Co_2L_2^1(H_2O)_4]$	1203.02	Red	361.66	67.98	4.29	4.51	9.78	5.26
				(69.89)	(4.36)	(4.66)	(9.80)	
$[Co_2L_2^2(H_2O)_4]$	1199.08	Red	358.12	70.06	4.78	4.62	9.81	5.68
				(70.12)	(4.71)	(4.67)	(9.83)	
$[[Co_2L_2^3(H_2O)_4]$	1291.13	Pale Red	360.97	66.53	4.70	4.34	9.10	5.12
				(66.98)	(4.68)	(4.34)	(9.12)	
$[Co_2L_2^4(H_2O)_4]$	1227.14	Red	289.44	70.42	4.98	4.50	9.58	4.98
				(70.47)	(4.93)	(4.57)	(9.61)	
$[Co_2L_2^5(H_2O)_4]$	1098.97	Brown	311.25	74.10	4.10	5.08	10.53	5.05
				(74.32)	(4.04)	(5.10)	(10.73)	
$[Ni_2L_2^1]$	1130.38	Green	419.60	71.78	3.84	4.84	10.37	2.70
				(72.25)	(3.92)	(4.96)	(10.38)	
$[Ni_2L_2^2]$	1126.54	Light Green	443.22	71.12	4.81	4.37	9.89	2..81
				(74.63)	(4.29)	(4.97)	(10.42)	
$[Ni_2L_2^3]$	1218.59	Light Green	333.12	70.25	4.36	4.55	9.61	2.78
				(70.96)	(4.30)	(4.60)	(9.63)	
$[Ni_2L_2^4]$	1154.59	Green	285.57	74.30	4.60	4.82	10.15	2.80
				(74.90)	(4.54)	(4.85)	(10.17)	
$[Ni_2L_2^5]$	1098.49	Green	317.87	74.35	4.04	5.10	10.65	2.82
				(75.75)	(2.04)	(5.11)	(10.69)	

*data in parenthesis are calculated ones # melting point obtained from DSC
[a] metal percentage calculated from ICP-MS analysis

Table 4A.2: *Physical, analytical and magnetic data of the biphenyl bridged Schiff base Cu(II) and Zn(II) complexes*

Complex	Mol. Wt	Color	M. P (^{0}C)	Elemental analysis*				μ_{eff} (BM)
				% C	% H	% N	% M[a]	
$[Cu_2L_2^1]$	1140.09	Brown	399.20	70.63 (71.63)	2.44 (3.89)	5.03 (4.91)	11.08 (11.15)	1.55
$[Cu_2L_2^2]$	1136.25	Black	351.37	73.78 (73.99)	4.34 (4.26)	4.95 (4.93)	11.15 (11.19)	1.72
$[Cu_2L_2^3]$	1228.3	Black	313.15	70.36 (70.40)	4.29 (4.27)	4.53 (4.56)	10.33 (10.35)	1.67
$[Cu_2L_2^4]$	1164.3	Black	302.67	74.20 (74.25)	4.45 (4.50)	4.85 (4.81)	10.85 (10.92)	1.72
$[Cu_2L_2^5]$	1108.25	Brown	304.71	73.36 (73.70)	3.59 (4.00)	5.15 (5.06)	11.41 (11.47)	1.76
$[Zn_2L_2^1(H_2O)_4]$	1215.9	Yellow	455.39	67.18 (67.17)	4.20 (4.31)	4.72 (4.61)	10.74 (10.76)	-
$[Zn_2L_2^2(H_2O)_4]$	1212.0	Yellow	372.86	69.35 (69.37)	4.54 (4.66)	4.64 (4.62)	10.77 (10.79)	-
$[Zn_2L_2^3(H_2O)_4]$	1303.0	Red	381.12	66.34 (66.37)	4.60 (4.56)	4.28 (4.30)	10.01 (10.04)	-
$[Zn_2L_2^4(H_2O)_4]$	1239.0	Pale Orange	283.13	69.50 (69.79)	4.79 4.80	4.43 4.52	10.15 10.55	-
$[Zn_2L_2^5(H_2O)_4]$	1182.9	Orange	323.67	68.35 (69.04)	3.92 (4.35)	5.04 (4.74)	11.01 (11.06)	-

*data in parenthesis are calculated ones [#] melting point obtained from DSC
[a] metal percentage calculated from ICP-MS analysis

Table 4A.3: *ICP-MS analysis of Co(II), Ni(II) and Cu(II) complexes*

Calibration Curve	^{59}Co	^{60}Ni	^{65}Cu
Concentration (ppm)	CPS	CPS	CPS
0	600	270	607
2	2.78×10^7	6.36×10^6	6.82×10^6
5	7.27×0^7	1.63×10^7	1.60×10^7
8	1.07×10^8	2.41×10^7	2.44×10^7
10	1.41×10^8	3.08×10^7	3.07×10^7

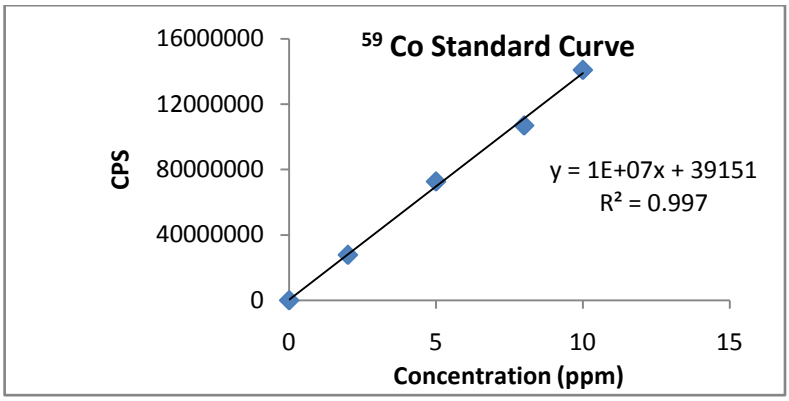

Figure 4A.1: Calibration curve of Cobalt (II) complexes

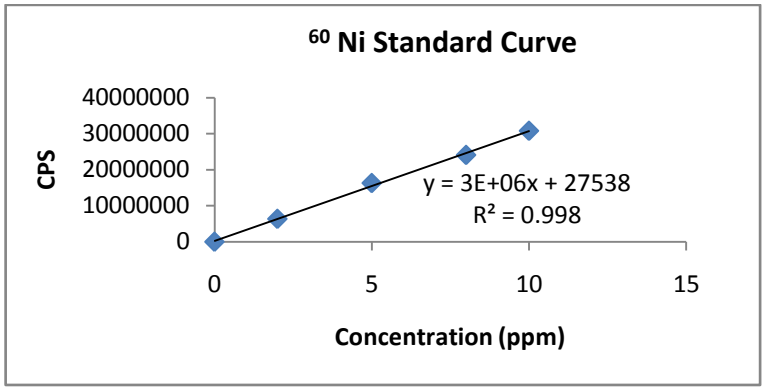

Figure 4A.2: Calibration curve of Nickel (II) complexes

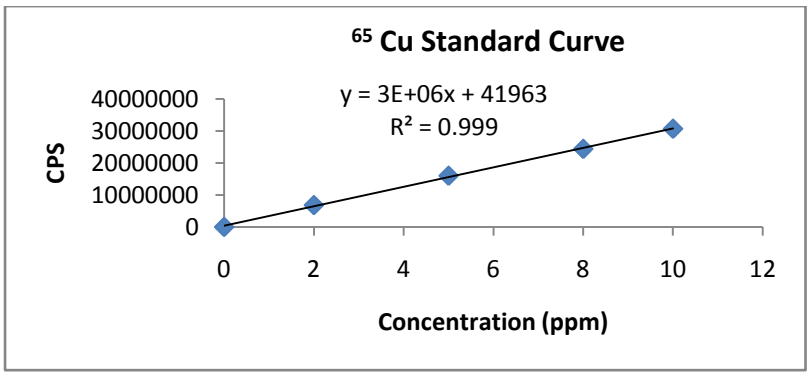

Figure 4A.3: Calibration curve of Copper (II) complexes

4A.2 Electronic absorption spectra of the Cu(II) complex with L^1 and L^2

Figures 4A.4 and **4A.5** shows the change in the UV–vis spectrum which occurs when L^1 and L^2 coordinates to Cu(II) ion in MeOH. Upon addition of Cu(II) ion to the ligand solution, the ligand π-π* band at 393 nm decreases, and a new band at 450 nm due to the deprotonation of the OH group and the N,O-coordination to Cu(II) ion emerges[1]. A mole ratio

plot using the change in absorbance at 393 nm clearly demonstrated the formation of the Cu(II): $\mathbf{L^1}$ and $\mathbf{L^2}$ =1:1 molar ratio complex, as judged by observing the clear inflection point at [CuII]/[$\mathbf{L^1}$ and $\mathbf{L^2}$] =1. However, further additions of Cu(II) ion lead to an additional increase in the absorbance at 400 nm and a saturation at [CuII]/[$\mathbf{L^1}$] (the inset in **1**). In addition, the isosbestic point at 375 nm shifts gradually to a shorter wavelength. The plateauing at two different CuII/$\mathbf{L^1}$ ratios suggests structure switching at the higher Cu(II) concentration.

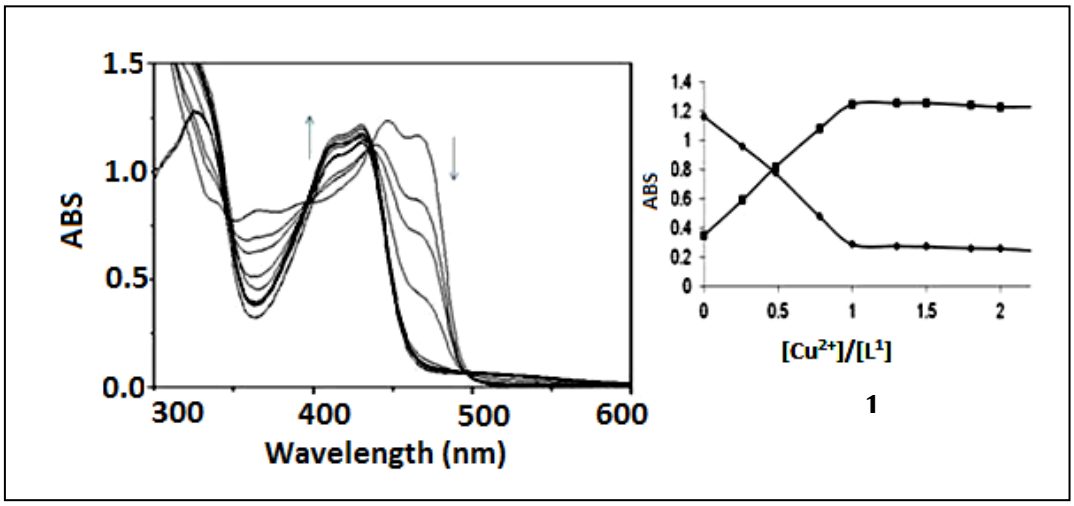

Figure 4A.4: Absorption spectral change of ligand L^1 in methanol upon addition of $Cu(CH_3COO)_2\ 2H_2O$. [L^1] = 2×10^{-5} M. [Cu^{II}] = 0, 0.3, 0.5, 0.7, 1.0, 1.3, 1.5, 1.7, 1.9, 2.1, 2.3, 2.5, 2.8, ($2x10^{-5}$ M) The spectrum for **1** coincides with the spectrum at λ_{max} = 465.5 nm

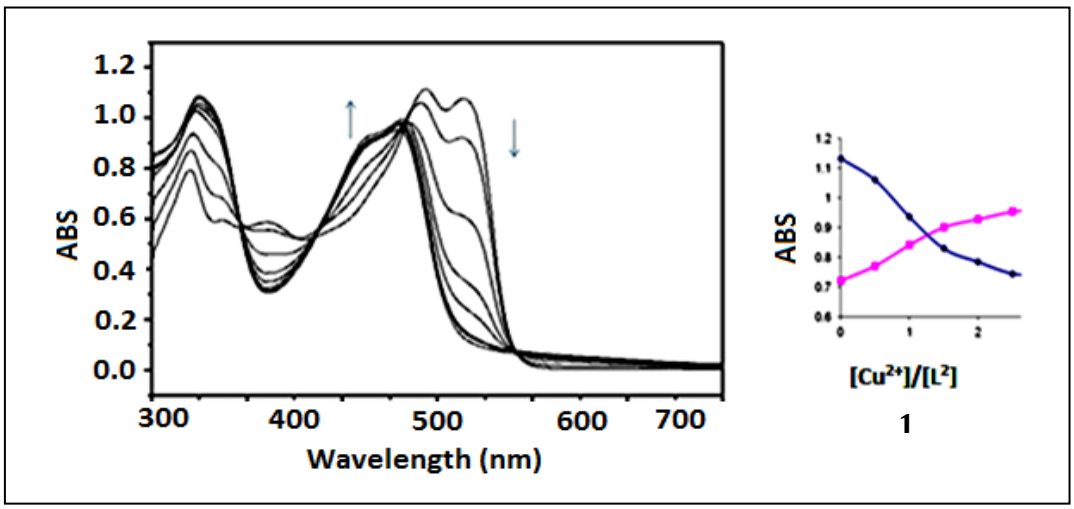

Figure 4A.5: Absorption spectral change of ligand L^2 in methanol upon addition of $Cu(CH_3COO)_2\ 2H_2O$. [L^1] = 2×10^{-5} M. [Cu^{II}] = 0, 0.3, 0.5, 0.7, 1.0, 1.3, 1.5, 1.7, 1.9, 2.3, 2.5, 2.8, ($2x10^{-5}$ M). The spectrum for **1** coincides with the spectrum at λ_{max} = 435.5 nm

4A.3 Infrared Spectral Studies

The FTIR spectra of some representative complexes are given in **Figure 4A.6**. Relevant spectral data are given in **Table 4A.4**. The spectra of the ligands display sharp peaks characteristics of the C=N bond at 1624-1618 cm^{-1}. The complexes exhibit a shift to lower frequency (1602-1616 cm^{-1}). This is due to the coordination of the imino nitrogen to the metal ion. The O–H stretching bands of the free Schiff bases are observed at 3411-3600 cm^{-1} are absence in the complexes. The IR spectra of the zinc(II) and cobalt(II) complexes show the strong bands at 3200 cm^{-1} and at ~860 cm^{-1}. This is suggest indicates the presence of coordinated water molecules due to their *ν*(-OH) stretching and bending modes of vibrations, respectively. In the low frequency region, the bands observed for the complexes in the region 500-550 cm^{-1} are attributed to M-O (phenolic) and those in the region 435-490 cm^{-1} to M–N(azomethanine) stretches. All the IR data suggest that the metal is bonded to the Schiff bases through the phenolic oxygen and iminonitrogen[2, 3].

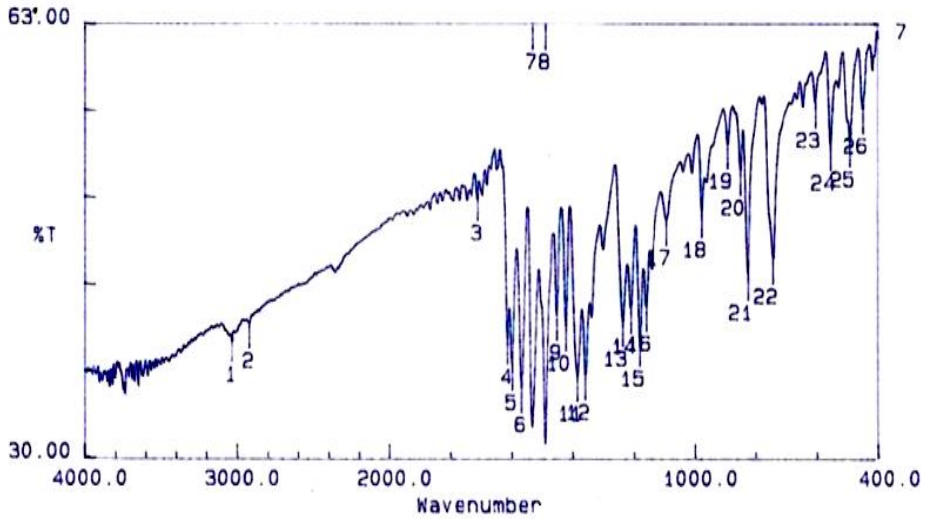

Condition
upper 63.00 lower 30.00 depth 2.00

Peak table

1:	3038.16 (39.2)	2:	2922.42 (40.3)	3:	1714.87 (50.0)	4:	1616.49 (39.1)
5:	1601.06 (37.1)	6:	1570.20 (35.4)	7:	1533.55 (32.3)	8:	1491.11 (31.1)
9:	1454.46 (40.9)	10:	1423.59 (40.1)	11:	1386.94 (36.3)	12:	1359.94 (36.4)
13:	1238.41 (40.4)	14:	1211.41 (41.4)	15:	1182.47 (38.9)	16:	1161.25 (41.5)
17:	1095.67 (48.1)	18:	979.93 (48.7)	19:	895.05 (54.0)	20:	852.61 (52.0)
21:	827.54 (44.0)	22:	744.59 (45.2)	23:	605.70 (57.0)	24:	557.48 (53.8)
25:	493.82 (54.1)	26:	451.38 (56.6)				

Figure 4A.6: FT-IR spectrum of $Co_2L_2^1$ complex

Table 4A.4: *Important IR freq. with assignment of Co(II), Ni(II),Cu(II) and Zinc(II) complexes*

Complex	IR spectral data (cm^{-1})					
	ν(C-H)	**ν(C=N)**	**ν(C-O)**	**ν(M-N)**	**ν(M-O)**	**Coordinated H_2O**
$[Co_2L_2^1(H_2O)_4]$	3038	1616	1211	557	451	827
$[Co_2L_2^2(H_2O)_4]$	3028	1614	1248	555	453	827
$[Co_2L_2^3(H_2O)_4]$	3040	1616	1211	525	493	825
$[Co_2L_2^4(H_2O)_4]$	3024	1618	1277	516	490	827
$[Co_2L_2^5(H_2O)_4]$	3038	1618	1211	520	489	815
$[Ni_2L_2^1]$	3042	1616	1240	484	422	-
$[Ni_2L_2^2]$	3024	1616	1188	589	418	-
$[Ni_2L_2^3]$	3034	1616	1211	555	447	-
$[Ni_2L_2^4]$	3030	1618	1205	518	434	-
$[Ni_2L_2^5]$	3034	1616	1211	565	424	-
$[Cu_2L_2^1]$	3032	1612	1211	543	453	-
$[Cu_2L_2^2]$	3026	1616	1184	545	451	-
$[Cu_2L_2^3]$	3045	1601	1184	552	458	-
$[Cu_2L_2^4]$	3036	1601	1180	561	460	-
$[Cu_2L_2^5]$	3030	1616	1215	561	462	-
$[Zn_2L_2^1(H_2O)_4]$	3026	1602	1238	449	553	850
$[Zn_2L_2^2(H_2O)_4]$	3030	1616	1211	447	551	854
$[Zn_2L_2^3(H_2O)_4]$	2939	1616	1211	451	552	866
$[Zn_2L_2^4(H_2O)_4]$	3034	1610	1207	434	505	862
$[Zn_2L_2^5(H_2O)_4]$	3040	1612	1211	489	550	852

4A.4 UV-Visible Absorption and Fluorescence Emission Spectral Studies

The UV-Vis spectra of metal(II) complexes, in chloroform solvent, are shown in **Figures 4A.7-4A.10.** Relevant electronic spectral data are collected into **Table 4A.5.** The absorptions observed at 320-400 nm are due to $\pi \rightarrow \pi^*$ transitions of the ligand origin. The band at ~450 nm with a shoulder at lower energy is attributed to the $n \rightarrow \pi^*$ transition associated with the azomethine linkage. This band in the complex has shown a bathochromic

shift when compared to the some ligand due to the donation of a lone pair of electrons to the metal by coordination of azomethine through its nitrogen.

The electronic spectral of binuclear Co(II) complexes in octahedral geometry are expected to show three d-d bands in the case of Co(II) complexes. The bands are observed at of ~410, ~330 and ~320 nm can be assigned to attributed, $4T_{1g}(F) \rightarrow 4T_{2g}(F)$, $4T_{1g}(F) \rightarrow 4T_{2g}(P)$, $4T_{1g}(F) \rightarrow 4A_{2g}(F)$, respectively.

The electronic transitions of Ni(II) complexes show 3 bands. $1A_{1g} \rightarrow 1A_{2g}$, $1A_{1g} \rightarrow 1B_{1g}$, $1A_{1g} \rightarrow 1E_g$. The ν_1 transition is rarely observed because of its weak transition. The ν_3 band usually merges with the ligand transitions resulting in a shoulder-like appearance in the spectrum. The bands at 440 and 325 nm for the present Ni(II) complexes can be assigned as ν_2 and ν_3, respectively. The high energy transitions in the complex are very close to those of the pure ligands suggesting negligible effect of the metal centre on the ligands electronic profile. The observed ν_2 and ν_3 are slightly on the higher side than expected for the Schiff base complexes. This might be due to the geometry having an enforced component of square planarity leading to C_{2V} point group. The fact that the observed magnetic moment value is slightly less than that expected for the square planar complex also suggests this possibility[5, 6].

Electronic spectra of Cu(II) complexes show a single broad band in the region 310-330 nm. There is also a low energy shoulder at ~435 nm for these complexes. Planar Schiff base Cu(II) complexes are known to have only one band in the range 320-340 nm while tetrahedral complexes are known to have absorption bands in the region 420-450 nm. For pseudo-tetrahedral Schiff base complexes the absorption bands are located at as high 440 nm with an additional band at ~310 nm. This additional band is assigned to the d_x^2-$_y^2 \rightarrow d_{yz}$ transition. The λ_{max} values are observed for present napthylidinimine Schiff base Cu(II) complexes do not represent proper planar or pseudotetrahedral geometries for Cu(II) complexes. As indicated in the shifts in the d-d absorption maxima to higher wavelengths. In the present complexes the napthyl groups are rigid and bulky. Further, some of the binucleating ligands with X= CH_3 or OCH_3 the situation is to enforce more distortion. Hence, it may be expected that the geometry at the two copper centres is substantially distorted towards tetrahedral from square planarity. The geometry is best described as pseudotetrahedral one. The low energy shoulder at ~430 nm may have similar origin as the 440 nm band observed for complexes which have pseudo tetrahedral geometry.

The electronic spectra of the binuclear Cu(II) complexes exhibit three spin allowed transitions, viz., $2B_{1g} \rightarrow 2A_{1g}$ ($d_{x^2-y^2} \rightarrow d_{z^2}$), $2B_{1g} \rightarrow 2B_{2g}$ ($d_{x^2-y^2} \rightarrow d_{xy}$), $2B_{1g} \rightarrow 2E_g$ ($d_{x^2-y^2} \rightarrow d_{xz}$), expected for square-planar complexes.

The $n \rightarrow \pi^*$ transition of the ligands associated with the azomethine linkage exhibit a bathochromic shift in the complexes due to the complexation. The moderately intense broad band for the Zn(II) complexes in the region 380-450 nm is assigned to the O→Zn(II), ligand to metal charge transfer transition (LMCT). The LMCT band of the phenolate complex shows line broadening, with a tail running into the visible part of the spectrum. The zinc complexes show no appreciable absorptions in the region above 400 nm in accordance with the d^{10} electronic configuration of the Zn(II) ion.

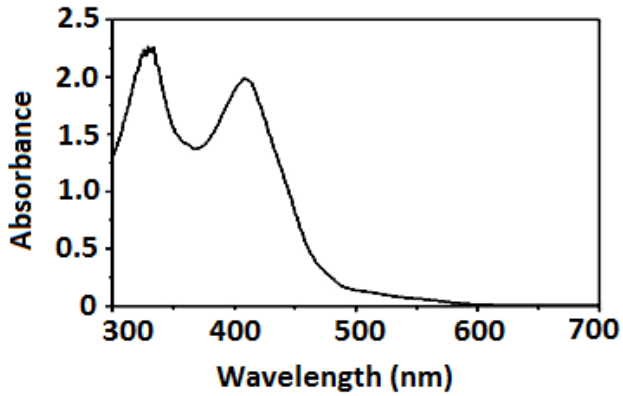

Figure 4A.7: UV-Vis absorption spectra of $Co_2L_2^1$(4 x 10^{-5} M) in chloroform solvent

The moderately intense broad band for the zinc complex in the region 380-450 nm is assigned to O→ Zn(II). The LMCT band of the phenolate complex shows line broadening with a tail running into the visible part of the spectrum.

Fluorescence spectra of the Zn(II) complex are shown in **Figure 4A.11** in **Table 4A.6**. Strong emission band at 490 nm along with some shoulders is observed when excited with 360 nm radiation.

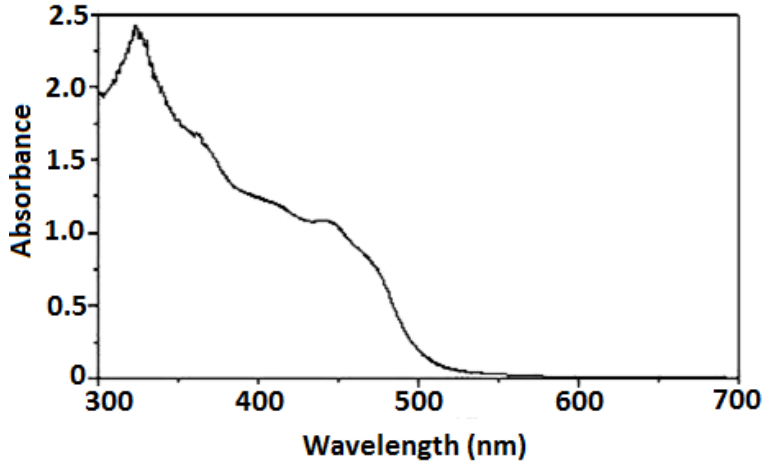

Figure 4A.8: UV-Vis absorption spectra of $Ni_2L_2^1$ (4x10^{-5}M) in chloroform

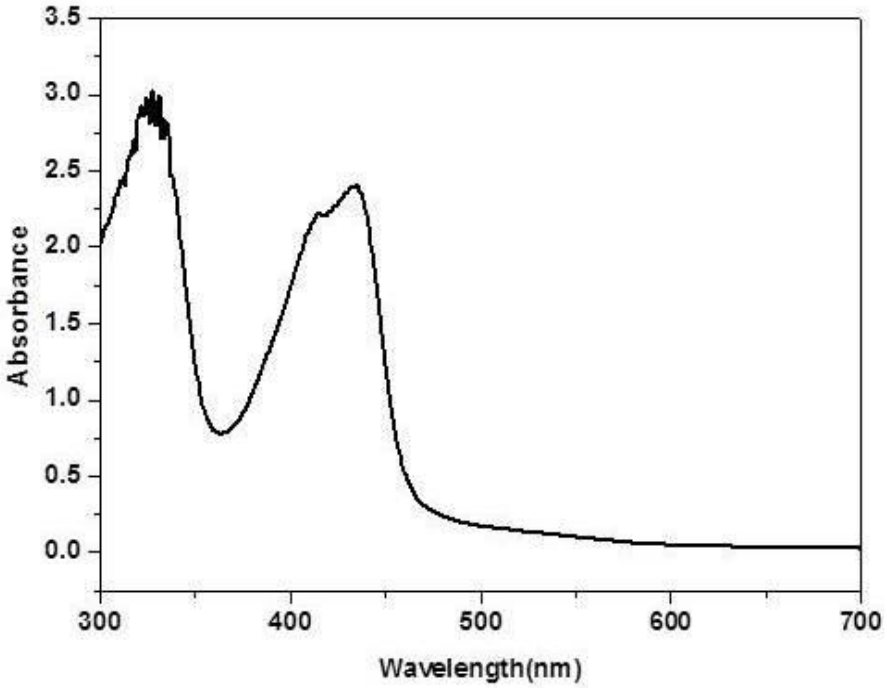

Figure 4A.9: UV-Vis absorption spectra of $Cu_2L_2^1$ ($4x10^{-5}$M) in chloroform

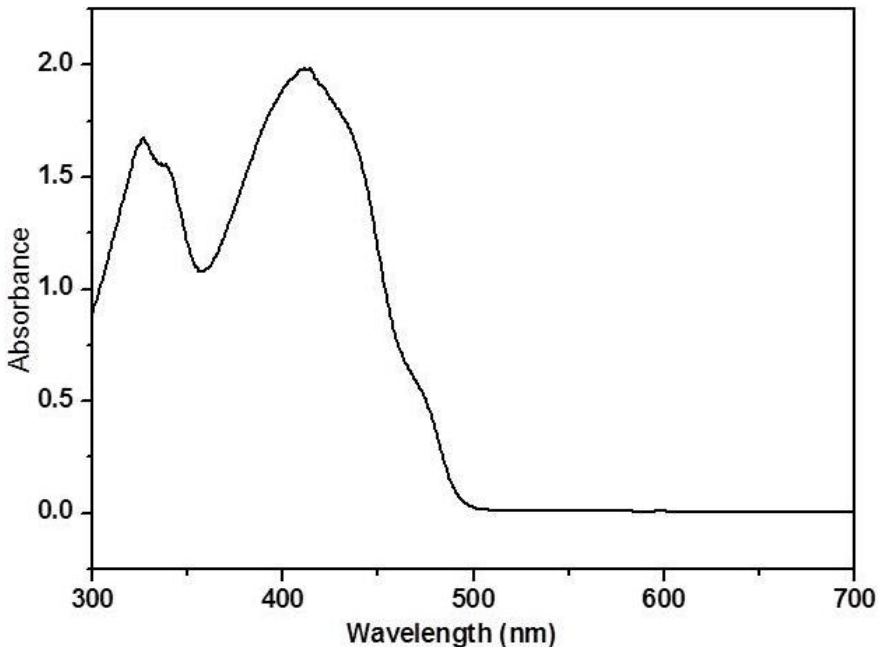

Figure 4A.10: UV-Vis absorption spectra of $Zn_2L_2^1$ ($4x10^{-5}$M) in chloroform

Table 4A.5: *Electronic spectral data of Co(II), Ni(II) and Cu(II) complexes*

Complex	**Electronic data in $CHCl_3$ λ_{max} ($\bar{\upsilon}$) (ε)[a]**
$[Co_2L_2^1(H_2O)_4]$	407(24,570)(48,750)
	328(30,487)(41,250)
$[Co_2L_2^2(H_2O)_4]$	407(24,570)(49500)
	327(30,769)(58,505)
$[Co_2L_2^3(H_2O)_4]$	472(21,186)(14,250)
$[Co_2L_2^4(H_2O)_4]$	401(24,937)(53,500)
	322(31,055)(34,780)
$[Co_2L_2^5(H_2O)_4]$	403(24,814)(58,001)
	327(30,581)(45,501)
$[Ni_2L_2^1]$	440.5(22,727)(28,250)
	323(30.959)(59.975)
$[Ni_2L_2^2]$	443(22,573)(16,235)
	322(21,250)(31,055)
$[Ni_2L_2^3]$	481.5(79,002)(14,750)
$[Ni_2L_2^4]$	404(47,524)(54,250)
	322(31,061)(59,320)
$[Ni_2L_2^5]$	399.5(25,626)(35250)
	326(25,250)(30,674)
$[Cu_2L_2^1]$	433(23,091)(59,790)
	327(30.581)(75,652)
$[Cu_2L_2^2]$	437(22,883)(51,210)
	325(30,771)(62,750)
$[Cu_2L_2^3]$	448(22,320)(67,001)
	327(30,581)(57,501)
$[Cu_2L_2^4]$	428(23,364)(56,001)
	322(31,055)(82,001)
$[Cu_2L_2^5]$	440(22,727)(51,501)
	326(30,670)(51,001)

a, λ_{max} (in nm), $\bar{\upsilon}$ (in cm^{-1}), ε (lit. $mol^{-1}.cm^{-1}$)

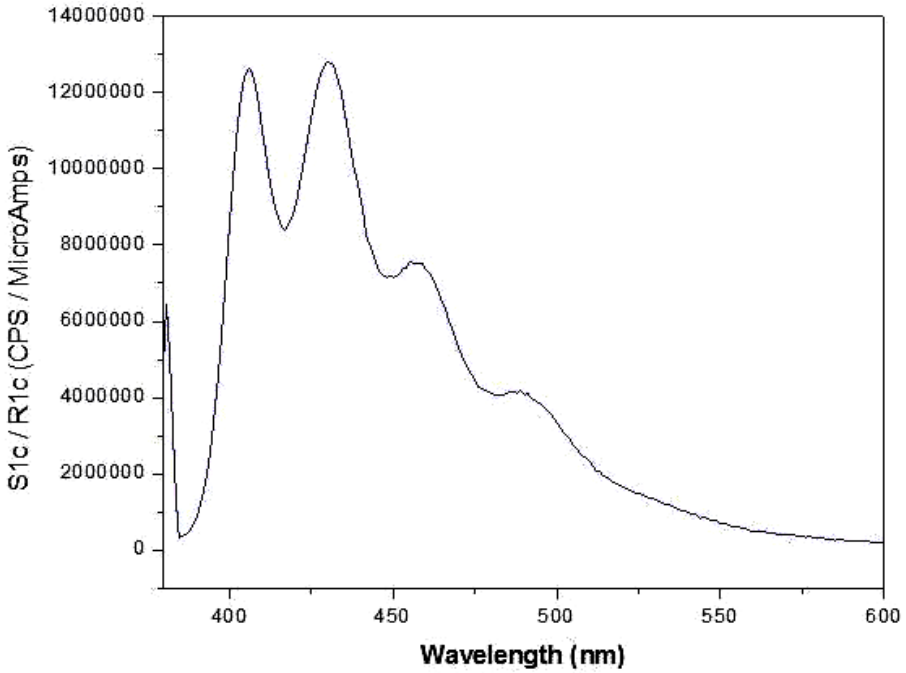

Figure 4A.11: Fluorescence spectrum of $Zn_2L_2^1$ (4 x 10^{-5}M) in chloroform

Table 4A.6: *Electronic spectral and fluorescence spectral data of Schiff base Zn(II) complexes*

Complex	**Electronic data in $CHCl_3$ λ_{max} ($\bar{\upsilon}$) (ε)[a]**	**Fluorescence data Exited (nm)**	**Fluorescence data Emission (nm)**
$[Zn_2L_2^1(H_2O)_4]$	410.5(24,361)(49.542)	360	434, 462,
	326.5(30,628)(41,915)		495
$[Zn_2L_2^2(H_2O)_4]$	435(22990)(42910)	360	404,465,489
	325(30771)(46550)		
$[Zn_2L_2^3(H_2O)_4]$	493.5(20,260)(21,285)	360	406,539
$[Zn_2L_2^4(H_2O)_4]$	401(24,940)(56,760)	380	407,430,524
	322(31,061)(36,601)		
$[Zn_2L_2^5(H_2O)_4]$	405(24690)(63700)	380	405,433, 525
	324(30860)(38610)		

a, λ_{max} (in nm), $\bar{\upsilon}$ (in cm^{-1}), ε (lit. $mol^{-1}.cm^{-1}$)

The solid-state magnetic susceptibility of crystalline samples was measured between 4 and 300 K at a field of 1 kOe using a Quantum Design Model MPMS SQUID magnetometer. Each sample was placed in a gelatine capsule. The susceptibility of the capsule was measured separately and its contribution was subtracted from the overall susceptibility. A temperature-independent susceptibility parameter χ_0 was included in the fitting procedures. This contribution is attributed to the combination of a negative contribution from Langevin diamagnetism through Pascal's constants a positive contribution from Van Vleck Paramagnetism[7].

Except Zn(II), the other complexes, viz, Co(II), Ni(II) and Cu(II) complexes are found to exhibit paramagnetic behaviour.

4B.1 Cryomagnetic Susceptibility Studies

The variable temperature magnetic χ_m values for $Cu_2L_2^1$ are given in **Table 4B.1**. The observed μ_{eff} values at room temperature are normal (~1.80 BM) and suggest the absence of any strong antiferromagnetic interactions between the two copper centres of the molecule. This is not unexpected since the two copper centres are not only separated by a distance of lesser than 10Å but also are bridged by non coplanar biphenyl moieties thereby diminishing the possibility of any electron delocalisation from one centre to the other by π conjugation. The Cu-Cu distance in the present complexes is ~12 Å. It has been claimed in certain biphenyl bridged Cu(II) complexes the presence of intramolecular inter ionic electronic interaction through the σ-bond pathway. However in the present $Cu_2L_2^1$ complexes the nitrogen attached to the metal and the biphenyl's benzene ring do not have any suitable orbital's to overlap with the metal d_{x2-y2} orbital. The p orbital on the nitrogen atom is involved in the azomethine π bond. This essentially any antiferromagnetic interaction.

The data plotted for Curie-Weiss Law are shown **Figure 4B.1**.

$$\chi_{m^{corr}} = \frac{C}{k(T-\theta)} \qquad 4.1$$

The curve fit plots of χ_M^{corr} versus temperature $\frac{1}{\chi_m corr}$ vs temperature shown in **Figure 4B.1**. Suggest a θ value of ~-4.6.

Magnetic susceptibility data, obtained for Cu_2L_2[1] from 4.5 to 300^{0}K, is also fitted to the modified Langevin dimer equation[8], as given below.

$$\chi_m = \frac{Ng^2\beta^2}{3k(T-\theta)}\left[1 + (\frac{1}{3})\exp(-\frac{2J}{kT})\right]^{-1} \qquad 4.2$$

where N is the Avogadro number, g = 2.023 is the spin-only Landé factor, β is the Bohr magneton, k is the Boltzmann constant, and T is the temperature, θ is the Weiss constant .

The fit was excellent, yielding the following values for the magnetic parameters: J = 20 cm^{-1} g = 2.19 θ = -0.38 for Cu_2L_2[1]. The fact that the 2J value is too considerable to be ignored suggests that there exits ferromagnetic interaction.

Magnetic susceptibility fitted curves of all binuclear Co(II), Ni(II) and Cu(II) complexes as shown in **Figures 4B.1- 4B.12** from 4.5 to 300 K, is also fitted to the modified Langevin dimer equation.

There have been extensive reports on spin coupling in "copper dimers" where the Cu-Cu distance is short and where incipient metal to metal bond have been postulated[11, 12]. A situation such as usually, is taken as the basis for the effect of Cu-O-Cu angle on the 2J value with sign. In the present case, such Cu-O-Cu linkage is not possible intermolecularity. We suggest a possibility such Cu-O-Cu linkage intermolecularity as follows in **Scheme 4B.1**.

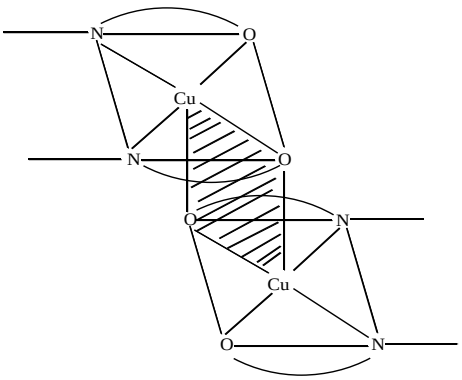

Scheme 4B.1

The shared zone provides a structural moiety as and these are may reports in the literature wherein two $M(N_2O_2)$ coordination centres are engaged in intermolecular. If the two M N_2O_2 coordination planes forming the intermolecular strait-bis-interactive core are parallels and Cu_1-O-Cu_2-O_2-Cu_1 parallelogram is rectangular, than Cu_1-O_1-Cu_2 and Cu_2-O_2-Cu_1 bond angles very close to 90^0. If either the above cyclic moiety deviates from rectangular shape or the two MN_2O_2 planes are not mutually parallel, the Cu-O-Cu bridging angle would deviate from 90^0. This would lead to a ferromagnetic interactions in +ve 2J value.

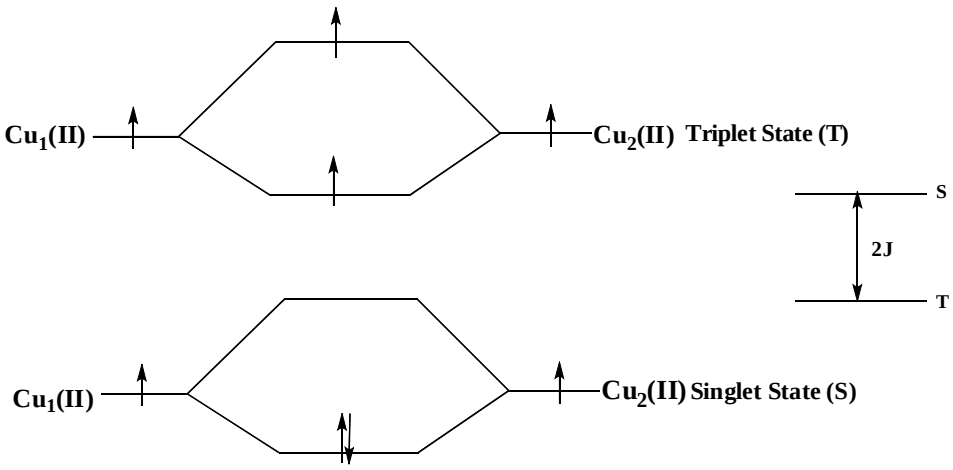

The room temperature and low temperature μ_{eff} values obtained from Co(II) and Ni(II) complexes are also found to be normal. Magnetic properties of binuclear Co(II), Ni(II) and Cu(II) complexes as given in **Table 4B.2**.

The validity of the above 2J value is further supporting the closeness of the g value obtained here with that evaluated from the polycrystalline ESR measurement[13].

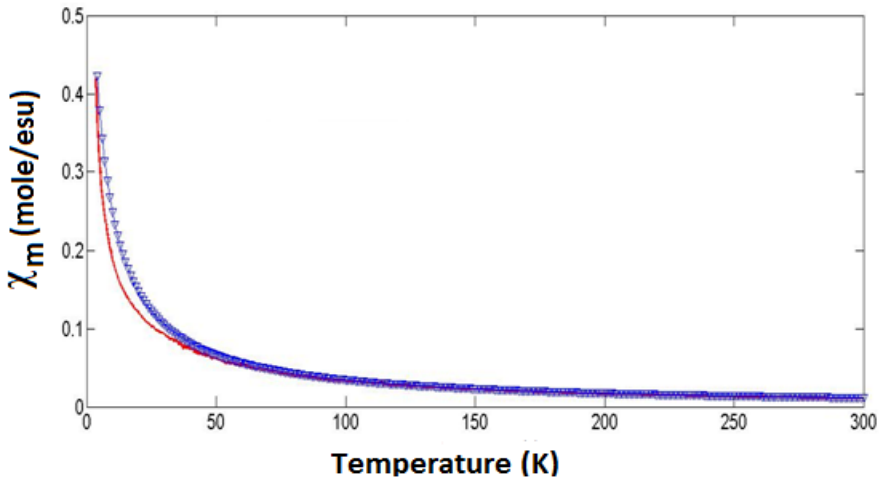

Figure 4B.1: Cryomagnetic susceptibility profile of $[Co_2L_2^1(H_2O)_4]$; (—▽—) experimental, (—) curve-fit line to eqn. 4.2 for g = 5.4, θ = -4.6 and J = 20 cm^{-1}

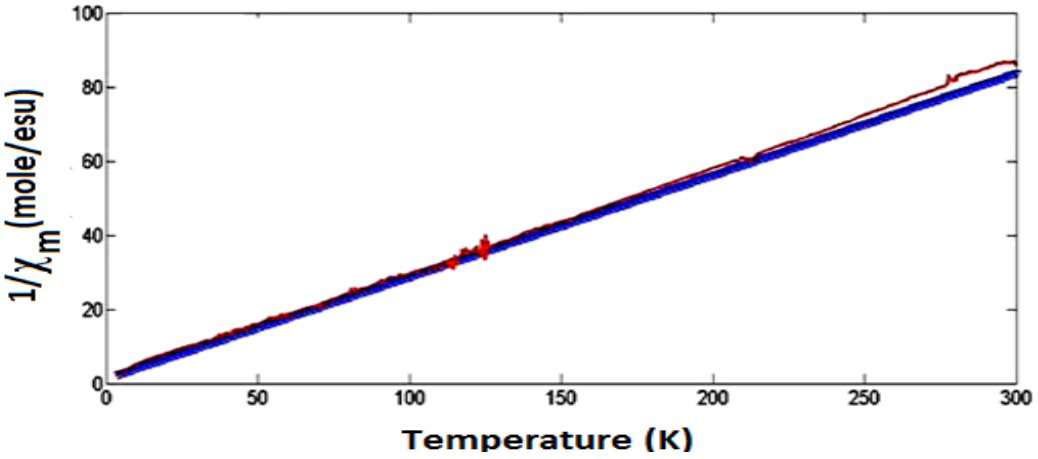

Figure 4B.2: Cryomagnetic susceptibility profile of $[Co_2L_2^1(H_2O)_4]$; (—▽—) experimental, (—) curve-fit line to eqn. 4.2 for g = 5.4, θ = -4.6 and J = 20 cm^{-1}

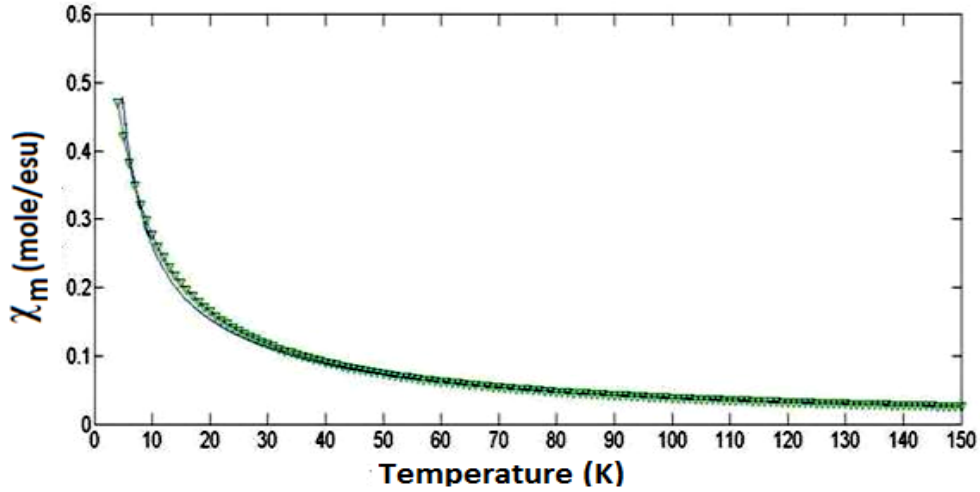

Figure 4B.3: Cryomagnetic susceptibility profile of $[Co_2L_2^2(H_2O)_4]$; (—▽—) experimental, (—) curve-fit line to eqn. 4.2 for g = 5.7, θ = -4.6 and J = 20 cm^{-1}

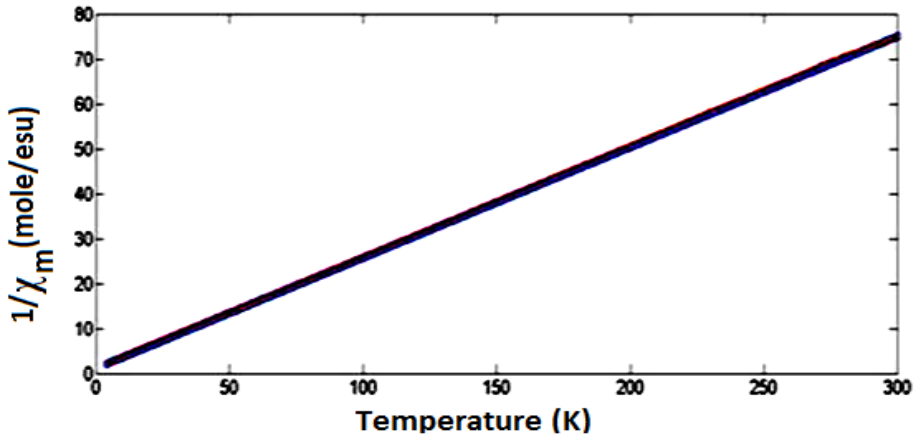

Figure 4B.4: Cryomagnetic susceptibility profile of $[Co_2L_2^2(H_2O)_4]$; (—▽—) experimental, (—) curve-fit line to eqn. 4.2 for g = 5.7, θ = -4.6 and J = 20 cm^{-1}

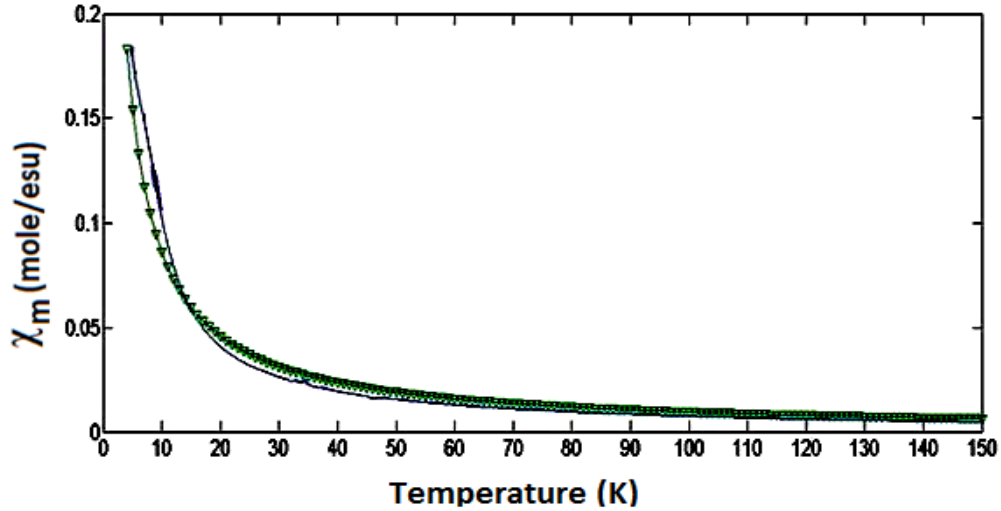

Figure 4B.5: Cryomagnetic susceptibility profile of $[Co_2L_2^5(H_2O)_4]$; (—▽—) experimental, (—) curve-fit line to eqn. 4.2 for g = 5.2, θ = -1.35 and J = 20 cm^{-1}

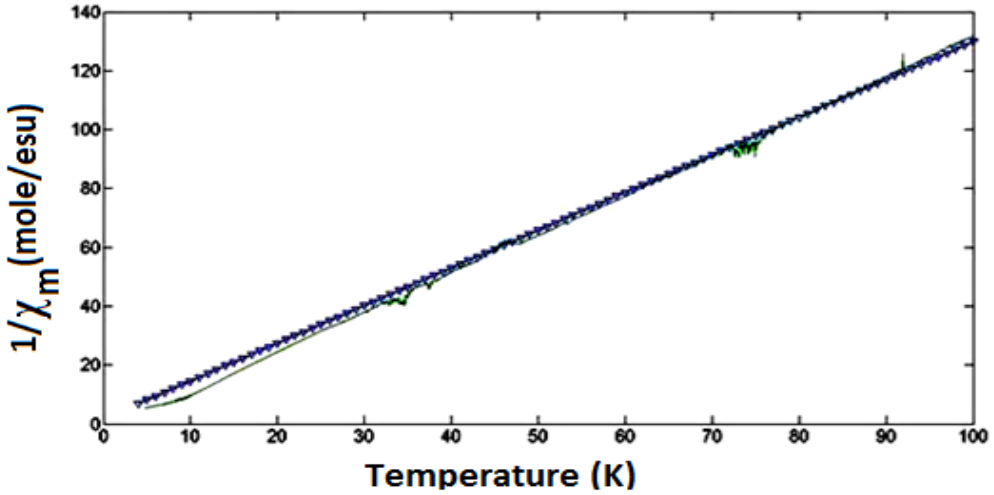

Figure 4B.6: Cryomagnetic susceptibility profile of $[Co_2L_2^5(H_2O)_4]$; (—▽—) experimental, (—) curve-fit line to eqn. 4.2 for g = 5.2, θ = -1.35 and J = 20 cm^{-1}

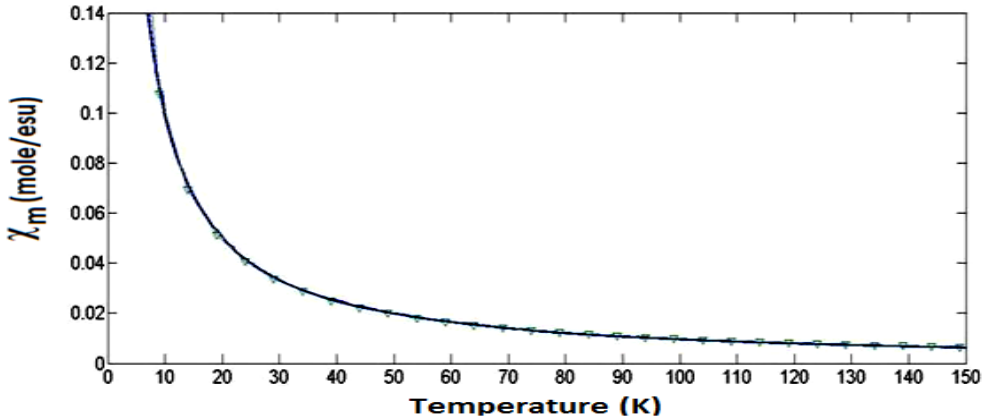

Figure 4B.7: Cryomagnetic susceptibility profile of $[Ni_2L_2^1]$; (—▽—) experimental, (—) curve-fit line to eqn. 4.2 for g = 2.8, θ = -0.1 and J = 20 cm^{-1}

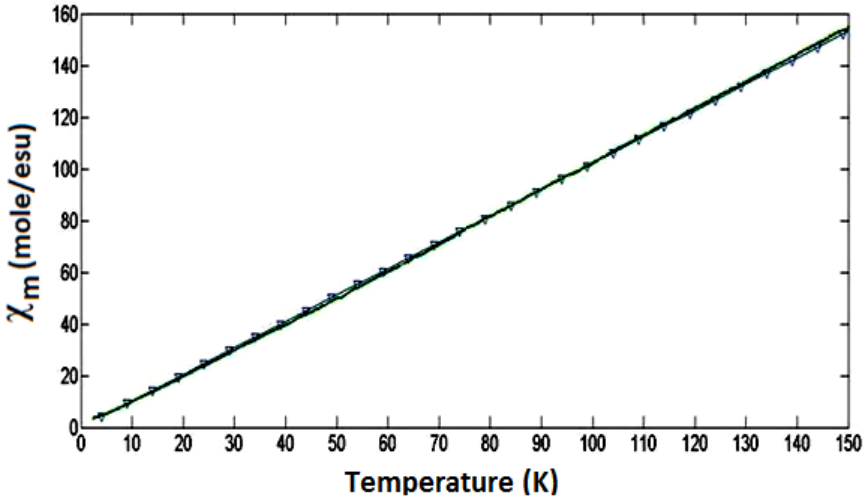

Figure 4B.8: Cryomagnetic susceptibility profile of [$Ni_2L_2^1$]; (—▽—) experimental, (—) curve-fit line to eqn. 4.2 for g = 2.8, θ = -0.1 and J = 20 cm^{-1}

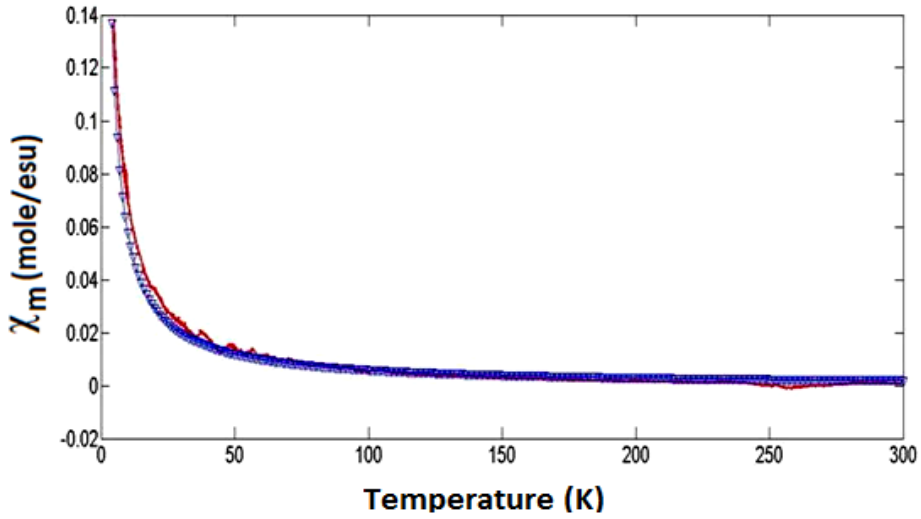

Figure 4B.9: Cryomagnetic susceptibility profile of [$Cu_2L_2^1$]; (—▽—) experimental, (—) curve-fit line to eqn. 4.2 for g = 2.19, θ = -0.38 and J = 20 cm^{-1}

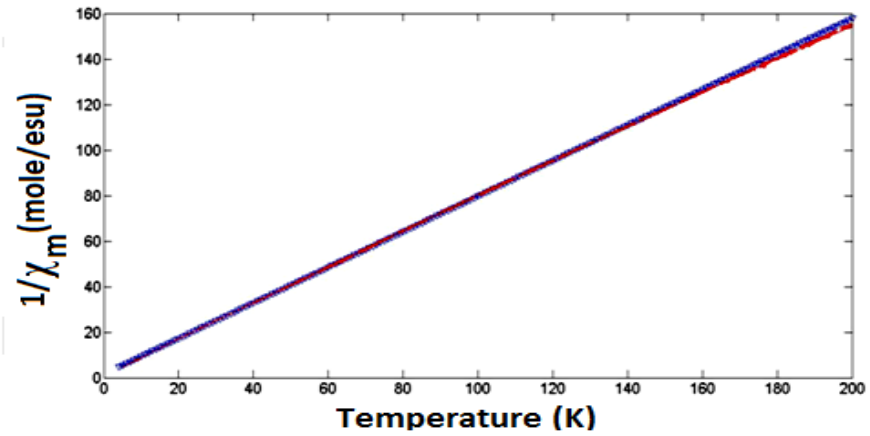

Figure 4B.10: Cryomagnetic susceptibility profile of [$Cu_2L_2^1$]; (—▽—) experimental, (—) curve-fit line to eqn. 4.2 for g = 2.19, θ = -0.38 and J = 20 cm^{-1}

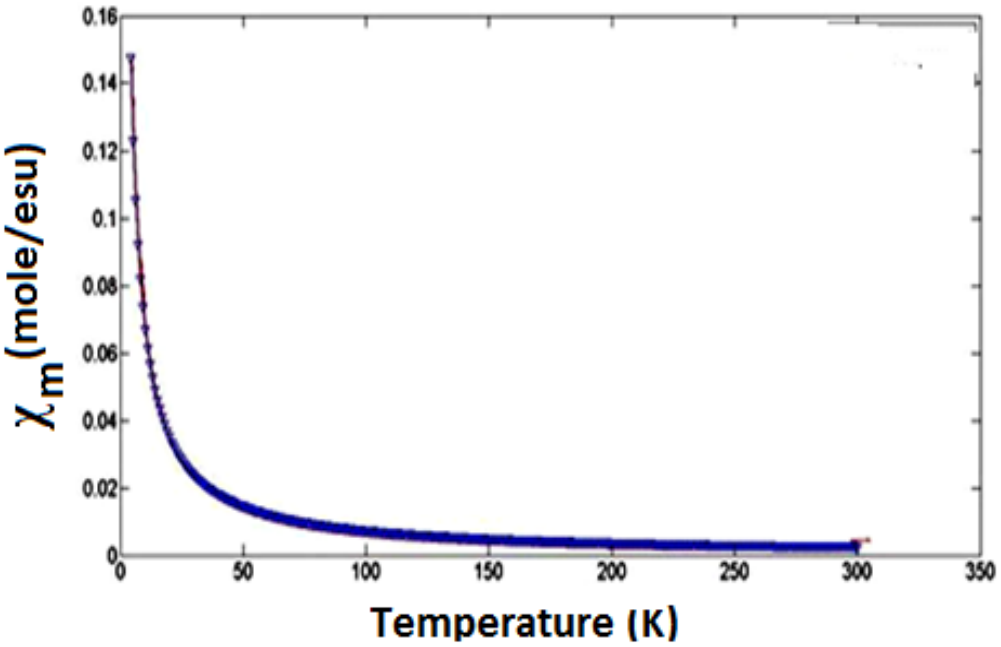

Figure 4B.11: Cryomagnetic susceptibility profile of $[Cu_2L_2^2]$; (—▽—) experimental, (—) curve-fit line to eqn. 4.2 for g = 2.43, θ = -1.0 and J = 20 cm^{-1}

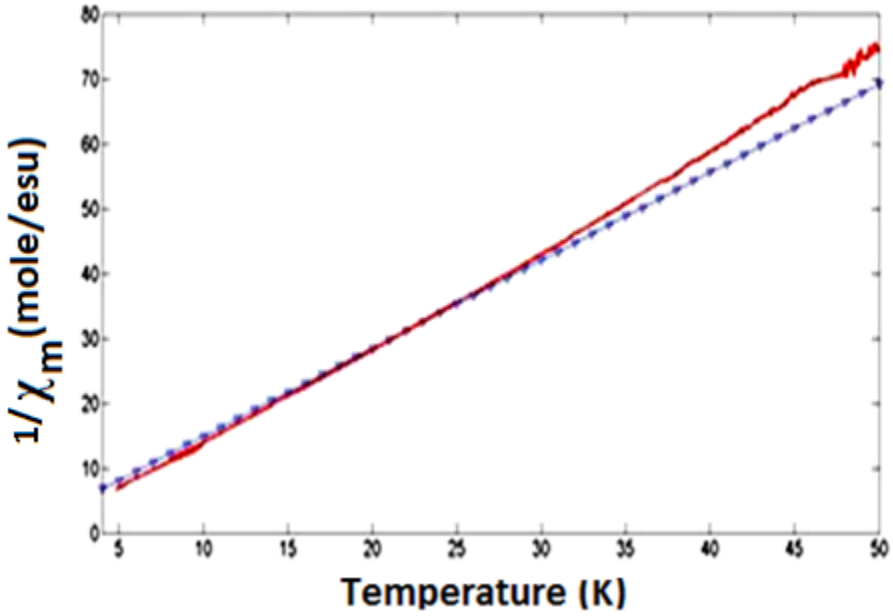

Figure 4B.12: Cryomagnetic susceptibility profile of $[Cu_2L_2^2]$; (—▽—) experimental, (—) curve-fit line to eqn. 4.2 for g = 2.43, θ = -1.0 and J = 20 cm

Table 4B.1: *Variable temperature magnetic susceptibility data of* $Cu_2L_2^1$

T ^{0}K	$\chi_{M \times 10^{-3}}$	μ_{eff}	T ^{0}K	$\chi_{M \times 10^{-3}}$	μ_{eff}
270.01	-0.14	1.41	28.018	24.87	2.43
260.01	-0.25	1.45	27.012	27.11	2.40
250.00	1.44	1.52	26.233	27.31	2.30
220.04	1.64	1.60	24.018	28.77	2.39
200.02	1.85	1.73	23.048	30.72	2.40
190.03	2.07	1.78	22.042	32.45	2.41
180.00	2.19	1.79	21.047	34.44	2.39
170.01	2.58	1.88	19.032	37.42	2.37
160.02	2.84	1.91	18.019	38.74	2.37
150.01	3.07	1.93	17.050	40.99	2.37
140.03	3.35	1.94	16.037	43.61	2.37
130.00	3.89	2.01	15.481	45.28	2.39
120.01	4.43	2.07	14.014	50.52	2.40
110.01	4.85	2.07	13.047	55.10	2.38
90.88	7.15	2.29	12.028	58.51	2.39
80.08	8.12	2.29	11.019	64.34	2.37
70.01	10.08	2.35	10.015	69.84	2.36
60.02	11.54	2.36	9.031	76.78	2.37
50.00	14.00	2.37	8.001	87.61	2.35
40.05	18.32	2.43	7.000	97.88	2.32
30.02	23.20	2.41	6.001	111.86	2.31

Table 4B.2: *Magnetic properties of binuclear Co(II), Ni(II) and Cu(II) complexes*

Complex	**J (cm^{-1})**	**g**	**θ (K)**
$[Co_2L_2^1(H_2O)_4]$	20	5.4	-4.6
$[Co_2L_2^2(H_2O)_4]$	20	5.7	-4.6
$[Co_2L_2^5(H_2O)_4]$	20	5.2	-1.35
$[Ni_2L_2^1]$	20	2.8	-0.1
$[Ni_2L_2^2]$	20	2.0	-1.6
$[Cu_2L_2^1]$	20	2.19	-0.38
$[Cu_2L_2^2]$	20	2.43	-1.06
$[Cu_2L_2^5]$	20	2.1	-2.2

4B.2 ESR Spectral Studies

The X- band powder and chloroform solution ESR spectra showed a strong absorption at ~3200 G (g ~2.12). The solution even after considerable dilution and freezing did not give any hyperfine splitting. The frozen glass esr spectra of the complexes are given **Figures 4B.13-4B.15.** Relevant esr data are presented in **Table 4B.3**. $A_{\parallel}$ and $A_{\perp}$ values are calculated by taking one third of the line widths at half maximum while A_0 is obtained by the relation $A_0 = 1/3(A_{\parallel} + A_{\perp})$. Normally in cases of server deviation from square planar geometry towards tetrahedral the A_0 values will be lowered by nearly three times from those of perfect square planar copper(II) complexes. A_0 value for tetrahedral geometry is of the order of 45 G (40 x 10^{-4} cm^{-1}), the observed A_0 values, in the present series of copper(II) complexes are about 35 G which is nearly, there are a series of pseudotetrahedral complexes which do not show any hyperfine esr spectra in solution. The absence of the splitting in solution even at liquid nitrogen temperature is due to dipolar line broadening. Due to the same effect the A_0 value is further reduced in the present Schiff base complexes. The above observation supports that the geometry around copper can best be described as pseudotetrahedral as predicted from the electronic spectral data[19]. The solution ESR spectra do not resolve the electron-nuclear spin coupling of the Cu(II) complexes. Computer simulation has been used to obtain the tensorial values of $g_{\parallel}$, $g_{\perp}$ and g_0 those of A_{xx}, A_{yy} and A_{zz} as shown in **Table 4B.3**.

Table 4B.3: *ESR spectral data of Cu(II) complexes*

Complex	$g_{\parallel}$	$g_{\perp}$	g_0 [a]	$A_{\parallel}$	$A_{\perp}$	A_0
$[Cu_2(NDADPE)_2]$	2.05	2.06	2.19	5.8	2.9	5.3
$[Cu_2(NDADPM)_2]$	2.07	1.96	1.98	21	1	1.4
$[Cu_2(NDADPD)_2]$	2.03	1.97	1.99	0.7	12	8.2
$[Cu_2(NDADPT)_2]$	2.04	1.99	2.01	1.2	18	12.4
$[Cu_2(NDADPB)_2]$	2.05	2.06	2.19	0.36	16	44

a : $g_0 = 1/3(g_{\parallel} + 2_{g_{\perp}})$b: room temperature (chloroform solution) c: $A_0 = 1/3(A_{\parallel} + 2_{A_{\perp}})$

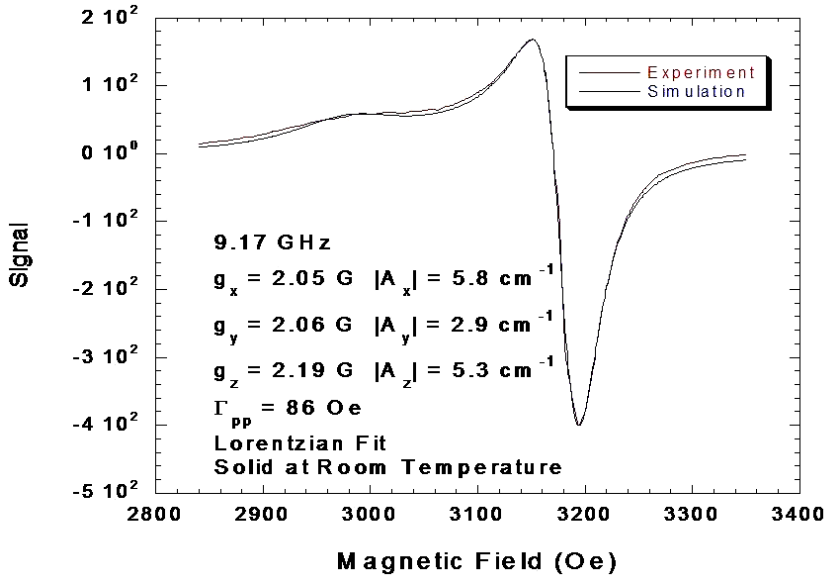

Figure 4B.13: Frozen glass EPR spectrum of $[Cu_2L_2^1]$ complex

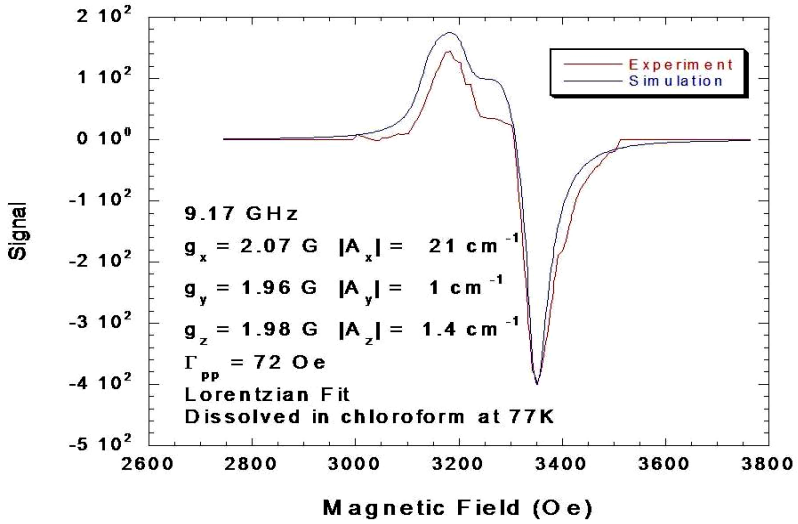

Figure 4B.14: Frozen glass EPR spectrum of $[Cu_2L_2^2]$ complex

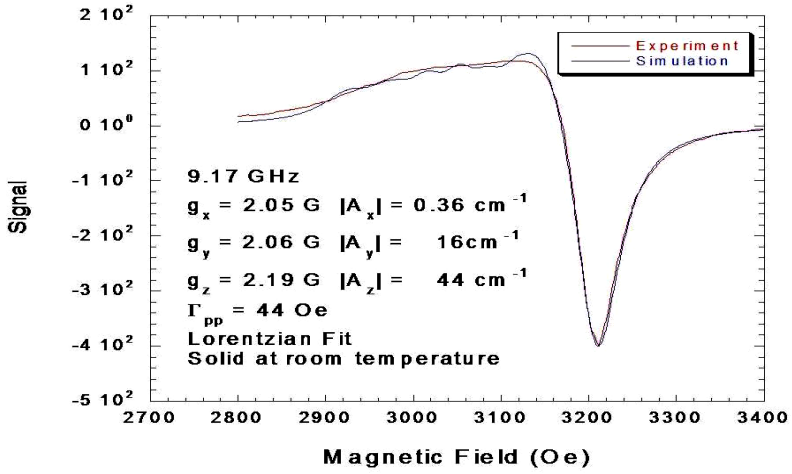

Figure 4B.15: Frozen glass EPR spectrum of $[Cu_2L_2^5]$ complex

PART C: THERMAL STUDIES

Thermometric studies have been carried out on under nitrogen atmosphere/static air at a heating rate of 20 °C min^{-1} from ambient temperature up to 1000 °C.

The decomposition stages, temperature range, decomposition products, as well as the found and calculated mass loss percentages of all the complexes are illustrated in **Table 4C**.1.

The TGA curve of Co(II) complex is shown in **Figure 4C**.1. $[Co_2L_2^1(H_2O)_4]$ complex was decomposed in two steps. The first step is occurring within the temperature range ~120^0C and it can be attributed to the loss of two coordinated water molecules and ligand molecule. The second and third step corresponds to the complete loss of ligand molecule in the temperature range between 308-408^0C with a mass loss of 81.16%. The remaining mass loss 12.48% is due to the formation of CoO as residue.

The TGA curve of Ni(II) complex is shown in **Figure.4C.2**. $[Ni_2L_2^1]$ complex was decomposed in one step. This step corresponds to the loss of ligand molecules within the temperature range of 358-700 ^{0}C with a mass loss of 87.05% . The residue with a mass loss of 13.3% is regarded as NiO.

The TGA and DTA Curves are shown in **Figures 4C.3** and **4C.4**. Thermal Data of acquired from there thermograms are presented in **Table 4C.1**. At step 1 obtained at ~173^0C a loss of 6% is observed. This suggests a loss of four water molecules. The temperature of the event supports the lost water is coordinated water. The DTA data at the high temperature the dehydrated complex was found thermal event at ~423^0C with a mass loss of 80.1%. The final mass loss 13.1% is due to the CuO as residue.

Thermometric studies have been carried out on under nitrogen atmosphere and static air. A few representative thermograms of TGA/DSC curves are shown in **Figure 4C.5.** Useful thermal data are collected in **Table 4C.1** for Zn(II) complexes. The molecular formulae of the complexes $Zn_2L_2^1$ deduced from elemental analysis indicate the presence of coordinated water. In the case of $Zn_2L_2^2$ and $Zn_2L_2^5$ complexes, there is no significant weight loss below 173 °C suggesting the absence of coordinated or lattice water, whereas in $Zn_2L_2^1$ complexes weight loss corresponding is observed at ~170^0C. This values match to the loss of 4 water

molecules per mole of the complex. Mass loss in the Pyrolytic cleavage of the complex. However, under nitrogen atmosphere the decomposition was not seen to even till 1000 ºC. This suggests that the dehydrated complex lignifies without any paralytics under inert condition.

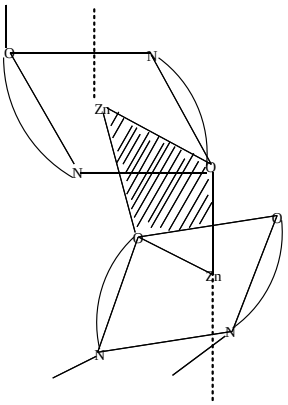

Scheme 4C.1

It can be seen that in like **Scheme 4C.1** in the case of Zn(II) complexes kinetics of copper(II) complexes also were investigated. Both Coats-Redfern and Horowitz-Metzger schemes were adopted.

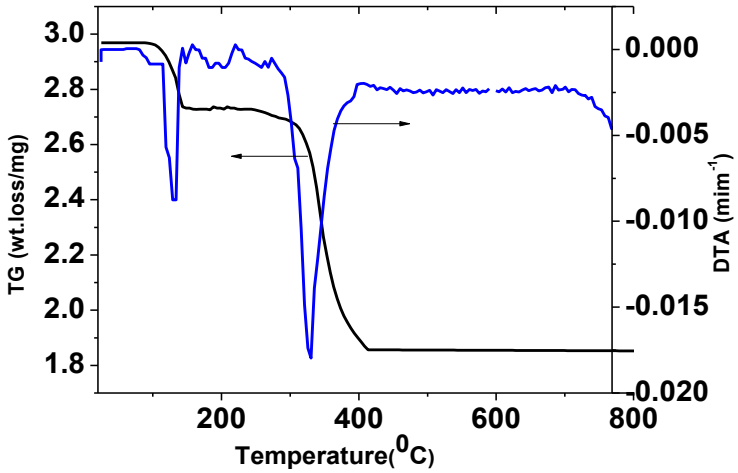

Figure 4C.1: Thermogravimetric (TG, Blue) and differential thermal analysis (DTA) curves of the Co_2L_2[1]

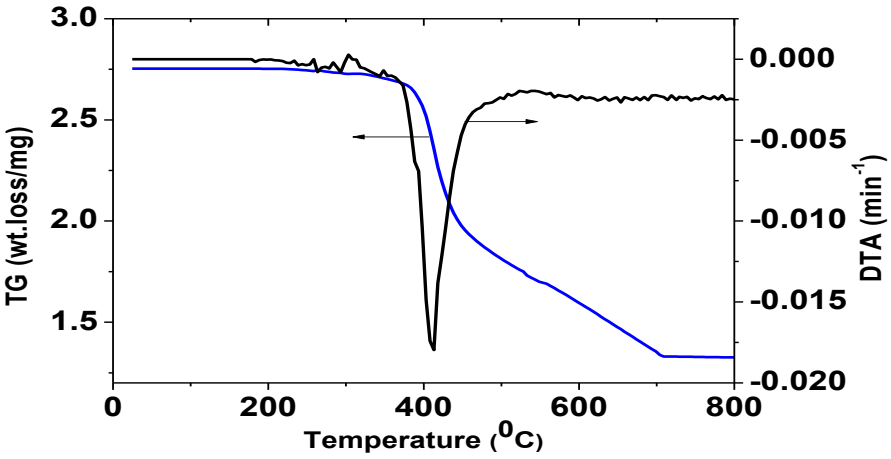

Figure 4C.2: Thermogravimetric (TG, Blue) and differential thermal analysis (DTA) curves of the Ni_2L_2[1]

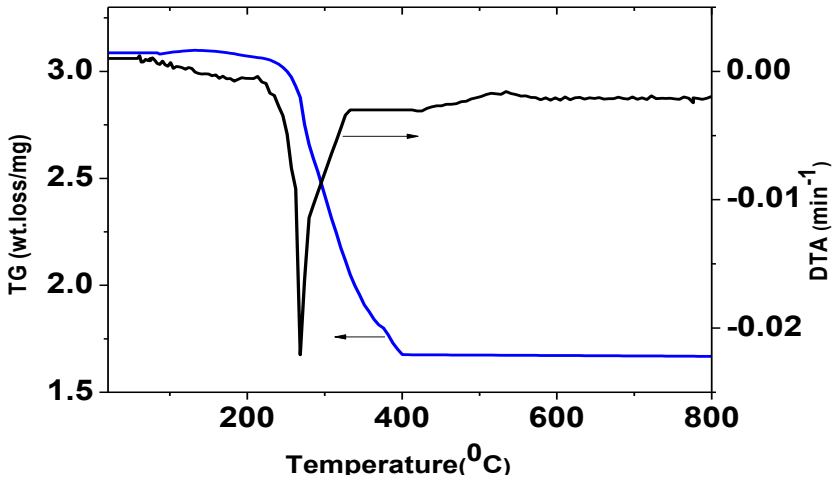

Figure 4C.3: Thermogravimetric (TG, Blue) and differential thermal analysis (DTA) curves of the $Cu_2L_2^1$

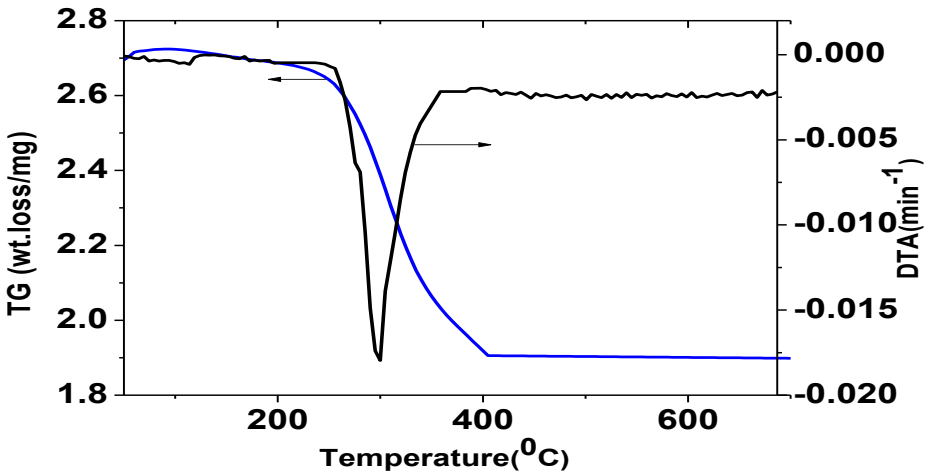

Figure 4C.4: Thermogravimetric (TG, Blue) and differential thermal analysis (DTA) curves of the $Cu_2L_2^2$

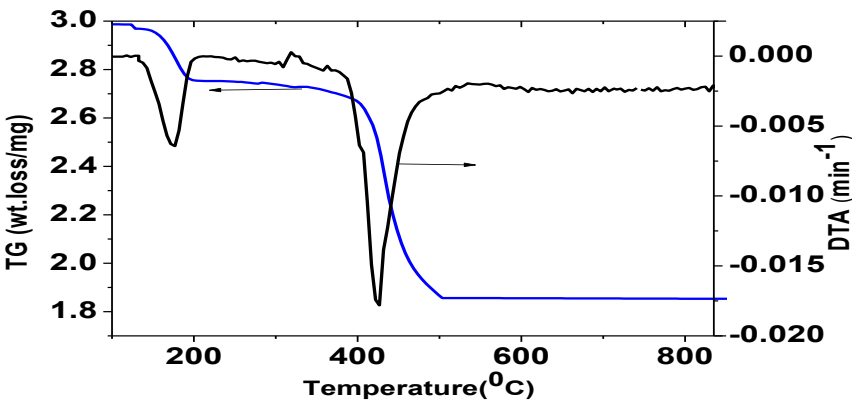

Figure 4C.5: Thermogravimetric (TG, Blue) and differential thermal analysis (DTA) curves of the $Zn_2L_2^1$

Table 4C.1: *Thermal behavior of Co(II), Ni(II), Cu(II) and Zn(II) complexes*

Complex	Temp. range (^{0}C)	Wt. loss (%)		Type of Peak	Assignment
		Found	Calcd		
$[Co_2L_2^1(H_2O)_4]$	118-148	5.8	5.9	Endo	$4H_2O$
	308-408	81.16	81.86	Endo	Organic part
	>410	13.1	13.2		Residue CoO
$[Ni_2L_2^1]$	358-700	87.03	87.15	Endo	Organic part
	>700	13.3	13.2		Residue NiO
$[Cu_2L_2^1]$	256-420	85.98	86.04	Endo	Organic part
	>422	14.0	13.9		Residue CuO
$[Cu_2L_2^2]$	245-415	86.05	89.88	Endo	Organic part
	>420	13.10	13.90		Residue CuO
$[Cu_2L_2^5]$	234-398	85.02	85.92	Endo	Organic Part
	>400	14.01	14.25		Residue CuO
$[Zn_2L_2^1(H_2O)_4]$	133-188	6.0	5.9	Endo	$4H_2O$
	383-498	80.97	81.01	Endo	Organic part
	>500	13.1	13.3		Residue ZnO
$[Zn_2L_2^2 (H_2O)_4]$	326-510	83.4	83.5	Endo	Organic part
	>510	12.9	13.0		Residue ZnO
$[Zn_2L_2^5(H_2O)_4]$	321-451	83.1	83.3	Endo	Organic Part
	>451	12.9	13.3		Residue ZnO

4C.1 Kinetics of Thermolysis

Non-isothermal calculations were used extensively to evaluate the thermodynamic and kinetic parameters for the different thermal decomposition steps of the metal complexes were determined using the Coats–Redfern[11] and Horowitz–Metzger[12]. The rate of decomposition of a solid depends upon the temperature, thermally conductivity amount of material, etc among others. The expression for the thermal decomposition of a homogeneous system has the following general

$$\frac{d\alpha}{dt} = k(T)g(\alpha) \qquad 4.3$$

where t is the time, T is the absolute temperature and α is the degree of transformation, defined as $\alpha = \frac{w_0 - w_t}{w_0 - w_\infty}$ wherein w_o, w_t and w_α are the weights of the sample before the degradation, at temperature t and after total conversion, respectively. K(T) is the rate coefficient that usually follows the Arrhenius equation. The differential conversion function, g(α) may present various functional forms but its most commonly form for solid-state reactions is g(α) = (1-α)n, where n is the reaction order, assumed to remain constant during the thermal reaction[13,14]. The rate constant is normally expressed by the Arrhenius equation:

$$K = A\, exp\left(-\frac{E_a}{RT}\right) \qquad 4.4$$

where E_a is the activation energy, A is the Arrhenius pre-exponential factor which indicates how frequents the reactant species attempt to undergo thermal process occurs and R is the gas constant in (J mol^{-1} K). Substituting in Eqn. (4.3) we get:

$$\frac{d\alpha}{dt} = A\, exp\left(-\frac{E_a}{RT}\right) g(\alpha) \qquad 4.5$$

when the reaction is carried out under a linear temperature program, ($T = T_o + \beta t$, where $\beta = dT/dt$ is the heating rate and T_o the starting temperature). A large number of decomposition processes can be represented as first order reaction[15]. Particularly, the degradation of the investigated series of metal complexes was suggested to be first order. Therefore we will assume n = 1 for the remainder of the present text. Under this assumption the integration of Eq. (4.5) leads to:

$$\ln(1-\alpha) = -\frac{A}{\beta}\int_{T_0}^{T} Exp\left(\frac{E}{RT}\right) dT \qquad 4.6$$

On the basis of Eq. (4.4), it is possible to analyze experimental data by the integral method, in order to determine the degradation kinetic parameters A, E_a. The temperature integral in the right hand side of Eqn. (4.6) has no exact analytical solution and several kinds of approximations are generally used. Two methods that differ on the way of resolving Eqn.

(4.6) are compared using the TGA data of the studied complexes. These methods are presented here

4C.1.1 *Coats–Redfern Method*

In this method the partiner equation is

$$ln\left[\frac{g(\alpha)}{T^2}\right] = ln\left(\frac{AR}{\beta E}\right) - \frac{E_a}{RT} \qquad 4.7$$

where $g(\alpha) = 1 - (1-\alpha)1 - n/1 - n$ for $n \neq 1$ and $g(\alpha) = -\ln(1-\alpha)$ for n =1, and R is the gas constant. The correlation coefficient, r, was computed using the least square's method for different values of n (n = 0.33, 0.5, 0.66 and n = 1) by plotting $ln\left[\frac{g(\alpha)}{T^2}\right]$ versus 1/T for the investigated metal complexes. The n-value which gave the best fit $(n \approx 1)$ was chosen as the order of the decomposition. From the slope of the straight line (E_a/R) in **Figures 4C.6-4C.9** for metal complexes, the activation energy E_a and from the intercept the pre-exponential factor, A could be determined. The data obtained are posted in **Table 4C.2.**

4C.1.2 *Horowitz–Metzger method*

The Horowitz–Metzger relation was also used to evaluate the degradation kinetics. The relevant relativities in this platform

$$ln[-\ln(1-\alpha)] = \frac{E_a\theta}{RT_s{}^2} \quad \text{for n=1} \qquad 4.8$$

$$ln\left[\frac{1-(1-\alpha)^{1-n}}{1-n}\right] = ln\left(\frac{A}{\beta}\frac{RT_s{}^2}{E}\right) - \frac{E_a}{RT_s} + \frac{E_a\theta}{RT_s{}^2} \quad \text{for } n \neq 1 \qquad 4.9$$

where h = T - T_s, T_s is the DTG peak temperature, T the temperature corresponding to weight loss, W_t. In this method a straight line should be observed between ln [ln(1-α)] and θ with a slope of $\frac{E_a}{RT_s{}^2}$ **Figures 4C.10-4C.13,** the Horowitz–Metzger plots for the metal complexes under study. The obtained data are recorded in **Table 4C.3**.

$$\Delta H^* = E_a - RT \quad 4.10$$

$$\Delta S^* = R\left(ln\frac{hA}{K_B T} - 1\right) \quad 4.11$$

$$\Delta G^* = \Delta H - T\Delta S \quad 4.12$$

where ΔH* is the enthalpy of activation (kJ/mol^{-1}), ΔS the entropy of activation (kJ/mol K) and ΔG* the Gibbs free enthalpy of activation (kJ/mol), h the Planck constant and K_B the Boltzmann constant. From the results obtained, the following remarks can be pointed out:

i. All decomposition steps show best fit for n = 1.
ii. The negative value of the entropy of activation, ΔS* of some decomposition steps in case of the ion exchange and its metal complexes with all investigated metal ions indicates that the activated fragments have more ordered structure than the undecomposed ones later.
iii. The positive sign of activation enthalpy change, ΔH* indicates that the decomposition stages are endothermic processes.
iv. The high values of the energy of activation, E_a of the complexes reveal the high
v. stability of such chelates due to their covalent bond character[16].
vi. The positive sign of ΔG* for the investigated complexes reveals that the free energy of the final residue is higher than that of the initial compound, and hence all the decomposition steps are nonspontaneous processes. Moreover, the values of ΔG* increase significantly for the subsequent decomposition steps of a given compound. The fact that the thermolytic precedent of temperature demand more TΔS* would image that thermolytic loss of structural portieres is gradually difficult.

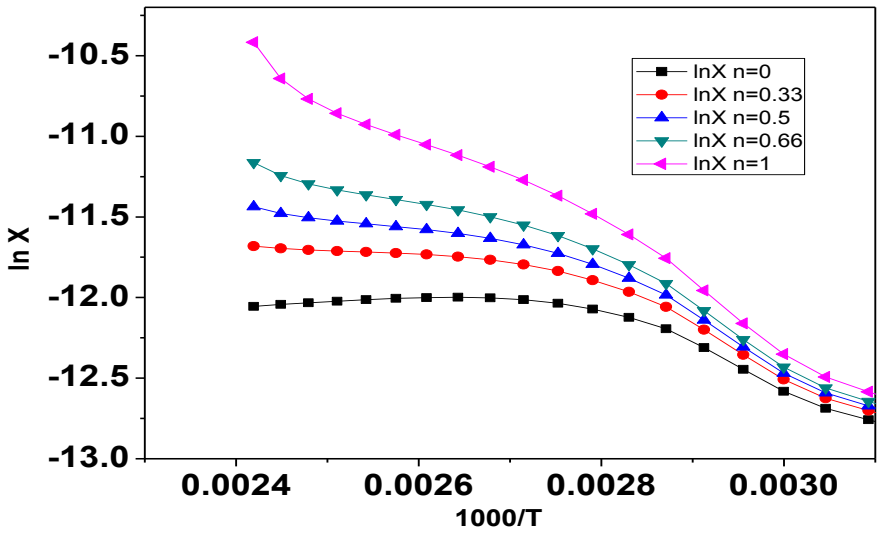

Figure 4C.6: Coats-Redfern plots of $Co_2L_2^1$ complex

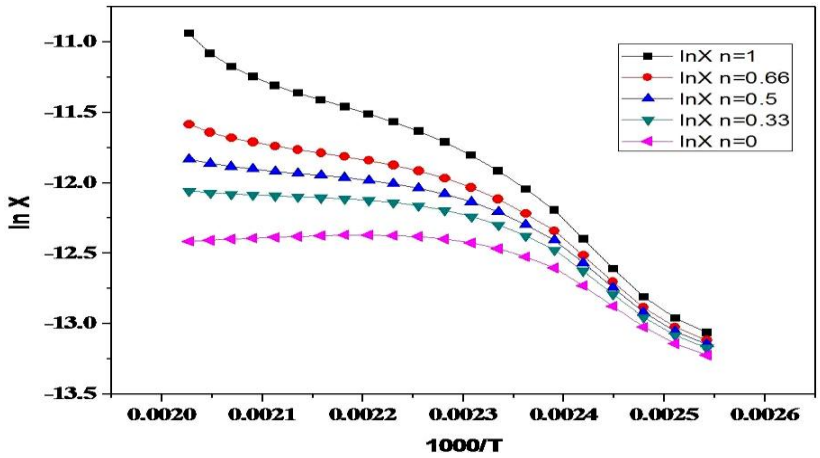

Figure 4C.7: Coats-Redfern plots of $Ni_2L_2^1$ complex

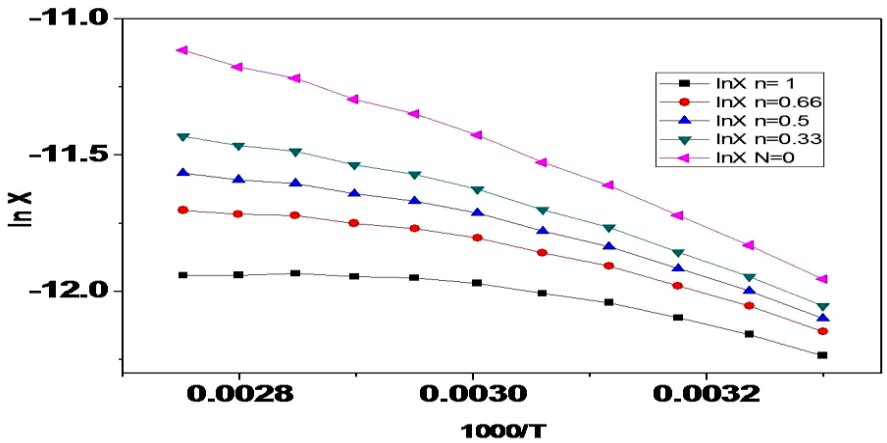

Figure 4C.8: Coats-Redfern plots of $Cu_2L_2^1$ complex

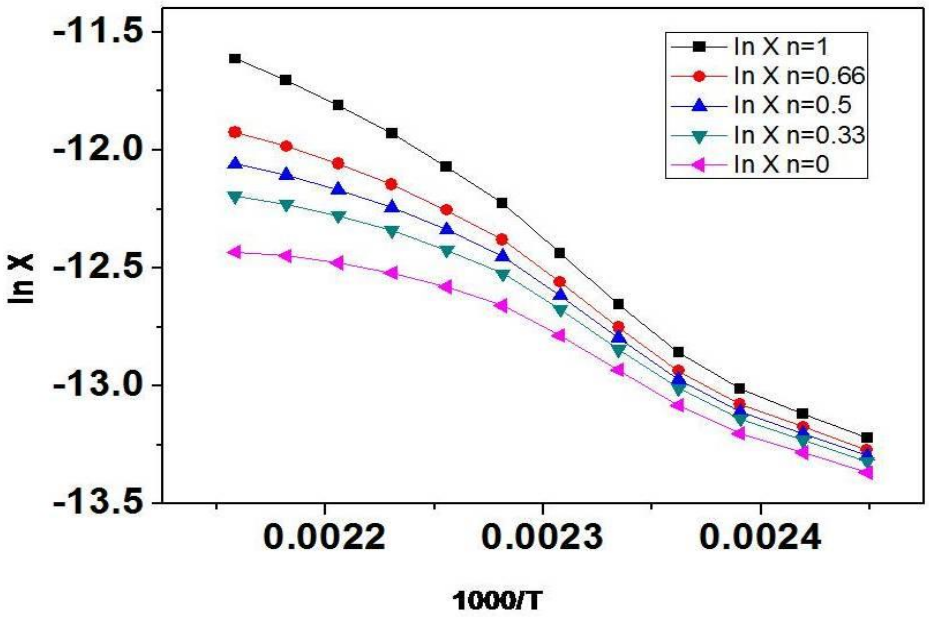

Figure 4C.9: Coats-Redfern plots of $Zn_2L_2^1$ complex

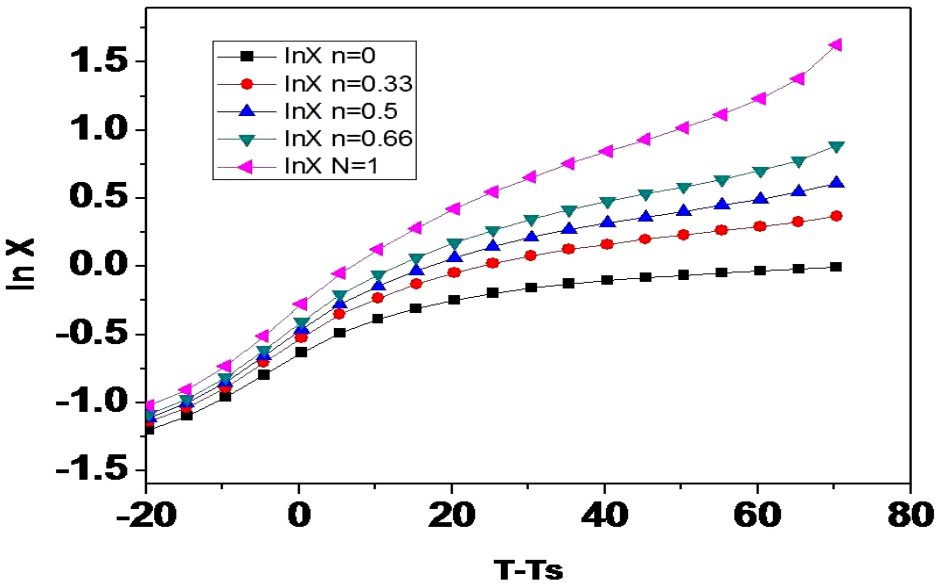

Figure 4C.10: Howoritz Metzer plots of $Co_2L_2^1$ complex

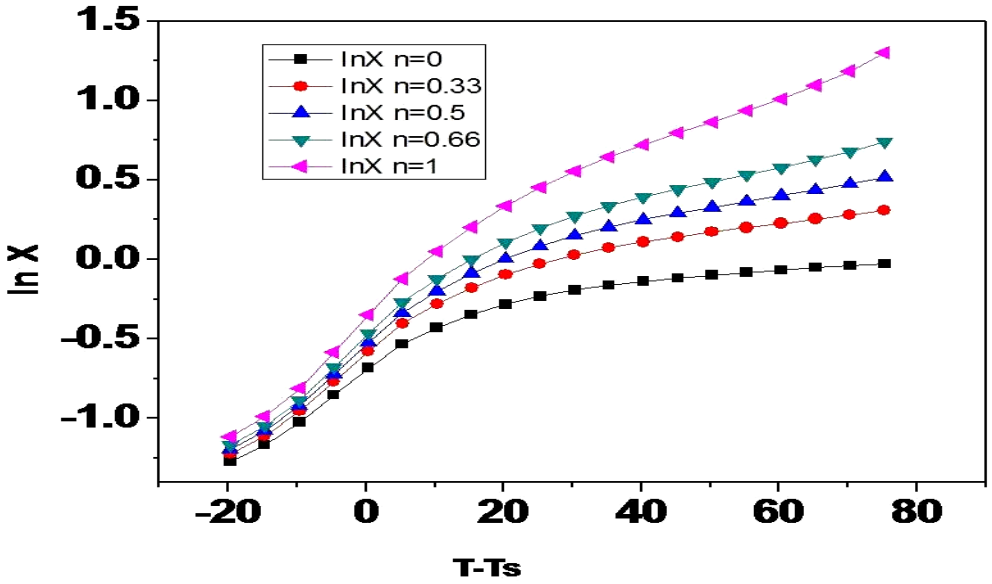

Figure 4C.11: Howoritz Metzer plots of $Ni_2L_2^1$ complex

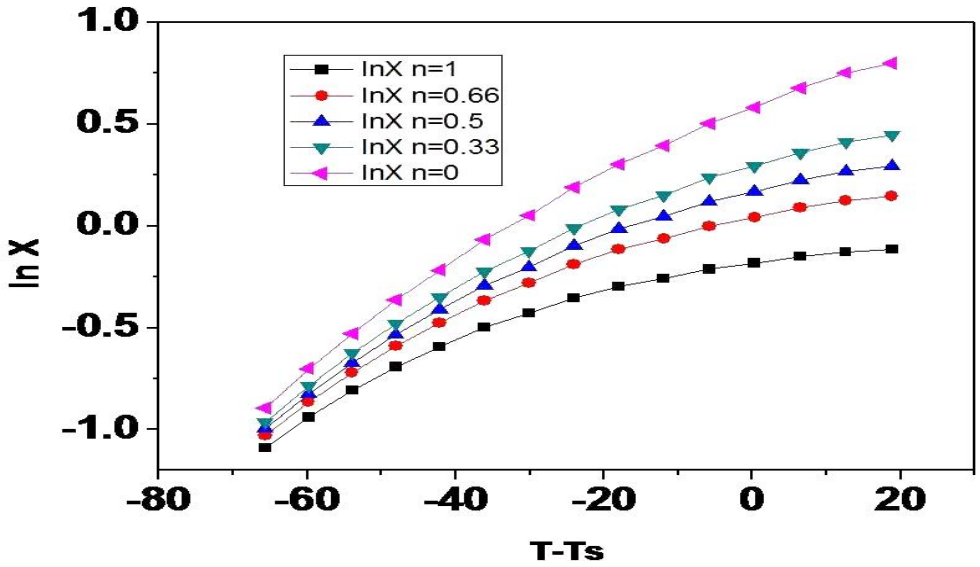

Figure 4C.12: Howoritz Metzer plots of $Cu_2L_2^1$ complex

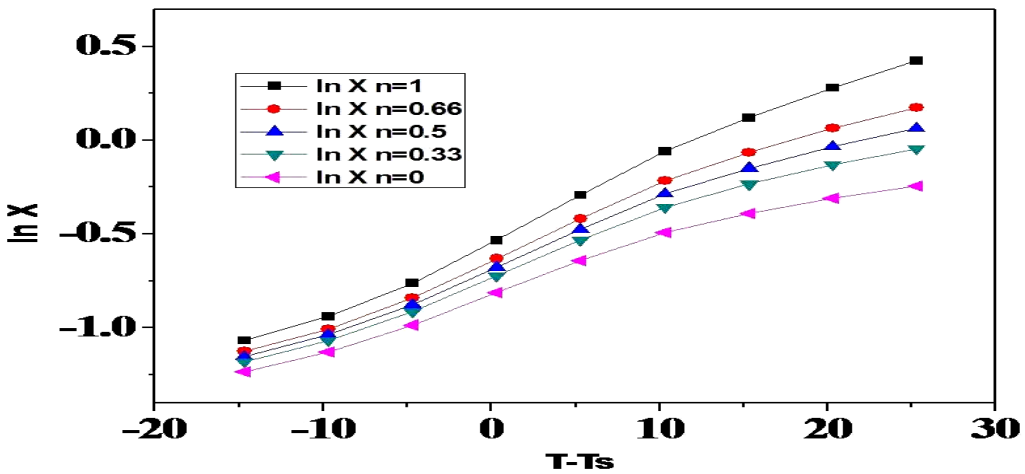

Figure 4C.13: Horowitz-Metzger plots of $Zn_2L_2^1$ complex

Table 4C.2: *Kinetic parameters of Co(II), Ni(II), Cu(II) and Zn(II) complexes evaluated by Coats-Redfern equation*

Complex	**Mid temp(K)**	**Ea (kJ/mol)**	**A (S^{-1})**	**ΔH (k_J/mol K)**	**ΔS (k_J/mol K)**	**ΔG (k_J/mol)**
$[Co_2L_2^1(H_2O)_4]$	133	35.8	13.21	34.78	-0.45	58
	343	44.7	7.37	44.8	-0.0955	47
$[Ni_2L_2^1]$	413	34.52	1.40	34.02	-0.0753	24
$[Cu_2L_2^1]$	268	54.12	26.25	53.56	-0.36	58.32
$[Cu_2L_2^2]$	305	28.23	7.25	27.86	-0.08	45.12
$[Cu_2L_2^5]$	398	31.22	17.8	30.52	-0.053	73.2
$[Zn_2L_2^1(H_2O)_4]$	173	25.91	18.18	24.94	-0.23	65.92
	433	50.08	1.43	41.57	-0.095	82.70
$[Zn_2L_2^2(H_2O)_4]$	447	45.02	2.01	38.25	-0.012	85.20
$[Zn_2L_2^5(H_2O)_4]$	388	32.12	17.8	31.22	-0.056	74.23

Table 4C.3: *Kinetic parameters of Co(II), Ni(II), Cu(II) and Zn(II) complexes evaluated by* Horowitz- Metzger

Complex	**Mid temp (K)**	**Ea (kJ/mol)**	**A(S^{-1})**	**ΔH (k_J/mol K)**	**ΔS (k_J/mol K)**	**ΔG (k_J/mol)**
$[Co_2L_2^1(H_2O)_4]$	133	35.2	12.35	34.25	-0.42	56
	343	43.7	7.37	42.8	-0.0954	46
$[Ni_2L_2^1]$	413	34.01	1.38	33.17	-0.0723	23
$[Cu_2L_2^1]$	268	54.10	25.22	52.56	-0.32	57.32
$[Cu_2L_2^2]$	305	27.02	7.22	26.06	-0.07	44.12
$[Cu_2L_2^5]$	398	31.02	17.2	30.29	-0.051	72.25
$[Zn_2L_2^1(H_2O)_4]$	173	25.81	18.09	23.94	-0.23	65.90
	433	50.02	1.39	41.57	-0.095	82.68
$[Zn_2L_2^2(H_2O)_4]$	447	45.01	2.00	38.24	-0.012	85.40
$[Zn_2L_2^5(H_2O)_4]$	388	31.25	17.2	30.29	-0.052	73.25

PART D: ELECTROCHEMICAL STUDIES

None of the metal complexes, $M_2L_2^i$ are soluble in water and hence the electrochemical studies of $M_2L_2^i$ could be carried out in non-aqueous media only. The electron transfer properties of the complexes were studied in DMF with tetra ethyl ammonium perchlorate (TEAP) as the supporting electrolyte. Cyclic voltammetry was used as the primary tool. The experimental details of sampling and electrochemical run are reported in **Chapter II**.

4D.1 Cobalt(II) Complexes

A typical cyclic voltammogram obtained in the potential range of -1.6 V to +1.6 V (Ag | AgCl) on GCE for $[Co_2L_2^1(H_2O)_4]$ is presented in **Figure 4D.1** and **4D.2**. An irreversible oxidation peak at ~ 0.850 V and another quasireversible reduction peak at ~-1.250 V are observed. The cathodic response is not very clean but seems to be arising from more than one reducible sites. The effect of scan rate, concentration, potential settings, etc on the cyclic voltammetric profiles suggest that the two electron transfer processes are diffusion controlled and that they belong to two different electrophores.

A comparision of the cyclic voltammograms of the complexes with those of the corresponding ligands indicates that the electron transfer processes due to reduction of azomethine group of the ligand frame work is slightly more cathodic. Free Co(II)|Co(III) redox couple appears at +1.59 V and Co(II)|Co(0) at -0.54V vs Ag | AgCl in aqueous media[17]. But when Co(II) is complexed, the Co(II)/Co(0) couple has a reduction potential more cathodically shifted such that it might join the hydrogen evaluation. We purpose that the multiple (shoulder like) cathodic peaks are due to the reduction of Co(II) and also that to the azomethine. In **Figure 4D.3** are shown the cyclic voltammogram of $[Co_2L_2^1(H_2O)_4]$ at various scan rates on the peak current. The fact that both cathodic and anodic current peaks are linear for the square root of scan rate suggests diffusion controlled electron transfer processes. The other $Co_2L_2^i$ behave similarly in DMF. Important electrochemical data such as Ep, ip, αn_a, k^0_h, D, etc, of all $Co_2L_2^1$ into **Table 4D.1**.

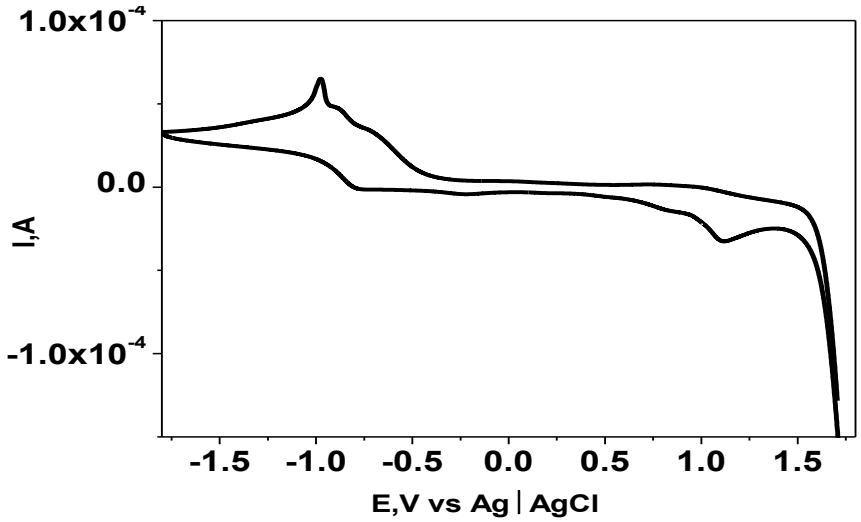

Figure 4D.1: Cyclic voltammogram of $Co_2L_2^1$ (3.06 x 10^{-4} M) in DMF on GCE at scan rate, 0.1 Vs^{-1}, with TEAP (0.1 M)

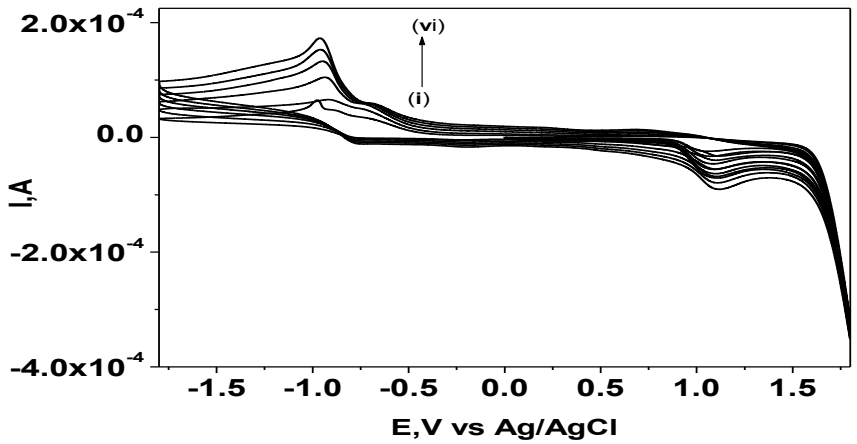

Figure 4D.2: Cyclic voltammograms of $Co_2L_2^1$ (3.06 x 10^{-4} M) in DMF on GCE at different scan rates, (i) 0.1, (ii) 0.2, (iii) 0.4, (iv) 0.6, (v) 0.8, (vi)1.0 Vs^{-1} with TEAP (0.1 M)

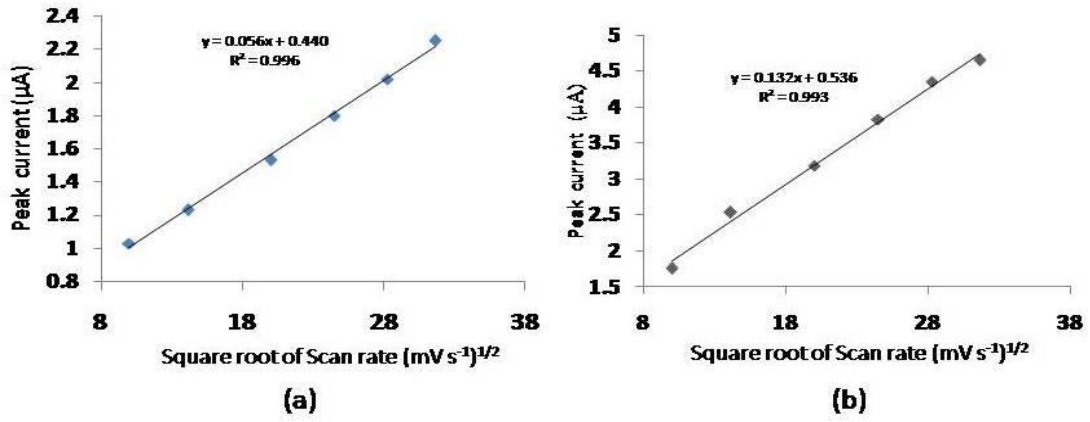

Figure 4D.3: Variation of peak current with scan rate of $Co_2L_2^1$ (3.06 x 10^{-4} M) at GCE; (a) for cathodic at ~0.1 V and (b) for anodic peak at ~ 1.0 Vs^{-1}

Table 4D.1: *Voltammetric data of* $Co_2L_2^1$ *complex*

Scan rate (mVs^{-1})	$-E_p$ (V)	α_{na}	k^o_h x10^9 (cm^2 /s)	D_o x 10^6 (cm^2 /s)
100	1.056	0.071	0.951	1.28
200	1.075	0.079	0.959	5.41
400	1.082	0.531	0.963	3.19
600	1.107	0.090	0.996	9.30
800	1.108	0.095	1.003	9.91
1000	1.122	0.096	1.012	7.88

4D.2 Electrochemical Studies of Ni(II) Complexes

Electrochemical studies for all the $Ni_2L_2^i$ have been investigated with cyclic voltammetry on this first method. In **Figures 4D.4** and **4D.5** are shown the CV profile of $Ni_2L_2^1$ as examples. Unlike in the case of $Co_2L_2^i$, the cathodic response for the reduction of the metal centre and the ligand part are well defined in the case of $Ni_2L_2^i$. The cathodic CV pattern may be visualised to have arisen by superposition of the Ni(II)|Ni(0) reduction and the reduction of the azomethine moiety[18]. The effect of scan rates and concentration on the ip and E_1 values are indicative of diffusion controlled electron transfer relevant electrochemical data of $Ni_2L_2^i$ are also collected.

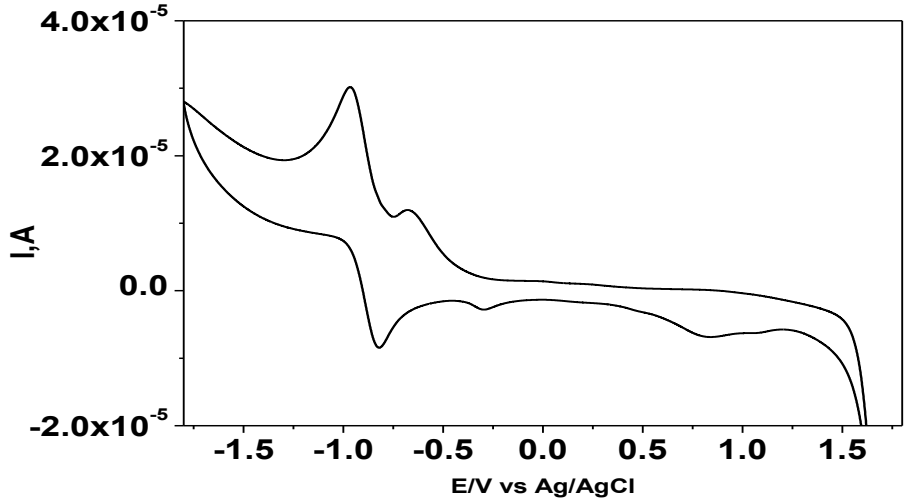

Figure 4D.4: Cyclic voltammogram of $Ni_2L_2^1$ (3.06×10^{-4} M) in DMF on GCE at scan rate, 0.1 Vs^{-1}, with TEAP (0.1 M)

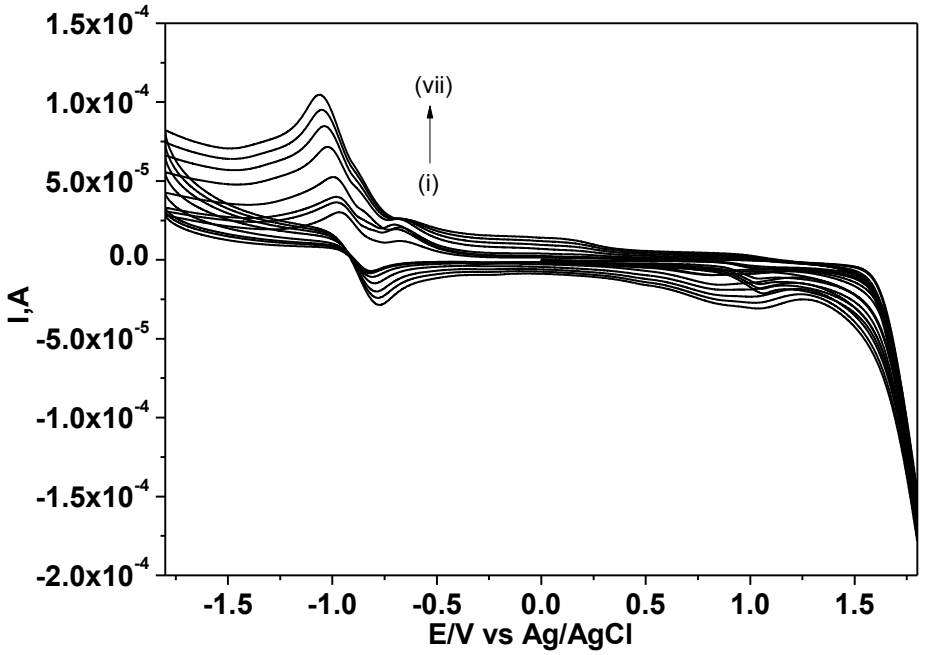

Figure 4D.5. Cyclic voltammograms of $Co_2L_2^1$ (3.06 x 10^{-4} M) in DMF on GCE at different scan rates, (i) 0.05, (ii) 0.08, (iii) 0.1, (iv) 0.2, (v) 0.4, (vi) 0.6, (vii) 0.8 Vs^{-1} with TEAP (0.1 M)

4D.3 Copper(II) Complexes

The Cu(II) analogous of $M_2L_2^i$ also exhibit both cathodic as well as anodic electron transfer characteristics. In **Figure 4D.6**, is shown a typical cyclic voltammogram. It can be observed from this figure, that there is a quasireversible reduction process at ~-0.7 V whereas a stepwise electron transfer at ~+0.2 and +0.8 in the anodic scan in **Figure 4D.7** are presented in **Table 4D.2,** overlapped cyclic voltammogram for this complex in the same medium for varied scan rates. From this figure, we can understand that complex exhibits greater reversibility at high scan rate than at lower scan rates. The cathodic response observed for this complex is attributed Cu(II) complexes. Usually Cu(II) undergoes reduction at ~0.3 V. In the present case, however, the reduction potential is at ~0.7 V. This greater cathodic drift for the reduction of copper(II) in the present complexes in the metal ions is greatly stabilized upon complexation. A cathodic drift of ~400 mV/s may be due to the stabilization alone. The copper(II) metal centres must have been rendered less reducible by charge transfer from ligand to metal (L→M). The near reversible electrochemical behaviour of $Cu_2L_2^1$-$Cu_2L_2^5$ complexes can be exploited for the electroanalytical assaying of copper(II) ion.

In the anodic region, one finds a set of 3 oxidation peaks with varied intensity. The low anodic and low intensity response is assigned to the low probable oxidation of Cu(II)|Cu(III). It is already reported in the literature for some binuclear copper complexes with N_2O_2 co-ordination geometry to exhibit Cu(II)|Cu(III)[19]. The more intense anodic response at ~0.8V is attributed to the usual azomethanine oxidation.

The reversible CV response at the cathodic zone is proposed as $Cu_2(II)L_2 + 2e \rightarrow Cu_2(I)L_2$ whereas reversible anodic peaks are as $Cu_2(II)L_2 \rightarrow Cu_2(II)L^+L + e$; $Cu_2(II)L^+L \rightarrow Cu_2(II)L^{2+}{}_2 + e$

Though the nonaqeuous (DMF) electrochemical response of $Cu_2L_2{}^i$ on the cathodic region on solid electrodes is either reversible (GCE) or quasireversible (platinum disc electrode) and mercury elctrode, it is totally different on the SMDE. In **Figure 4D.8** is shown the set of cyclic voltammograms of $Cu_2L_2{}^1$ in DMF on SMDE for various scan rates. A pair of widely separated reduction peaks appears. The lower cathodic peak position corresponds to the electrochemical reduction of Cu(II) centres whereas the more cathodic peak (with a further cathodic shoulder) to that of the azomethine site in **Figure 4D.9**. For want of hydrogen ion the reduction of the azomethine moiety must be involving free radical mechanism eqn.4.12, any as

$$Cu_2L_2{}^i + e^- \rightarrow Cu_2L^{i-\bullet}L^i + e^- \rightarrow Cu_2L_2{}^{i\,2-\bullet} \qquad 4.13$$

The effect of scan rate on both Cu(II)|Cu(I) and $Cu_2L_2{}^i$.| $Cu_2L_2{}^{2-}$. is not similar. The $Cu_2L_2{}^i$| $Cu_2L_2{}^{2-}$, exhibits linearity of ip vs ν with R^2 =0.942 and 0.997, respectively, in **Figure 4D.10** is presented as a representative case for $Cu_2L_2{}^1$. Usually, reduction of organic unsaturated sites on mercury electrode with free radical mechanism occurs by adsorptive manner. The linearity of i_p vs ν supports an adsorption complicated reduction of the azomethine sites.

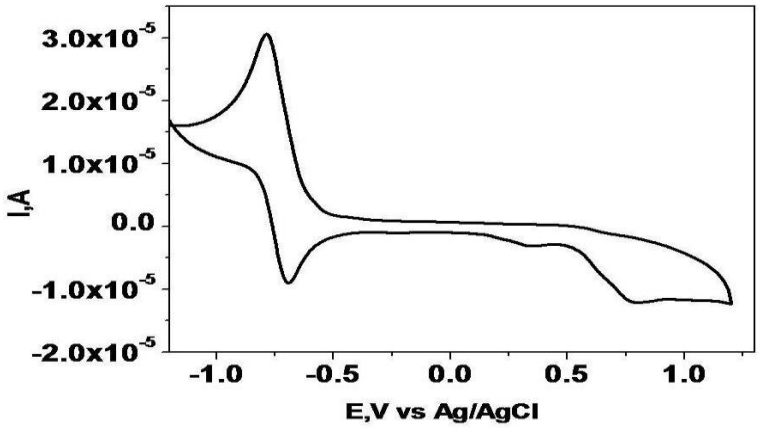

Figure 4D.6: Cyclic voltammogram of $Cu_2L_2{}^1$ (3.06×10^{-4} M) in DMF on GCE at scan rate, 0.1 Vs^{-1}, with TEAP (0.1 M)

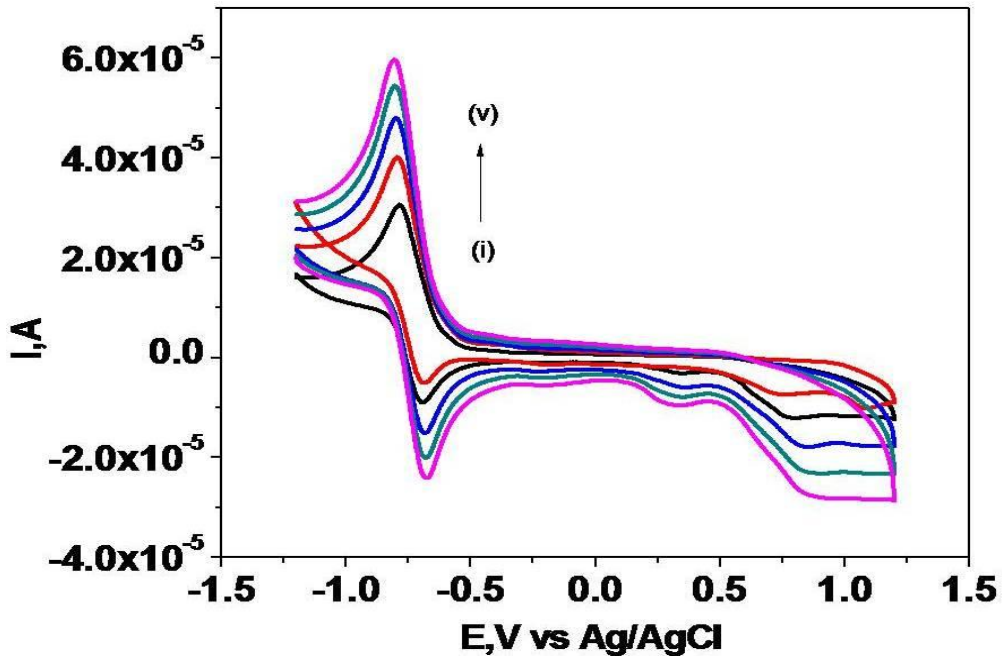

Figure 4D.7: Cyclic voltammograms of $Cu_2L_2^1$ (3.06 x 10^{-4} M) in DMF on GCE at different scan rates, (i) 0.1, (ii) 0.2, (iii) 0.3, (iv) 0.4, (v) 0.5, Vs^{-1} with TEAP (0.1 M)

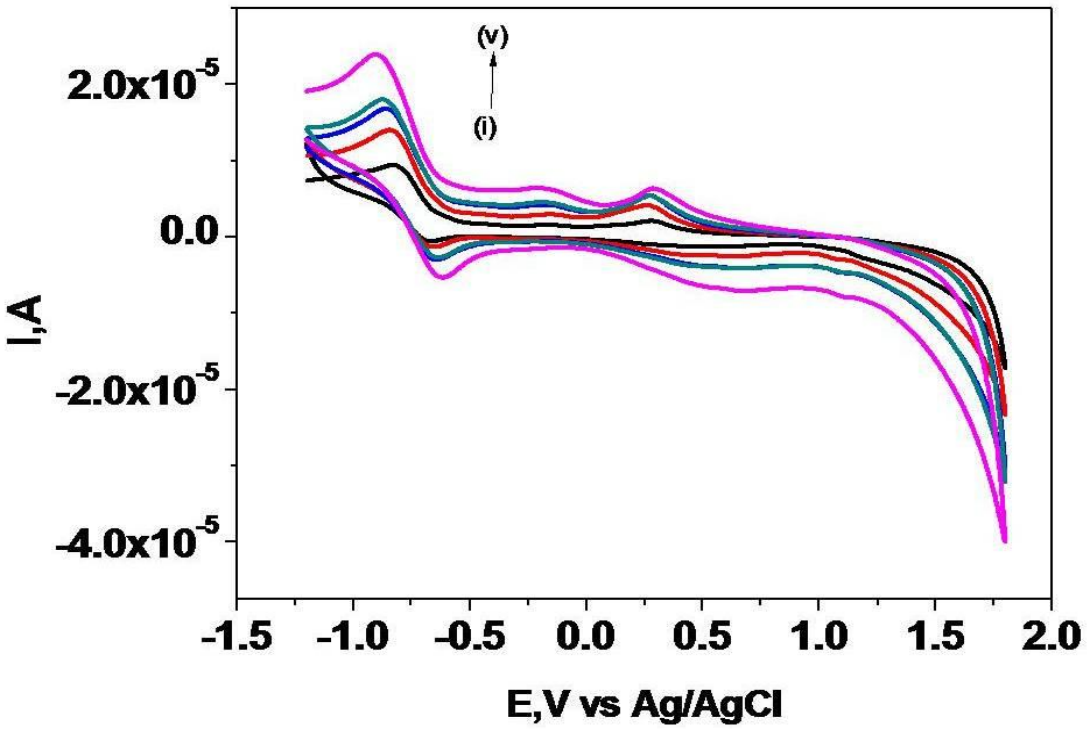

Figure 4D.8: Cyclic voltammograms of $Cu_2L_2^1$ (3.06 x 10^{-4} M) in DMF on Pt at different scan rates, (i) 0.1, (ii) 0.2, (iii) 0.3, (iv) 0.4, (v) 0.5, Vs^{-1} with TEAP (0.1 M)

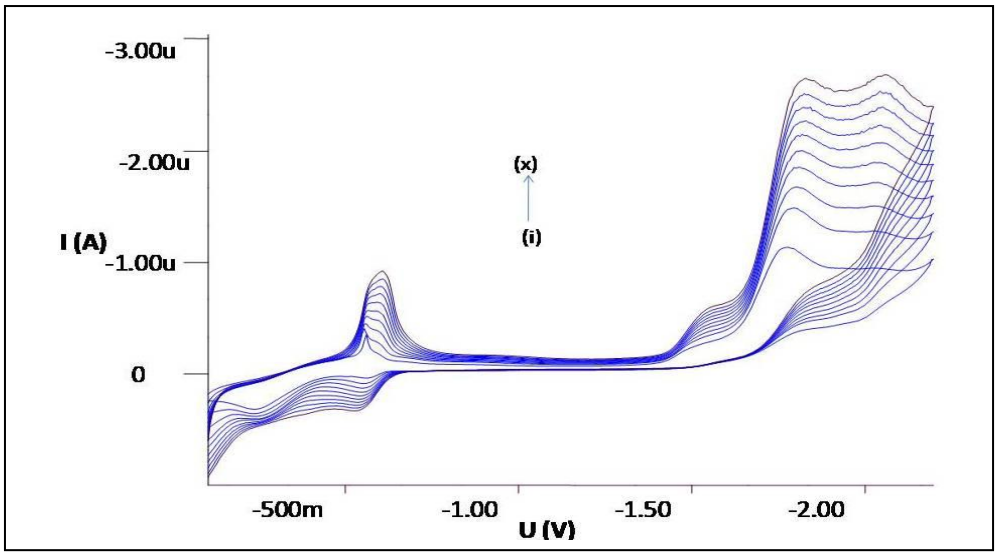

Figure 4D.9: Cyclic voltammograms of $Cu_2L_2^1$ (3.06 x 10^{-4} M) in DMF on SMDE at different scan rates, (i) 0.1, (ii) 0.2, (iii) 0.3, (iv) 0.4, (v) 0.5, (vi) 0.6, (vii) 0.7, (viii) 0.8, (ix) 0.9, (x) 1.0 Vs^{-1} with TEAP (0.1 M)

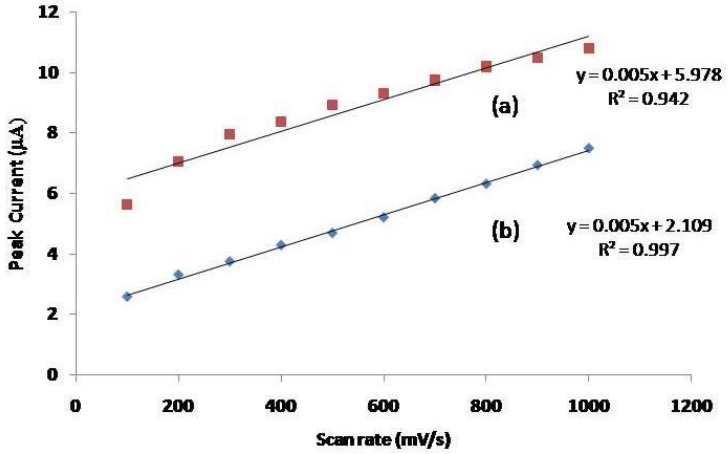

Figure 4D.10: Variation of peak current with scan rate of $Cu_2L_2^1$ (3.06 x 10^{-4} M) at SMDE ;(a) for cathodic at ~0.1 V and (b) for anodic peak at ~ 1.0 Vs^{-1}

Table 4D.2*: Cyclic voltammetry data of* $Cu_2L_2^1$ *complex on GCE*

Scan rate (mV/s)	E_{pc} (V)	E_{pa}(V)	ΔE_p(mV)	E^0(V)	i_{pa}/i_{pc}
100	0.140	0.367	222	0.251	0.82
200	0.125	0.380	255	0.252	0.97
300	0.090	0.400	310	0.245	1.00
400	0.070	0.425	355	0.247	1.01
500	0.069	0.433	364	0.251	1.00

4D.4 Zinc(II) Complexes

A typical cyclic voltammogram obtained in the cathodic region on GCE for $Zn_2L_2^1$ is presented in **Figure 4D.11**. An irreversible reduction peak at ~ -0.850 V and another irreversible oxidation peak at ~-1.250 V are observed. The effect of scan rate, concentration, potential settings, etc on the cyclic voltammetric profiles suggest that the two irreversible peaks are diffusion controlled and that they belong to two different electrophores[20]. Usually, the Zn(II)|Zn(0) couple in aqueous media shows up its CV reduction peak at ~ -0.700 V against Ag|AgCl . The reduction peak observed for the $Zn_2L_2^1$ is attributed to the 2-electron reduction of the metal ion. The greater cathodic potential for the present complexed zinc ion than the standard reduction potential of Zn^{2+}/Zn is attributed to the poorer dielectric constant of DMF than water and to the additional stabilisation of the ion by complexation, Further, the crowding of the bulky napthylidinimine around the metal ion on the equatorial plane and the presence of 2 water molecules on the axial ends of the octahedral geometry around the metal ion would hinder the facile electron transfer. Presence of only one peak in the cathodic scan indicates that the two metal centres of the binuclear complex undergo near-simultaneous reduction. This is further proven by the coulometric studies which reveal the transfer of 4 faradays per mole.

Hence, the non-aqueous cathodic electron transfer of $Zn_2L_2^1$ is assigned as

$$\mathbf{Zn(II)_2L_2^i + 2e \xrightarrow{k_{1c}} Zn(II)Zn(0)L_2^i} \quad (4.1a)$$

$$\mathbf{Zn(II)Zn(0)L_2^i + 2e \xrightarrow{k_{2c}} Zn(0)_2L_2^i} \quad (4.1b)$$

$$\mathbf{Zn(0)_2L_2^i \xrightarrow{k_{dc}} dissociated\ species} \quad (4.1c)$$

with the first cathodic heterogeneous electron transfer rate constant, k_{1c} being far higher than the second one, k_{2c}, while the electrochemical event having a following-chemical dissociation reaction with a high rate constant, k_{dc}.

The anodic peak is attributed to the oxidation of the azomethine moiety. It is well known that azomethine moieties exhibit characteristic oxidation in non-aqueous media at ~ 1.00 V vs Ag|AgCl through a free radical mechanism. The near similar current heights of the cathodic and the anodic responses (**Figure 4D.11**) of the complex suggests a similar 2 consecutive electrochemical steps with following-chemical dissociation event as

$$Zn(II)_2L_2{}^{i}\boxed{\{(-C{=}N\text{-})(N{=}C\text{-})\}_2} \xrightarrow[-2e]{k_{1a}} Zn(II)_2L_2{}^{i}\boxed{\{(-C^{\bullet}\text{-}N^{+}\text{-})(N{=}C\text{-})(-C^{\bullet}\text{-}N^{+}\text{-})(N{=}C\text{-})\}} \quad (4.2a)$$

$$Zn(II)_2L_2{}^{i}\boxed{\{(-C^{\bullet}\text{-}N^{+}\text{-})(N{=}C\text{-})(-C^{\bullet}\text{-}N^{+}\text{-})(N{=}C\text{-})\}} \xrightarrow[-2e]{k_{2a}} Zn(II)_2L_2{}^{i}\boxed{\{(-C^{\bullet}\text{-}N^{+}\text{-})(N^{+}\text{-}C^{\bullet}\text{-})\}_2} \quad (4.2b)$$

$$Zn(II)_2L_2{}^{i}\boxed{\{(-C^{\bullet}\text{-}N^{+}\text{-})(N^{+}\text{-}C^{\bullet}\text{-})\}_2} \xrightarrow{k_{da}} \textbf{dissociated species} \quad (4.2c)$$

with the first anodic heterogeneous electron transfer rate constant, k_{1a} being far higher than the second one, k_{2a}, while the electrochemical event having a following-chemical dissociation reaction with a high rate constant, k_{da}.

Interestingly, the $Zn_2L_2{}^{2}$ has quasireversible reduction behaviour in the cathodic scan on the GCE in DMF. In **Figure 4D.12** is shown this behaviour. However, the $Zn_2L_2{}^{5}$ complexes, where in L are of class B (with Z=nil), show no oxidation response peak corresponding to the azomethine sites. This may be attributed to the extended difficult of electron transfer due to denser molecular Skelton. Further, the cathodic response is also very complicated seeming to be involved with an irreversible and a quasi reversible reduction steps. In **Figures 4D.13** and **4D.14** are shown in these features. The effect of scan rates and concentration on the ip and E_1 values are indicative of diffusion controlled electron transfer relevant electrochemical data of $Zn_2L_2{}^{i}$ are also collected in **Table 4D.3**.

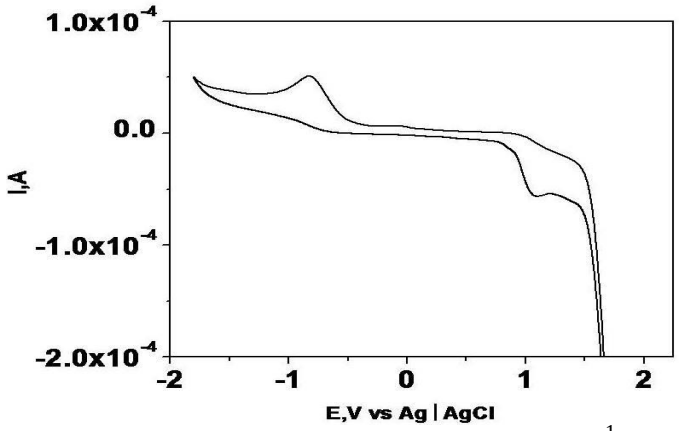

Figure 4D.11: Cyclic voltammogram of $Zn_2L_2{}^{1}$ (3.06×10^{-4}M) in DMF on GCE at scan rate, 0.1 Vs^{-1}, with TEAP (0.1M)

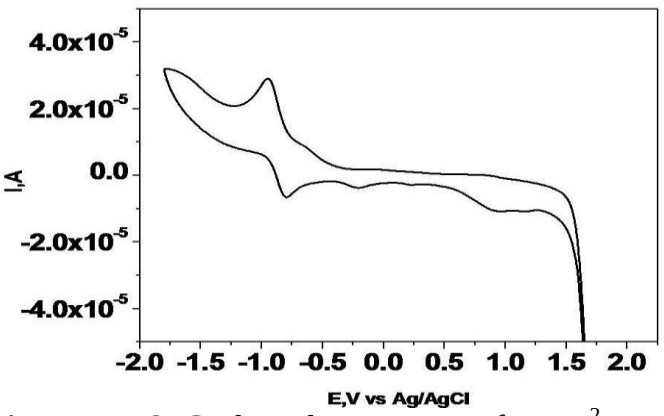

Figure 4D.12: Cyclic voltammogram of $Zn_2L_2{}^{2}$ (3.06×10^{-4}M) in DMF on GCE at scan rate, 0.1 Vs^{-1}, with TEAP (0.1M)

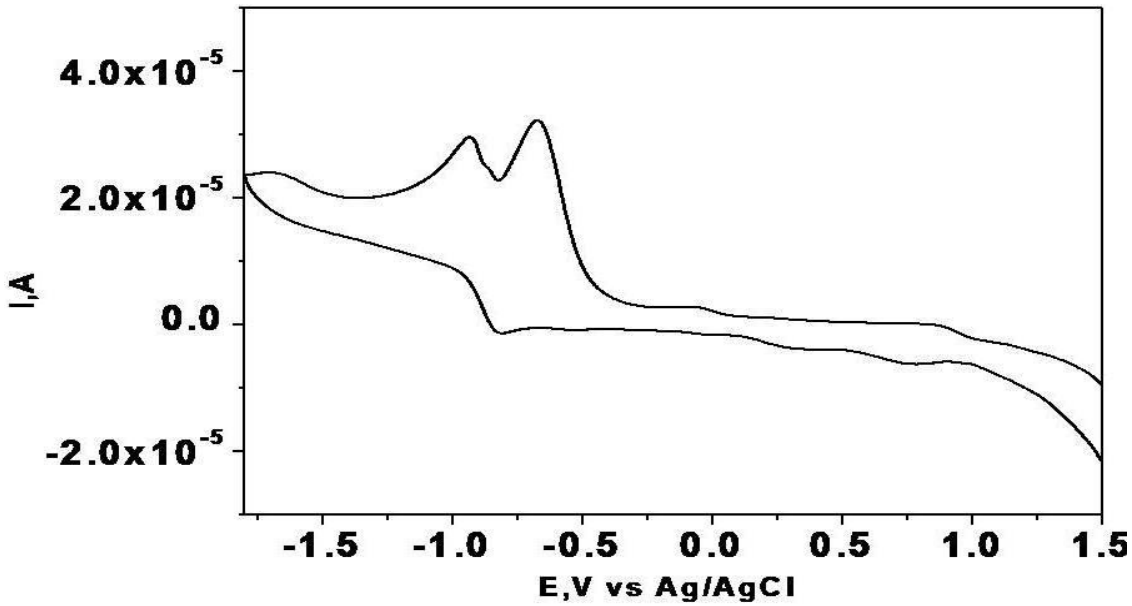

Figure 4D.13: Cyclic voltammogram of $Zn_2L_2^5$ (3.06 x 10^{-4} M) in DMF on GCE at scan rate, 0.1 Vs^{-1}, with TEAP (0.1 M)

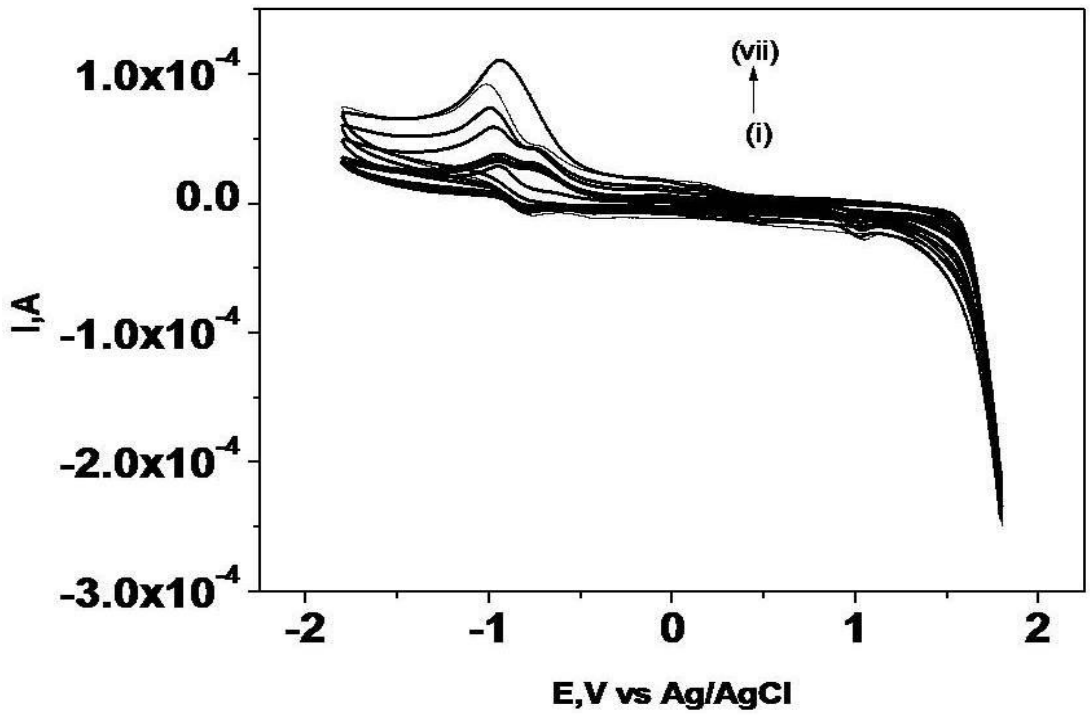

Figure 4D.14: Cyclic voltammograms of $Zn_2L_2^5$ (3.06 x 10^{-4} M) in DMF on GCE at different scan rates, (i) 0.1, (ii) 0.2, (iii) 0.3, (iv) 0.4, (v) 0.5, (vi) 0.6, (vii) 0.7 Vs^{-1} with TEAP (0.1 M)

Table 4D.3: *Cyclic voltammetric data of Zn(II) complexes*

Complex	Scan rate (mV/s)	E_{Pc} (V)	E_{Pa}(V)	ΔE_P(mV)	E^0(V)
$[Zn_2L_2^1(H_2O)_4]$	50	0.786	0.924	138	0.855
	80	0.781	0.932	151	0.856
	100	0.779	0.934	155	0.856
	200	0.768	0.961	193	0.864
	400	0.764	0.981	216	0.873
	600	0.762	1.020	255	0.892
	800	0.762	1.040	278	0.901
$[Zn_2L_2^2(H_2O)_4]$	50	0.796	0.949	153	0.872
	80	0.784	0.951	167	0.867
	100	0.781	0.952	171	0.866
	200	0.782	0.962	180	0.872
	400	0.767	0.982	215	0.874
	600	0.767	1.004	237	0.885
	800	0.767	1.025	258	0.896
	1000	0.767	1.049	282	0.908
$[Zn_2L_2^3(H_2O)_4]$	50	0.683	1.016	333	0.849
	80	0.704	1.025	321	0.864
	100	0.714	1.029	315	0.871
	200	0.732	1.033	301	0.882
	400	0.748	1.04	292	0.894
	50	0.676	0.933	257	0.804
$[Zn_2L_2^5(H_2O)_4]$	100	0.682	1.036	354	0.859
	200	0.692	1.038	346	0.865
	400	0.713	1.041	328	0.877
	600	0.716	1.046	330	0.881
	800	0.724	1.052	328	0.888
	1000	0.732	1.056	324	0.894

References

1. Noboru Yoshida, Hiroki Oshio, Tasuku Ito, *J Chem Soc Perkin Trans*, 2, **1999**, 975–983
2. G Wang, J C Chang, *Synth React Inorg Met-Org Chem*, 24, **1994**, 1091
3. O A Rajan, A Chakravorty, *Inorg Chem*, 20, **1981**, 660
4. H D Bian, J Y Xu, W Gu, S P Yan, P Cheng, D Z Dao, Z H Jiang, *Polyhedron*, 22, **2003**, 2927-2932
5. B Sarkar, M S Ray, M.G Drew, A Figuerola, C Diaz, A Ghosh, *Polyhedron*, 25, **2006**, 3084-3094
6. C Kittel, *Introduction to Solid State Physics*; Wiley, New York, **1996**
7. J W van Vleck, *The theory of electric and magnetic susceptibilities*, Oxford Univ, Press, Lonclon, **1832,** 188
8. J F Villa and W E Hatfield, *Chem Commun*, **1971**, 101
9. W E Hatfield, J A Barnes, D Y Jeter, R Whyman, E R Jones Jr, *J Am Chem Soc*, 92 **1970**, 4982
10. P B Ayscough, *Electron spin resonance in chemistry*, Methuen. London, 6, **1967**
11. A W Coats, J P Redfern, *Nature*, 20, **1964**, 68–69
12. H H Horowitz, G Metzger, *Anal Chem*, 25, **1963**, 1464–1468.
13. M S Abu-Bakr, H Sedaira, E Y Hashem, *Talanta*, 10, 1994, 1669–1674
14. D Kara, M Alkan, *Talanta*, 55, **2001**, 415–423
15. A Broido, *J Polym Sci A*, 27, 1969, 1761–1773
16. D J Hodgson, Znorg, *Chim Acta*, 75, **1983**, 225
17. M Amirnasr, R Vafazadeh, A Mahmoudkhani, Can J Chem, 80, **2002**, 1196
18. A Anthonysamy, S Balasubramanian, *Inorg Chem Commun*, 8, **2005,** 908–911
19. P S Zacharias, A Ramachandraiah, *Polyhedron*, 4, **1985**, 1013-1017
20. N H Pilkington, R Robson, *Aust J Chem*, 23, **1970**, 2225

CHAPTER V

BIS-BIPHENYL BRIDGED 2,6-DIFORMYLIDINIMINE TETRAAZOMETHINE CYCLICS AND THEIR BINUCLEAR AND TETRANUCLEAR METAL COMPLEXES AS POSSIBLE HOSTS

Portions of the results of this chapter are presented in conference *"Spectral and supramolecular studies of the Schiff base cryptands of substituted 4-(4-aminophenoxy)benzenamine and 2, 6- diformyl-4-methylphenol*" International Conference on Supramoleculer Chemistry and Nanomaterials, 14-16th Feb. 2011, Page-82 at University of Mumbai, Mumbai

In this chapter, the characterization of bis-biphenyl bridged 2,6-diformylidinimine tetraazomethine cyclic hosts is discussed. These ligands were characterized by spectral (IR, electronic, NMR and mass), elemental, electrochemical, thermal and molecular modeling studies.

Aromatic diamines such as 4-(4-aminophenoxy)aniline, 4.4'-diamino biphenyls, when treated with 2,6-diformyl-4-methyl phenol give bis-biphenyl bridged 2,6-diformylidinimine tetraazomethine cyclic hosts. The details of synthesis are described in **Chapter II**.

The bis-biphenyl bridged 2,6-diformylidinimine tetraazomethine cyclic hosts reported in this chapter have been complexed with various metal ions such as cobalt(II), nickel(II), copper(II), zinc(II), etc. The details of synthesis and purification are also presented in **Chapter II**. These complexes have been characterized by physical, analytical, spectral, thermal, cryomagnetic, electron spin resonance and electrochemical studies and the details are presented in this chapter.

Based on the structural vividity, this Chapter is divided into two parts, **PARTS, A** and **B**.

In **PART A**, the physical, analytical, spectral and electrochemical characterization and molecular modeling studies of the tetraazomethine Schiff base ligands are present and discussed.

In **PART B**, the binuclear and tetranuclear complexes of the tetraazomethine Schiff base ligands are reported.

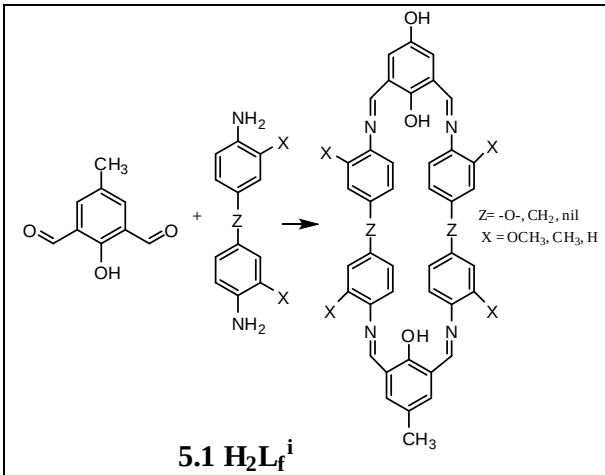

5.1 $H_2L_f^i$

Z	X	row combination $H_2L_f^i$
-O-	H	DFMDPE or $H_2L_f^1$
$-CH_2-$	H	DFMDPM or $H_2L_f^2$
nil	OCH_3	DFMDPD or $H_2L_f^3$
nil	CH_3	DFMDPT or $H_2L_f^4$
nil	H	DFMDPB or $H_2L_f^5$

PART A: SPECTRAL AND ELECTROCHEMICAL CHARACTERIZATION OF TETRAAZOMETHINE SCHIFF BASE LIGANDS

The structure of the class of the tetraazomethine Schiff base ligands is furnished in **5.1**. Since **5.1** is a macrocyclic tetraazomethanine-diphenolic poly Schiff base, the voide size in **5.**1 is highly decided by Z. If there no –Z-, like in the benzidine, o-tolidine and o-diansidine bridges, the void Z size is very small because then 1, 4, 1', 4' carbons of the bridging moiety are linear. Hence, the **5.1** with Z= nil is in a greater strain than that with Z = -CH_2- or Z= -O- wherein the void is wider because of the angularity expansion provided by the –CH_2- or the –O- linkage. The voide size in **5.1** is schematically depicted in **Scheme 5.1** with Z = nil and Z = -O-. On the basis of this difference in void size the catenand application of **5.1** is likely to be sensitrue to the presence or absence of Z. **5.1** is referred to here after as $\mathbf{H_2L_A^i}$ or $\mathbf{H_2L_B^i}$ with Z= CH_2 or –O- for A and Z = nil for respectively.

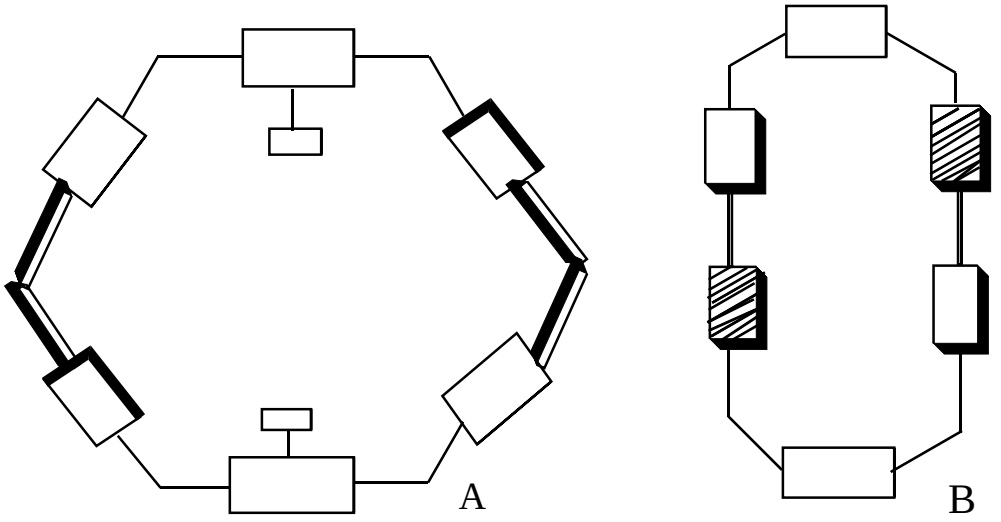

Scheme 5.1

5A.1 General Characterization of the Macrocyclic Schiff base Ligands

The physical and analytical data of the $\mathbf{H_2L_f^i}$ are presented in **Table 5A.1.** The elemental data are in good agreement with the structure shown in **5.1.**

5A.2 Mass Spectral Studies

The Electron ionization and Electro spray ionization (MS-ES^+ and ESI^+) mass spectra of $H_2L_f^1$ and $H_2L_f^3$ have been investigated. Typical such spectra are presented in **Figures 5A.1** and **5A.2** for DFMDPE and DFMDPD, respectively. The molecular ion peaks were obtained

at 659(45%), 653(100%), 745(100%), 681(100%), 625(100%) values, respectively. This data are in good agreement with the respective molecular formulae.

5A.3 Infrared Spectral Studies

The FT- IR data are presented in **Table 5A.2.** The band in the IR spectra of ligands in the range of 1624-1619 cm^{-1} is attributable to $\nu_{C=N}$ and provides a strong evidence for the condensation of aldehyde group with amine[1]. In the ligands a medium intensity band is present around 3415 cm^{-1} corresponding to the ν_{OH} stretch. The aromatic ring stretching frequencies are observed for the ligands in the range of 1409-1319 cm^{-1} and wagging frequencies are observed in the range of 3045-2914 cm^{-1}. The FTIR of DFMDPE and DFMDPD are shown in **Figures 5A.3** and **5A.4,** respectively.

5A.4 UV-Visible Absorption and Fluorescence Spectra of $H_2L_f^i$

The UV-Vis electronic spectra of DFMDPE and DFMDPD are shown in **Figures 5A.5** and **5A.6,** respectively**.** The ligands show absorption bands of $\pi\rightarrow\pi^*$ and $n\rightarrow\pi^*$ at 380 and 500 nm, respectively arising from the –C=N- moiety. The relevant spectra data are collected in **Table 5A.3.**

Fluorescence properties of the Schiff bases have been checked by using Spectrofluorometer model number RF5301. A Xe laser lamp was used for excitation and emission spectra were scanned from the range 220 to 750 nm. For fluorescence study of the Schiff bases, dimethylformamide is used as solvent and reference material. The excitation of the molecule is occurred due to the $n\rightarrow\pi^*$ and $\pi\rightarrow\pi^*$ transitions. The fluorescence data can be shown in following data. The fluorescence emission spectrums of a selected DFMDPD are present in **Figure 5A.6**.

5A.5 ^{1}H NMR and ^{13}C NMR Spectral Studies

Compound **5.1** was studied by its ^{1}H NMR and ^{13}C NMR spectra in $CDCl_3$. Whether amine-carbonyl condensation at the four position and thus whatever cyclisation effected to get the spectra and shown in **Scheme 5.2** were confirmed by ^{1}H NMR spectra. It incomplete

condensation was these have yielded compounds like **5.2**, then would be addition NH_2 and CHO kind protons in the ^1H NMR spectrum.

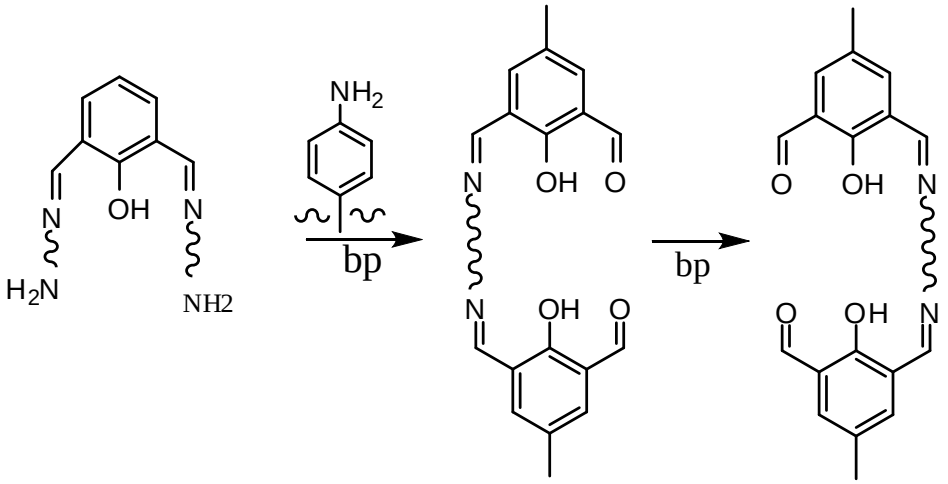

Scheme 5.2

However the ^1H NMR and ^{13}C NMR are not indicate of any NH_2 broad triplet (I=1 for N) or CHO with a ^{13}C doublet (in OH resonance). However there is a singlet ^1H NMR peak for CH=N and a multiplet ^{13}C for CH=N carbon.

In all the Schiff bases a distinctly characteristic ^1H peak is observed due to the deshielded CH=N protons (4H). A signal appeared around δ 11.5 due to the OH (2H) protons in **Figure 5A.7**. All the ligands contain signals in the range of δ 154-165 characteristic of the azomethinine carbon signals in **Figure 5A.8**.

Table5A.1: *Physical and analytical data of bis-biphenyl bridged 2,6-diformylidinimine tetraazomethine cyclic ligands*

Compound	**Appearance**	**M. P#** (^{0}C)	**M. Formula (M. Weight)**	**Elemental analysis***		
				%C	**%H**	**%N**
DFMDPE	Pale Red	336.83	$C_{42}H_{32}N_4O_4$	76.78	4.93	8.52
			(656.73)	(76.81)	(4.91)	(8.53)
DFMDPM	Yellow	338.27	$C_{44}H_{36}N_4O_2$	79.95	5.64	8.49
			(652.78)	(80.96)	(5.56)	(8.58)
DFMDPD	Blue	475.77	$C_{46}H_{40}N_4O_6$	74.14	5.42	7.51
			(744.83)	(74.18)	(5.41)	(7.52)
DFMDPT	Pale Orange	372.54	$C_{46}H_{40}N_4O_2$ (680.84)	80.75 (81.15)	5.95 (5.92)	8.15 (8.23)
DFMDPB	Orange	370.03	$C_{34}H_{24}N_4O_2$ (520.58)	78.15 (78.44)	4.25 (4.65)	10.81 (10.76)

* data in parenthesis are calculated ones # melting point obtained from DSC

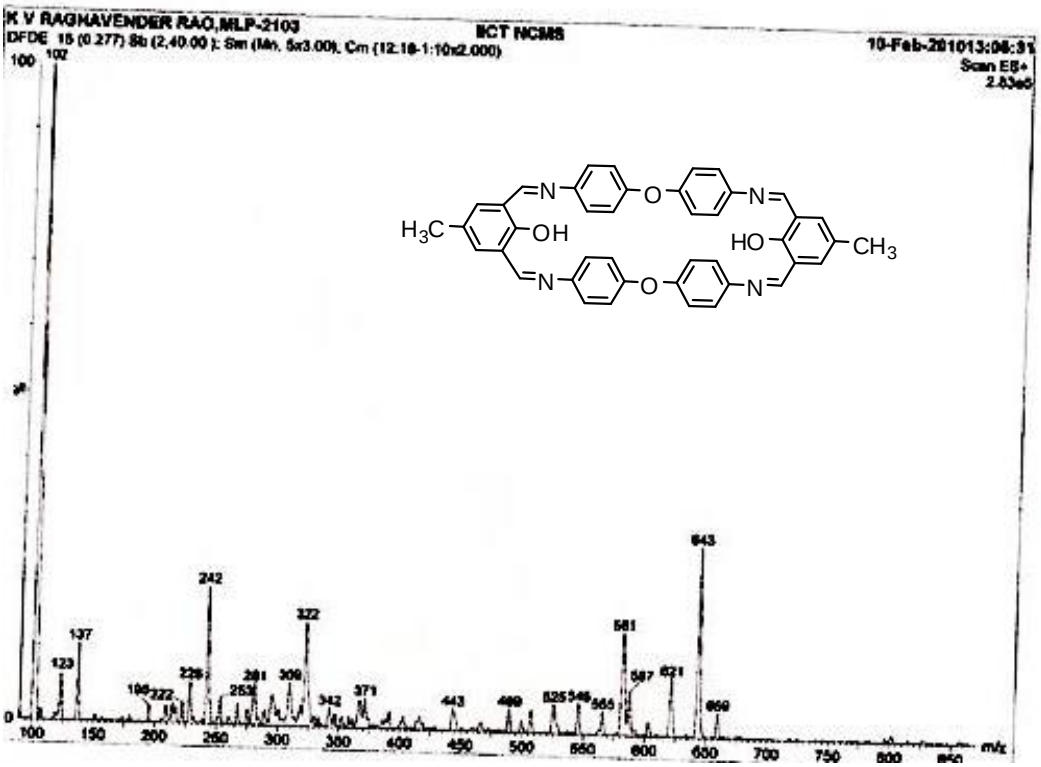

Figure 5A.1: ESI^+ mass spectrum of DFMDPE

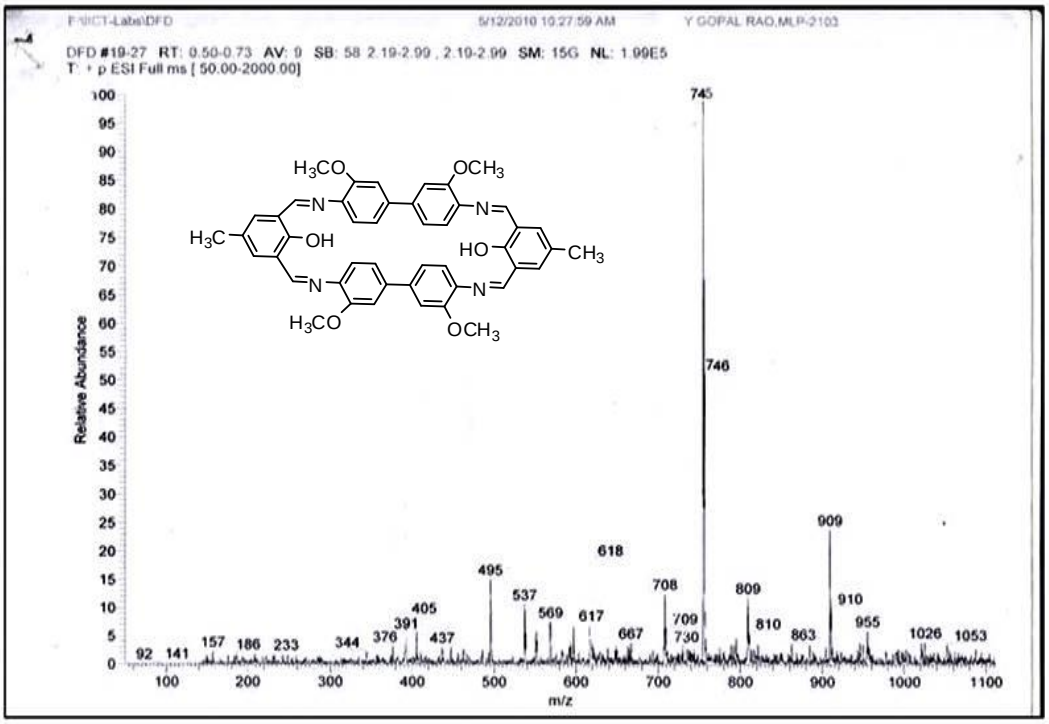

Figure 5A.2: ESI^+ mass spectrum of DFMDPD

Table 5A.2: *Infrared spectral data of bis-biphenyl bridged 2,6-diformylidinimine tetraazomethine cyclic ligands*

Compound	IR spectral data (cm^{-1})*			
	$\nu_{C=N}$	ν_{OH}	ν_{C-O}	Aromatic
DFMDPE	1621	3415	1541	3045w 1494, 1323
DFMDPM	1621	3410	1543	3042 w, 1510, 1319
DFMDPD	1620	3377	1540	2914 w, 1489, 1321
DFMDPT	1619	3341	1542	3024w, 1405, 1331
DFMDPB	1624	3415	1540	3038 w, 1409, 1317, 1348

***** In KBr pellet (cm^{-1})

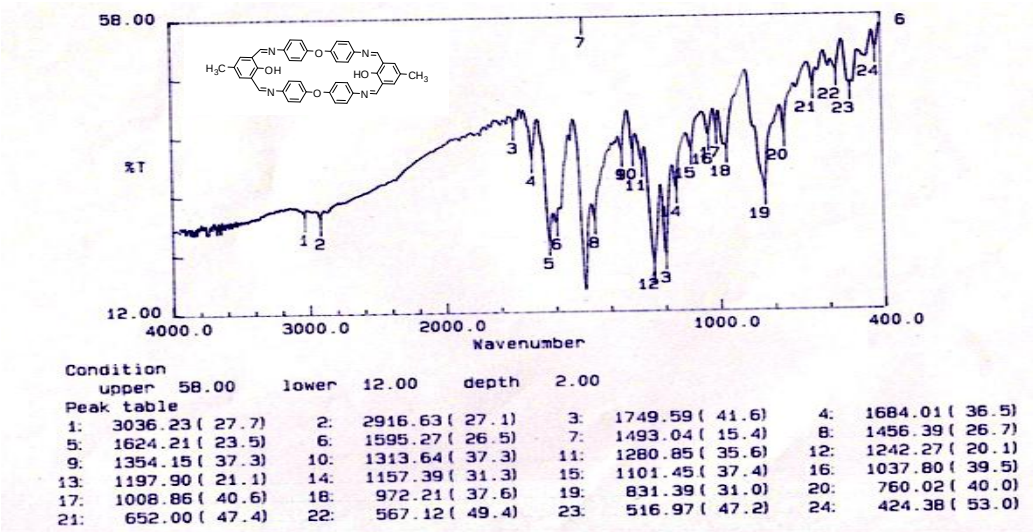

Figure 5A.3: FT-IR spectrum of DMFDPE

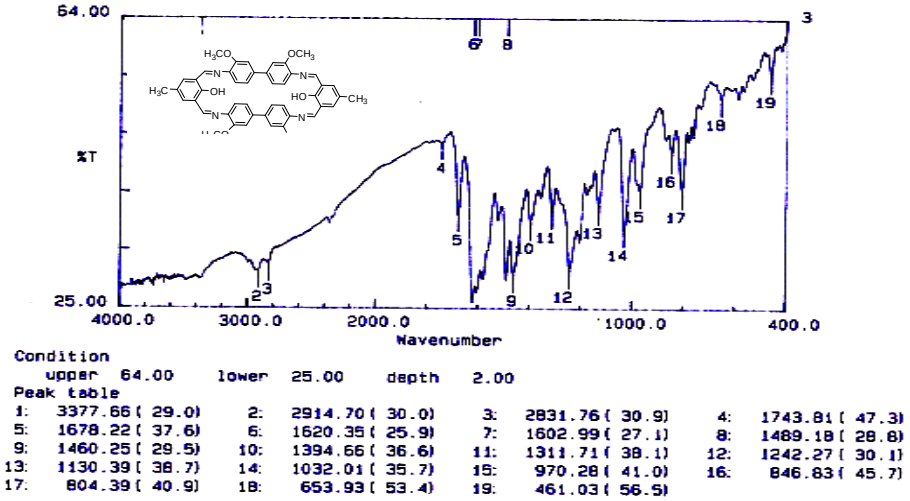

Figure 5A.4: FT-IR spectrum of DMFDPD

Table 5A.3: *UV-Visible and fluorescence spectral data of bis-biphenyl bridged 2,6-diformylidinimine tetraazomethine cyclic ligand*

S. No.	Compound	Electronic data in $CHCl_3$ λ_{max} ($\bar{\upsilon}$) (ε)[a]	Fluorescence data Exited (nm)	Fluorescence data Emission (nm)
1.	DFMDPE	390(25,640)(34,812)	370	500
2.	DFMDPM	382.5(26,145)(58,082)	360	435,480
3.	DFMDPD	398(25,126) (34256), 550(18,182)	370	508,690
4.	DFMDPT	392.5(25,195)(30,722)	370	430
5.	DFMDPB	382(26,171)(31,460)	360	410

a, λ_{max} (in nm), $\bar{\upsilon}$ (in cm^{-1}), ε (lit. $mol^{-1}.cm^{-1}$)

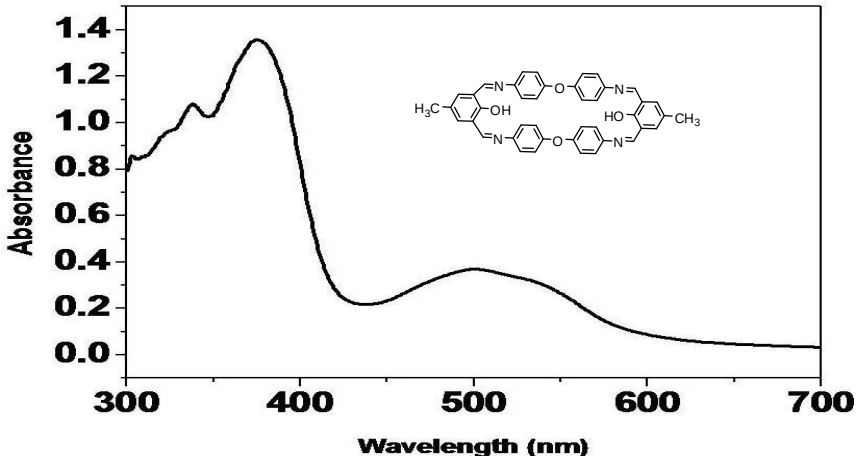

Figure 5A.5: UV-Visible spectrum of DFMDPE (4 x 10^{-5} M) in $CHCl_3$

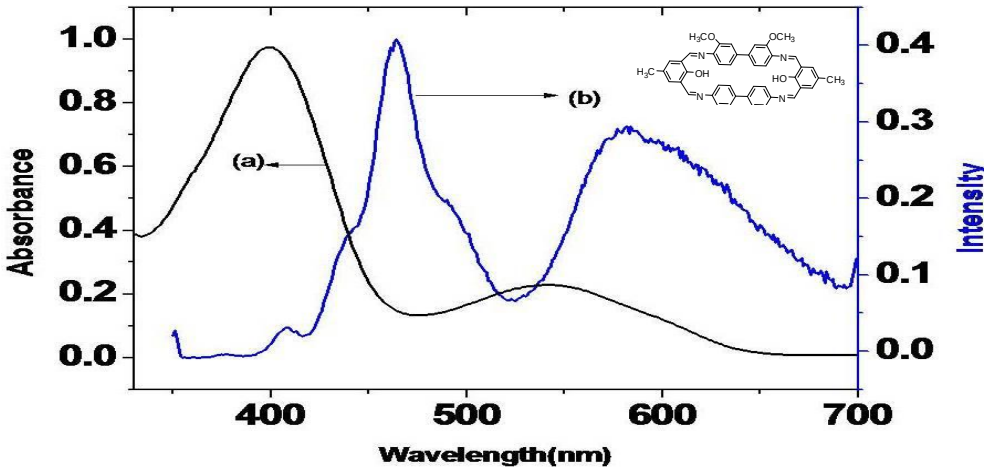

Figure 5A.6: Electronic spectra of (a) UV-Visible and (b) Fluorescence of DFMDPD (4 x 10^{-5} M) in $CHCl_3$

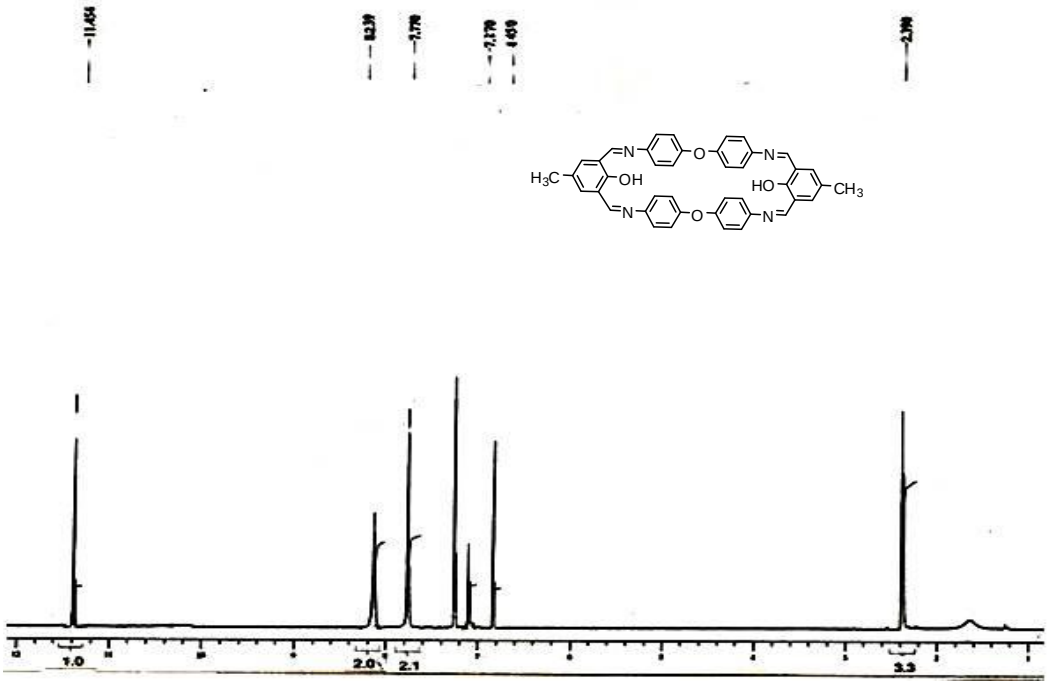

Figure 5A.7: ^{I}H NMR spectrum of DFMDPE

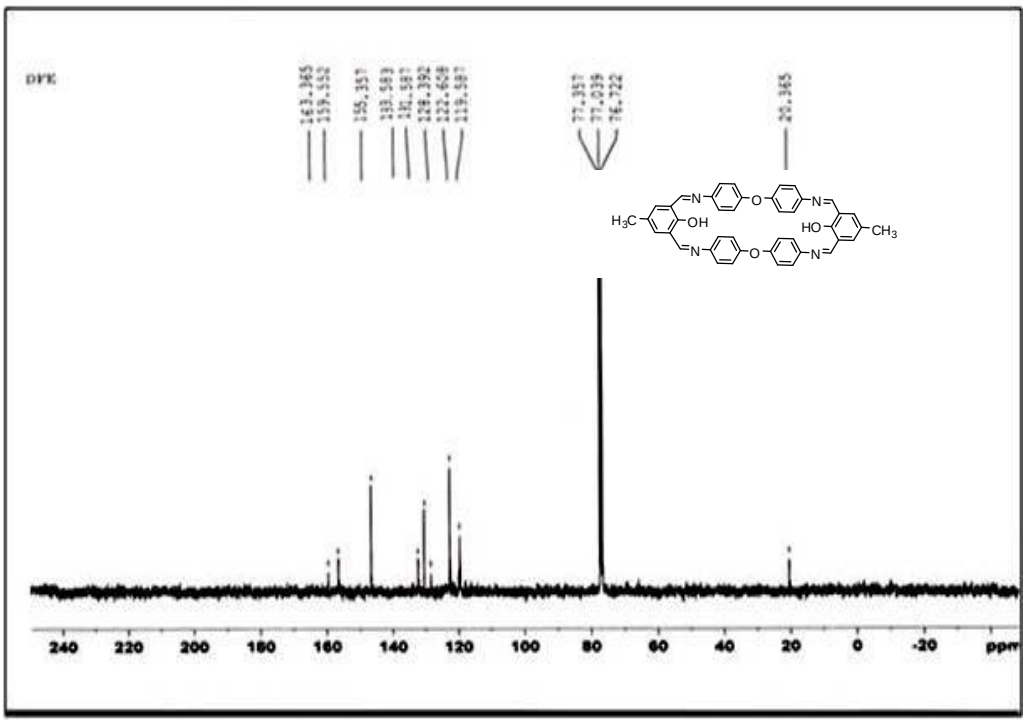

Figure 5A.8: ^{I3}C NMR Spectrum of DFMDPE

5A.6 Thermal Analysis

The series of **5.1** were also characterized by thermal studies with differential scanning calrometry (DSC). The DSC thermograms of DFMDPE and DFMDPD are given in **Figures 5A.9** and **5A.10**. The exothermic peak at ~ 403ºC corresponds to its melting point. There is no other thermal event till 600 ^{0}C before or after the melting point. It means that no solvent molecules has included in the crystal structure.

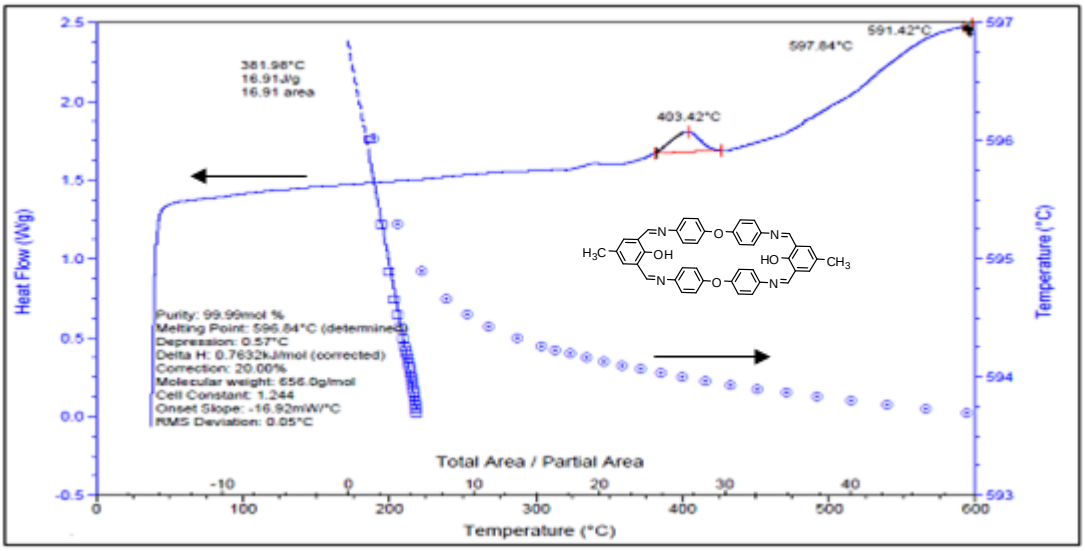

Figure 5A.9: Differential scanning calorigram of DFMDPE (3 mg) under N_2 atmosphere

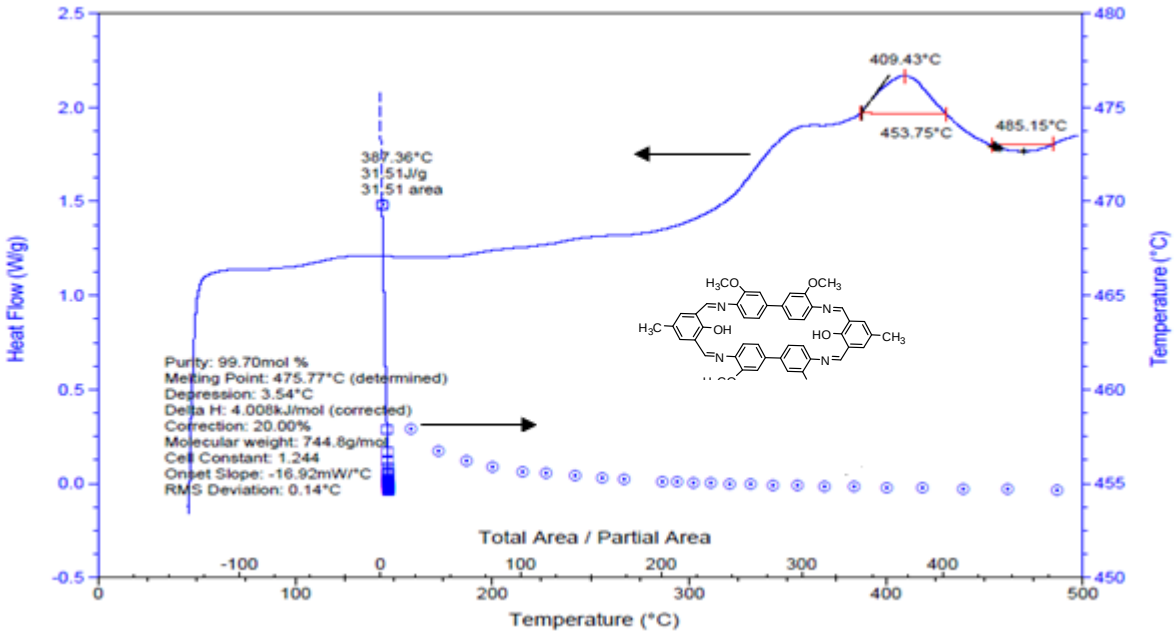

Figure 5A.10: Differential scanning calorigram of DFMDPD (3 mg) under N_2 atmosphere

H_2L^iA and **H_2L^iB** are likely to be exhibit different trends of thermal behaviour because of their varied structural stability. **Figure 5A.9** is a representative thermogram of **H_2L^iA** system where as **Figure 5A.10** is that of **$H_2L^i_B$**. One can see a single and sharp thermal process of **$H_2L^i_A$** due to their stable form. However there seems to be a conseqative thermal event of fusion for $H_2L^i_B$ type system, which is under strain. To establish the temperature of the two conseqative thermal process. The first event is attributed to a thermally assisted relaxation. Whereas the second one to the actual fusion process.

5A.7 Acid -Base Equilibria

The Schiff base ligands **5.1** have two phenolic sites and four azomethine cyclic moieties Hence, they can exist as LH_6^{4+}, LH_5^{3+}, LH_4^{2+}, LH_3^{+}, LH_3, LH_2^{-}, LH^{2-} and L^{3-} depending on the pH. Acid–base equilibria of **5.1** have been monitored by P^H-metric spectrophotometry in buffer solutions of variable P^H. A representative such P^H-metric spectral titration DFMDPD is presented in **Figure 5A.11.** Other **5.1** also exhibit similar profiles. All compounds exhibit well defined isosbestic point at ~470 nm in the pH range 4-10 with their λ_{max} at ~ 370 and ~ 470 nm. The bathochromic shift seen in the pH range, 4 –10, must be linked to certain structural alterations upon deprotonation of **5.1**.

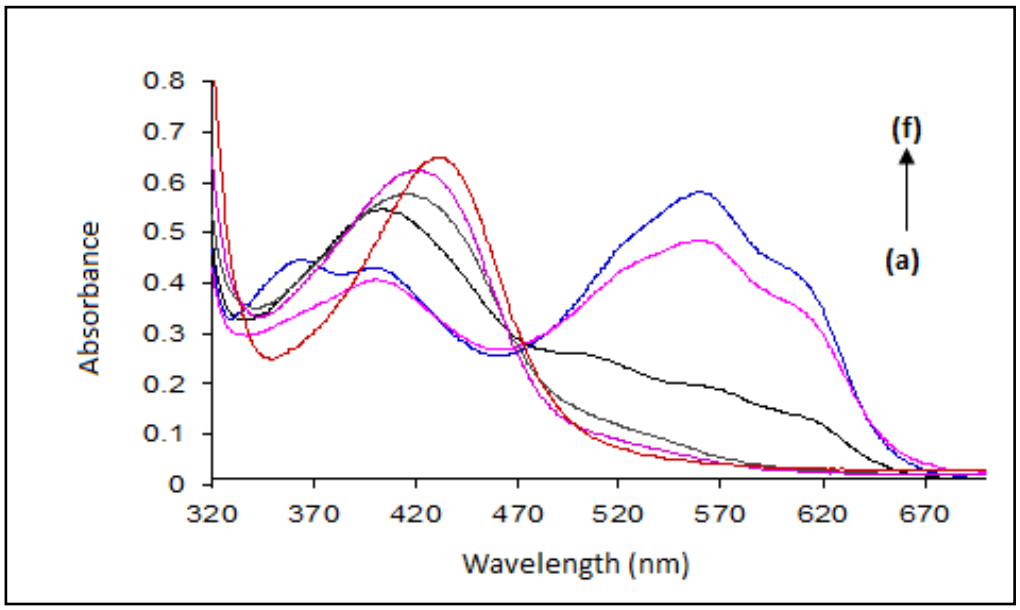

Figure 5A.11: Electronic spectral profile of DFMDPD (4 x 10^{-5} M) in the media of varying pH (a) 2.07, (b) 4.02, (c) 6.01, (d) 8.20, (e) 10.12, (f) 12.01

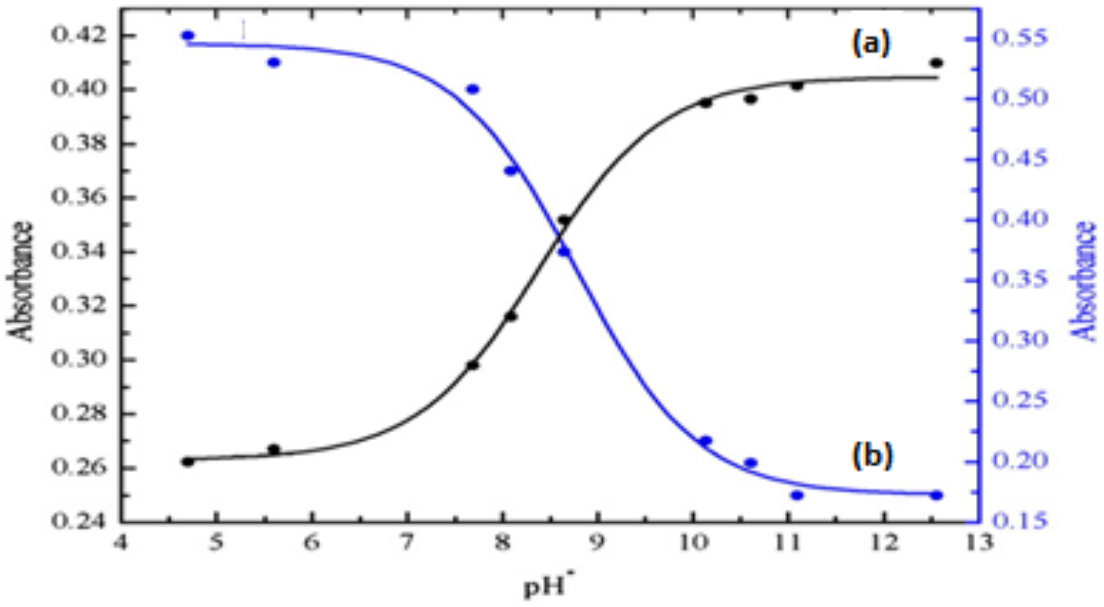

Figure 5A.12: Variation of absorbance with pH of DFMDPD at (a) 370 nm (b) 472 nm

May acid-base indicators such as phenolphthalein, methyl orange, etc one then pH-dependent colour change to bezenoid to quinonoid isomergation upon the resulting in bathochromic shift observed for DFMDPD is attributed to an isomerisation. A careful observatory of **Figure 5A.12** reveals that the spectra are out crossing cleanly at a specific set of isosbestic points. These spectra drift from isosbesticity after attaining a particular p^H and again gradually reestablish isosbesticity at a different wavelength. This type of 'set, left and reset' type of isosbesticity is indicative of polyprotic and polydeprotic consecutive acid-base equilibria. On the basis of the plots of absorbance vs pH at the two λ_{max} ~370 and ~472 nm, it was possible to obtain the pKa = 8.7 of DFMDPD.

5A.8 Electrochemical Studies

The title compounds, **5.1** have different electrochemical redox sites. It has been also said that these compounds exists LH_6^{4+},LH_5^{3+}, LH_4^{2+}, LH_3^{+}, LH_2, LH and L^{2-} conjugates with populations decided by the pH in **Figure 5A.13** and **Table 5A.4** . The electrochemical studies are earlier reported in **Chapter III**.

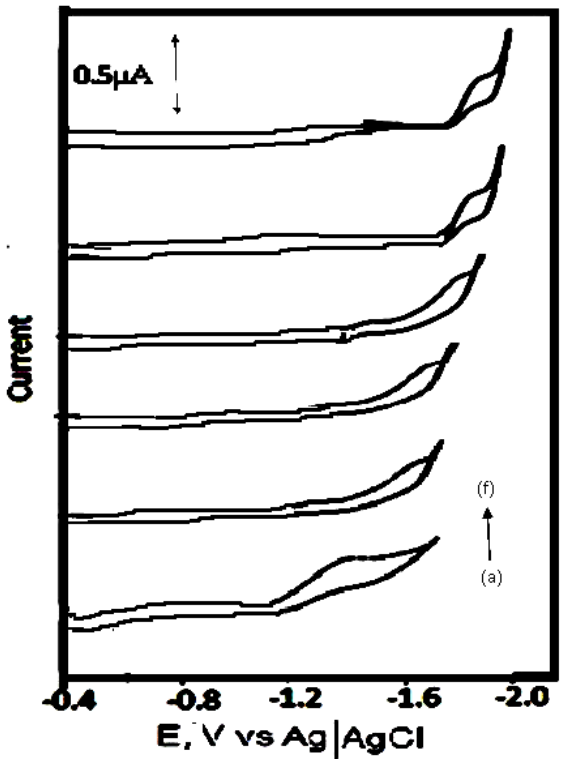

Figure 5A.13: Cyclic voltammograms of DFMDPD **(**4 x 10^{-5} M) at a pH of (a) 2.07, (b) 4.02, (c) 6.01, (d) 8.20, (e) 10.12, (f) 12.01 (scan rate, 50 mV/s) on SMDE

Table 5A.4: *Cyclic voltammometry data of DFMDPD*

pH	$-E_p$ (V)	α_{na}	k^o_h x10^9 (cm^2 /s)	D_o x 10^6 (cm^2 /s)
2.07	0.698	0.58	6.21	1.21
4.02	0.842	0.54	1.68	3.00
6.01	0.952	0.67	1.02	6.22
8.20	1.086	0.28	2.62	1.62
10.12	1.282	0.52	1.15	3.31
12.01	1.342	0.48	5.92	2.30

5A.9 Non-aqueous Electrochemistry

The electron transfer properties of the ligands were studied in acetonitrile with tetra ethyl ammonium perchlorate (TEAP) as the supporting electrolyte. Cyclic voltammetry was used as the primary tool. The experimental details of sampling and electrochemical run are reported in **Chapter II**. A typical cyclic voltammogram obtained in the anodic region on GCE

for all ligands is presented in **Figures 5A.14** and **5A.15**. An irreversible reduction peak at ~ -0.850 V is observed.

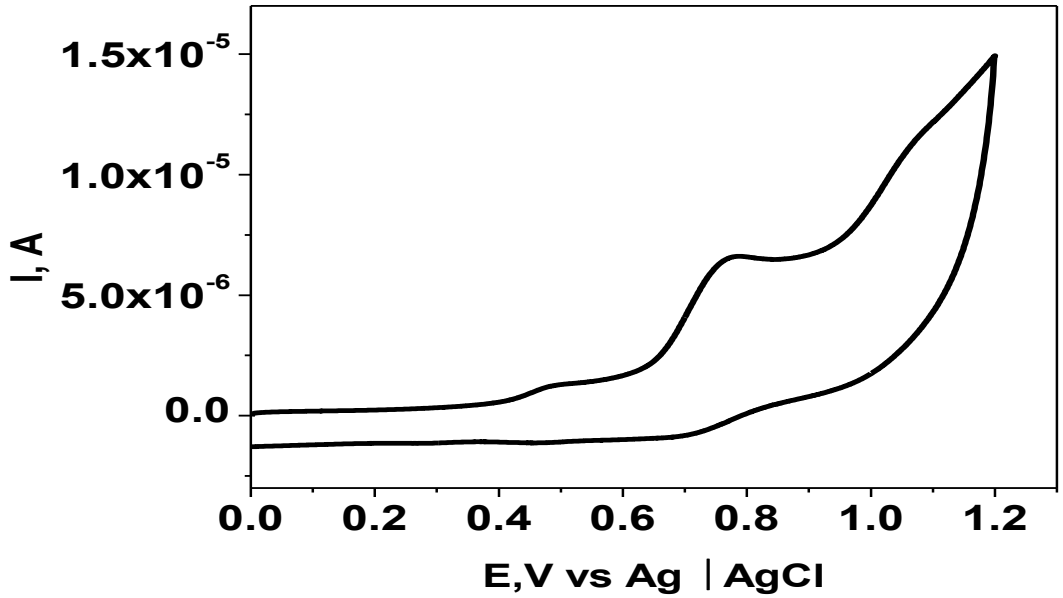

Figure 5A.14: Cyclic voltammogram of DFMDPE (3.06 x 10^{-4} M) in DMF on GCE at scan rate, 0.1 Vs^{-1}, with TEAP (0.1 M)

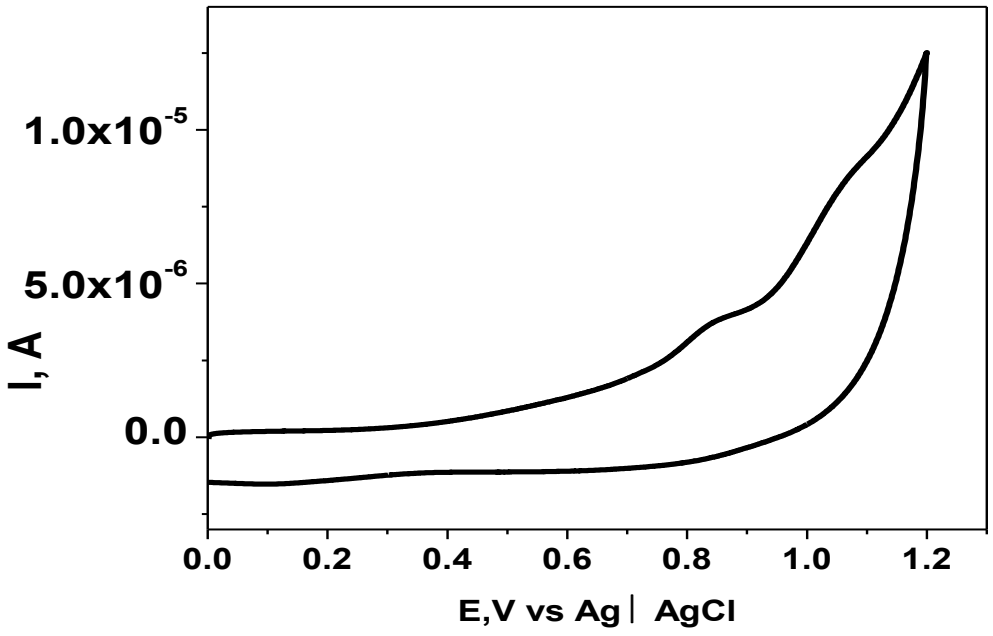

Figure 5A.15: Cyclic voltammogram of DFMDPM (3.06 x 10^{-4} M) in DMF on GCE at scan rate, 0.1 Vs^{-1}, with TEAP (0.1 M)

5A.10 Molecular Modeling

Molecular modeling studies have been done on **5.1** to understand the stability, intramolecular hydrogen bonding and to verify whether the mechanisms proposed for the thermodynamic, spectroscopic and electrochemical behavior of the compound are tenable.

The possible energy minimized structure of DFMDPE and DFMDPD shown in **Figures 5A. 16** and **5A.20** along with stereographical projection and the numbering pattern is follows as shown in energy minimized structure in shown **Figures 5A.17** and **5A.21**, as resulting of $H_2L^i_A$ or $H_2L^i_b$, respectively.

The quantum mechanical HOMO-LUMO orbital energy calculations have been used for computing the expected gas-phase electronic transitions. Some of the important molecular LUMO, HOMO orbitals are shown in **Figures 5A.18** and **5A.20.** These values are collected in **Table 5A.6** along with the experimental spectral data. The theoretical and experimental absorption maxima are in great agreement. The deviation from the modeled and experimental data of DFMDE may be attributed to salvation effect in **Figure 5A.20**. Some of the important geometric parameters of DFMDPE and DFMDPD in **Tables 5A.5** and **5A.7.**

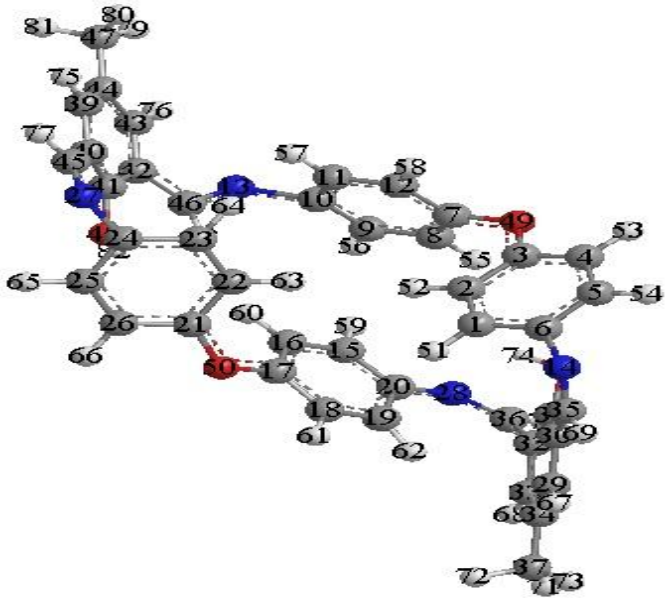

Figure 5A:16: Energy minimized monographic stereographic image of DFMDPD generated from energy minimization through MM_2 calculations (lone pairs of electrons are removed for clarity)

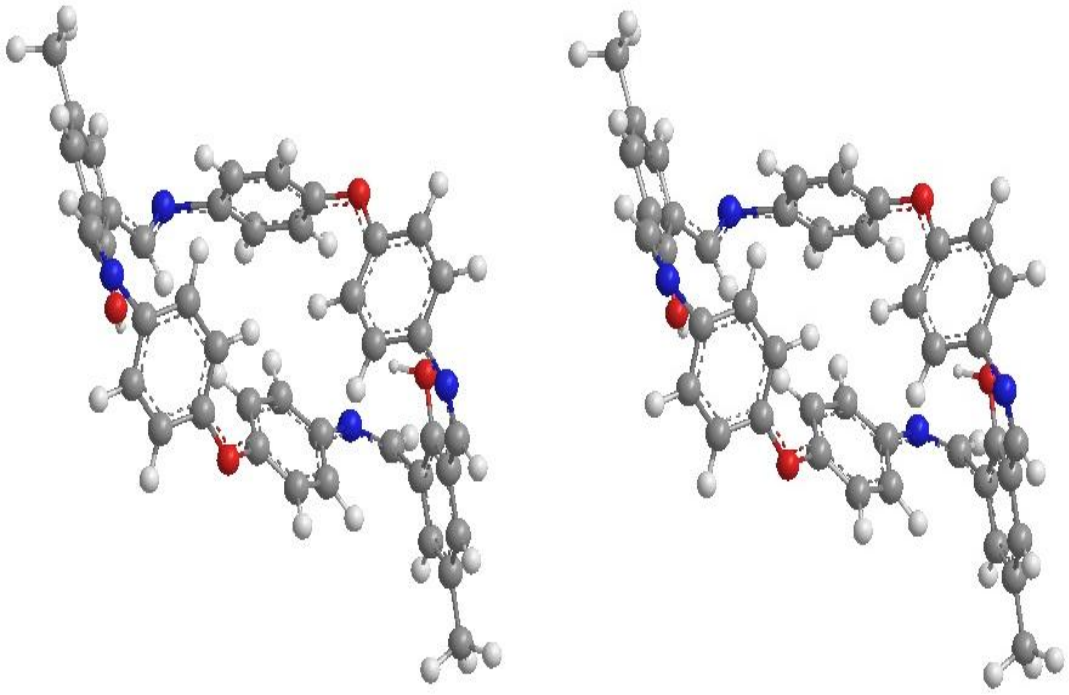

Figure 5A.17: Energy minimized structure and stereographic image of DFMDPE generated from energy minimization through MM_2 calculations (lone pairs of electrons are removed for clarity)

Table 5A.5: *Some of the important geometric parameters of DFMDP*

Bond	Bond length (A^o)	Bond	Bond angle (deg)	Bond	Dihedral angle (deg)
C_{42}-O_{46}	1.47	C_6-N_{14}-C_{35}	125.3	-C_6-N_{14}-C_{35}-C_{30}-	9.3
C_{46}-N_{13}	1.28	N_{14}-C_{35}-C_{30}	134.0	-N_{14}-C_{35}-C_{30}-C_{29}-	-150.2
C_{10}-N_{13}	1.43	C_{35}-C_{30}-C_{31}	121.0	-C_{35}-C_{30}-C_{31}-O_{38}-	-0.8
C_{41}-O_{48}	1.35	C_{30}-C_{31}-O_{38}	120.5	-O_{38}-C_{31}-C_{32}-C_{36}-	-3.2
C_{40}-C_{45}	1.47	C_{32}-C_{31}-O_{38}	120.8	-C_{32}-C_{36}-N_{28}-C_{20}-	177.3
C_{45}-N_{27}	1.28	O_{32}-C_{36}-N_{28}	125.9	-C_{10}-N_{13}-C_{46}-C_{42}-	177.7
C_{24}-N_{27}	1.42	C_{36}-N_{28}-C_{20}	124.4	-C_{40}-C_{45}-N_{27}-C_{24}-	-8.7
C_{17}-C_{50}	1.36	C_{17}-O_{50}-C_{21}	114.1	-C_{46}-C_{42}-C_{41}-C_{48}-	4.3
C_{50}-C_{21}	1.36	C_3-O_{49}-C_7	118.0		
C_{20}-N_{28}	1.42	C_{10}-N_{13}-C_{46}	121.2		
C_{36}-N_{28}	1.28	N_{13}-C_{46}-C_{42}	126.9		
C_{32}-C_{36}	1.47	C_{40}-C_{45}-N_{27}	135.2		
C_{31}-O_{38}	1.36	C_{24}-N_{27}-C_{45}	125.9		
C_{30}-C_{35}	1.48				
C_{35}-N_{14}	1.27				
N_{14}-C_6	1.42				
C_3-O_{49}	1.36				
O_{49}-C_7	1.36				

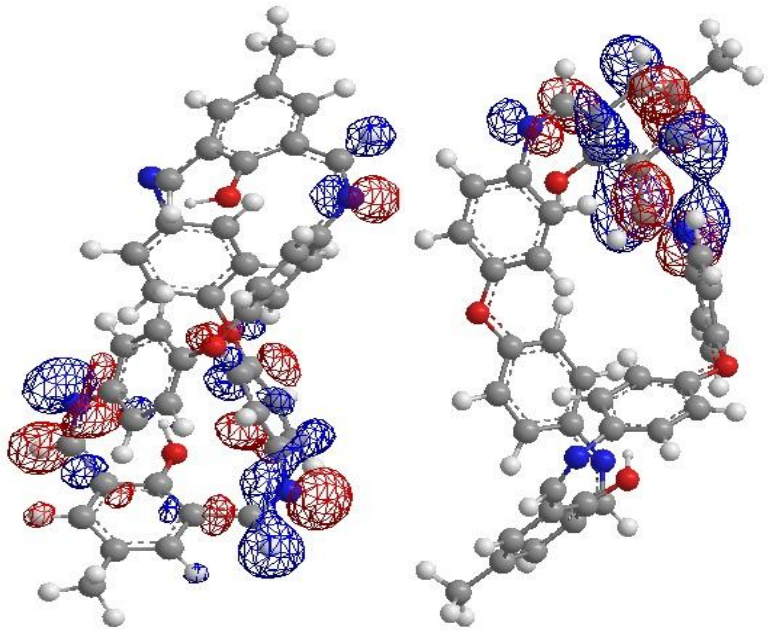

HOMO **LUMO**

Figure 5A.18: High dense HOMO, LUMO molecular orbitals of DFMDPE in wire mesh format

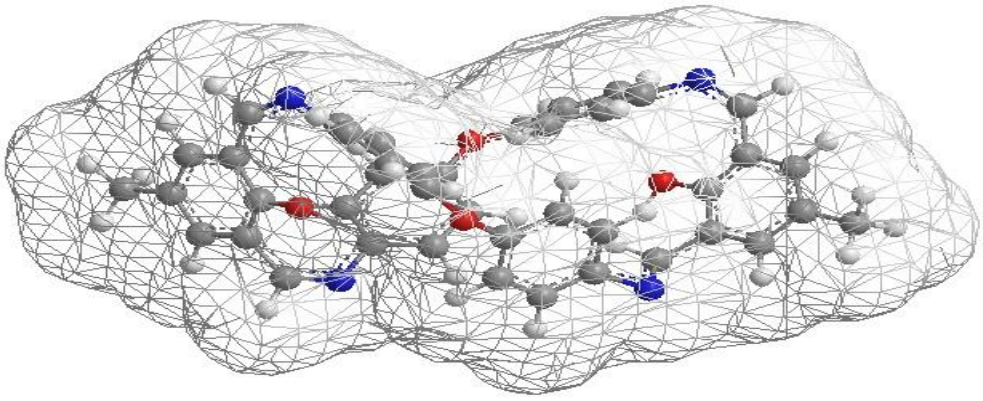

Figure 5A.19: Solvent accessible zone cloud of DFMDPE in wire mesh found

Table 5A.6: *Molecular modeling data of* $H_2L_f^i$

Compound	$\Delta H^o_{f(kcal/mol)}$	HOMO (eV)	LUMO (eV)	Calculated λ_{max} (nm)	Observed λ_{max} (nm)
DFMDPE	210.89	-9.37	-4.22	364	390
DFMDPD	-170.11	-9.482	-4.118	354	398

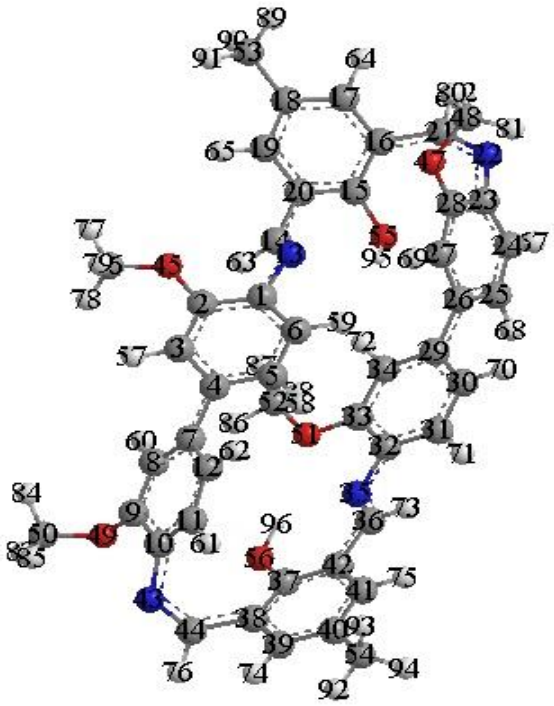

Figure 5A:20: Energy minimized monographic stereographic image of DFMDPD generated from energy minimization through MM_2 calculations (lone pairs of electrons are removed for clarity)

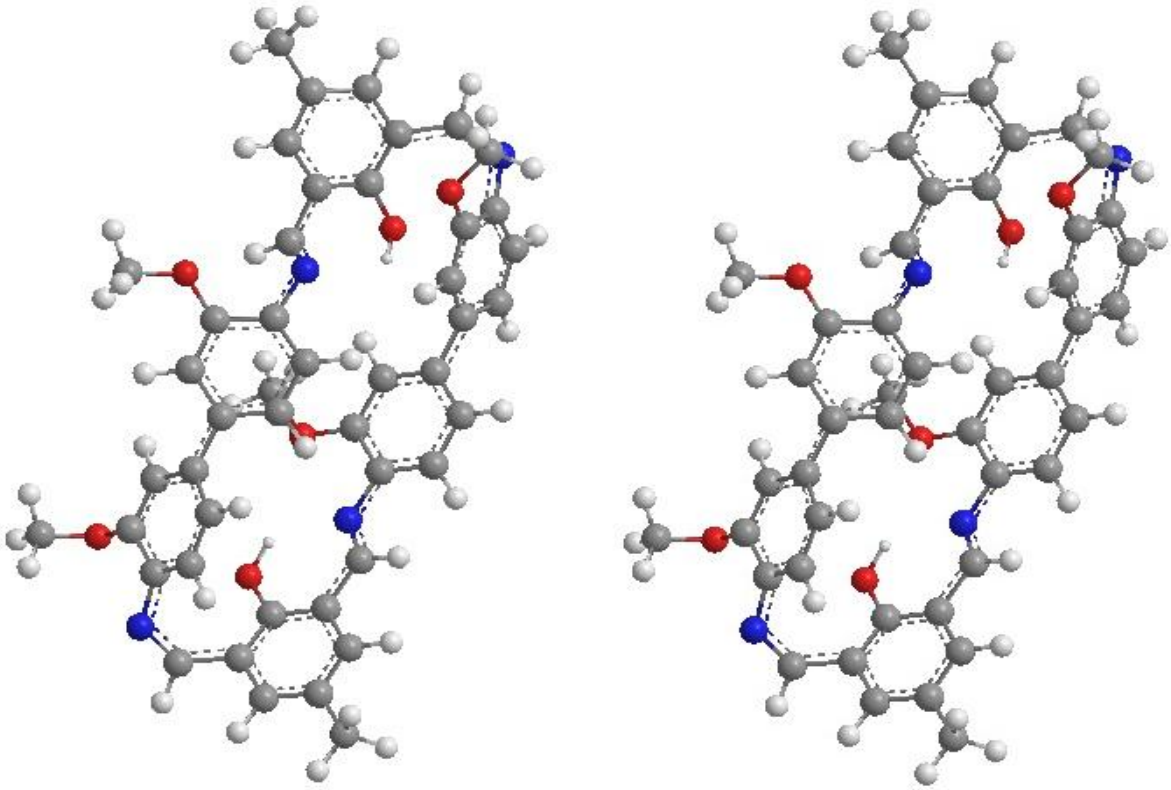

Figure 5A.21: Energy minimized structure and stereographic image of DFMDPD generated from energy minimization through MM_2 calculations (lone pairs of electrons are removed for clarity)

Table 5A.7: *Some of the important geometric parameters of DFMDPD*

Bond	Bond length (A^o)	Bond	Bond angle (deg)	Bond	Dihedral angle (deg)
C_{31}-O_{56}	1.36	C_{32}-N_{35}-C_{36}	125.7	-C_{32}-N_{35}-C_{36}-C_{42}-	174.4
C_{42}-C_{36}	1.47	C_{42}-C_{36}-N_{35}	124.6	-C_{36}-C_{42}-C_{37}-O_{56}-	3.2
C_{36}-N_{35}	1.28	C_{38}-C_{44}-N_{43}	130.5	-C_{38}-C_{44}-N_{43}-C_{10}-	-2.7
N_{35}-N_{14}	1.42	C_{44}-N_{43}-C_{10}	120.9	-O_{55}-C_{15}-C_{20}-C_4-	7.0
C_{38}-C_{44}	1.48	C_9-O_{49}-C_{50}	113.1	-C_{20}-C_{14}-N_{13}-C_1-	177.0
C_{44}-N_{43}	1.28	O_{55}-C_{15}-C_{20}	118.0	-C_{14}-N_{13}-C_1-C_2-	-5.5
N_{43}-C_{10}	1.43	C_{15}-C_{20}-C_{14}	121.2	-N_{22}-C_{21}-C_{16}-C_{23}-	-1.2
C_{29}-C_{26}	1.50	C_{20}-C_{14}-N_{13}	123.4	-O_{55}-C_{15}-C_{16}-C_{21}-	-6.4
C_9-O_{49}	1.37	-C_2-C_{45}-O_{46}-	119.4		
O_{49}-C_{50}	1.40	-C_{23}-N_{22}-C_{21}-	122.9		
C_4-C_7	1.48				
C_{37}-O_{56}	1.36				
-C_{15}-O_{55}-	1.35				
C_{14}-C_{20}	1.47				
N_{13}-C_{14}	1.28				
C_1-N_{13}	1.44				
C_{16}-C_{21}	1.48				
C_{21}-N_{22}	1.28				
N_{22}-C_{23}	1.44				

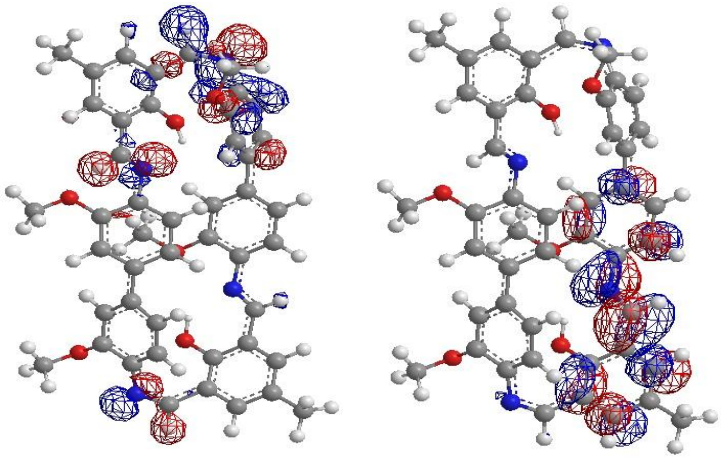

HOMO **LUMO**

Figure 5A.22: High dense HOMO, LUMO molecular orbitals of DFMDPD in wire mesh format

By altering the metal to ligand stiochiometry and by manipulating counter series of ligand. One may arrive at either a binuclear complexes or a series of tetranuclear complexes as shown in **Scheme 5B.1.**

2,6-diformyl-4-methyl phenols have attracted the attention of coordination chemists recently by virtue of their sidereal left-right double condensation character[2]. The presence of phenolic and azomethine sites at vintage position make the Schiff bases arising out of 2,6-diformyl-4-methyl phenols as one of the best classes of binucleating ligands that bring the two metal ions to single atom bridged proximity[3-5]. A typical such case is shown here in **5b.1** as a representative of that class of compounds.

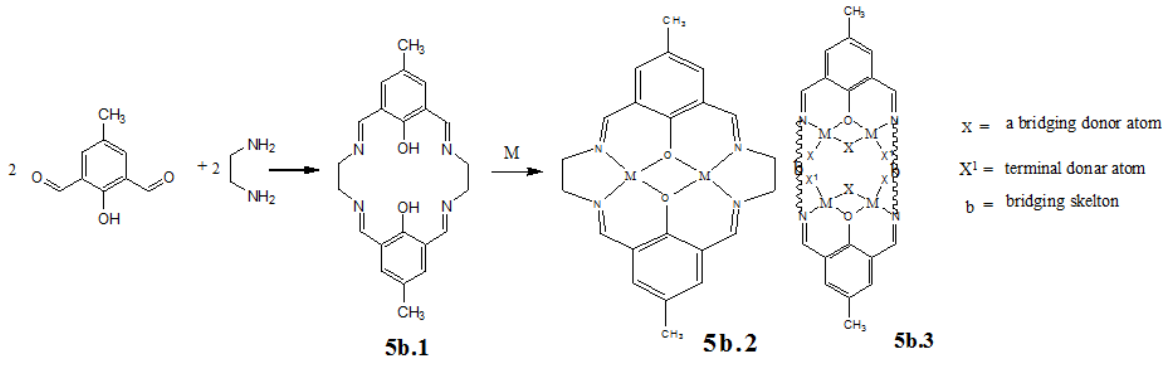

5b.1 **5b.2** **5b.3**

Scheme 5B.1

Complexation of **5b.1** with bivalent metal ions gives **5b.2**. Hence a great deal of supramolecular chemistry around the magnetic, electronic spin resonance, redox catalytic, thermodynamic and optical properties. Instead of ethylenediamine if one uses a longer slightly lower diamine, the hexdentate collective coordination of **5b.1** may lead to a tetranuclear complex, as like in **5b.3**.

Each of this series is discussed separately the following sections:

The general structures of complexes $M_2L^i X_n$ is shown in structure **5B.1** dependant on the co-ordinating number of the metal, the value of n where n = 2,6 usual X = halide, water) Zachiras et,al prepared binuclear copper complexes of $[Cu_2L^{ia}Cl_2]$. However neither supramolecular characteristics of this complex or binuclear complexes with $H_2L^i_b$ are reported

anywhere. Hence, we investigated the metal complexes of $M_2L^i_a$ X_n. However the electrochemical properties have been reported but not studies of supermolecules and magnetic properties.

Binuclear Complexes of $H_2L_f^i$ ($M_2L_f^i.X_n$)

5B.1 Physical, Analytical and Spectral Studies

The structure of the class of binuclear bivalent metal complexes is furnished in **5B.1a** and is referred to as $M_2L_f^i$, hereafter.

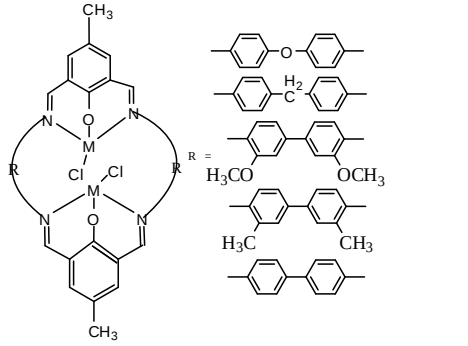

5B.1a $M_2L_f^i$

L	i	$M_2L_f^i$
DFMDPE	1	$M_2L_f^1$
DFMDPM	2	$M_2L_f^2$
DFMDPD	3	$M_2L_f^3$
DFMDPT	4	$M_2L_f^4$
DFMDPB	5	$M_2L_f^5$

5B.2 General Characterizations of the Metal (II) Complexes

The physical and analytical data of the metal (II) complexes are given in **Table 5B.1.** These analytical data are consistent with the proposed binuclear structure shown in **5B.1a.**

5B.3 FT-IR Spectral Studies

The FTIR spectra of some representative complexes relevant spectral data are given in **Table 5B.2**. The spectra of the ligands display sharp peaks characteristics of the C=N bond at 1624-1618 cm^{-1}. The complexes exhibit a shift to lower frequency (1602-1616 cm^{-1}) this is with the coordination of the imino nitrogen to the metal ion. The band observed for the complexes in the region 505–553 cm^{-1} is attributed to (M-phenolic O) and that in the region 434– 489 cm^{-1} to (M–N). All the i.r. data suggest that the metal is bonded to the Schiff bases through the phenolic oxygen and imino nitrogen.

5B.4 ^{1}H NMR and ^{13}C NMR Spectral Studies

The ^{1}H NMR and ^{13}C NMR spectra of some representative complexes as shown in **Figures 5B.1** and **5B.2.** The spectrum of the ligand assigned to the enolic OH, phenyl, groups protons respectively. In the ^{1}H NMR and ^{13}C NMR spectrum of Zn(II) complex in $CDCl_3$, the zinc complex, the enolic, OH proton signal is found to be absent, confirming deprotonation and its subsequent involvement in coordination.

5B.5 Electronic Spectral Studies

The Cu(II) complex exhibited a high intensity band at 480 cm^{-1} in the UV region in **Figure 5B.3**. Appearance of this band is due to π-π* transition associated with the azomethine linkage and L→M charge transfer transition. The Cu(II) and Ni(II) complex may be suggested to the geometry is trigonal bipyrimidal. The Co(II) and Zn(II) complexes may be suggested to the geometry is tetrahedral geometry as shows in the relevant spectral data in **Table 5B.3.**

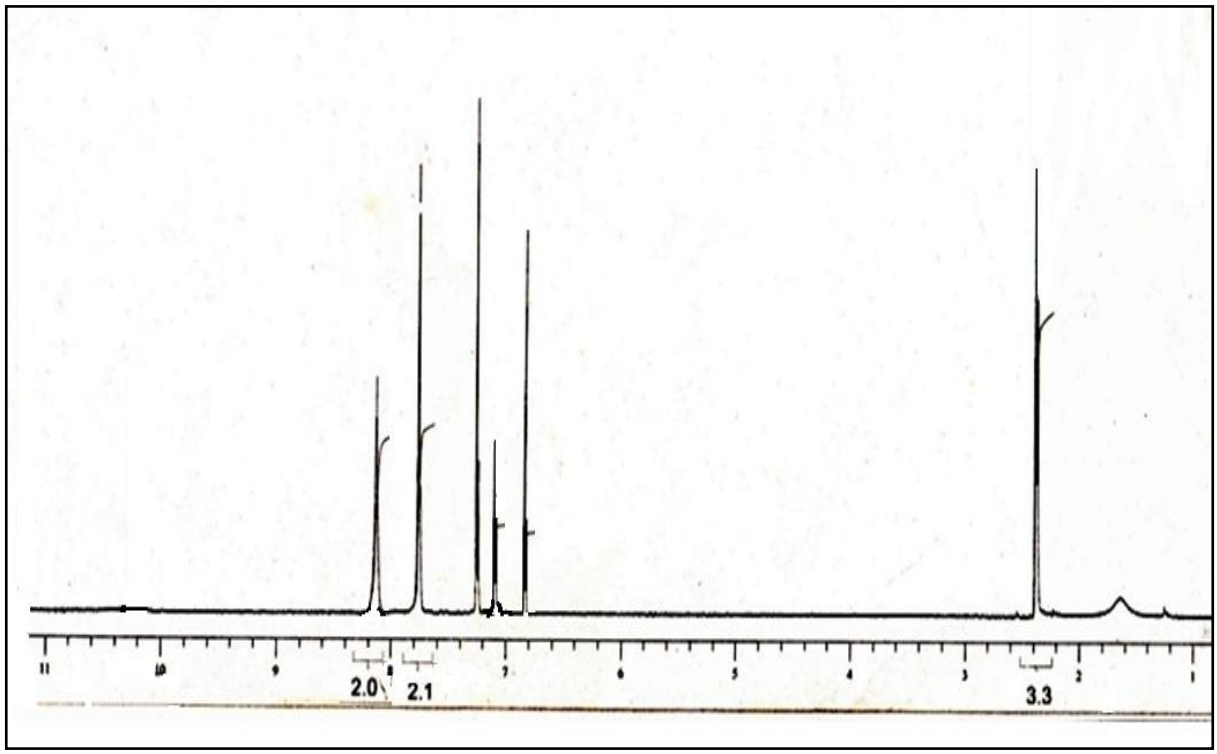

Figure 5B.1: ^{I}H NMR spectrum of $Zn_2(DFMDPE)Cl_2$

Table 5B.1: *Physical, analytical and magnetic data of the biphenyl bridged Schiff base $M_2L_f^i$ complexes*

Complex	**Mol. Formula (mol.weight)**	**Melting Point (^{0}C)$^{\#}$**	**Elemental analysis ***				**μ_{eff} (BM)**
			% C	**% H**	**% N**	**% M**	
$[Cu_2(DFMDPE)(Cl)_2]$	$Cu_2C_{42}H_{30}Cl_2N_4O_4$(852.71)	363.81	59.16	3.55	6.57	14.90	1.70
			(58.98)	(3.60)	(6.28)	(14.01)	
$[Cu_2(DFMDPM)(Cl)_2]$	$Cu_2C_{44}H_{34}Cl_2N_4O_2$(848.76)	350.81	62.26	4.04	6.60	14.97	1.53
			(61.95)	(4.12)	(6.45)	(14.85)	
$[Cu_2(DFMDPD)(Cl)_2]$	$Cu_2C_{46}H_{38}Cl_2N_4O_6$(940.82)	463.81	58.72	4.07	5.96	13.51	1.69
			(58.23)	(4.98)	(5.92)	(13.28)	
$[Cu_2(DFMDPT)(Cl)_2]$	$Cu_2C_{46}H_{38}Cl_2N_4O_2$ (876.82)	423.81	63.01	4.37	6.39	14.49	1.68
			(62.95)	(4.42)	(6.32)	(14.38)	
$[Cu_2(DFMDPB)(Cl)_2]$	$Cu_2C_{42}H_{30}Cl_2N_4O_4$(852.71)	363.81	61.46	3.68	6.83	15.49	1.71
			(61.34)	(3.70)	(6.76)	(15.34)	
$[Co_2(DFMDPE)(Cl)_2]$	$Co_2C_{42}H_{30}Cl_2N_4O_2$(843.48)	481.61	59.84	3.59	6.65	13.92	5.21
			(58.35)	(3.92)	(6.64)	(13.01)	
$[Ni_2(DFMDPE)(Cl)_2]$	$Ni_2C_{42}H_{30}Cl_2N_4O_4$(843.00)	484.48	59.84)	3.59	6.65	13.92	2.72
			(59.50)	(3.79)	(5.53)	(13.15)	
$[Zn_2(DFMDPE)Cl_2]$	$Zn_2C_{42}H_{30}Cl_2N_4O_4$(856.40)	384.38	58.90	3.53	6.54	15.27	-
			(58.35)	(3.54)	(5.64)	(15.10)	

* values in parentheses are theoretical ones $^{\#}$ melting point obtained from DSC

Table 5B.2: *Important IR freq. with assignment of $M_2L^i_f$ complexes*

Complex	IR frequencies [a] (cm^{-1})				
	ν(C-H)	**ν(C=N)**	**ν(C-O)**	**ν(M-N)**	**ν(M-O)**
$[Cu_2(DFMDPE)(Cl)_2]$	3034	1616	1211	555	447
$[Cu_2(DFMDPM)(Cl)_2]$	3031	1630	1231	560	435
$[Cu_2(DFMDPD)(Cl)_2]$	3029	1624	1221	570	440
$[Cu_2(DFMDPT)(Cl)_2]$	3024	1631	1214	565	425
$[Cu_2(DFMDPB)(Cl)_2]$	3025	1614	1216	562	422
$[Co_2(DFMDPE)(Cl)_2]$	3034	1616	1211	565	424
$[Ni_2(DFMDPE)(Cl)_2]$	3030	1618	1205	518	434
$[Zn_2(DFMDPE)Cl_2]$	3024	1616	1188	589	418

a, recorded in KBr (cm^{-1})

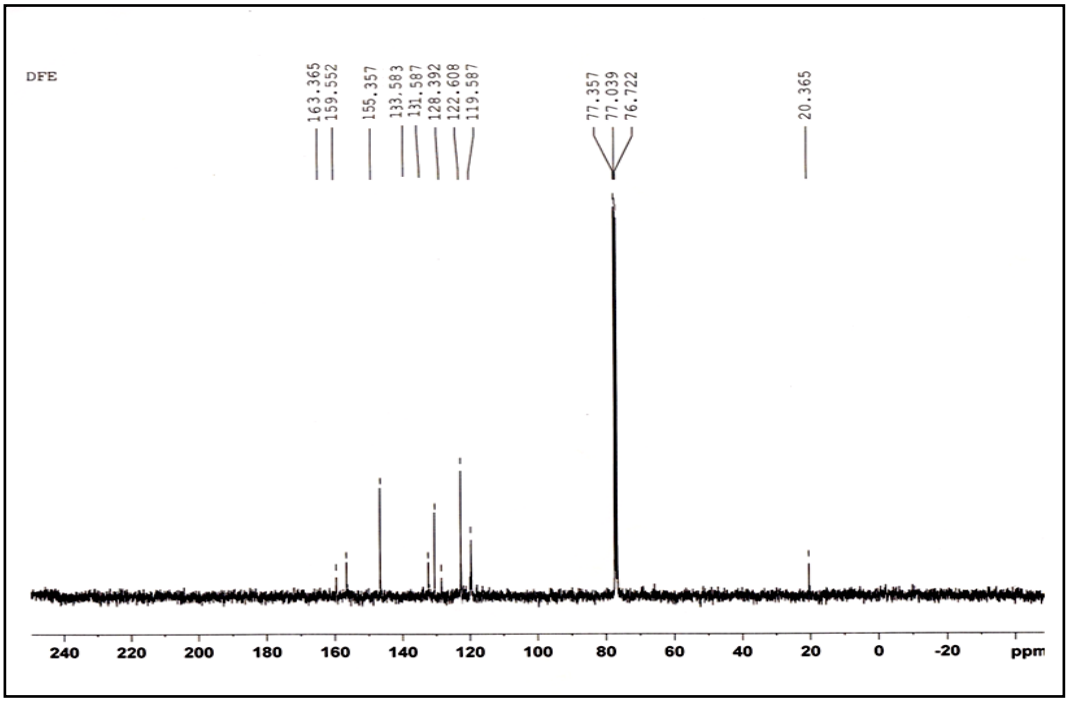

Figure 5B.2: ^{13}C NMR spectrum of $Zn_2(DFMDPE)Cl_2$

Table 5B. 3. *Electronic spectral data of $M_2L_f^i$ complexes*

Complex	Electronic data in DMF λ_{max} ($\bar{\upsilon}$) (ε)[a]
$[Co_2(DFMDPE)(Cl)_2]$	399.5(25,626)(35250)
	326(25,250)(30,674)
$[Ni_2(DFMDPE)(Cl)_2]$	404(47,524)(54,250)
	322(31,061)(59,320)
$[Cu_2(DFMDPE)(Cl)_2]$	481.5(79,002)(14,750)
$[Zn_2(DFMDPE)Cl_2]$	443(22,573)(16,235)
	322(21,250)(31,055)

a, λ_{max} (in nm), $\bar{\upsilon}$ (in cm^{-1}), ε (lit. $mol^{-1}.cm^{-1}$)

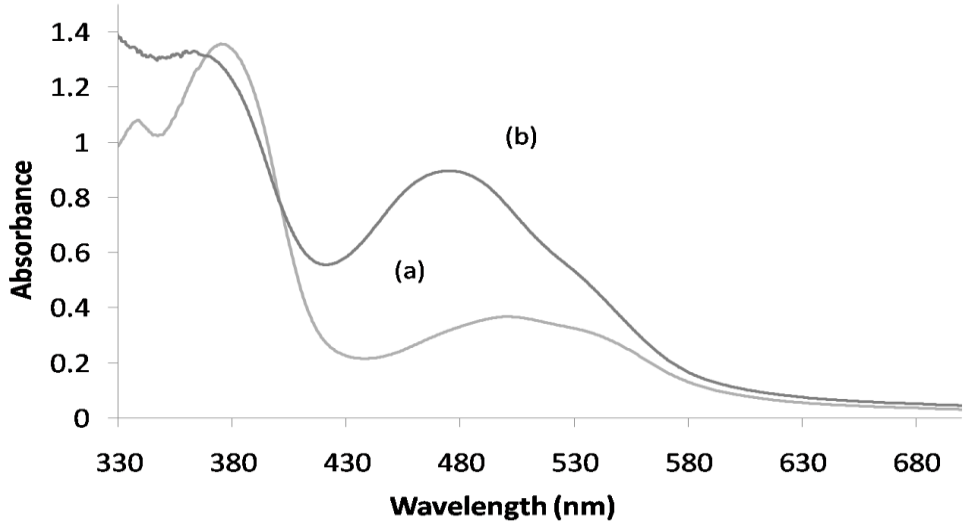

Figure 5B.3: Electronic spectra of (a) ligand of DFMDPE, (b) complex of $Cu_2(DFMDPE)Cl_2$ of (4 x 10^{-5} M) in DMF

5B.6 Magnetic Susceptibility Studies

The magnetic moments of the Co(II), Ni(II) and Cu(II) complexes obtained at room temperature are listed in **Table 5B**.1. The Co(II) and Ni(II) complexes shown magnetic moment values around 5.21 and 2.72 BM, respectively, which are lower than the respective spin values only and indicates weak antiferromagnetic coupling interaction between the metal ions which further confirm the dinuclear nature of the complexes. The Cu(II) complex showed a magnetic moment around 1.70 BM, which is considerably lower than the spin only value for Cu(II) complexes. The low value of the magnetic moment is attributed to the antiferromagnetic coupling interaction between two metal ions. This fact suggests the dinuclear nature of the Co(II), Ni(II) and Cu(II) complexes magnetic susceptibility data were

obtained for $Co_2(DFMDPE)Cl_2$, $Ni_2(DFMDPE)Cl_2$ and $Cu_2(DFMDPE)Cl_2$ from 4.5 to 300^{0}K, in **Figures 5B.4** and **5B.7** fitted to the modified Langevin in dimer equation. The fit was excellent, yielding the following values for Cu(II) the magnetic parameters: J = 20 cm^{-1}, g = 2.15 and θ= -2.06 ^{0}K. The compound possesses a triplet ground state with a singlet state 20 cm^{-1} as shown in **Figure 5B.1**. The fit was excellent, yielding the following values for Co(II) the magnetic parameters: J = 20 cm^{-1}, g = 5.4 and θ= -3.2 ^{0}K as shown in **Figure 5B.4**.

The fit was excellent, yielding the following values for Ni(II) the magnetic parameters: J = 20 cm^{-1}, g = 2.8 and θ= -3.2 ^{0}K as shown in **Figure 5B.5**. The experimental data are shown as open circles and the lines represent the theoretical values obtained using the modified Langevin equation[6].

$$\chi = \frac{Ng^2\beta^2}{3k(T-\theta)}\left(1+\left(\frac{1}{3}\right)exp\left[-\frac{2J}{kT}\right]\right)^{-1} \qquad 5.1$$

and the values of 2J= +20 cm^{-1}, g = 2.15 and θ = -2.06^{0}K. The calculations were carried out with matlab programs written by us for a windows 7 computer.

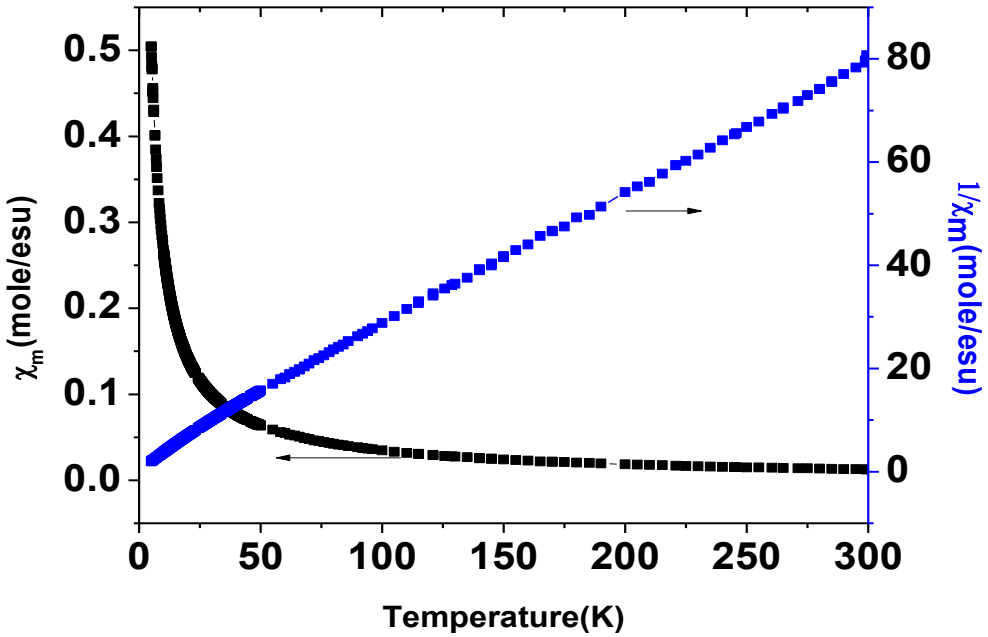

Figure 5B.4: Cryomagnetic susceptibility profile of [$Co_2(DFMDPE)Cl_2$]; (□) experimental, (—) curve-fit line to eqn. 5.1 for g = 5.4, θ = -3.2 and J = 20 cm^{-1}

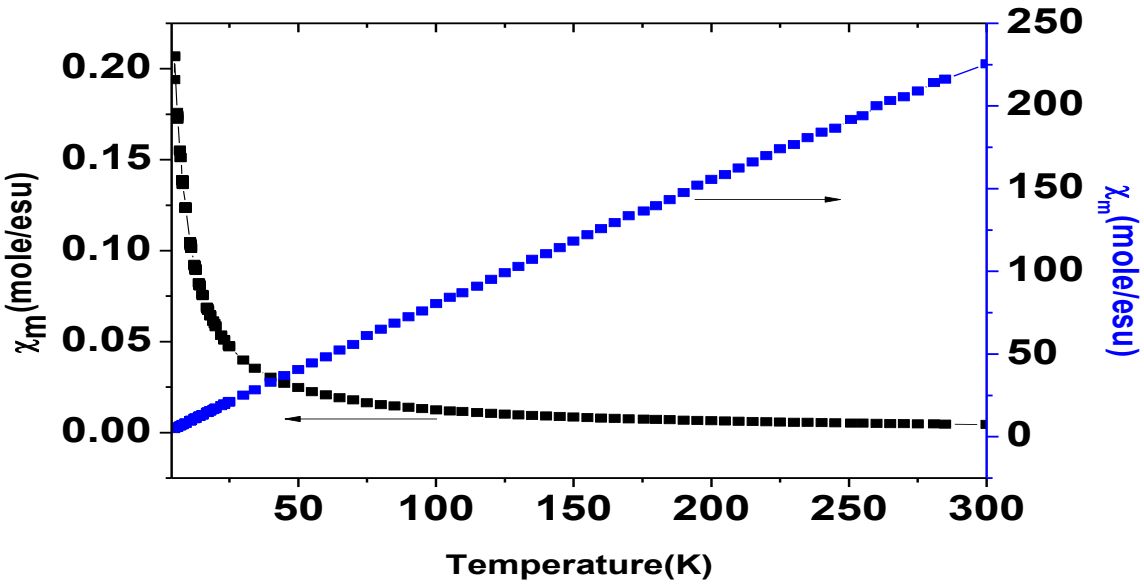

Figure 5B.5: Cryomagnetic susceptibility profile of $[Co_2(DFMDPE)Cl_2]$; (□) experimental, (—) curve-fit line to eqn. 5.1 for g = 2.8, θ = -3.2 and J = 20 cm^{-1}

5B.7 ESR Spectral Studies

The X- band powder and chloroform solution ESR spectra showed a strong absorption at ~3200 G (g ~2.12). The solution even after considerable dilution and freezing did not give any hyperfine splitting. A∥ and A⊥ values are calculated by taking one third of the line widths at half maximum while A_0 is obtained by the relation $A_0 = 1/3(A∥ + A⊥)$. Normally in cases of servere deviation from square planar geometry towards tetrahedral the A_0 values will be lowered by nearly three times from those of perfect square planar copper(II) complexes. A_0 value for tetrahedral geometry is of the order of 45G (40 x 10^{-4} cm^{-1}), the observed A_0 values, in the present series of copper(II) complexes are about 35G which is nearly, there are a series of pseudotetrahedral complexes which do not show any hyperfine ESR spectra in solution. The absence of the splitting in solution even at liquid nitrogen temperature is due to dipolar line broadening. Due to the same effect the A_0 value is further reduced in the present Schiff base complexes. The above observation supports that the geometry around copper can best be described as pseudotetrahedral as predicted from the electronic spectral data. The solution ESR spectra do not resolve the electron-nuclear spin coupling of the Cu(II) complexes. Computer simulation has been used to obtain the tensorial values of $g_{\|}$, $g_{\perp}$ and g_0 those of A_{xx}, A_{yy} and A_{zz} as shown in **Table 5B.4**.

The 77K temperature liquid state ESR spectra of the Cu(II) complex in **Figure 5B.6** show d_{x2-y2} as a ground state, suggesting distorted octahedral or tetrahedral geometries around Cu(II) centres The molar conductance measurements proved that the complexes are non-electrolytes.

Table 5B.4: *ESR spectral data of $Cu_2L_2^i$ complexes*

Complex	$g_{\parallel}$	$g_{\perp}$	g_0 [a]	$A_{\parallel}$	$A_{\perp}$	A_0 [b]
$[Cu_2(DFMDPE)Cl_2]$	2.04	2.04	2.32	11.8	53.6	39.6
$[Cu_2(DFMDPM)Cl_2]$	2.02	2.16	2.11	54.2	77.5	69.7
$[Cu_2(DFMDPD)Cl_2]$	2.10	2.24	2.19	70.2	84.5	79.73
$[Cu_2(DFMDPT)Cl_2]$	2.06	2.18	2.14	50.2	80.2	70.4
$[Cu_2(DFMDPB)Cl_2]$	2.08	2.21	2.16	61.5	92.0	81.83

a : $g_0 = 1/3(g_{\parallel} + 2_{g_{\perp}})$; b: room temperature (DMF solution); b: $A_0 = 1/3(A_{\parallel} + 2_{A_{\perp}})$

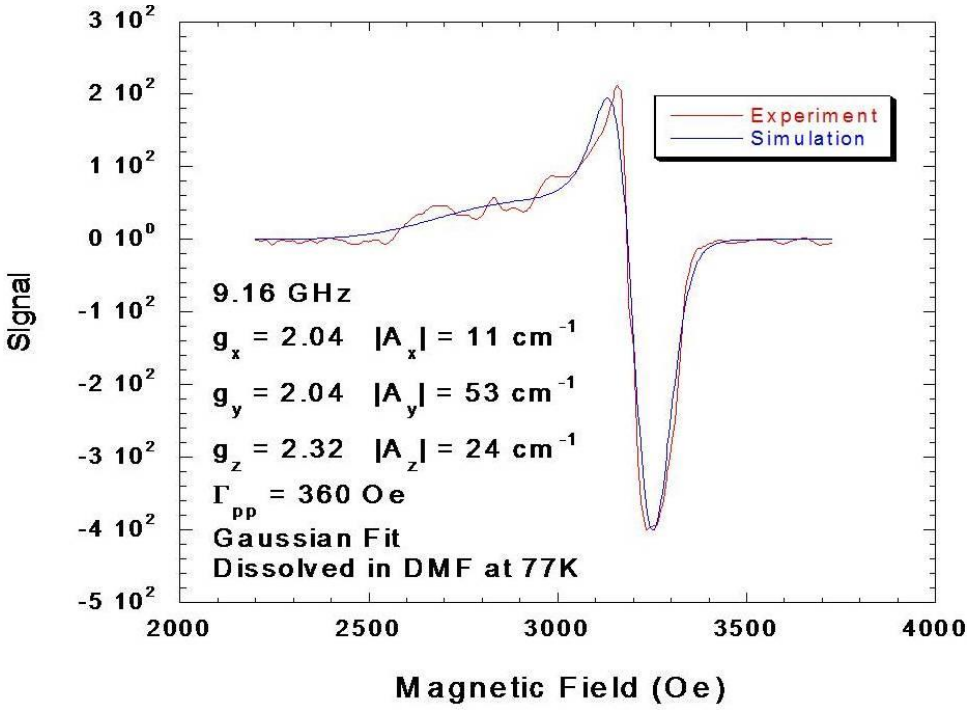

Figure 5B.6: Frozen glass EPR spectrum of $[Cu_2(DFMDPE)Cl_2]$

5B.8 Electrochemical Studies

The electron transfer properties of the complexes were studied in DMF with tetra ethyl ammonium perchlorate (TEAP) as the supporting electrolyte. Cyclic voltammetry was used as the primary tool. The experimental details of sampling and electrochemical run are reported in **Chapter II.**

The cyclic voltammograms (CVs) of the complex $[Co_2(DFMDPE)Cl_2]$ in the potential range 1.10–1.50 Vs^{-1} (versus Ag/AgCl) and for scan rates of 0.1–1.0 V in DMF solutions containing 0.1 M TEAP supporting electrolyte are shown in **Figures 5B.7** and **5B.8** for $[Co_2(DFMDE)Cl_2]$ displays two well defined reversible reduction processes with the corresponding cathodic waves. The half-wave potentials for the reversible and Co(II)/Co(I) redox couples were calculated as the average of the cathodic and anodic peak potentials of the processes. The half-wave potentials of the first and second reduction processes are and $E_{1/2}$ = -1.21 V (scan rate: 0.1 V) in DMF. The first reduction process has about a unit ratio of anodic to cathodic peak currents (ip_a/ip_c). The ratio observed for the second reduction process deviates from unity due to the residual current at low potential. These results are assigned to simple one-electron processes: $[Co(II)L]^- + -e \rightarrow [Co(I)L]^{2-}$,The value of the anodic to cathodic peak separation of the Co(II)/Co(I) couples are 100-1000 mV (scan rate 0.1-1.0 V/s) in DMF. These values are a little larger than expected theoretically for a reversible one electron process.

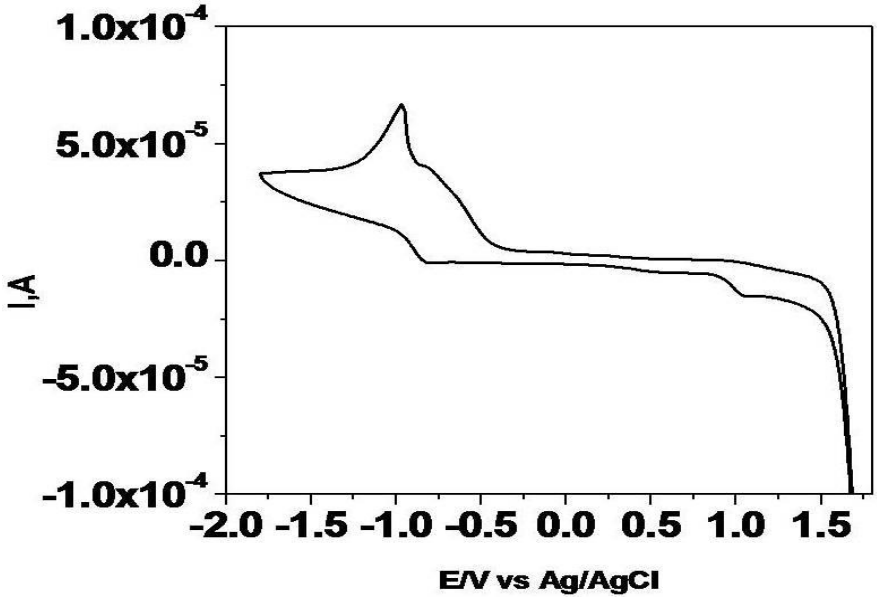

Figure 5B.7: Cyclic voltammogram of $Co_2(DFMDPE)Cl_2$ (3.06×10^{-4} M) in DMF on GCE at scan rate, 0.1 Vs^{-1}, with TEAP (0.1 M)

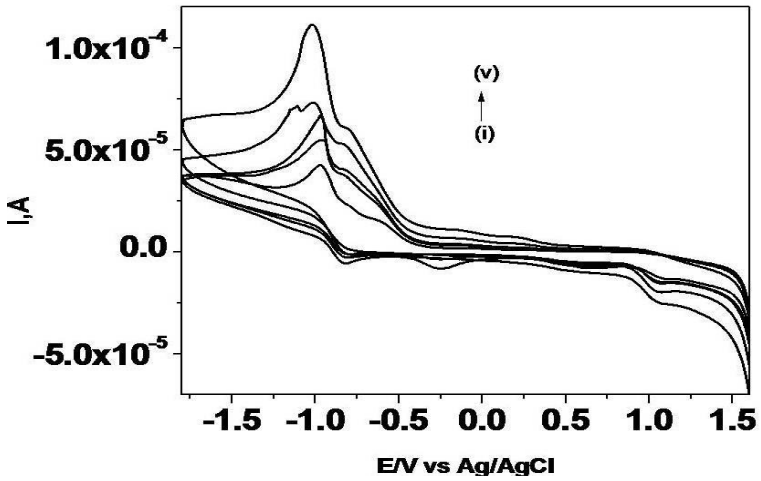

Figure 5B.8: Cyclic voltammograms of $Co_2(DFMDPE)Cl_2$ (3.06 x 10^{-4} M) in DMF on GCE at different scan rates, (i) 0.1, (ii) 0.2, (iii) 0.4, (iv) 0.6, (v) 0.8, Vs^{-1}, with TEAP (0.1 M)

The Ni(II) complex exhibited a reduction peak at Epc = 0.332 With a direct oxidation peak at Epa = 0.280 V corresponding to the formation of Ni(II)/Ni(I) couple. The peak separation of this couple ($^{-}$Ep) is 0.052 V at 0.1 V and increases with scan rate. These characteristic features are consistent with the quasi-reversibility of Ni(II)/Ni(I) couple Cyclic voltammograms of the ligand and complexes were run in DMF 0.1M TEAP as supporting electrolyte at 293 K. unless otherwise stated all potentials quoted refer to measurements run at scan rates of 100 mV/s and against an internal Ag/AgCl. The electrochemical data of the ligand and its complexes are summarised. The CV curves of the ligand at the 100 mV/s scan rates in DMF solution show the reversible process (Ipa: Ipc=1.0)). The electrochemical curves of the Ni(II) complexes at 100 mVs^{-1} scan rate are shown in the **Figure 5B.9.** In addition to the ligand-based processes, all complexes show an irreversible or quasi-reversible two-electron reduction.

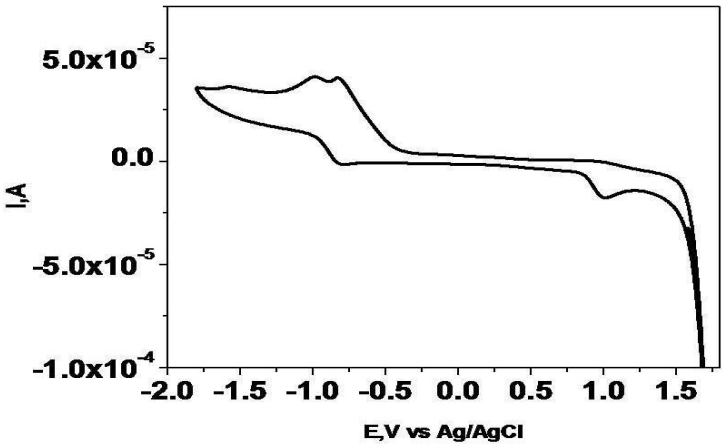

Figure 5B.9: Cyclic voltammogram of $Ni_2(DFMDPE)Cl_2$ (3.06 x 10^{-4} M) in DMF on GCE at scan rate, 0.1 Vs^{-1}, with TEAP (0.1 M)

The electrochemical behavior of Cu(II) complex was examined by employing glassy carbon as working electrode, Ag/AgCl as reference electrode and platinum wire as auxiliary electrode (**Figure 5B.10**). The working media consisted of DMF and n-$Bu_4N^+ClO_4^-$ as supporting electrolyte. The cyclic voltammogram of Cu(II) complex in 10^{-3} M solution was recorded at room temperature in the potential range -3.0 V to +2.4 V with a scan rate 100 mV /s. The complex shows a redox process corresponding to the Cu(II)/Cu(I) couple at E_{pa}= -1.40 V and associated cathodic peak at E_{pc} = -0.60 V. This couple is found to be quasi-reversible as the peak separation between the anodic and cathodic potential is very high. But the ratio between the anodic and cathodic currents suggests that the process is simple one-electron transfer, quasi-reversible process[7, 8]. On comparing the cyclic voltammograms, we observed that the variation in oxidation and reduction potential may be due to distortion in the geometry of the complex which arises due to different anions coordinated to the metal ion [9]. The λ_{max} of Schiff base undergoes red shift in DMF may be due to the hydrogen bond formation.

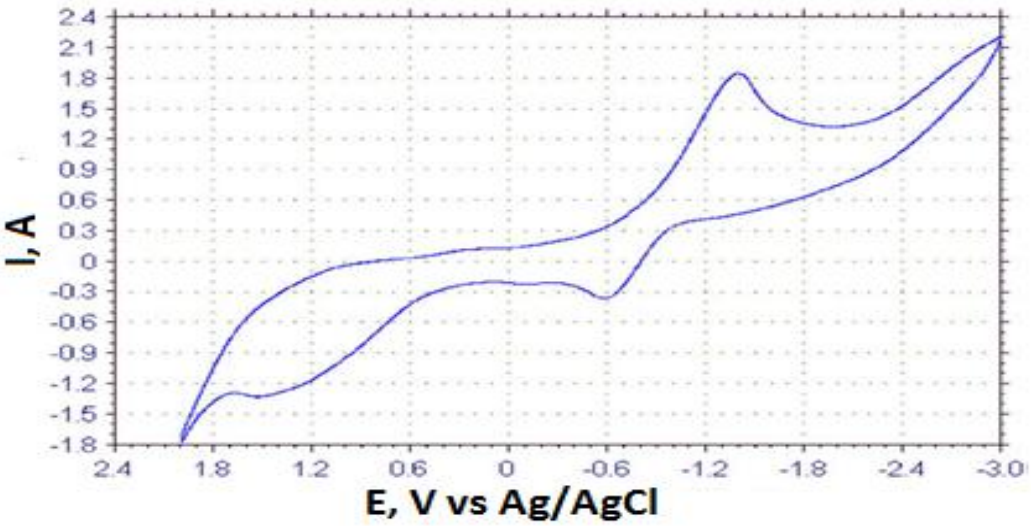

Figure 5B.10: Cyclic voltammogram of $Cu_2(DFMDPE)Cl_2$ (3.06×10^{-4} M) in DMF on GCE at scan rate, 0.1 Vs^{-1}, with TEAP (0.1 M)

The electron transfer properties of the complexes were studied in DMF with tetra ethyl ammonium perchlorate (TEAP) as the supporting electrolyte. Cyclic voltammetry was used as the primary tool. The experimental details of sampling and electrochemical run are reported in **Chapter II**. A typical cyclic voltammogram obtained in the cathodic region on SMDE/GCE for $Zn_2(DFMDE)Cl_2$ is presented in **Figure 5B.11.** An irreversible reduction peak at ~ 0.850 V and another irreversible oxidation peak at ~ 1.250 V are observed. The effect of scan rate, concentration, potential settings, etc on the cyclic voltammetric profiles suggest that the two irreversible peaks are diffusion controlled and that they belong to two different electrophores. Usually, the Zn(II)/Zn(0) couple in aqueous media shows up its CV reduction peak at ~ -0.700

V against Ag|AgCl. The reduction peak observed for the $Zn_2(DFMDPE)Cl_2$ is attributed to the 2-electron reduction of the metal ion. The greater cathodic potential for the present complexed zinc ion than the standard reduction potential of Zn^{2+}/Zn is attributed to the poorer dielectric constant of DMF than water and to the additional stabilisation of the ion by complexation, Further, the crowding of the bulky naphthylidinimines around the metal ion on the equatorail plane and the presence of 2 water molecules on the axial ends of the octahedral geometry around the metal ion would hinder the facile electron transfer. Presence of only one peak in the cathodic scan indicates that the two metal centres of the binuclear complex undergo near-simultaneous reduction. This is further proven by the coulometric studies which reveal the transfer of 4 faradays per mole. Hence, the non-aqueous cathodic electron transfer of Zn_2L^1 is assigned as

$$\mathbf{Zn(II)_2L^1 + 2e \xrightarrow{k_{1c}} Zn(II)Zn(0)L^1} \quad \textbf{(}5.1a)$$

$$\mathbf{Zn(II)Zn(0)L^1 + 2e \xrightarrow{k_{2c}} Zn(0)_2L^1} \quad \textbf{(}5.1b)$$

$$\mathbf{Zn(0)_2L^1 \xrightarrow{k_{dc}} dissociated\ species} \quad \textbf{(}5.1c)$$

with the first cathodic heterogeneous electron transfer rate constant, k_{1c} being far higher than the second one, k_{2c}, while the electrochemical event having a following-chemical dissociation reaction with a high rate constant, k_{dc}.

The anodic peak is attributed to the oxidation of the azomethine moiety. It is well known that azomethine moieties exhibit characteristic oxidation in non-aqueous media at ~ 1.000 V vs Ag|AgCl through a free radical mechanism. The near similar current heights of the cathodic and the anodic responses (**Figure 5B.11**) of the complex suggests a similar 2 consecutive electrochemical steps with following-chemical dissociation event as

$$\mathbf{Zn(II)_2L^1\boxed{\{(-C{=}N-)(N{=}C-)\}_2} \underset{-2e}{\overset{k_{1a}}{\longrightarrow}} Zn(II)_2L^1\boxed{\{(-C^{\bullet}\text{-}N^{+}\text{-})(N^{+}\text{-}C^{\bullet}\text{-})(-C{=}N-)(N{=}C-)\}}} \quad (5.2a)$$

$$\mathbf{Zn(II)_2L^1\boxed{\{(-C^{\bullet}\text{-}N^{+}\text{-})(N^{+}\text{-}C^{\bullet}\text{-})(-C{=}N-)(N{=}C-)\}} \underset{-2e}{\overset{k_{2a}}{\longrightarrow}} Zn(II)_2L^1\boxed{\{(-C^{\bullet}\text{-}N^{+}\text{-})(N^{+}\text{-}C^{\bullet}\text{-})\}_2}} \quad (5.2b)$$

$$Zn(II)_2L^1\boxed{\{(-C^{\bullet}\text{-}N^{+}\text{-})(N^{+}\text{-}C^{\bullet}\text{-})\}_2} \xrightarrow{k_{da}} \textbf{dissociated species} \quad (5.2c)$$

with the first anodic heterogeneous electron transfer rate constant, k_{1a} being far higher than the second one, k_{2a}, while the electrochemical event having a following-chemical dissociation reaction with a high rate constant, k_{da}.

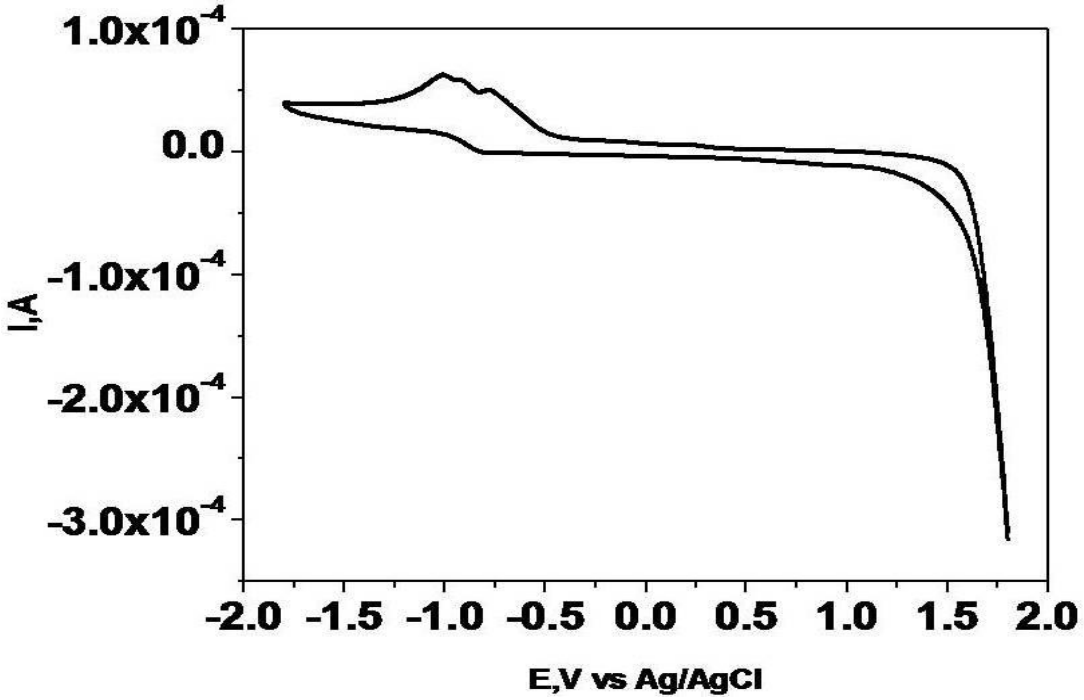

Figure 5B.11: Cyclic voltammogram of $Zn_2(DFMDPE)Cl_2$ (3.06×10^{-4} M) in DMF on GCE at scan rate, 0.1 Vs^{-1}, with TEAP (0.1 M)

Tetranuclear complexes of H_2L^i ($M_4L^i.X_n$)

The structure of all these compounds reported fall under any one of the general structures shown in structures **2A.3b**. But no Macrocyclic compartmental ligands where biphenyl pillar bridges were used, are reported[11], excepting the recent report by P.S.Zacharis et al, that the structure proposed by them is to certain extent untenable because it involves coordination of copper, through three nearly collinear ligands atoms, ON of a tridentate 2,6 bis(azomethanine)phenolic Schiff base moiety[12-19]. The strain involved in such complexation was also evident to us through construction models.

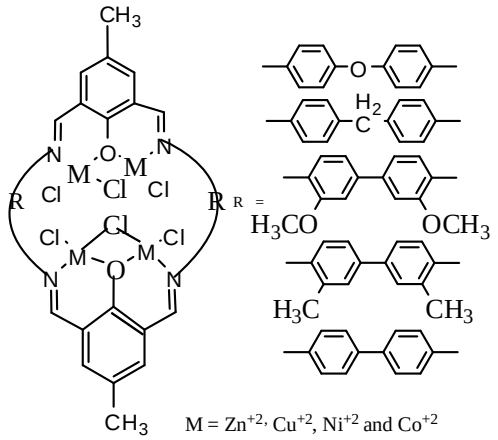

5.1b $M_4L_f^i$

$H_2L_f^i$	$M_4L_f^i$
DFMDPE or $H_2L_f^1$	$M_4L_f^1$
DFMDPM or $H_2L_f^2$	$M_4L_f^2$
DFMDPD or $H_2L_f^3$	$M_4L_f^3$
DFMDPT or $H_2L_f^4$	$M_4L_f^4$
DFMDPB or $H_2L_f^5$	$M_4L_f^5$

To ascertain whether the complexes would have more meaningful structure and to develop macropolynuclear coordination compounds as in structure **5B.1b.** We have proceeded to synthesize and characterize a few representative compounds

The synthetic procedure adapted to prepare the target compound as in structure is **5B.1b,** discussed in **Chapter II**, **PART A**. The physical and elemental data are presented in **Table 5B.14**. The elemental data is consistent with the formula $M_4L_f^i$ where $H_2L_f^i$ is the Schiff base ligand obtained by mixing appropriate diamine with 2,6-diformyl 4-methyl phenol. For subsequent reference, the L part will be expressed through DFMDPE, DFMDPM, DFMDPD, DFMDPT, and DFMDPB. For instance, the L obtained from 2,6-diformyl-4-methyl phenol and benzidine will be referred to as DFMDPB. The compounds are insoluble in routine solvents.

Table 5B.5: *Physical, analytical and magnetic data of the tetranuclear Schiff base ligands $M_4L_f^i$ complexes*

Compound	**Mol. Formula (mol.weight)**	**Color**	**Elemental analysis ***					**μ_{eff} (BM)**
			% C	% H	% N	% M	**% Yield**	
$[Cu_4(DFMDPE)Cl_6]$	$Cu_4C_{42}H_{30}Cl_6N_4O_4$(1121.61)	Black	44.98 (44.05)	2.70 (2.78)	5.00 (4.88)	22.66 (22.01)	89	1.76
$[Cu_4(DFMDPM)Cl_6]$	$Cu_4C_{42}H_{34}Cl_6N_4O_2$(1093.65)	Black	46.13 (66.34)	3.13 (4.60)	5.12 (4.28)	23.24 (10.01)	89	1.74
$[Cu_4(DFMDPD)Cl_6]$	$Cu_4C_{46}H_{38}Cl_6N_4O_6$(1169.66)	Black	45.67 (66.34)	3.17 (4.60)	4.63 (4.28)	21.01 (10.01)	89	1.72
$[Cu_4(DFMDPB)Cl_6]$	$Cu_4C_{42}H_{30}Cl_6N_4O_2$(1089.62)	Black	46.30 (66.34)	2.78 (4.60)	5.14 (4.28)	23.33 (10.01)	89	1.70
$[Ni_4(DFMDPE)Cl_6]$	$Ni_4C_{42}H_{30}Cl_6N_4O_4$(1102.20)	Pale Green	45.72 (66.34)	2.74 (4.60)	5.08 (4.28)	21.30 (10.01)	70	2.72
$[Co_4(DFMDPE)Cl_6]$	$Co_4C_{42}H_{30}Cl_6N_4O_4$(1103.16)	Orange	45.73 (68.35)	2.74 (3.92)	5.08 (5.04)	21.37 (11.01)	82	5.21
$[Zn_4(DFMDPE)Cl_6]$	$Zn_4C_{42}H_{30}Cl_6N_4O_4$(1128.99)	Yellow	44.68 (69.35)	2.68 (4.54)	4.96 (4.64)	23.17 (10.77)	87	-

* data in parenthesis are calculated ones

Table 5B.6: *Infrared and thermal data of the tetranuclear Schiff base ligands $M_4L_f^i$ complexes*

Complex	Infrared frequencies [a] (cm^{-1})				
	C=N	C-O	Cu-Cl-Cu	Cu-Cl	ΔH^b_d
$[Cu_4(DFMDPE)Cl_6]$	1621	1342	302	332	44.22
$[Cu_4(DFMDPM)Cl_6]$	1620	1340	300	320	44.48
$[Cu_4(DFMDPD)Cl_6]$	1624	1338	302	323	44.20
$[Cu_4(DFMDPB)Cl_6]$	1622	1340	301	322	45.12
$[Ni_4(DFMDPE)Cl_6]$	1620	1342	302	325	42.26
$[Co_4(DFMDPE)Cl_6]$	1622	1341	301	331	44.21
$[Zn_4(DFMDE)Cl_6]$	1624	1342	300	328	44.22

a, recorded in KBr pellet b, in Kcal/mole d, measured at room temperature (per metal centre)

Table 5B.7: *ESR spectral data of the tetranuclear Schiff base ligands Cu_4L^i complexes*

a, calculated from equation

Complex	$g_{\parallel}$	$g_{\perp}$	g_0 [a]	$A_{\parallel}$ (cm^{-1} x 10^4)	$A_{\perp}$ (cm^{-1} x 10^4)	A_0 [a] (cm^{-1} x 10^4)
$[Cu_4(DFMDPE)Cl_6]$	2.13	2.18	2.17	61.2	73.2	69.2
$[Cu_4(DFMDPM)Cl_6]$	2.02	2.16	2.11	54.2	77.5	69.73
$[Cu_4(DFMDPD)Cl_6]$	2.10	2.24	2.19	70.2	84.5	79.73
$[Cu_4(DFMDPB)Cl_6]$	2.08	2.21	2.16	61.5	92.0	81.83

a : $g_0 = 1/3(g_{\parallel} + 2_{g_{\perp}})$; b: room temperature (DMF solution); c: $A_0 = 1/3(A_{\parallel} + 2_{A_{\perp}})$

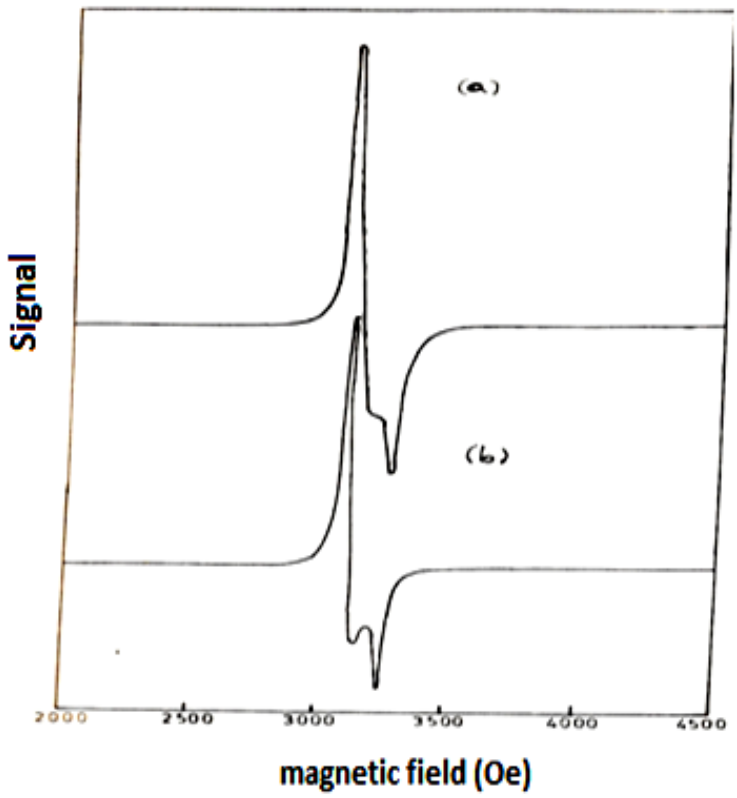

Figure 5B.12: X-band polycrystalline ESR spectra of $[Cu_4(DFMDPM)Cl_6]$ (ν= 9.235) (a) Room temperature (b) -120^0C

The infrared spectral data of the compounds for a few band assignments are also shown in **Table 5B.6**. Bands characteristic to Cu-Cl and Cu-Cl-Cu were observed in the lower energy from ~350 cm^{-1} to ~320 cm^{-1}. Presence of water is also confirmed by stong IR band at ~3200 cm^{-1}. The room temperature magnetic moment data for the formula Cu_4LCl_6 are collected in **Table 5B.5**. The magnetic moment data are obviously subnormal even at room temperature indicating the presence of strong antiferromagnetic interaction.

The ESR spectra of these compounds exhibited characteristic trigonal bipyrimidal ESR profiles where g is considerably lower than g. The representative ESR spectrum is shown in **Figure 5B.12**. The ESR profiles are very close to those reported for similar macrocyclic compartmental binuclear complexes involving trigonal bipyrimidal geometry. The relevant ESR data are also collected in **Table 5B.7**.

In the synthetic process of the compound obtained was found to have molecules evidenced from the elemental (table) and IR data (table). The ESR spectrum of this compound is very close to that expected for a tetrahedral Cu(II) geometry.

References

1. K Nakamoto, Infrared and Raman Spectra of Inorganic and Coordination Compounds, John Wiley, New York, 3rd edn, **1978**, 232
2. R R Gange, C L Spiro, T J Smith, C A Hamann, W R Thies, A K Shiemke, J Am Chem Soc, 103, **1981**, 4073
3. N H Pilkington, R Robson, Aust, J, Chem, 23, **1970**, 2225
4. S K Mandal, L K Thompson, K Nag, J P Charland, *Inorg Chem*, 26, **1987**, 1391
5. R P Das, K Nag , *Inorg Chem*, 30, **1991**, 2831
6. J F Villa and W E Hatfield, *Chem Commun*, **1971**, 101
7. Z Shirin, R M Mukherjee, *Polyhedron*, 11, **1992**, 2625
8. A. Shyamala, A R Chakravarty, *Polyhedron* 12, **1993**, 1545
9. S Chandra, L K Gupta, Sangeetika, *Synth, React Inorg Met Org Chem*, 34, **2004** 1591.
10. H Okawa , M Honda, S Kida, *Chem Le*t, **1972**, 1027
11. B Srinivas, N Arulsamy, P S Zacharias, *Polyhedron*, **1992**, 11, 211
12. B Srinivas, N Arulsamy, P S Zacharias, *Polyhedron*, **1991**, 731
13. H Okawa , M Tanaka, S Kida, *Chem Let*, **1974**, 987
14. M Mikuriya, H Okawa , S Kida, I Ueda, *Bull Chem Soc*, **1972**, 1027
15. H Okawa, Y Nishida, M Tanaka, S Kida, *Bull Chem Soc*, Jpn, 50, **1977**, 127
16. M Tanaka, M Kitaoka, H Okawa, S Kida , *Bull Chem Soc*, Jpn, 49, **1976**, 2469
17. O Kahn, P Tola, J Galy, H Coudane, *J Am Chem Soc*, 100, **1978**, 3931
18. O Kahn, J Galy, Y Journaux, J Jaud, I Morgenstern Badarau, H Coudane, *J Am Chem Soc*, 104, **1982**, 2165
19. O Kahn, R Claude, H Coudane, *J Chem Soc*, 100, **1978**, 3931

CHAPTER VI

STUDIES OF KINETICS OF HYDROLYSIS AND BIOLOGICAL ACTIVITY OF THE BINUCLEATING AND TETRANUCLEATING LIGANDS AND THEIR COMPLEXES

Portions of the results of this chapter are published as *"synthesis and characterization of antimicrobial activity of the binuclear Ni(II), Co(II), Cu(II) and Zn(II) complexes of a novel macrocyclclic biphenyl bridged Schiff base ligand*" Indian Council of Chemists**,** (Accepted), 2012

The azomethine site, –C=N–, is known for its hydrolytic cleavage as –C=N– + H_2O → -CHO + H_2N– under suitable conditions. The biological functions of many drugs, enzymes[1,2], other biochemicals possessing azomethine site are attributed primarily to the chemistry of the hydrolysis of their –C=N– bond. In this chapter are presented the results of the kinetics of hydrolysis of various biphenyl bridged binucleating and tetranucleating ligands that have been discussed in the earlier chapters, besides their biological activities[3-7]. The hydrolysis is found to be either minimized or ceased upon complexation. Spectrophotometry, fluorescence spectro-photometry, cyclic voltammetry were used to monitor the hydrolysis of the ligands. The rate of hydrolysis is found to be very sensitive to pH. Finally, all the ligands and their metal complexes have been screened for their antimicrobial activity. The results reveal that many of them are gram positive.

6.1 Kinetics of Hydrolysis of NDADPE, NDADPM, NDADPO, NDADPT and NDADPB

The studies of kinetics of hydrolytic cleavage of the two azomethine sites have been done in aqueous methanol/ water (v/v) mixtures covering a wide pH range. Repetitive scan spectral profiles of NDADPE, NDADPM, NDADPD, NDADPT and NDADPB in an acidic, neutral and basic media at time intervals of 1 minute are shown in **Figures 6.1-6.5.**

In the same respective figures are shown the spectral scan recorded at infinite time (solution kept overnight and recorded under similar conditions).

In all the cases, it is observed that infinite spectrum first retraces (resembles) the mathematical sum of the spectrum of the corresponding aromatic diamine and naphlaldhyde recorded independently more similar experimental and stoichiometric conditions. Such spectrum taken at the alkaline medium (pH ≥ pk_a) resembles that of the first spectrum recorded for each of the Schiff base indicating fast a hydrolytic cleavage to be monitored. **Figure 6.6** presents the integrative plot of log A_0-A_t is time for NDADPE for the fall of absorbance (due to n→π* of the –C=N-) at ~400 nm at pH ≈ 2.0. The data seen to be well fit to a first order (in the Schiff base) kinetics. Since the structure of the molecule itself is pH dependent, the rate constants also being different for different pHs is not a surprising phenomenon. We propose the low and monitorable hydrolytic kinetics of NDADPE at pH =2.0 in **Figure 6.7** is stabilization of the protonated –NH=CH- moiety enjoying more ways of intramolecular hydrogen bonding as shown in **Scheme 6.1 (**repeated from **Scheme 6.3).**

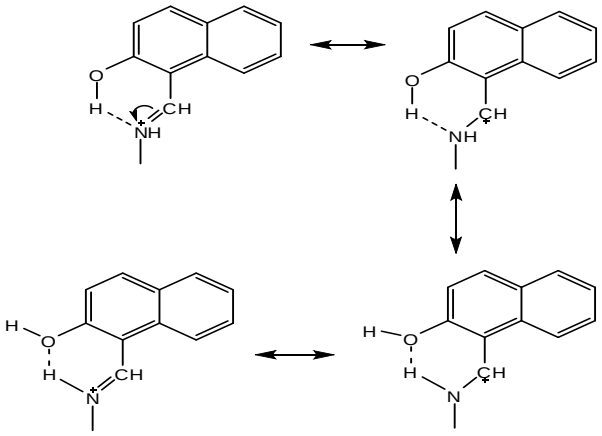

Scheme 6. 1

However, in the Schiff bases of class 'B' (i.e. those with Z= nil), kinetics of hydrolysis was found to be slow even in alkaline medium in **Scheme 6.4**, except in the case of NDADPD **(Figures 6.1 - 6.5).**

In the recent past the kinetics of hydrolysis of biphenyl bridged Schiff basses was reported. Comparative spectral scans for DADPM sal and NDADPM are presented in **Figures 6.2**. Similarly, the seams of NDADPD and o-dia sal are also shown in **Figure 6.3.**

A proton- involved mechanism as shown in **Scheme 6.2** is proposed for the kinetics of hydrolysis of their NDADP Schiff bases.

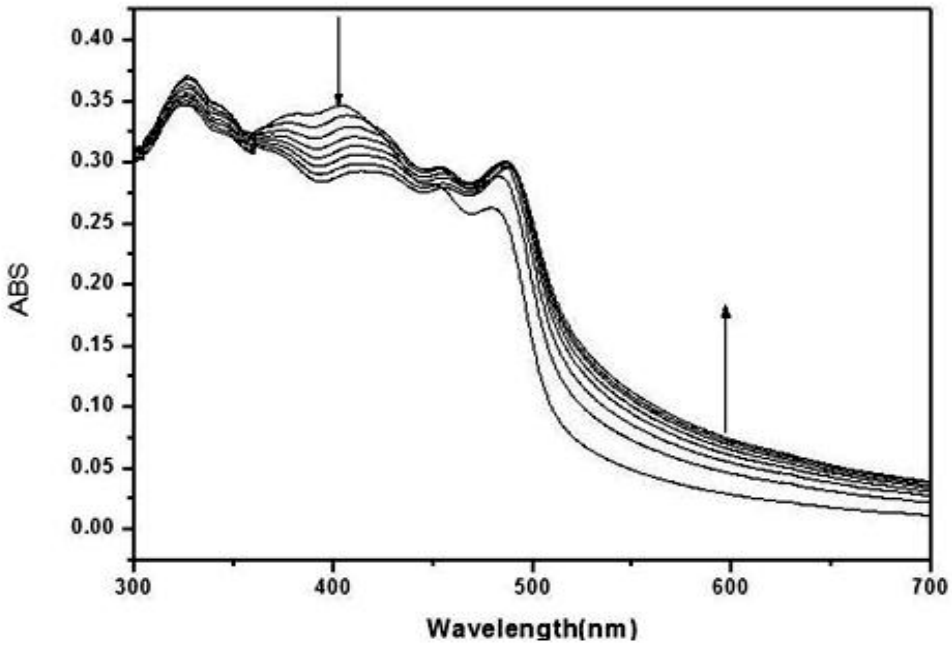

Figure 6.1: Repetitive spectral profiles of NDADPE (4×10^{-5}M; μ = 0.1M) at pH =2.01 at 30^0C (time interval, 1 min)

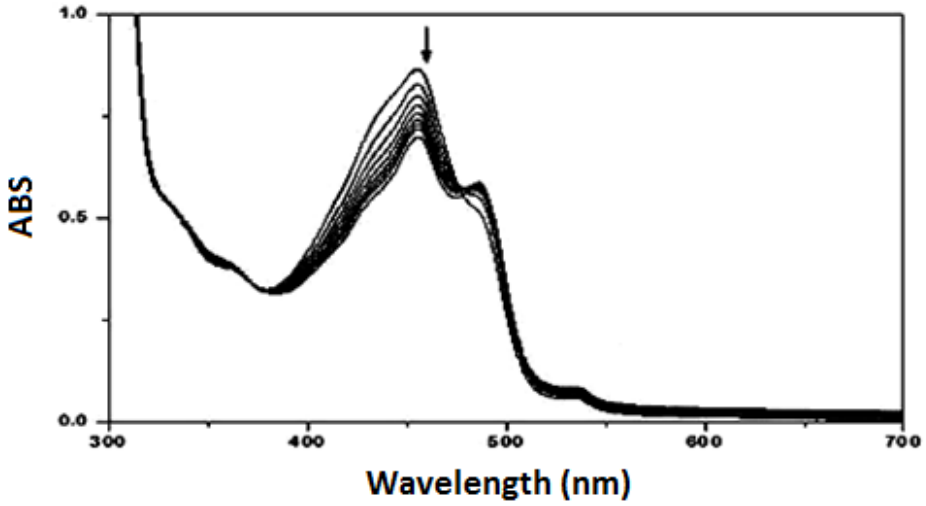

Figure 6.2: Repetitive spectral profiles of NDADPM (4 x 10^{-5}M; μ = 0.1M) at pH =3.84 at 30^0C (time interval, 1 min)

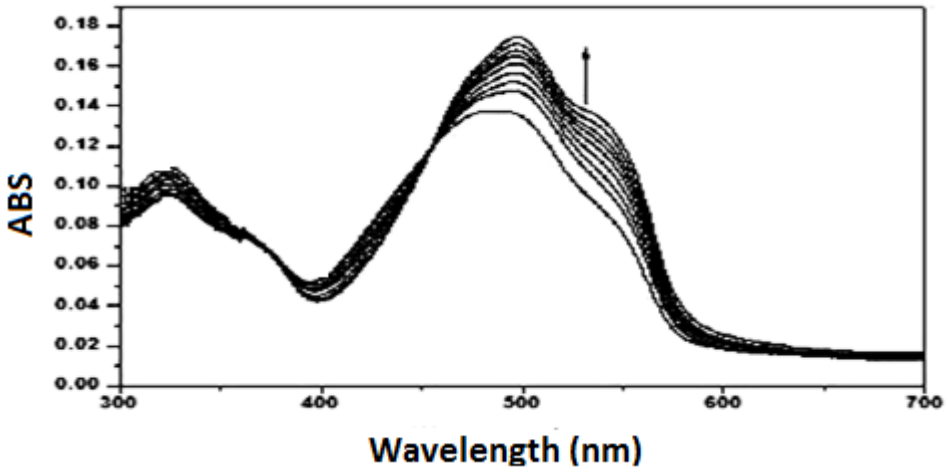

Figure 6.3: Repetitive spectral profiles of NDADPD (4 x 10^{-5}M; μ =0.1M) at pH =2.01 at 30^0C (time interval, 1 min)

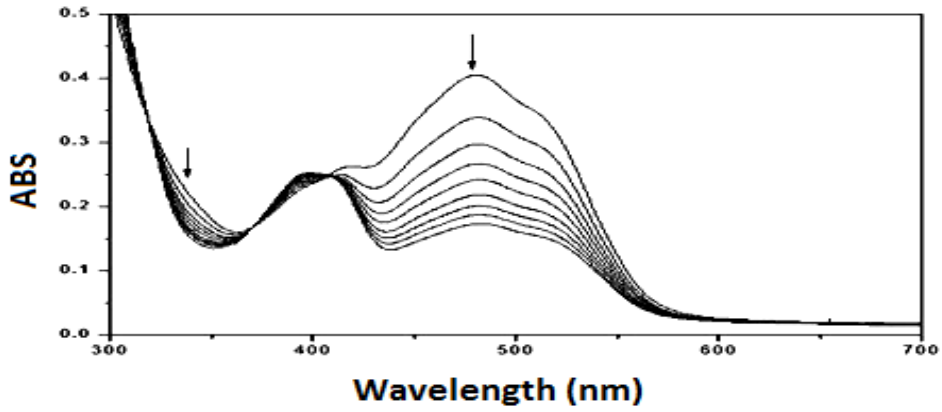

Figure 6.4: Repetitive spectral profiles of NDADPT (4 x 10^{-5}M; μ =0.1M) at pH =12.0 at 30^0C (time interval, 1 min)

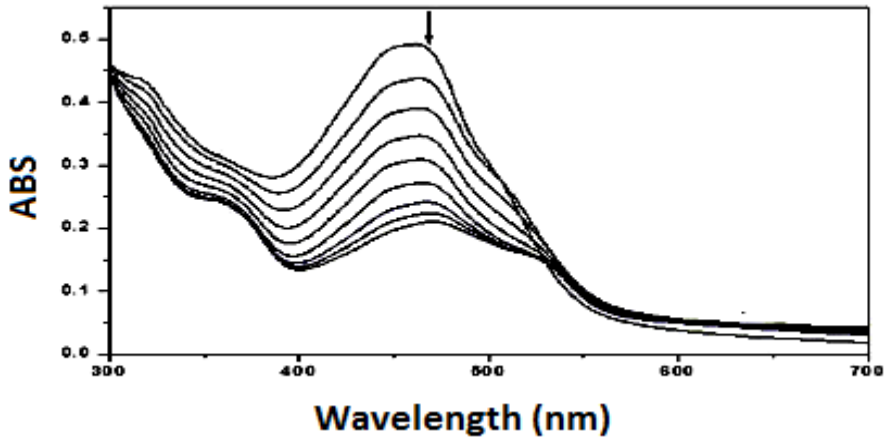

Figure 6.5: Repetitive spectral profiles of NDADPB (4 x 10^{-5}M; μ =0.1M) at pH =3.20 at 30^0C (time interval 1 min)

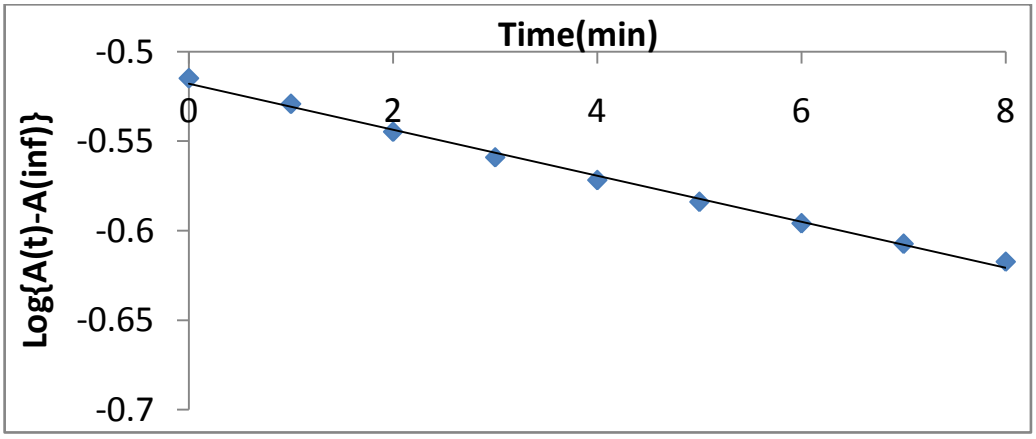

Figure 6.6: Hydrolysis of NDADPE in pH = 2.0: data fitting to first order kinetics at 30^0C

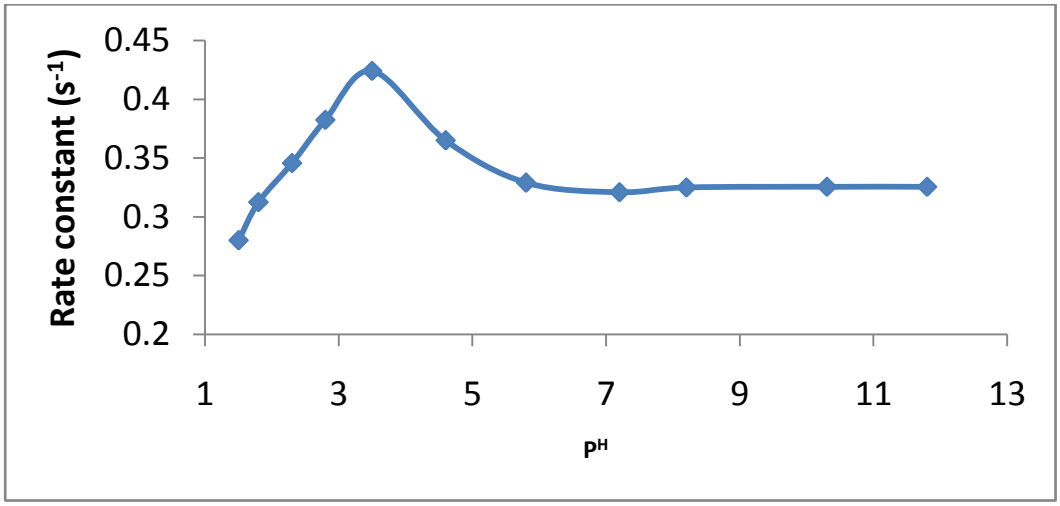

Figure 6.7: Effect of pH on first order rate constant of the hydrolysis of NDADPE at 30^0C

Scheme- 6.2

LH_4^{+2} $\overset{Ka1}{\rightleftharpoons}$ LH_3^{+} $\overset{Ka2}{\rightleftharpoons}$ LH_2 $\overset{Ka3}{\rightleftharpoons}$ LH^{-} $\overset{Ka4}{\rightleftharpoons}$ L^{-2}

Where

LH_4^{2+} = 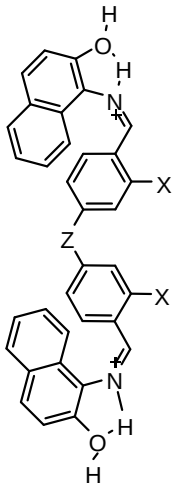

LH_3^{+} = 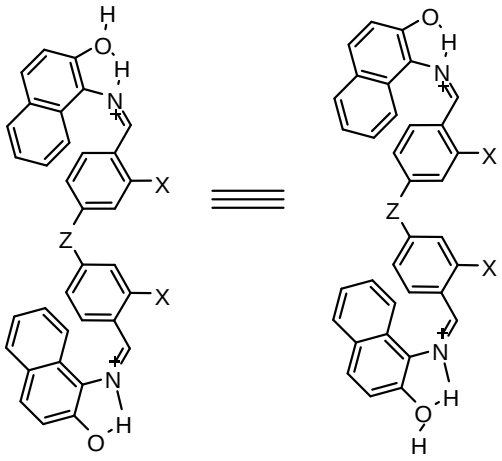

LH_2 = 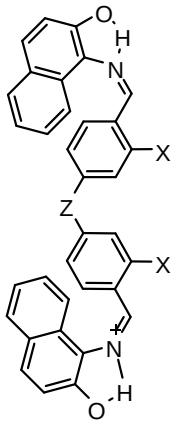

Z= nil or O,CH_2 X= H, CH_3, OCH_3

LH^{-} 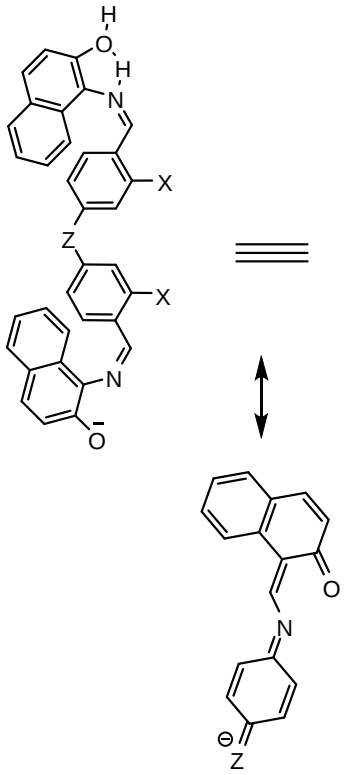

L^{2-} 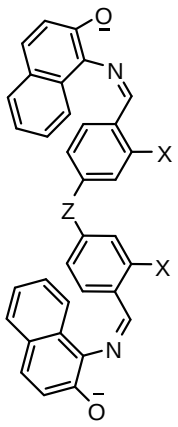

Scheme-6.3

LH_4^{+2} $\overset{Ka1}{\rightleftharpoons}$ LH_3^{+} $\overset{Ka2}{\rightleftharpoons}$ LH_2 $\overset{Ka3}{\rightleftharpoons}$ LH^{-} $\overset{Ka4}{\rightleftharpoons}$ L^{-2}

Where

LH_4^{2+} =

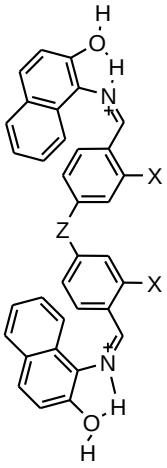

LH_3^{+} =

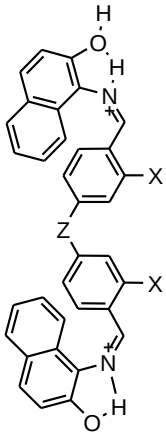

≡

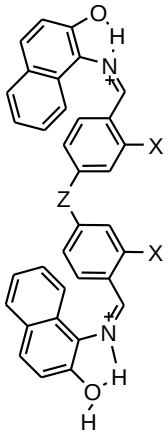

LH_2 =

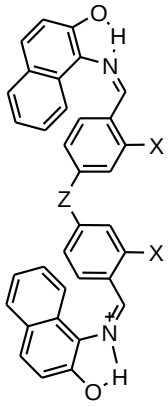

Z= nil or O,CH_2 X= H, CH_3, OCH_3

LH^{-}

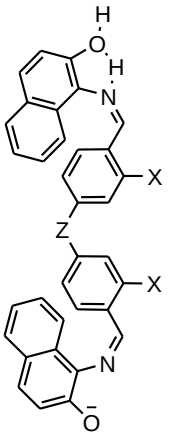

≡

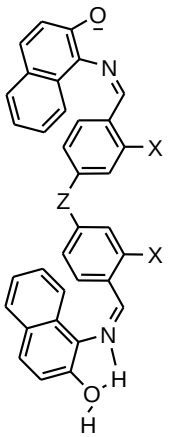

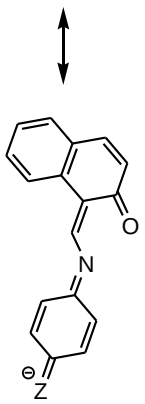

L^{2-}

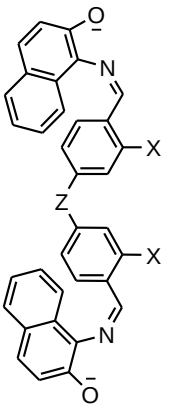

Scheme-6.4

In Acid Range

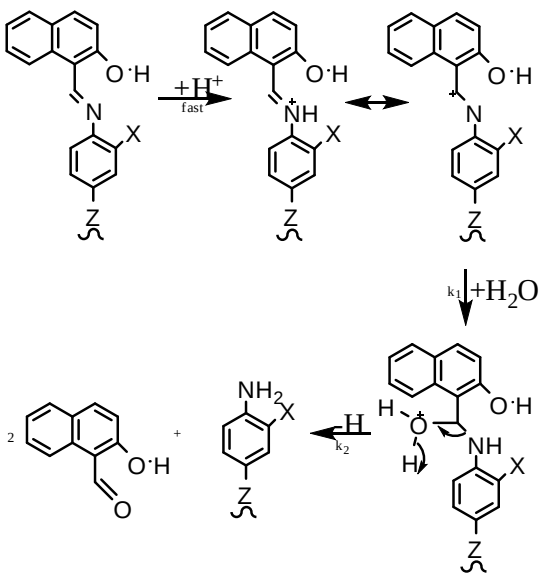

In Neutral Range

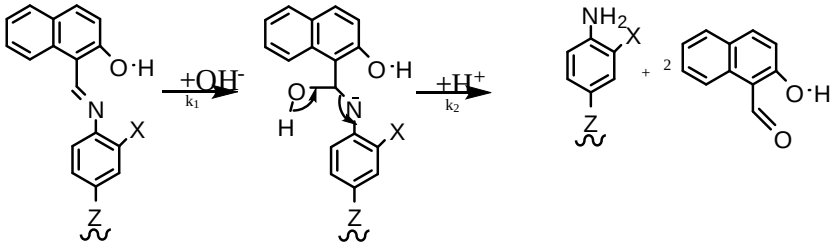

In Basic Range

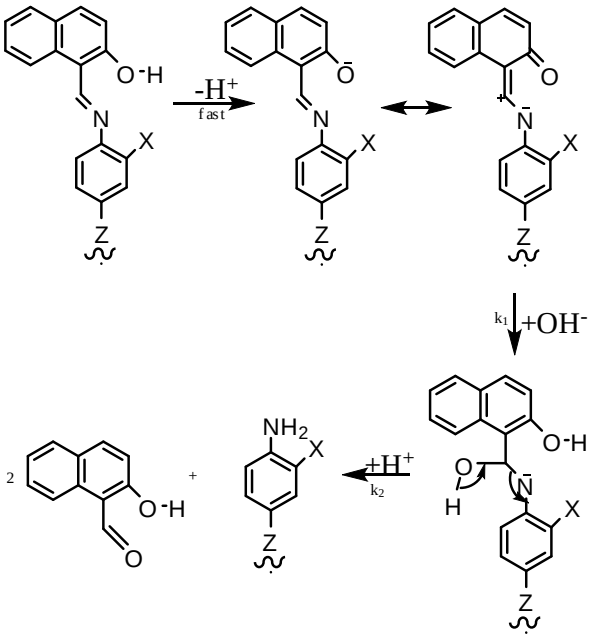

6.2 Kinetics of Hydrolysis of DFMDPE, DFMDPM, DFMDPD, DFMDPT and DFMDPB

The studies of kinetics of hydrolytic cleavage of the four azomethine sites have been done in aqueous methanol/ water (v/v) mixtures covering a wide pH range. Repetitive scan spectral profiles of DFMDPE, DFMDPM, DFMDPD, DFMDPT and DFMDPB in an acidic, neutral and basic media at time intervals of 1 minute are shown in **Figure 6.8.**

In the same respective figure are shown the spectral scan recorded at infinite time (solution kept overnight and recorded under similar conditions).

A proton- involved mechanism as shown in **Scheme 6.5** is proposed for the kinetics of hydrolysis of their DFMDPD Schiff bases.

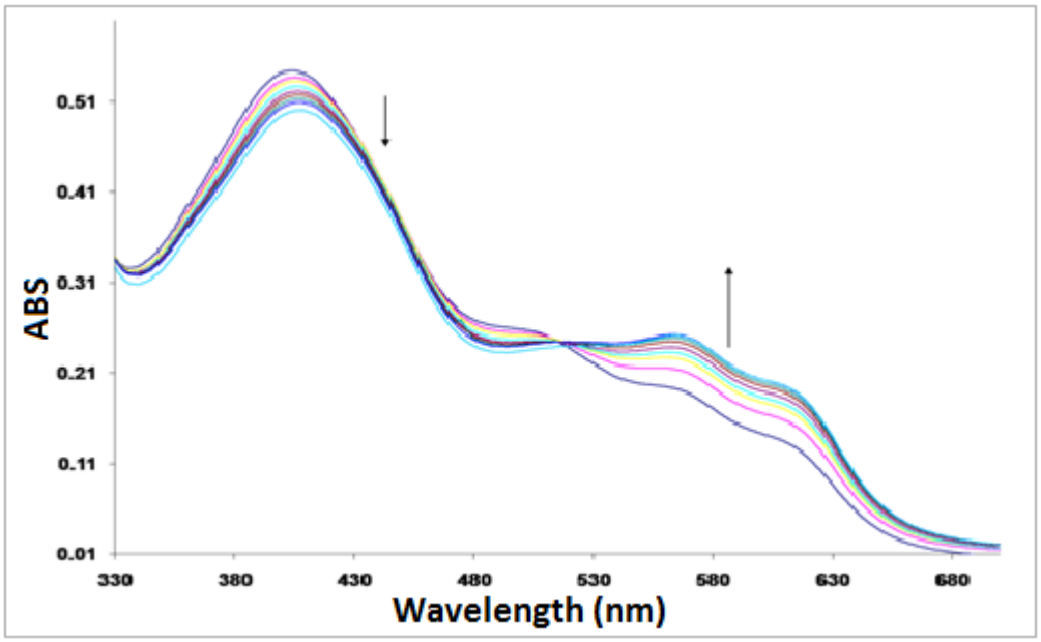

Figure 6.8: Repetitive spectral profiles of DFMDPD (4×10^{-5}M; μ = 0.1M) at P^H =6.0 at 30^0C (time interval, 1 min)

Scheme 6.5

in Acid range

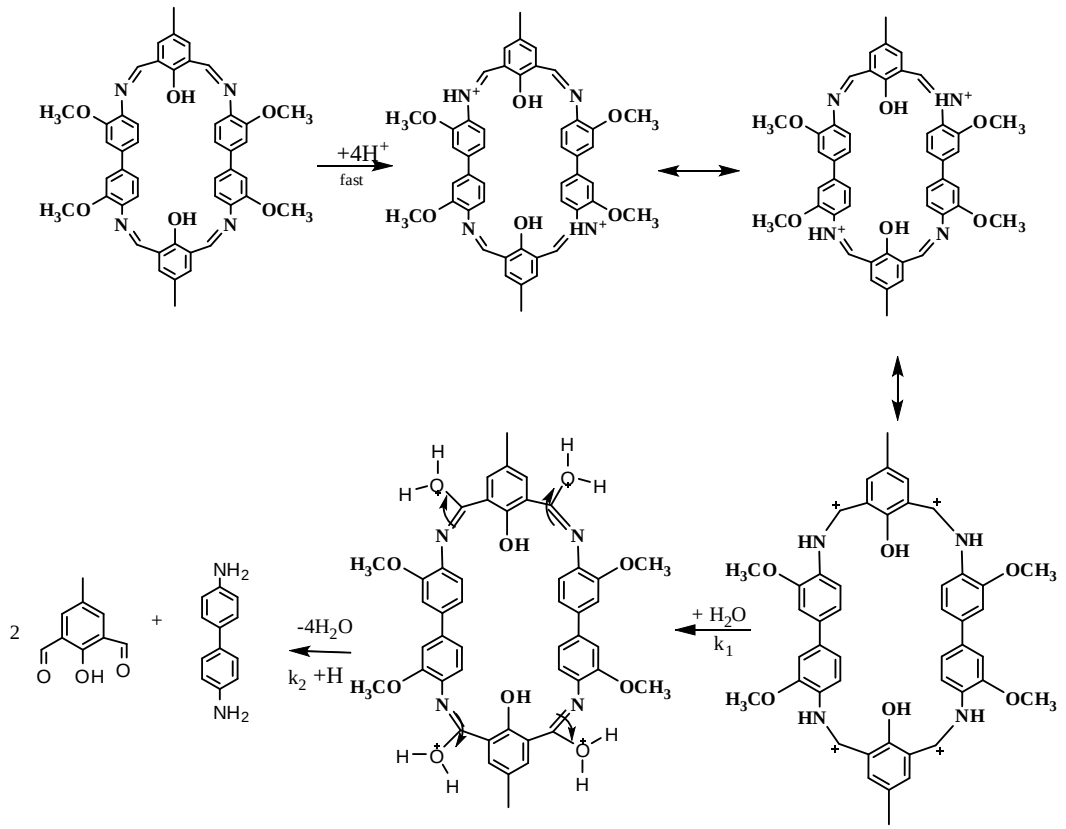

Neutral range

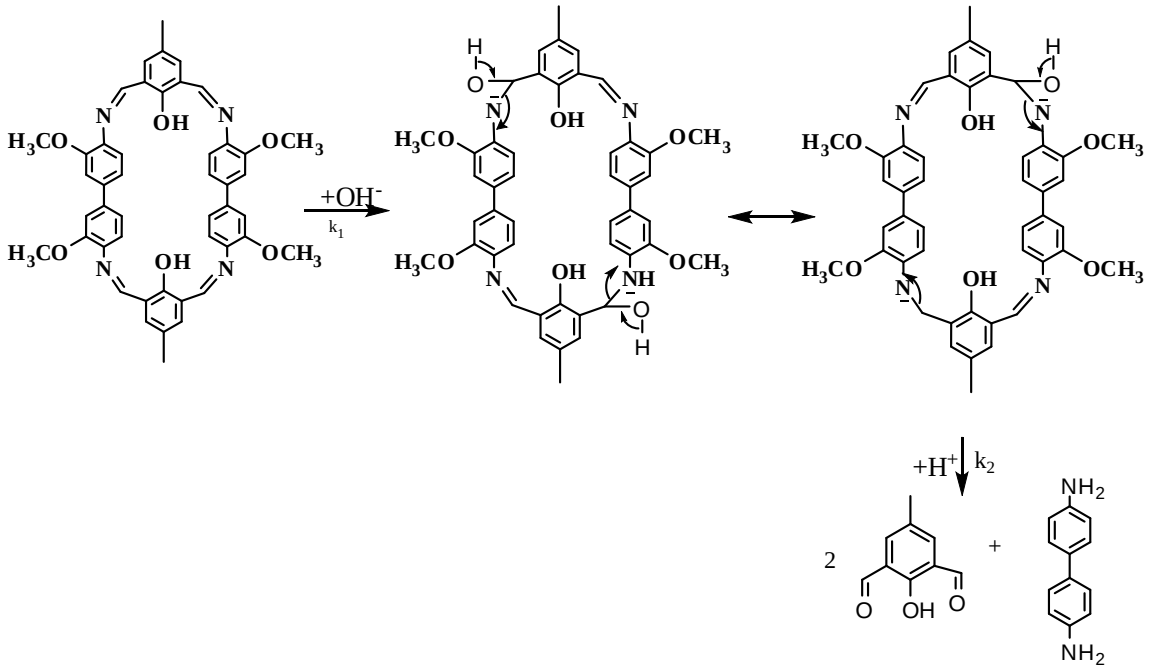

in Basic range

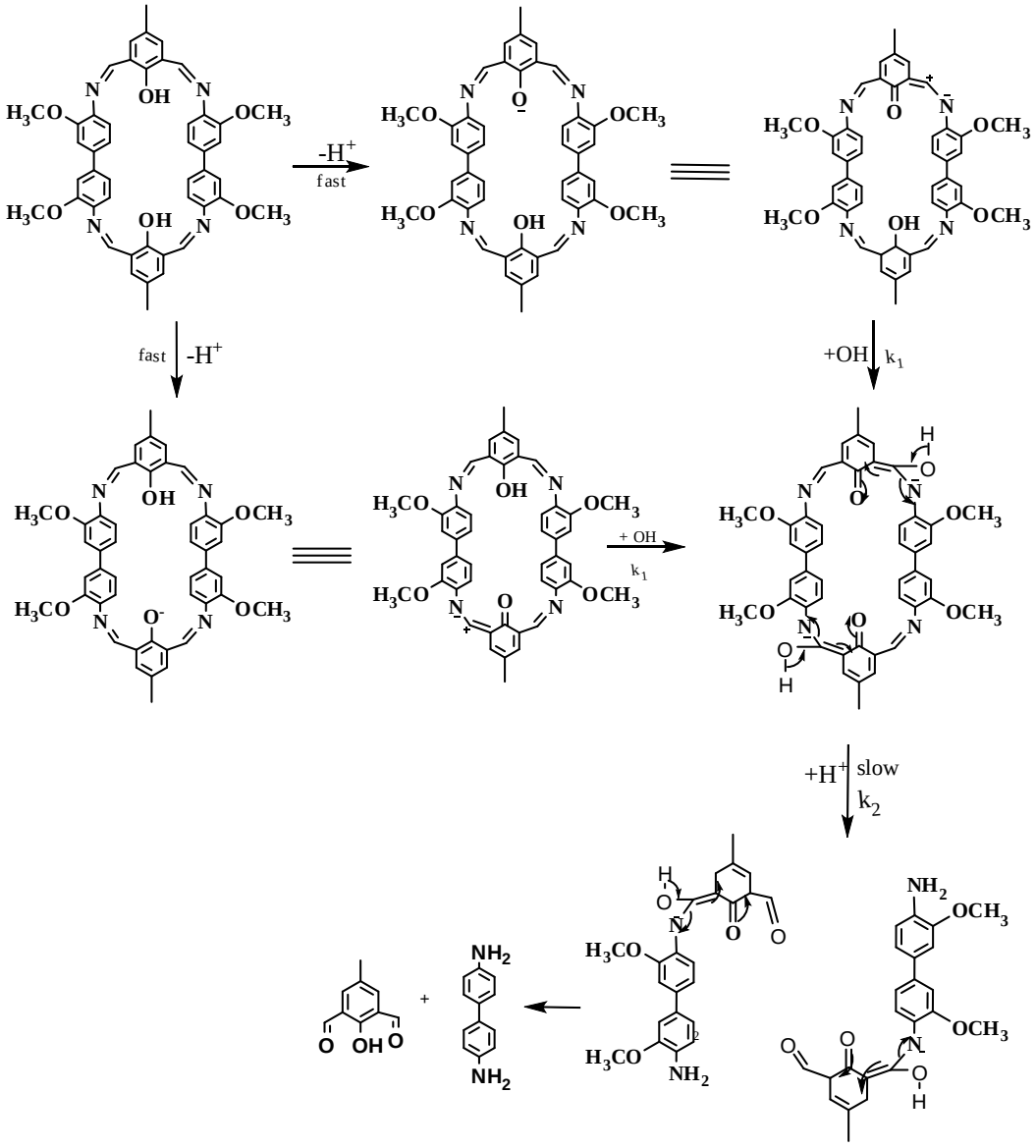

6.3 Biological Activity Applications

The biphenyl bridged Schiff base ligands and their complexes, have been found to shown biological activity. The binucleating ligands, shown in structure **2A.1** were reported to be successful fungicides, insecticides and antituberculer agents[8, 9]. The compounds also claimed to have certain degree of plant growth regulating activity[10]. Their complexes especially those of 2-hydroxy-benzamide showed synergistic herbicidal activity[11]. The metal complexes contains azomethine group have been found to show antifungal and antibacterial activity [12,13].

In the present studies binucleating ligands extend their utility as antibacterial agents. The biphenyl bridged binucleating ligands also are anticipated to have such activity.

The ligands, NDADPE, NDADPM, NDADPD, NDADPT and NDADPB were tested for their antibacterial activity against different bacteria and fungi. The bacterial strains including *Bacillus subtilis*, *Escherichia coli*, *Staphylococcus* aureu, *Shigella spp*. and *Klebsiella neumonia* were used in present study and *Aspergillus flavus, A. niger*, *Fusarium oxysporum, F. verticillioides* and *Penicillium chrysogenum* and *P. verrucosum* were used in present study to assess the antimicrobial activities of synthesized ligands. The ligands, containing napthyl group showed more activity than those of sal groups. The ligands containing OCH_3, and CH_3 groups (electron dontating groups) show more activity than others. In the case of binucleating napthyl systems the studies have been carried out in DMF medium as a control, since these ligands are sparingly soluble in common organic solvents like acetone, ethanol, methanol, acetonitrile, etc.

The compounds were dissolved in DMF and tried at different concentrations (400 µg and 600 µg). The Whatman filter paper discs (6 mm diameter) with different compounds were placed aseptically on seeded nutrient agar plates with different bacteria and incubated for 72 hours at 37^0C. At the end of the incubation period, the diameters of the growth inhibition zones were measured. The results are depicted in **Figure 6.9**. Among the complexes were screened Ni-NDADPE and Cu- NDADPD were show activity at 0.5 mg/ml against *Shigella* spp. and *Staphylococcus aureus* of among the tested organisms. In the case of antifungal activity most of the compounds show reasonable activity against *Aspergillus* and *Fusarium* species,

6.4. Pharmacology

6.3.1 *In vitro antibacterial and antifungal assays*

The biological activities of the newly synthesized macro cyclic Schiff base (**2A.3**) and its metal complexes (**2A.3a**) were studied for their antibacterial and antifungal properties by disc diffusion method[14,15]. The antibacterial activities of synthesized compounds were assessed against of gram negative and gram positive bacteria including *Escherichia coli*, *Staphylococcus* aureus, *Shigella dysentery, Klebsiella pneumonia, Micrococcus* species, *Bacillus subtilis, Bacillus cereus* and *Pseudomonas aeruginosa*. These bacterial strains have been chosen as they are the known pathogens of humans and other animals. In the case of antifungal activity *Aspergillus niger, Penicillium verrucosum*, *Fusarium oxysporum* and *Candida albicans* were used by above mentioned method. For antimicrobial assay various

concentrations of compounds ranging from 10, 25, 50 and 100 $mgmL^{-1}$ was used, DMF solvent was used as control assay standard. Standard antibiotics Gentamycin and Nistatin were used as positive controls for antibacterial and antifungal activity respectively. Nutrient agar media for antibacterial assay and potato dextrose agar medium for antifungal assay were used. Swab cultures were made and different concentrations of compounds were applied on to respective wells in agar media along with standard antibiotics. Cultured plates were incubated for 24 h to 48 hrs at 37^0C in incubator. After incubation the zone of inhibition was calculated and compared with negative and positive controls of respective compounds. The zones are shown in **Figures 6.10** and **6.11**. Diameters of the zones are calculated and represented in **Table 6.1**.

6.3.2 *Minimum inhibitory concentration (MIC)*

Compounds showing promising antibacterial/antifungal activities were selected to determine minimum inhibitory concentration by dilution method. The minimum inhibitory concentrations were determined by assaying at 100, 50 and 25 $mgmL^{-1}$ concentrations of selected by compounds comparison with the standard antibiotics of antibacterial and antifungal at the same concentrations.

6.3.3 *Pharmacology results*

The biological activity of the Schiff base exhibited a considerable enhancement on coordination with the metal ions against all fungal strains in **Table 6.1**. However, the metal complexes showed good antifungal activity against tested fungal strains in present study. It is evident from the data that, this activity was increases significantly in relation with coordination. This enhancement in the activity may be rationalized on the basis that their structures mainly possess an additional C=N bond. It has been suggested that the Schiff base with nitrogen and oxygen donor systems inhibit enzyme activity, since the enzymes which require these groups of their activity appear to be especially more susceptible to deactivating by metal ions on coordination. Moreover, coordination reduces the polarity[16,17] of the metal ion mainly because of the partial dampening of its positive charge with the donor groups[18,19] within the chelate ring system formed during coordination. This process, in turn, increases the lipophilic nature of the central metal atom, which favours its permeation more efficiently through the lipid layer of the microorganism[20,21] thus destroying them more aggressively. Some important factors such as the nature of the metal ion, nature of the ligand, coordinating

sites and geometry of the complex, concentration, hydrophilicity, lipophilicity and presence of coligands have considerable influence on antibacterial activity of the compound. Certainly, steric and pharmacokinetic factors also play a decisive role in deciding the potency of an antimicrobial agent. Apart from this, the mode of action of these compounds may also invoke hydrogen bond through the -C=N- group with the active centres and thus interfere with normal cell process. The presence of lipophilic and polar substituents is expected to enhance antibacterial activity. Heterocyclic ligands with multi functionality have a greater chance of interaction either with nucleoside bases (even after complexation with metal ion) or with biologically essential metal ions present in the biosystem and can be promising candidates as bactericides since they always tend to interact especially with some enzymatic functional groups, in order to achieve higher coordination numbers[22]. Thus antibacterial property of metal complexes cannot be ascribed to chelation alone, but it is an intricate blend of several contributions.

6.3.4 *In vitro cytotoxicity*

The synthesized Schiff base and its Co(II), Ni(II) and Cu(II) complexes were screened for their cytotoxicity (brine shrimp bioassay) by using the protocol of Meyer et al[18]. Brine shrimp (Artemia salina leach) eggs were hatched in a shallow rectangular plastic dish (22 - 32 cm) filled with artificial seawater, which was prepared with a commercial salt mixture and double distilled water. An unequal partition was made in the plastic dish with the help of a perforated device. Approximately 50 mg of eggs were sprinkled into the large compartment, which was darkened while the minor compartment was open to ordinary light. After two days nauplii were collected by a pipette from the lighter side. A sample of the test compound was prepared by dissolving 20 mg of each compound in 2 mL of DMF. From this stock solution 100, 50 and 10 $mgmL^{-1}$ was transferred to nine vials (three for each dilutions were used for each test sample and LD50 is the mean of three values) and one vial was kept as control having 2 mL of DMF only. The solvent was allowed to evaporate overnight. After two days, when shrimp larvae were ready, 1 mL of seawater and 10 shrimps were added to each vial (30 shrimps/ dilution) and the volume was adjusted with seawater to 5 mL per vial. After 24 h the number of survivors was counted. Data were analyzed by a Finney computer program to determine the LD50 values. In the case of cytotoxic activity it was observed that the Schiff base and its Co(II), Ni(II) and Cu(II) complexes displayed weak cytotoxic activity against A. salina, therefore they can be considered non-cytotoxic.

6.5 Biological studies

The microbial results of Schiff base and its Co(II), Ni(II) Cu(II) and Zn(II) complexes are systematized in **Table 6.1**. The biological activity of the Schiff base exhibited a considerable enhancement on coordination with the metal ions against all fungal strains. However, the metal complexes showed good antifungal activity against A. niger, Penicillium and C. albicans as shown in **Figures 6.10** and **6.11**.

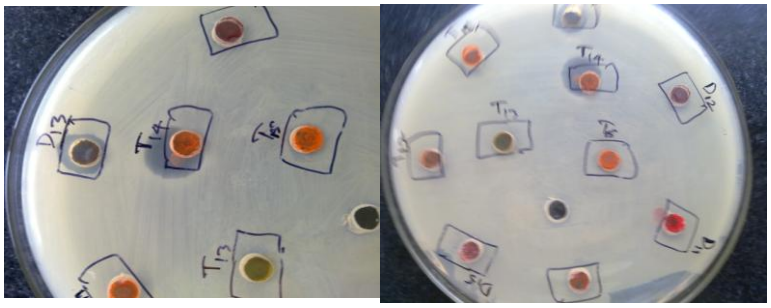

Figure 6.9: Photograph (*Shigella s*pp. And *Staphylococcus aureus*) showing antibacterial screening of biphenyl bridged ligands and their complexes

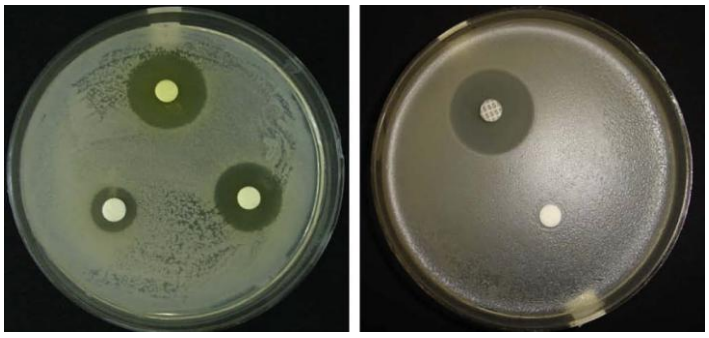

Figure 6.10: Photograph (Bacillus subtilis) showing antibacterial screening of Schiff base and Gentamycin

Figure 6.11: Photograph (A. niger) showing antifungal screening of Schiff base and Fluconazole

Table 6.1: *Bacteriological results of Schiff base and its Co(II), Ni(II) Cu(II) and Zn(II) complexes at 10 mg mL^{-1} concentration*

Compound	**Activity against bacteria (mm)**							**Activity against bacteria (mm)**		
	E.coli	**P.aeruginasa**	**b. cereus**	**s. aureus**	**s. dysentery**	**micrococus**	**b.subtilis**	**A.nigar**	**pencillium**	**c. albicans**
DFMDPE	18	16	18	12	16	15	20	22	20	18
$[Zn_2(DFMDPE)Cl_2]$	12	14	10	16	12	10	14	18	20	20
$[Cu_2(DMFDPE)(Cl)_2]$	14	16	12	18	14	12	16	20	22	22
$[Ni_2(DMFDPE)(Cl)_2]$	16	14	16	12	18	18	18	22	20	20
$[Co_2(DMFDPE)(Cl)_2]$	12	18	18	14	16	14	14	22	20	20
gentamycin	22	22	22	22	22	22	22	-	-	
fluconazole	-	-	-	-	-	-	-	26	26	26
DMF	14	14	14	14	14	14	14	14	14	14

Key for interpretation: less than 14 mm – inactive; 14–16 mm – weakly active; 16–18 mm – moderately active; above 18 mm – highly active

References

1. P A Villanova, NCCLS, *Performance standerds for Antimicrobial Disk Suspectibility Tests Approved Standard NCCLS Publication M2-A5, USA*, **1993**
2. C H Collins, PM Lyre, J M Grange, "*Microbiological Methods"*, ed. 6th ed., **1989**, Butterworths, Co Ltd, London
3. A Ramachandraiah, *Investigations on a new series of binuclear and tetranuclear complexes of copper(II) and other bivalent metal ions*, PhD thesis, University of Hyderabad, **1985**
4. P S Zacharias, A Ramachandraiah, *Polyhedron*, 4 , **1985**, 1013
5. A Ramachandraiah, P Nageswara Rao, M Ramaiah, *Indian J Chem*, 28A, **1989**, 309
6. Sarojini T, *Studies of some new classes of polynuclear coordination compounds*, PhD thesis, Regional Engg College Warangal, **1993**
7. S Suryanarayana Rau, *Intramolecular interactions and kinetics of hydrolysis of some bridged homo bifunctional organic compounds*, PhD thesis, Regional Engg College, Warangal, **1997**
8. B Ramamurthy, R K Maller, G R Rao, T Ramakrishnan, M V Bhatt, *J Indian Inst Sci*, 58, **1967**, 557
9. Debrecen, K N Ludovico, Sero, *Phys Chim*, 12, **1966**, 145
10. M Kovaes, G Pfeifer, I Pragal, *Plant growth Regul*, Proc, **1977**, 366
11. N M Golyshin, V I Abelenstev, *Mikol Fitopatol*, 7, **1973**, 498
12. K Y Lau, A Mayr, K K Cheung, *Inorg. Chem. Acta*, 285, **1999**, 223.
13. A S Shawali, N M S Harb, K O Badahdah, *J Heterocylic Chem*, 22, **1985**, 1397
14. E O Offiong, S Martelli, Il Farmaco 49, **1994**, 513
15. J G Collee, J P Duguid, A G Farser, B D Marmion (Eds), *Practical Medical Microbiology*, Churchill Livingstone, New York, **1989**
16. C J Balhausen, *An Introduction to Ligand Field*, McGraw Hill, New York, **1962**
17. A B P Lever, *Inorganic Electronic Spectroscopy*, Elsevier, Amsterdam, **1984**, 23
18. B N Meyer, N R Ferrigni, J E Putnam, L B Jacobsen, D E Nichols, J L McLauhglin, *Planta Med*, 45, **1982**, 31
19. Z H Chohan, A Scozzafava, C T Supran, *J Enzyme Inhib Med Chem*, 17, **2003**, 261
20. Z H Chohan, H Pervez, M K Khan, A Rauf, C T Suuran, *J Enzyme Inhib Med Chem*, 19 **2004**, 85
21. Z H Chohan, *Synth React Inorg. Met-Org Chem*, 34, **2004**, 833
22. W Levingson, P Mikeleus, J Jackson, W Kaska, G N Schranzer (Ed), *Inorganic and Nutritional Aspects of Cancer*, Plenum Press, New York, **1978**

LIST OF THE PUBLICATIONS / CONFERENCES

1. Crystal structure analysis and conformational isomerism of 2,2'-(4,4'-oxybis(4,1-phenylene)bis(azan-1-yl-1-ylidene))bis(methan-1-yl-1-ylidene)dinaphthalen-1-ol
   Krishna V, Srinivas Basavoju and Ramachandraiah A "*Molecular Crystals and Liquid Crystal*s" (Taylor and Francis), **2012** (1) 265-29
2. Synthesis, electrochemical and molecular modeling studies of Schiff bases of some hydrazinylthiazocoumarins and 2-acetyl pyridine
   Vijaybhaskar P, Krishna V and Ramachandraiah A, *J Pharm Chem*, **2010**; 4, 10-16
3. Synthesis and spectral characterization of antimicrobial activity of the binuclear Ni(II), Co(II), Cu(II) and Zn(II) complexes of a novel macrocyclclic biphenyl bridged Schiff base ligand
   Krishna V and Ramachandraiah A, *Indian Council of Chemists***,** (Accepted), **2012**
4. Synthesis and characterization of the binuclear Ni(II), Co(II), Cu(II) and Zn(II) complexes of a novel macrocyclic biphenyl bridged Schiff base ligand
   Krishna V and Ramachandraiah A
   6th International Symposium on "*Macro-and Supramolecular Architectures and Materials"* held on 21-25th November, **2012** at K.S. Rangasamy College of Technology, Tamilnadu
5. Electrochemical behavior of a double diphenylether-bridged binuclear copper(II) Schiff base complexes in non-aqueous media
   Krishna V, Srinivasa Rao G and Ramachandraiah A
   2nd International Conference On "*Trends in Chemical Sciences Going Beyond Frontiers*" held on 10-12th June **201**2 at India Council of Chemist, Malaysia
6. Spectral and supramolecular studies of the Schiff base cryptands of substituted 4-(4- aminophenoxy)benzenamine and 2, 6- diformyl-4-methylphenol
   Krishna V and Ramachandraiah A
   International Conference on "*Supramoleculer Chemistry and Nanomaterials*" held on 14-16th Feb. **2011**, Page-82 at University of Mumbai, Mumbai
7. Synthesis and characterization of a novel series of homo aryl bridged binuclear and tetranuclear of Co(II), Ni(II), Cu (II) and Zn (II) complexes
   Krishna V and Ramachandraiah A
   International Conference on "*3rd Asian Conference Coordination Chemistry*" held on 17-20th Oct. **2011**, PP-108 at IIT, Delhi

8. Spectral and magnetic characterisation and studies of antimicrobial activity of the binuclear Ni(II), Co(II), Cu(II) and Zn(II) complexes of the Schiff base, 2,2'-(4,4'-oxybis(4,1-phenylene)bis(azan-1-yl-1ylidene)bis(methan-1-ylylidene)dinaphthalen- 1-ol

   Krishna V**,** Prabhakarachary D and Ramachandraiah A

   National Conference On "*Interface between Chemical Sciences and Technologies*" held on 29-30th December **2011** at National Institute of Technology, Warangal

9. Thermal studies to visualise a binuclear Zinc (II) Schiff base complex as a Supramolecular catenand

   Krishna V and Ramachandraiah A

   National Conference On "*Interface between Chemical Sciences and Technologies*" held on 29-30th December **2011** at National Institute of Technology, Warangal

10. Supramoleculer encapsulation of organic and heavy metal pollutants by a novel series of Quadridentate cavitands ligands

    Krishna V, Prabhakarachary D and Ramachandraiah A

    National Seminar on "*Green Chemistry an Sustainable Innovation Development*" held on 29-30th march **2010** at Kakitiya University, Warangal

11. Spectral electrochemical and molecular modeling studies of a new class of Supramolecular cavitands as Ion-transport and drug delivery systems

    State Level Seminar on "*Applications and Impacts of Chemicals in Day to Day Life in Particular to Pharmaceuticals and Agriculture*" held on 17th & 18th July, **2009** at S.V.R.K. Govt.Degree College, Nidadavole

    Krishna V and Ramachandraiah A

12. Spectral and supramolecular studies of the Schiff base cryptands of substituted benzidines and 2, 6-diformyl-4-methylphenol

    Krishna V. Sarojini T and Ramachandraiah A

    National Seminar on "*Recent Trends in Organic and Medicinal Chemistry*" held on 16-17th January **2009** at National Institute of Technology, Warangal